Visible Light Active Photocatalysts for the Degradation of Drug Residues in Polluted Waters

Von der Naturwissenschaftlichen Fakultät der

Gottfried Wilhelm Leibniz Universität Hannover

zur Erlangung des Grades

Doktorin der Naturwissenschaften

(Dr. rer. nat.)

genehmigte Dissertation von

Arsou Arimi, M. Sc. (Iran)

2020

Referent: Apl. Prof. Dr. rer. nat. habil. Detlef Bahnemann

Korreferent: Prof. Dr. rer. nat. Jürgen Caro

Tag der Promotion: 09.01.2020

For My Family

II

Acknowledgments

discussions in our weekly seminars and also for our non-scientific, nice conversations and the fun time we had in the office.

I would like to also thank my close friends, Yalda, Parisa, Golnar and Marzie for becoming somehow my Iranian family in Germany and a special thank goes to Sona for her kindness and for all the memorable moments we have had together in TCI.

I was lucky to find the coolest group of friends one could have here in TCI: Lena, Sona, Steffi, Carsten, Manuel, Christoph, Ana and Björn (from Bibliothek), and Camilla, Maryam and Fabian (from LNQE). You guys mean a lot to me and I will never forget the amazing time we have had together during the past years.

My special thanks go of course to my best friend. Thank you Lena, for standing by my side at all costs, for taking care of me when I faced problems, for motivating me even in your hardest moments, and for being the best friend, sister, roommate and anything I needed to survive here in Germany.

And, last but by no means least:

No words can express how grateful I am to my family. Their absolute support, kindness, love, patience, encouragement and trust throughout my whole life have made it possible for me to reach where I am right now. My thanks also go to my cousin, Mohabbat, who has always been like a sister for me and to my sister-in-law, Mahboobeh for being as kind as she is. I dedicate this achievement to my parents, Mahmood and Rafat and to my brother, Alireza. You three are all I have got. Thanks for being the best family that I could imagine to have.

Zusammenfassung

Die Entfernung von Pharmazeutika und deren Rückständen aus Wasser- und Abwasserströmen ist ein wichtiges Umweltproblem, das in den letzten Jahrzehnten große Aufmerksamkeit erlangt hat. Dabei ist die Photokatalyse einer der Ansätze, die im Bereich der Wasser- und Abwasserbehandlung untersucht werden. In jüngster Zeit standen photokatalytische Prozesse, die durch Sonnenlicht oder sichtbares Licht angetrieben werden, und Materialien, die sichtbares Licht absorbieren, im Mittelpunkt vieler wissenschaftlicher Studien. In der vorliegenden Arbeit werden zwei Mitglieder der Phenothiazin-Gruppe (Antipsychotika), Methylenblau und Chlorpromazin, als Modellschadstoffe untersucht.

Im Rahmen dieser Doktorarbeit wird zunächst die photokatalytische Umsetzung von Methylenblau in Gegenwart von sieben selbst hergestellten halbleitenden Zinkferritpulvern untersucht. Hierbei werden die Zinkferritproben charakterisiert und der Einfluss verschiedener Synthesemethoden auf deren Eigenschaften, einschließlich der Kristallgröße und -reinheit, der Oberfläche, des Flachbandpotentials und der Bandlückenenergie, bestimmt. Darüber hinaus wird die berichtete Aktivität von Zinkferriten durch Bestrahlung mit sichtbarem Licht, sowie die Fähigkeit von Methylenblau, die Aktivität dieses halbleitenden Materials zu bestimmen, durch eine Reihe detaillierter wellenlängenabhängiger Messungen für die photokatalytische Umwandlung von Methylenblau untersucht. Die experimentellen Ergebnisse zeigen, dass das beobachte Photobleichen von Methylenblau durch Bestrahlung mit sichtbarem Licht in Gegenwart von Zinkferriten durch Elektronentransfer von den photoangeregten Methylenblau-Molekülen, die auf der Oberfläche des Ferrits adsorbiert sind, in das Leitungsband des Zinkferrits zu erklären ist.

Darüber hinaus wird in der vorliegenden Arbeit die photokatalytische Umwandlung von Chlorpromazin, einem weiteren sehr wichtigen Mitglied der Phenothiazin-Gruppe, untersucht. Da bislang sehr wenig über die photokatalytische Umwandlung von Chlorpromazin und seiner Metabolite unter Bestrahlung mit sichtbarem Licht bekannt ist, wird dieses in der vorliegenden Arbeit ausführlich untersucht. Aufgrund dessen wird die photokatalytische Umwandlung von Chlorpromazin in Gegenwart von KRONOClean 7000 (K-7000) unter verschiedenen Versuchsbedingungen bewertet. K-7000 ist ein Halbleitermaterial, das sichtbares Licht absorbiert, genauer ein kohlenstoffbasiert modifizierter Titandioxid-Photokatalysator. Es wird gezeigt, dass trotz der hohen Stabilität von Chlorpromazin unter Bestrahlung mit sichtbarem Licht, in Gegenwart von K-7000 eine vollständige Umwandlung dieses organischen Moleküls erreichbar ist. Darüber hinaus wird in der vorliegenden Arbeit ein detaillierter Vergleich zwischen den photokatalytischen und den photolytischen Umwandlungswegen von Chlorpromazin und seinen Reaktionsprodukten / Zwischenprodukten, die bei Bestrahlung mit UV- und sichtbarem Licht unter anaeroben und aeroben Bedingungen gebildet werden, vorgestellt. Die Zwischenproduktanalyse unter Verwendung der Hochleistungsflüssigkeitschromatographie (HPLC-MS) zeigt, dass das Hauptreaktionszwischenprodukt der photokatalytischen Umwandlung von Chlorpromazin sein Sulfoxidmetabolit ist. Chlorpromazinsulfoxid ist bei Bestrahlung mit sichtbarem Licht, selbst in Gegenwart von K-7000, sehr beständig. Diese Beobachtung zeigt, dass unter verschiedenen Umständen die Fähigkeit von K-7000 zur photokatalytischen Umwandlung einiger organischer Materialien unzureichend sein kann.

Daher werden eingehendere Untersuchungen zum Ursprung der Aktivität durch Anregung mit sichtbarem Licht von K-7000 durch diffuse-Reflexions-Transienten-Absorptionsspektroskopie durchgeführt. Die Dynamiken der Ladungsträger, die alternativ durch Laserbestrahlung mit UV-

oder sichtbarem Licht unter inerten oder reaktiven Atmosphären erzeugt werden, wird untersucht, indem K-7000, als Titandioxid, das durch eine kohlenstoffbasierte Schicht sensibilisiert ist, betrachtet wird. Die experimentellen Ergebnisse zeigen, dass die Fähigkeit von K-7000 zur Oxidation von Methanol unter Bestrahlung mit sichtbarem Licht äußerst begrenzt ist, während dieser Photokatalysator Chlorpromazin erfolgreich umwandeln kann. Diese Beobachtungen, die durch Transienten-Absorptionsspektroskopie-Messungen gemacht wurden, werden auch durch eine Reihe von photokatalytischen Experimenten gestützt, die durchgeführt wurden, um Chlorpromazin und Methanol unter identischen Bedingungen umzusetzen. In diesem Zusammenhang werden die möglichen photokatalytischen Reaktionen mit Chlorpromazin und Methanol nach UV- und sichtbarer Lichtanregung von K-7000 bestimmt und miteinander verglichen. Unter Berücksichtigung der Redoxpotentiale der entsprechenden Reaktionen wird ein Mechanismus vorgeschlagen, anhand dessen die unterschiedliche Fähigkeit von K-7000 zur photokatalytischen Umwandlung verschiedener organischer Verbindungen (Chlorpromazin, Methanol und Chlorpromazinsulfoxid) erklärt wird.

Insgesamt bietet diese Dissertation einen tieferen Einblick in die Prinzipien der photokatalytischen Umwandlung von organischen Molekülen durch sichtbares Licht, insbesondere der Gruppe der Phenothiazin-Antipsychotika. Diese Studie bestätigt, dass die photogenerierten Ladungsträger in Halbleitern, die mit sichtbarem Licht angeregt werden können, eine begrenzte Fähigkeit haben können, Oxidationsreaktionen zu steuern. Diese Eigenschaft kann jedoch gezielt genutzt werden, um die Selektivität der Oxidationshalbreaktion bei photokatalytischen Prozessen zu verbessern, so dass ein unerwünschter Schadstoff selektiv oxidiert und in ein wertvolles Produkt umgewandelt werden kann.

Schlüsselwörter: Photokatalyse mit sichtbarem Licht; KRONOClean 7000; Zinkferrit; Chlorpromazin; Methylenblau; Wasser- und Abwasserbehandlung; pharmazeutische Rückstände; Hochleistungsflüssigkeitschromatographie (HPLC-MS); diffuse-Reflexions-Transienten-Absorptionsspektroskopie.

Abstract

Removal of pharmaceuticals and their residues from water and wastewater streams is an important environmental issue which has gained a huge amount of attention over the past decades. Photocatalysis is one of the remediation approaches to be considered in this regard in the field of water and wastewater treatment. Hence, solar- or visible light- driven photocatalytic processes and visible light-absorbing materials have recently been the focus of many scientific studies. In the current work, two members of the phenothiazine group of antipsychotic pharmaceuticals, namely, methylene blue and chlorpromazine are considered as model pollutants.

Within the scopes of this doctoral thesis, initially, the photocatalytic conversion of methylene blue in the presence of seven self-prepared zinc ferrite semiconducting powders is evaluated. Herein, the zinc ferrite samples are characterized and the impact of different synthetic methods on their properties including the crystalline size and purity, the surface area, the flat band potential and the bandgap energy is determined. Moreover, the reported visible light-activity of zinc ferrite as well as the usefulness of methylene blue to determine the activity of this semiconducting material are investigated through a series of detailed wavelength dependent measurements for the photocatalytic conversion of methylene blue. The experimental results reveal that the observed photobleaching of methylene blue under visible light irradiation in the presence of zinc ferrite is rather contributed to the electron transfer from the photo-excited methylene blue molecules adsorbed at the surface of zinc ferrite into the latter's conduction band.

In addition, the photocatalytic conversion of chlorpromazine, another very important member of the phenothiazine group of antipsychotics is studied. Since very little is known about the possibility of the photocatalytic conversion of chlorpromazine and its metabolites under visible light irradiation, this issue is assessed in detail in the current study. Accordingly, the photocatalytic transformation of chlorpromazine in the presence of KRONOClean 7000 (K-7000) under different experimental conditions is evaluated. K-7000 is a visible light-absorbing semiconducting material, more specifically, a carbon-based modified titanium dioxide photocatalyst. It is shown that despite the high stability of chlorpromazine under visible light irradiation, in the presence of K-7000 a complete conversion of this organic compound is achievable. Moreover, a detailed comparison between the photocatalytic and the photolytic conversion pathways of chlorpromazine and the reaction products/intermediates formed upon UV and visible light irradiation under both anaerobic and aerobic conditions is presented in the current study. The intermediates analysis employing the high performance liquid chromatography (HPLC-MS) technique reveals that the main reaction intermediate of the photocatalytic conversion of chlorpromazine is its sulfoxide metabolite. Chlorpromazine sulfoxide is highly persistent upon visible light irradiation even in the presence of K-7000. This observation evinces that under different circumstances, the ability of K-7000 for the photocatalytic conversion of some organic materials might be inadequate.

Thus, deeper investigations are carried out concerning the origin of the visible light activity of K-7000 by means of diffuse reflectance transient absorption spectroscopy. The dynamics of the charge carriers alternatively induced by UV or visible light laser irradiation under inert or reactive atmospheres are studied by considering K-7000 as TiO_2 sensitized by a carbon-based layer. The experimental results reveal that the ability of K-7000 for the oxidation of methanol under visible light irradiation is extremely limited, while, this photocatalyst is able to successfully oxidize chlorpromazine. These observations obtained from the transient absorption spectroscopy measurements are also supported by a series of photocatalytic experiments performed to convert

chlorpromazine and methanol under identical conditions. In this regard, the possible photocatalytic reactions with chlorpromazine and methanol after UV and visible light excitation in K-7000 are determined and compared with each other. Hence, by considering the one-electron redox potentials of the corresponding reactions, a mechanism is proposed from which the varying ability of K-7000 for the photocatalytic conversion of different organic compounds, (i.e., chlorpromazine, methanol and chlorpromazine sulfoxide), is explained.

In total, this doctoral dissertation provides a closer insight into the principles of the visible-light driven photocatalytic conversion of organic molecules, specifically the group of phenothiazine antipsychotic pharmaceuticals. This study confirms that the photogenerated charge carriers formed in visible light active semiconductors are likely to have a limited ability to drive oxidation reactions. This property can, however, be used to improve the selectivity of the oxidation half-reaction in photocatalytic processes, so that an undesired pollutant can be oxidized selectively and be transformed into a valuable product.

Keywords: Visible light-driven photocatalysis; KRONOClean 7000; zinc ferrite; chlorpromazine; methylene blue; water and wastewater treatment; pharmaceutical residues; high performance liquid chromatography (HPLC-MS); transient absorption spectroscopy.

Table of Contents

X

Chapter 1: Introduction

1.1. Pharmaceuticals as Pollutants

During the last decades, the appearance of trace amounts of pharmaceutical residues in water and wastewater streams has gained a huge amount of attention. The presence of these compounds was reported for the first time in the late 1970s; however, this could have been a problem even before that time. Despite the low concentration of these compounds, their continuous consumption and release in aquatic systems throughout the whole year rises up a big concern [1]. Pharma-residues have already been detected globally in various aquatic systems such as drinking water [2–4], surface water [5–7] and inlet or outlet of water/wastewater treatment plants [8–12]. In many cases, the observed pharmaceutical compounds were reported to originate from improper disposal of unused drugs into the urban sewage systems [13]. They were also found in landfill leachates resulting from the inappropriate discharge of drugs into normal garbage [14].

Most of the pharmaceuticals are designed in a way to have specific biological impact on living tissues; this also leads to their adverse environmental effects. Pharma-residues are mainly resistant to biodegradation and can hence also totally or partially escape the conventional water/wastewater treatment plants [15] and in many cases extra very costly treatment steps for their removal are required. Therefore, this group of contaminants are considered as a serious threat for the environment as well as for the human health [16,17].

Among the huge variety of most frequently detected pharma-residues in water and wastewater streams, the group of "psychiatric drugs" including the four categories of antipsychotics, antidepressants, anxiolytics, and antiepileptics represent almost 17% occurrence in the environmental systems [18]. The global production as well as consumption of this group of drugs are generally increasing [19]. Psychiatric pharmaceutical residues are often found worldwide in aqueous environments, for instance in psychiatric hospital wastewater and municipal wastewater treatment plants in China [20,21], in wastewaters from a hospital and a wastewater treatment plant in the urban region of Porto, Portugal [22], or in raw and treated wastewater from a wastewater treatment plant, drinking water and lake water collected in New York State, USA [23].

Antipsychotics are a type of psychiatric drugs which are prescribed to treat patients with specific psychiatric disorders affecting the mind. In this case, the patient suffers from loss of contact with the reality and shows symptoms such as delusion or hallucination. This situation might be reflected in form of a physical condition or a mental disorder like schizophrenia or even as an extreme depression [24]. Antipsychotic medications are normally used to mitigate these severe symptoms of mental disorders. The first generation of antipsychotic drugs or the "typical" antipsychotics, also known as neuroleptics, include pharmaceuticals such as chlorpromazine, haloperidol, perphenazine, thioridazine, flupenthixol, thiothixene, and trifluoperazine. Neuroleptics block the rational dopamine receptors and can thus have mood-changing properties, without affecting the intellectual skills [25].

1.2. Phenothiazines

Phenothiazines, one of the largest categories of antipsychotic drugs, is among the most frequently prescribed medications to treat severe mental disorders around the world [26,27]. Phenothiazines are able to block the dopamine receptors in the basal ganglia (a group of clusters of neurons in the brain), the hypothalamus (a complex area of the brain with a number of important functions), and the limbic system (a connection of many brain structures that help control emotions, memory, learning, motivation, and bodily functions like appetite and sex drive). Besides psychosis, phenothiazines are also used to treat hyperemesis, a pregnancy complication that is characterized by severe nausea, vomiting, weight loss, and possibly dehydration; since they can also block the histamine receptors [25].

All the members of the phenothiazine group share a sulfur-containing tricyclic ring with different substituents at the R_1, R_2 and R_3 positions (**Figure 1**) and are divided based on the substitutions on the nitrogen into three sub-categories: (i) the aliphatic phenothiazines (with acyclic substitutions), (ii) the piperidine phenothiazines (with piperidine-derived group substituents), and (iii) the piperazine phenothiazines (with piperazine-derived substituents). Chlorpromazine is the major representative member of the aliphatic phenothiazines [28,29].
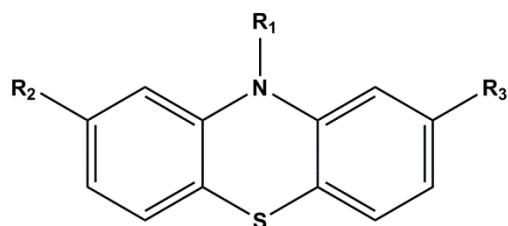
Figure 1-1. Chemical structure of the phenothiazine group

The origin of phenothiazines goes back to the 19th century accompanied by the development of the dye industry at that time [30]. In 1876, Heinrich Caro, a German chemist who worked at the Badische Anilin und Soda Fabrik (Baden Aniline and Soda Factory; BASF) synthesized a phenothiazine derivative aniline dye ($C_{16}H_{18}ClN_3S$) and named it as "methylene blue" [IUPAC name: 3,7-bis(Dimethylamino)-phenothiazin-5-ium chloride] (**Figure 1-2**). This was the beginning of the evolution of a new antipsychotic group of drugs, the "phenothiazines" [31].
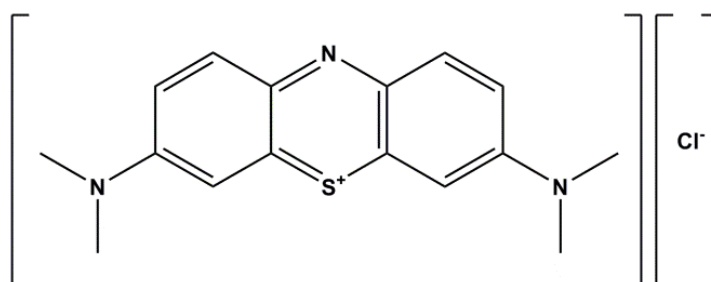
Figure 1-2. Chemical structure of methylene blue

Methylene blue was the first dye tested for medical purposes in human patients and in 1891 Paul Ehrlich was able to show that this dye was effective to treat malaria [32]. Eversince, this compound and its derivatives have been investigated in several therapeutic aspects such as chemotherapy, bacterial and viral infections, cancer, psychotic and neurological problems, and even Alzheimer's disease [33]. Besides being a pharmaceutical and a textile dye, methylene blue has also been very popular as a model pollutant in water remediation studies [34].

In 1883, with methylene blue as the lead compound, August Bernthsen reported the synthesis of the 10*H*-phenothiazine molecule (**Figure 1-3**) and was able to characterize its structure [32].

Figure 1-3. Chemical structure of phenothiazine

About seventy years later, the hunt for antimalarial drugs led to the synthesis of a new member of phenothiazines by Paul Charpentier at Rhône-Poulenc, Paris in 1950; "chlorpromazine" (**Figure 1-4**) which was reported to be the first effective antipsychotic drug [31].
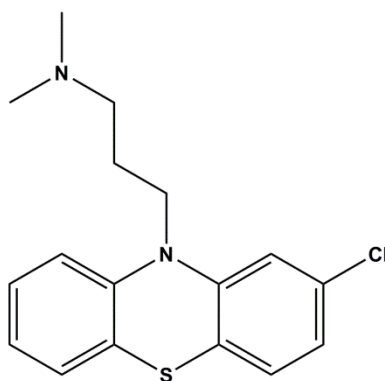
Figure 1-4. Chemical structure of chlorpromazine

Chlorpromazine, with the IUPAC name of 3-(2-chloro-10*H*-phenothiazin-10-yl)-*N*,*N*-dimethyl-propan-1-amine, was introduced to the pharmaceutical market in 1952, as the most popular member of the phenothiazine group [35]. However, there have been negative reports about the toxicity symptoms in patients taking this medication after exposure to sunlight [36]. It has been shown that this compound is highly photosensitive and that some genotoxic effects were resulted from the formation of short-lived radicals in the body [37]. It has also been observed that taking this drug and being exposed to solar irradiation at the same time could result in the formation of dechlorinated free radicals in the patient's body which could react subsequently with DNA and produce singlet oxygen [38].

Obviously, the remains of this pharmaceutical as well as its transformation intermediates end up in the municipal or industrial water and wastewater streams. Similar to many other pharmaceuticals, there have been several reports on detected residues and possible harmful ecotoxicological effects of phenothiazines or their transformation products in the effluents

of treatment plants or pharmaceutical companies [39–43]. Therefore, finding an effective method to remove these organic structures and their reaction intermediates from the aquatic systems is of high importance.

1.3. Photocatalysis

One of the possible approaches for the treatment of pharmaceutical-containing water or wastewater is the application of photocatalytic reactions [1,44]. As recommended by the International Union of Pure and Applied Chemistry (IUPAC), photocatalysis is defined as "change in the rate of a chemical reaction or its initiation under the action of ultraviolet, visible, or infrared radiation in the presence of a substance (the photocatalyst) that absorbs light and is involved in the chemical transformation of the reaction partners" [45].

Following the pioneering work of Fujishima and Honda in 1972 which reported for the first time the photocatalytic activity of TiO_2 for splitting water into molecular hydrogen and oxygen upon UV irradiation [46], photocatalysis has gained a huge amount of scientific attention. Eversince, many efforts have been done in this field to find proper semiconducting materials as photocatalysts for the degradation of organic and inorganic molecules.

Heterogeneous photocatalysis is considered as one of the advanced oxidation processes (AOPs) in the field of air/water/wastewater treatment [47]. Over the past decades, several investigations related to solar-light driven heterogeneous photocatalytic reactions with the purpose of wastewater treatment have been performed [48–53]. Heterogeneous photocatalysis enables the chemical destruction of pharmaceutical residues and their transformation products present in wastewater. This is one of the advantages of this treatment method which leads to the reduction of ecotoxicity and other harmful effects of these compounds on the environment [19].

An ideal semiconducting material to be used as a photocatalyst needs to be stable, available, biologically and chemically inactive, simply produced and employed, efficient in catalyzing the reaction, optimally activated by sunlight, inexpensive, and environmentally-friendly [54].

1.3.1. Titanium Dioxide (TiO_2)

Most of the available photocatalysts are inorganic solids having various crystalline phases. Among the available semiconducting oxides, TiO_2 is the most intensely investigated and the most commonly used photocatalyst, *inter alia*, due to its low toxicity, its reasonable price and its high photo- and chemical stability [55–58]. Among the three available polymorphs of TiO_2 (**Figure 1-5**), namely, anatase (tetragonal), brookite (orthorhombic), and rutile (tetragonal) [59], the latter is known to be thermodynamically the most stable form of titanium dioxide at ambient temperature. This leads to a transformation of all metastable phases to the rutile phase at temperatures higher than 600°C [60,61].
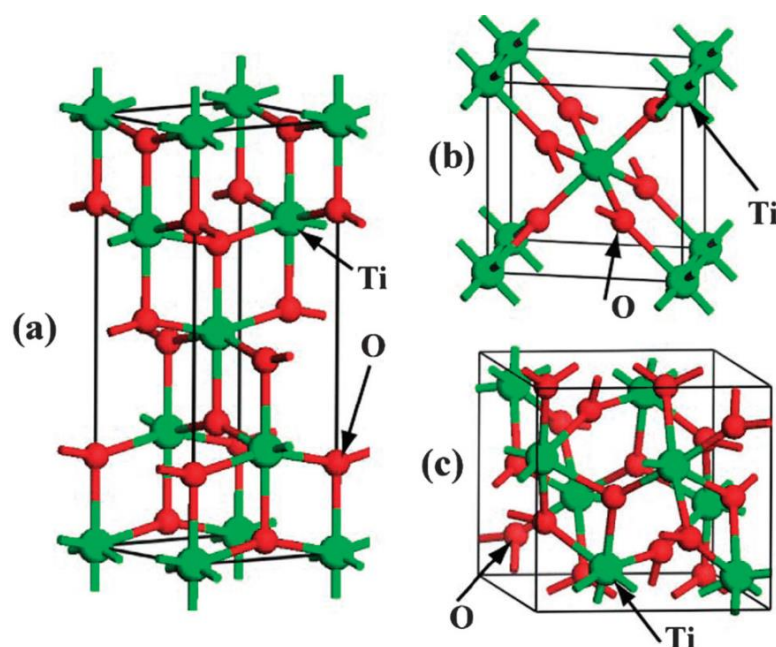
Figure 1-5. The schematic structures of TiO_2 polymorphs (a) anatase, (b) rutile, and (c) brookite [62]. Reproduced from Ref. [62], copyright (2014), with permission of Royal Society of Chemistry.

With a bandgap of ~3.2 eV, anatase TiO_2 is a semiconductor which absorbs light in the UV range ($\lambda < 387$ nm) [47]. When such a semiconductor absorbs photons with an energy equal to or higher than its bandgap energy, this light energy excites electrons from the filled valence band of the semiconductor to its conduction band (**Figure 1-6**).
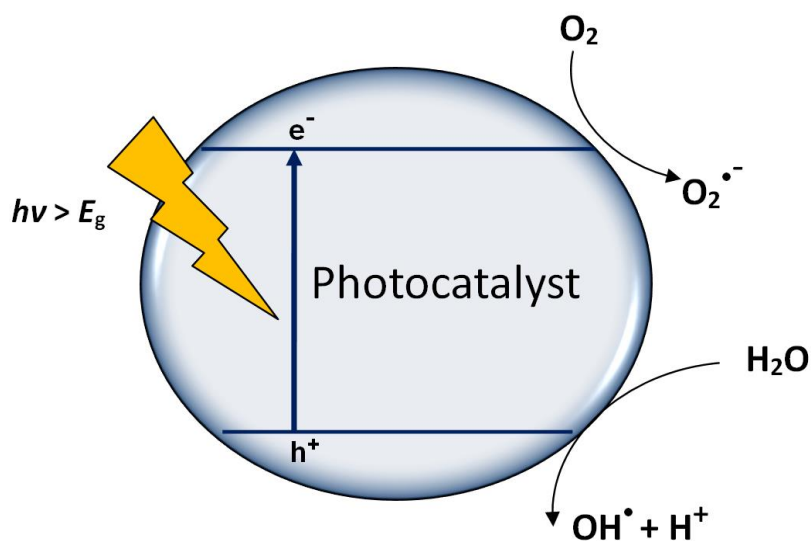
Figure 1-6. Schematic representation of photocatalyst excitation

Therefore, charge carriers or better to say, electrons in the conduction band (the reducing species) and positively charged holes in the valence band (the oxidizing species), will be generated (**Equation 1-1**) and will migrate to the surface of the semiconductor. In the presence of an organic molecule adsorbed on the surface of the photocatalyst (OM_s), an oxidation or a reduction reaction might occur. The oxidation reaction can proceed through two different mechanisms, namely, direct oxidation or indirect oxidation. In the direct oxidation, the photogenerated holes in the valence band (h_{VB}^+) are transferred directly to the adsorbed organic compound resulting in its direct oxidation (**Equation 1-2**). However, if the organic molecule is only weakly adsorbed at the photocatalyst surface, the indirect mechanism is more likely to take place. In this case, the valence band holes will be first transferred to water molecules adsorbed on the surface of the photocatalyst resulting in the formation of surface hydroxyl radicals ($^{\bullet}OH_s$) (**Equation 1-3**). These radicals can then react, still being adsorbed on the surface, with the organic molecule in the solution (OM) resulting in the formation of oxidation products (**Equation 1-4**). Another possibility is that the surface hydroxyl radicals will first be desorbed into the solution (**Equation 1-5**) and then react with the organic molecule as free hydroxyl radicals yielding oxidation products (**Equation 1-6**). It is worth mentioning that the hydroxyl radicals can also be formed through the reduction reaction in which the photogenerated conduction band electrons (e_{CB}^-) react with molecular oxygen (O_2) forming a superoxide radical ($O_2^{\bullet -}$) (**Equation 1-7**) and eventually hydrogen peroxide (H_2O_2) (**Equation 1-8** and **Equation 1-9**). After a further

reduction step, hydrogen peroxide will be converted to hydroxyl radicals (**Equation 1-10**). All these pathways are summarized in the following chemical equations [52,63]:

$$TiO_2 \xrightarrow{h\nu} e_{CB}^- + h_{VB}^+ \tag{1-1}$$

Direct oxidation pathway:

$$h_{VB}^+ + OM_s \rightarrow \text{Oxidation Products} \tag{1-2}$$

Indirect oxidation pathway:

$$h_{VB}^+ + H_2O \rightarrow {}^\bullet OH_s + H^+ \tag{1-3}$$

$${}^\bullet OH_s + OM \rightarrow \text{Oxidation Products} \tag{1-4}$$

$${}^\bullet OH_s \xrightarrow{desorption} {}^\bullet OH_{free} \tag{1-5}$$

$${}^\bullet OH_{free} + OM \rightarrow \text{Oxidation Products} \tag{1-6}$$

Reduction pathway:

$$e_{CB}^- + O_2 \rightarrow O_2^{\bullet -} \tag{1-7}$$

$$O_2^{\bullet -} + H^+ \rightarrow HO_2^\bullet \tag{1-8}$$

$$O_2^{\bullet -} + HO_2^\bullet + H_2O \rightarrow O_2 + H_2O_2 + OH^- \tag{1-9}$$

$$H_2O_2 + e_{CB}^- \rightarrow {}^\bullet OH + OH^- \tag{1-10}$$

For the photocatalytic degradation of organic compounds, each of these reactions has an important role in the overall process. The hydroxyl radical produced through the oxidation or the reduction reactions is the main oxidant, while the presence of molecular oxygen can inhibit the recombination of electron-hole pairs to some extent. Depending on the nature of the absorbed compound, different intermediates can be produced from its reaction with the hydroxyl radical, yielding eventually the degradation products, that is, water and carbon dioxide. In addition, the organic compound can also be directly oxidized by trapped holes [63–65]. The aforementioned equations are a simplified description of a photocatalytic reaction. However, the mechanism of the overall photocatalytic degradation of a real

organic pollutant mixture is a much more complicated process. This is due to the, *inter alia,* different possible reaction pathways, the formation of intermediates or by-products, and varying reaction steps depending on the nature of the degraded compound. It becomes even more complex when trying to determine the actual function of electrons, holes, free radicals and the surface chemistry in this system. Despite all the efforts which have been undertaken to understand the mechanism of photocatalysis, there are still several open questions in this field which have not been clarified until now [66,67].

For the transfer of the photoinduced electrons or holes to surface species, the quasi-Fermi levels of electrons and holes upon bandgap illumination of the semiconductor, the bandgap energy, the energetic positions of the valence band and the conduction band, respectively, as well as the redox potential of the adsorbates are the key factors to be considered. The energy level of the valence band indicates the hole oxidizing ability, while the conduction band energy level determines the electron reduction potential of the semiconductor [54].

To explain this from a thermodynamic standpoint, first the concept of Fermi level and quasi-Fermi levels have to be introduced. The Fermi level (E_F) is the electrochemical potential of the electrons in a semiconductor and is a measure of the free energy of electrons (see **Figure 1-7**). In an n-typed semiconductor such as TiO_2, the Fermi level is positioned below the conduction band edge (E_C) at thermodynamic equilibrium (**Figure 1-7(a)**) [68–70]. The higher the n-doping, the closer E_F will be to E_C [70]. Under illumination however, this equilibrium will not be held anymore. Since excess electrons and holes will be photogenerated upon bandgap excitation, the electron and hole densities will be enhanced to values above their equilibrium values. In this case, the electron and hole densities in the conduction and valence band of the semiconductor cannot be determined by the same Fermi level. Thus, for a semiconductor under illumination, a quasi-Fermi level for electrons ($*E_{Fn}$) and a quasi-Fermi level for holes ($*E_{Fp}$) are defined (shown in **Figure 1-7(b)**) [68,69].
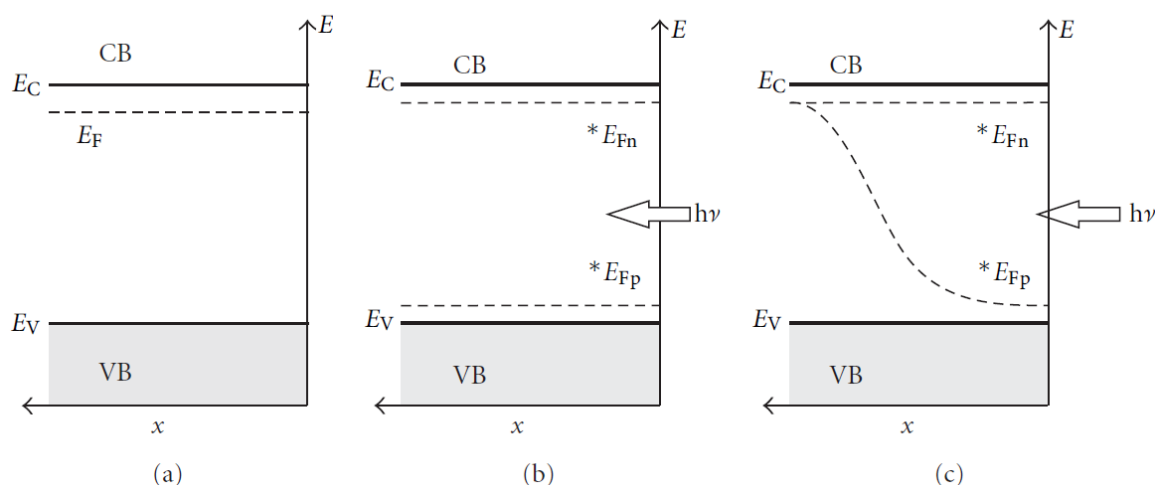
Figure 1-7. Fermi levels and quasi-Fermi levels of electrons and holes for an n-type semiconductor: (a) at thermodynamic equilibrium (in the dark); (b) and (c) under illumination; (c) local excitation; x is the distance from the semiconductor surface [68]. Reproduced with permission from ref. [68], copyright (2011).

In the case of n-type semiconductors, electrons are the majority carriers and holes are the minority carriers. Accordingly, upon illumination, the electron density does not change significantly and hence the quasi-Fermi level of electrons, $*E_{Fn}$, remains almost the same as Fermi level under equilibrium (E_F). On the contrary, the shift of the quasi-Fermi level of holes, $*E_{Fp}$, with respect to E_F is considerable, as the hole density might be increased by many orders of magnitude. Thus, $*E_{Fp}$ will be shifted downwards and to a position near to the valence band edge (E_V) of the semiconductor (**Figure 1-7(b)**) [68,69]. In many cases, due to the small light penetration depth, the electron-hole pairs are generated locally near the surface of the semiconductor. Therefore, $*E_{Fp}$ varies with the distance from the excited surface of the semiconductor (**Figure 1-7(c)**) [68,69].

The quasi-Fermi levels are of high importance regarding the reactions taking place at the semiconductor-adsorbate interface. In case of TiO_2, being a heavily-doped n-type semiconductor, the position of E_C, and $*E_{Fn}$, almost merge with each other. Thus, by determining the $*E_{Fn}$, the position of E_C and consequently that of the valence band, E_V, can be obtained. The latter can be easily calculated by adding the value of E_C to the value of bandgap energy (normally determined by optical or photoelectrochemical approaches) [68].

According to these explanations, upon bandgap illumination of the semiconductor, if the adsorbed organic molecule has a more negative redox potential than $*E_{Fp}$, the

photogenerated holes in the valence band of the semiconductor will be able to oxidize it. On the other hand, if the redox potential of the organic molecule is more positive than $*E_{Fn}$, the photogenerated electrons of the conduction band are capable of reducing the adsorbed molecule [71].

1.3.2. Visible light-active Photocatalysts

As described above, the potential to be activated by sunlight counts as an optimal characteristic of an ideal photocatalyst. Although TiO_2 is a very good candidate for photocatalytic reactions, with its relatively wide bandgap of about 3.2 eV, it is only able to absorb UV light with wavelengths up to maximum 387 nm [72]. Nevertheless, only a small fraction of the sunlight, ~3.5%, consists of UV light (λ: 200-400 nm) [73], while the visible light fraction (λ: 400-800 nm) contributes ~43 % [74]. Therefore, many attempts have been made to develop visible light-absorbing semiconductors to enhance the application of solar light in photocatalytic systems.

1.3.2.1. Ferrites

One of the semiconducting materials reported as visible-light active oxides are ferrites having the general formula of MFe_2O_4, with M being a metal ion. Most ferrites exhibit a spinel structure with oxide anions positioned in a cubic close-packed lattice and M and Fe cations occupying tetrahedral and/or octahedral sites [75]. Besides being chemically and thermally stable, and having a reasonable price, ferrites also benefit from their narrow bandgap (~1.9 eV) which allows them to absorb visible light with wavelengths up to 653 nm. These materials have already been studied for water splitting [75–79], for the reduction of carbon dioxide [80], artificial photosynthesis [75], and water treatment [81,82].

Among the spinel ferrites, zinc ferrites, $ZnFe_2O_4$, have been widely studied for their potential application in photocatalytic and photoelectrocatalytic processes. They exhibit a spinel structure (**Figure 1-8**), with Zn^{2+} and Fe^{3+} cations, occupying the tetrahedral and octahedral sites, respectively [78,83,84].
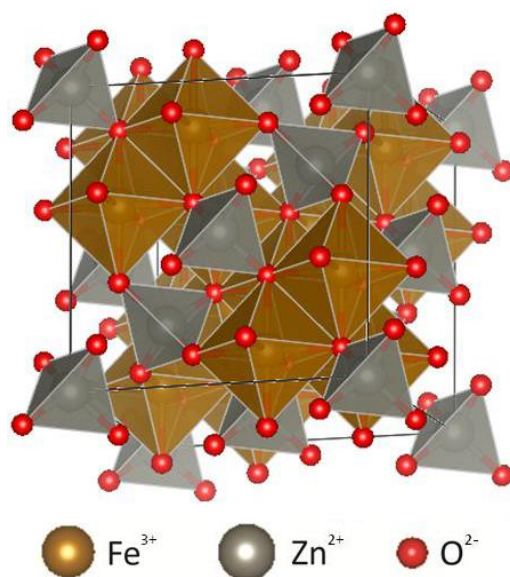
Figure 1-8. Crystallographic 3D structure of zinc ferrite with a normal spinel arrangement [85]. Reproduced from Ref [85].

Zinc ferrites can be prepared through various synthetic methods such as co-precipitation [86], sol-gel reactions [87,88], reflux procedures [89], hydrothermal processes [89], solid state reactions [90,91], polymer complex method [90,91], hybrid microwave annealing [76], *etc*. However, for the zinc ferrites prepared by different methods, also different photocatalytic activities have been reported [75,79]. These differences in photocatalytic activities are expected to result from the variation of properties such as the BET surface area [92], the crystalline size [75], the energetic bandgap position [93], and the degree of inversion [94,95].

Several reports are available regarding the evaluation of the photocatalytic activity of zinc ferrites [92,96–101]. Šutka *et al.* have investigated the effect of different excess iron contents in the structure of zinc ferrites ($ZnFe_{2+z}O_4$) prepared through a sol–gel auto-combustion method [92]. They have observed that by increasing the iron content (from $z = 0$ to $z = 0.15$), the energetic bandgap of the prepared samples decreased. Also, the photocatalytic activity was reduced from 40% to zero for the degradation of methylene blue after three hours visible light irradiation. This effect was contributed to the formation of Fe^{2+} species in the octahedral sites of the spinel structure acting as recombination centres [92].

In another study, Qiu *et al.* prepared zinc ferrite films through a sol-gel method followed by a calcination at four different temperatures and claimed that the absorption onset of these films were shifted to the visible region up to 540 nm (compared to TiO_2 films) [100]. These authors have investigated the photocatalytic conversion of methyl orange as a probe molecule irradiated by a xenon lamp in a wavelength range of 200 to 700 nm and have reported that the sample calcined at 450°C revealed the highest photocatalytic activity [100]. Sharma and Singhal synthesized zinc doped nickel ferrites with varying zinc to nickel ratios using a sol-gel method followed by annealing at 400 to 1000°C [101]. They reported an increased electrical resistivity as well as an increased photocatalytic activity for the degradation of methylene blue under visible light irradiation with increasing the zinc content in the structure. This was explained by the authors through the wider bandgap of nickel ferrite as compared to zinc ferrite [101].

1.3.2.2. KRONOClean 7000

Despite the efforts to develop new photocatalytic materials with activity in the visible range, TiO_2 still continues to be the most commonly used photocatalyst. Although, as mentioned above, TiO_2 is able to harvest only up to 3.5 % of the solar energy [73], its photocatalytic activity under UV irradiation is much higher than that of the materials with a strong absorption in the visible range, such as iron based photocatalysts [93,102]. Thus, another approach which can be considered other than replacing TiO_2 with new visible light active materials is to apply some strategies to increase its light absorption; for instance, doping of TiO_2 with metal or non-metal ions or modifying the TiO_2 surface by the deposition of sensitizers. Doping TiO_2 may result in a narrowing of the bandgap [103,104], while dye-sensitization of TiO_2 through its coupling with a strongly absorbing dye molecule enhances the overall visible light absorption of the photocatalyst [105]. The latter approach is widely applied not only in the field of dye sensitized solar cells [106], but also for photocatalysis [107,108].

One example of the application of this method is KRONOClean 7000 (from this point in the current study: K-7000), a commercially available photocatalyst developed by Kronos International Inc., prepared through the modification of TiO_2 with pentaerythritol [109]. This product was initially assumed to be a carbon-doped TiO_2, however, Ząbek *et al.* were able to exclude this possibility and showed that this photocatalyst (named as VLP by these

authors) actually consists of anatase particles with a carbon-based sensitizer layer covering their surface [109]. This could be convincingly shown since these authors removed the layer around the particles and separated it into a pale brown powder (SENS$_{ex}$) and an extracted colorless powder (VLP$_{res}$) which was washed several times to remove all organic and inorganic impurities. Afterwards, they could reconstruct it using some well-designed straightforward experiments. As shown in **Figure 1-9**, they could confirm that the sample after the reassembling process (VLP$_{reas}$) had identical photocatalytic properties as compared with the initial sample (VLP) [109].
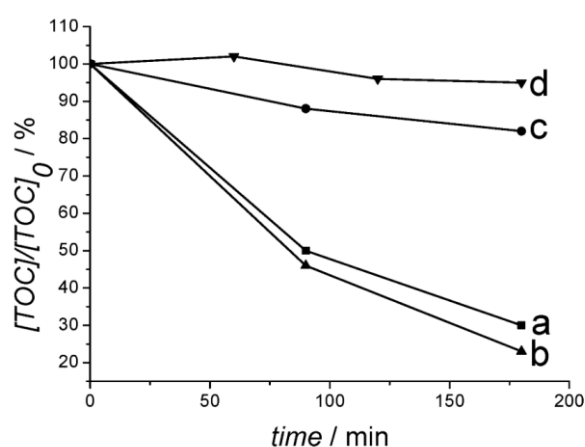
Figure 1-9. Photomineralization of 4-chlorophenol with visible light ($\lambda \geq 455$ nm) in the presence of (a) VLP, (b) VLP$_{reas}$, (c) VLP$_{res}$, and (d) SENS$_{ex}$, Suspensions [109]. Reproduced from Ref. [109], copyright (2009), with permission of Royal Society of Chemistry.

The activity of K-7000 was also compared with that of Evonik P25. K-7000 showed a better performance than P25 for the photocatalytic abatement of NO$_x$ under white light excitation [110] as well as for the degradation of acetone under visible light irradiation [111]; confirming that the carbon-based sensitizer layer could enhance the visible light absorption of this photocatalyst. Nevertheless, understanding the underlying mechanism of the extended visible light response of TiO$_2$ and its enhanced visible light activity is of great importance. Thus, in the current work, this issue will be discussed in more detail in **Chapter 4**.

1.4. Model Compounds

An important issue regarding the evaluation of the activity of a photocatalyst is the choice of a proper model compound. Organic dye molecules are most commonly chosen as probe

compounds for the analysis of the photocatalytic activity of photocatalysts, due to the possibility of an uncomplicated determination of the dye concentration *via* spectrophotometric methods.

1.4.1. Methylene Blue

Methylene blue (from this point in the current study: MB) is the first member of the phenothiazine antipsychotic drugs. This blue colored dye ($\varepsilon_{660} = 10^5$ $dm^3 \cdot mol^{-1} \cdot cm^{-1}$) has λ_{max} values at 660, 614 and 292 nm [112]. The degradation of MB has been introduced by the international standard organization (ISO) as a reference method from which the self-cleaning photocatalytic activity of surfaces in aqueous medium can be determined [113]. Thus, this dye is one of the most popular organic dyes chosen as a model pollutant in photocatalytic investigations [114–121].

Owing to its high molar absorptivity, this dye only requires small concentration changes to convert its color from blue to pale or colorless upon photocatalytic-oxidation and this change can be readily monitored and followed. Moreover, it is also possible to simply analyze the photobleaching rate of the dye *via* spectrophotometric methods [34].

However, it is worth mentioning that a dye molecule in principle might not be a good option for the evaluation of the photocatalytic activity of a photocatalyst. As simple as it might be assumed, an irradiated suspension containing a dye molecule together with a photocatalyst can be a complicated system. Often, the dye molecule might undergo a photocatalytic reduction reaction leading to its bleaching as discussed for MB by Mills *et al.* [112]. It should be considered that the doubly reduced form of MB (LMB, $\lambda_{max} = 256$ nm) is colorless and stable in de-aerated aqueous solutions [122]. However, the singly reduced form of MB (MB$^{\bullet-}$, $\lambda_{max} = 420$ nm) is pale yellow and can disproportionate to form MB and LMB according to the following equation [112]:

$$2\ MB^{\bullet-} \rightarrow MB + LMB \tag{1-11}$$

The oxidized form of MB (MB$^{\bullet+}$, $\lambda_{max} = 520$ nm) can be easily reduced back to MB in acidic media [123], while in slightly alkaline (pH 9.1) solutions, it decomposes irreversibly [124]. According to Mills *et al.*, MB can be completely mineralized photocatalytically upon ultra-band gap irradiation under oxygen-saturated conditions as following [112]:

$$\underbrace{C_{16}H_{18}N_3SCl}_{(MB)} + 25\frac{1}{2}O_2 \xrightarrow{\text{TiO}_2(hv \gg 3.2\ eV)}$$

$$HCl + H_2SO_4 + 3HNO_3 + 16CO_2 + 6H_2O \hspace{2cm} (1\text{-}12)$$
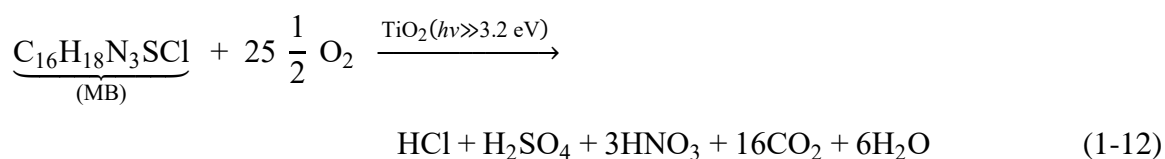
This reaction results into the bleaching of MB and is an irreversible process.

On the other hand, under anaerobic conditions, MB will be reduced to LMB upon irradiation in the presence of TiO_2 and a sacrificial electron acceptor (SED) [112]:

$$MB + SED \xrightarrow{\text{TiO}_2\ (hv \gg 3.2\ eV)} LMB + SED^{2+} + 2\ e^- \hspace{2cm} (1\text{-}13)$$
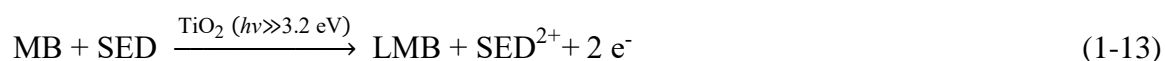
Thus, also here, a bleaching effect will be observed which is in this case due to the colorless LMB. However, this reaction can be reversed by addition of O_2 to the anaerobic system, which results into oxidation of LMB back to MB [112].

Since these two reactions both give the same superficial result, namely, bleaching of the MB dye over ultra-band gap irradiation of TiO_2, in many cases, they are mistaken with each other. Hence, the initially observed photobleaching of the dye does not necessarily prove its mineralization. This misinterpretation most often happens when the reaction conditions favor the formation of LMB. These conditions include for instance, a low, easily depleted dissolved oxygen level or a low pH value [112].

In some cases, upon visible light irradiation the dye molecule is able to absorb the incoming light itself resulting into its photobleaching which is usually mistaken with its photocatalytic degradation [125].

As reported by Zhao *et al.*, in case of having a dye molecule sensitized on the surface of a semiconducting material, the sensitized photocatalytic reaction can be explained as following [126]. After excitation of the dye (Dye*) under visible light illumination, the electrons generated in the LUMO of the dye are likely to be transferred to the conduction band of the semiconductor (illustrated in **Figure 1-10**). Thus, in the presence of an electron acceptor such as molecular oxygen, the conduction band electrons can reduce molecular oxygen yielding $O_2^{\bullet-}$. The remained free radical cation of the dye (Dye$^{\bullet+}$) is able to react further. For example in an aqueous solution, Dye$^{\bullet+}$ can oxidize water to hydroxyl radicals.
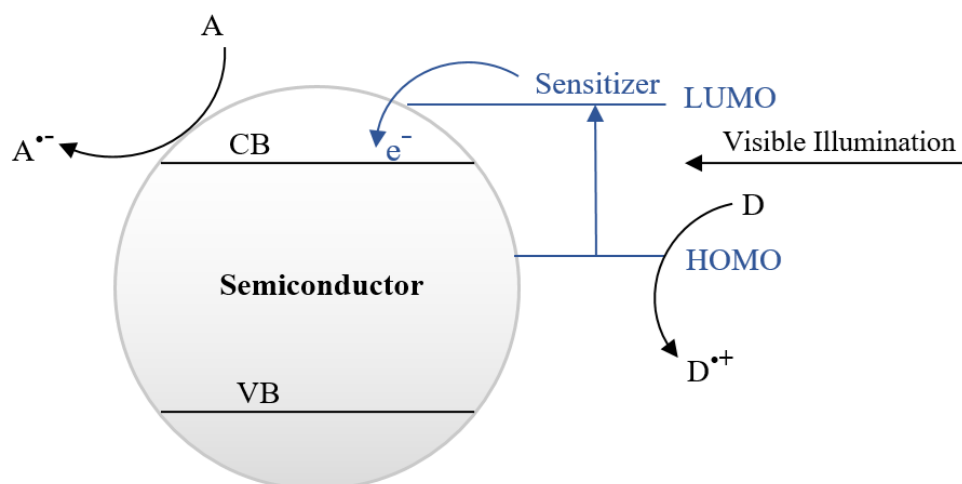
Figure 1-10. Proposed mechanism for visible-light-induced dye-sensitized photocatalysis

In the current work, this aspect is investigated in detail in terms of evaluation of the photocatalytic activity of different self-prepared zinc ferrites using MB as a model compound (**Chapter 2**).

1.4.2. Chlorpromazine

Another member of the phenothiazine antipsychotics is chlorpromazine. The early worry concerning its photochemistry originated from the frequently noticed strong skin rashes being observed for patients who were treated with high dosages of this medication [127]. Under UV irradiation, this compound was found to be transformed into its metabolites *via* ring hydroxylation, demethylation on the N-chain, or sulfur or nitrogen oxidation [41,128]. As determined by Bahnemann *et al.*, in aqueous solution, chlorpromazine has an absorption maximum at 305 nm ($\varepsilon = 4500 \ \mathrm{mol^{-1} \cdot dm^3 \cdot cm^{-1}}$) [37] thus it can be excited by UV irradiation yielding its excited singlet state which converts into its triplet state [129]. Chlorpromazine can then either fragment to form radicals or photo-ionize to form radical cations and electrons (**Figure 1-11**) as proposed by Kochevar [130].
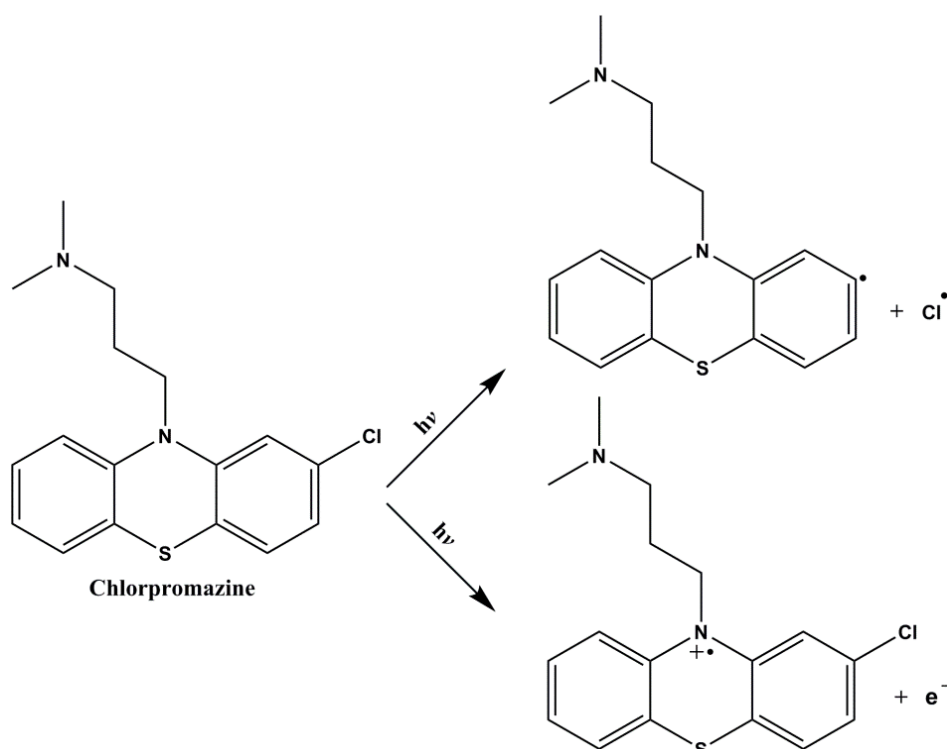
Figure 1-11. Proposed pathways for the photodegradation of chlorpromazine under UV irradiation [130]

As shown in **Figure 1-11**, photoionization of a chlorpromazine (CPZ) molecule results into the formation of a chlorpromazine radical cation ($CPZ^{\bullet+}$) and an electron (**Equation 1-14**). In an aqueous solution, the released electron can react further with water (**Equation 1-15**), yielding a hydrated electron (e_{aq}^-). This hydrated electron is an active reductant species.

$$CPZ \xrightarrow{h\nu} CPZ^{\bullet+} + e^- \tag{1-14}$$

$$e^- + H_2O \rightarrow e_{aq}^- \tag{1-15}$$

As reported by Davies *et al.* [131], in the absence of molecular oxygen, this e_{aq}^- can be added into the aromatic system of chlorpromazine, possibly yielding a short-living radical anion (**Equation 1-16**) and remove the chloride ion by the end of the reaction (**Equation 1-17**).

$$CPZ + e_{aq}^- \longrightarrow CPZ^{\bullet-} \tag{1-16}$$

$$CPZ^{\bullet-} \longrightarrow PZ^{\bullet} + Cl^- \qquad\qquad (1\text{-}17)$$

The promazine radical which is produced simultaneously can react with another chlorpromazine molecule to produce a cyclohexadienyl type radical [131].

In a study on the free radical induced one-electron oxidation of phenothiazines, Bahnemann *et al.* [37], also investigated the reduction of chlorpromazine by hydrated electrons through pulse radiolysis experiments. The characteristic optical absorption of the e_{aq}^- ($\lambda_{max} = 720$ nm) was observed to decay exponentially with the half-lives inversely proportional to the chlorpromazine concentrations. In another study, Bahnemann *et al.* [132], were able to derive the one-electron redox potentials of phenothiazine radical cations by pulse radiolysis. According to their studies with $I_2^{\bullet}$ and chlorpromazine, these authors estimated the redox potential of the $CPZ^{2+\bullet}/CPZ^+$ couple and determined an upper limit of $\Delta E^{\circ} = E^{\circ}(CPZ^{2+\bullet}/ CPZ^+) - E^{\circ}(I_2^{\bullet} / 2I^-) \leq -0.19$ V which agreed well with the calculated $\Delta E^{\circ} = -0.22$ V value, taking $E^{\circ}(CPZ^{2+\bullet}/ CPZ^+) = +0.78$ V and $E^{\circ}(I_2^{\bullet} / 2I^-) = +1.0$ V. These authors suggested that bases on the measured absolute rate constants for the reaction of phenothiazine and its related radical cations (including chlorpromazine radical cation) with ascorbate and α-tocopherol, electron transfer equilibria are likely to exist also with other phenothiazine cations and strongly reducing compounds [132].

As mentioned before, besides the formation of electrons through photoionization of chlorpromazine, also a radical cation intermediate will be produced (**Equation 1-14**). According to Ateş and Somer [133], regarding the photo-degradation of chlorpromazine under UV(A) irradiation, most of the radical intermediates formed during the oxidation such as its excited singlet and triplet states are unstable, while its radical cation ($CPZ^{\bullet+}$, $\lambda_{max} = 530$ and 275 nm) which is a colored free radical intermediate (red) could be identified in aqueous solutions at pH values of 1.5-6.5. This radical intermediates is known as the chlorpromazine radical cation [133]. As reported by Felmeister and Discher several resonance forms of the chlorpromazine free radical cation (**Figure 1-12**) may be envisioned [134]. However, Borg and Cotzias were able to rule out important contributions of the resonance form (b) through electron spin resonance (ESR) evaluations [135].
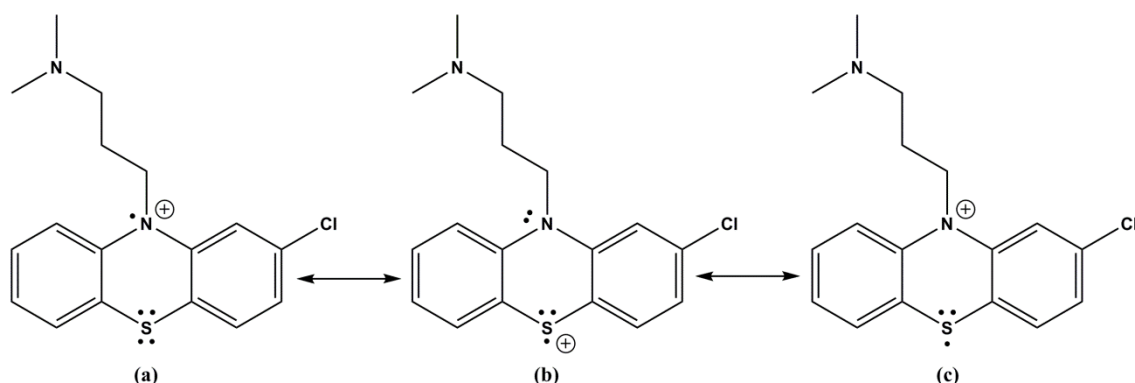
Figure 1-12. Resonance forms of chlorpromazine free radical of chlorpromazine; adapted from Ref. [134], copyright (1964), with permission from Elsevier.

Merkle and Discher performed an electrochemical investigation to elucidate the oxidation mechanism of chlorpromazine hydrochloride in aqueous media [136]. They proposed that in dilute aqueous acidic solution (1 N sulfuric acid), chlorpromazine undergoes a single-electron oxidation reaction to form the red chlorpromazine free radical intermediate ($CPZ^{\bullet+}$). This radical intermediate is unstable and disproportionates rapidly to form chlorpromazine (CPZ, colorless) and chlorpromazine sulfoxide (CPZ-O, colorless). The overall reaction taking place in dilute aqueous acidic media can be represented as following [136]:

$$2\ CPZ \xrightarrow{\text{1 N sulfuric acid (+0.70 V. }\textit{vs.}\text{ SCE)}} \underbrace{2CPZ^{\bullet+}}_{} + 2e^- \tag{1-18}$$

$$CPZ \xleftarrow{\text{Spontaneous}} CPZ\text{-}O$$
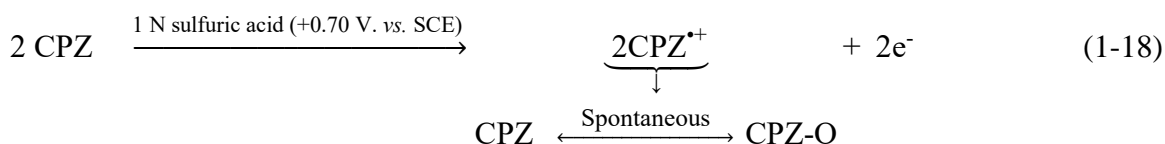
However, by using a 9 N sulfuric acid aqueous solution as the supporting electrolyte, these authors were able to confirm the occurrence of two separate one-electron oxidation steps as well as a one-electron reduction step. They could isolate a one-electron oxidation step by electrolysis at a potential of +0.50 V. *vs.* SCE [136]:

$$CPZ \xrightarrow{\text{9 N sulfuric acid (+0.50 V. }\textit{vs.}\text{ SCE)}} CPZ^{\bullet+} + e^- \tag{1-19}$$

It was shown that under these conditions, the free radical intermediate stabilizes. Thus, depending on the selected oxidation potentials it was possible to selectively either oxidize or reduce this free radical. The oxidation of $CPZ^{\bullet+}$ *via* a further one-electron step resulted into the formation of chlorpromazine sulfoxide (**Equation 1-20**), while the complete

reduction of $CPZ^{\bullet+}$ yielding chlorpromazine was also possible at lower potentials *via* a one-electron reduction step (**Equation 1-21**) [136].

$$CPZ^{\bullet+} \longrightarrow CPZ\text{-}O + e^- \tag{1-20}$$

$$CPZ^{\bullet+} + e^- \longrightarrow CPZ \tag{1-21}$$
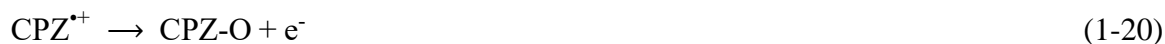
Nevertheless, the kinetic data obtained by Cheng *et al.* [137] for the decomposition of the chlorpromazine radical in aqueous buffers in the pH range between 2 and 7, using electrochemical and spectrophotometric measurements were inconsistent with a mechanism involving a disproportionation of the free radical cation. As an alternative, based on their kinetic data, these authors suggested that a cation radical/buffer adduct will be formed (**Equation 1-22**) which will be further oxidized by another chlorpromazine radical cation (**Equation 1-23**), leading eventually to its rearrangement to the sulfoxide metabolite (**Equation 1-24**). According to these observations, the mechanism of the hydrolysis of $CPZ^{\bullet+}$ in aqueous buffers was represented by the following equations in which RCO_2^- refers to a representative buffer constituent [137]:

$$CPZ^{\bullet+} + RCO_2^- + H_2O \leftrightarrows [CPZ(RCO_2)(OH)]^{\bullet-} + H^+ \tag{1-22}$$

$$[CPZ(RCO_2)(OH)]^{\bullet-} + CPZ^{\bullet+} \leftrightarrows CPZ + [CPZ(RCO_2)(OH)] \tag{1-23}$$

$$[CPZ(RCO_2)(OH)] \longrightarrow CPZ\text{-}O + RCO_2H \tag{1-24}$$

These observations rather indicated a direct reaction of the formed radical cation either with the buffer elements or with water [137].

Chlorpromazine sulfoxide (**Figure 1-13**) has been reported to be the ultimate photo-oxidation product of chlorpromazine [136–139].
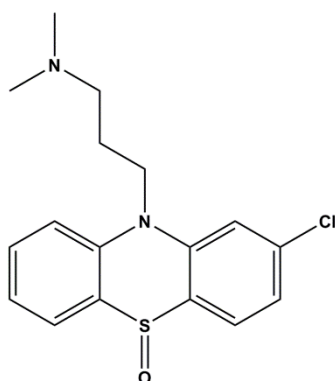
Figure 1-13. Chemical structure of chlorpromazine sulfoxide

Iwaoka and Kondo performed a mechanistic study regarding the photo-oxidation of chlorpromazine in water and ethanol employing both, a steady light photo-oxidation method as well as transient absorption spectroscopy [139]. According to their findings, the sulfoxide metabolite is formed *via* the chlorpromazine radical cation and the presence of dissolved molecular oxygen is essential for the formation of this radical cation as well as the chlorpromazine sulfoxide. They concluded that the oxygen atom in the sulfoxide structure originates from molecular oxygen and not from water [139]. According to Davies and Navaratnam, following the photochemistry of chlorpromazine transformation is much easier in solvents such as propan-2-ol rather than in aqueous solutions [140]. They were able to show that in the absence of molecular oxygen, the excited chlorpromazine is subjected to a C-Cl bond splitting by which a free promazine radical (PZ$^\bullet$) is formed as follows:

$$CPZ \quad \xrightarrow{\textit{hv}, \text{ anaerobic}} \quad PZ^\bullet + Cl^\bullet \tag{1-25}$$

These radicals can react with the solvent yielding products such as promazine, isopropoxypromazine, HCl, and acetone. On the other hand, in an oxygen-saturated solution, the excited chlorpromazine is quenched by molecular oxygen to form singlet oxygen [140]. In another work, Motten *et al.* applied the spin trapping technique and investigated the fate of the light-induced free radical intermediates formed during the photolysis of chlorpromazine at 330 nm [138]. They presented evidence for three main photoreactions of chlorpromazine: (I) dechlorination of chlorpromazine to form a radical, (II) direct reaction of chlorpromazine with molecular oxygen and formation of the

corresponding sulfoxide, and (III) photoelectron ejection (only when excited into the second excited singlet state, $\lambda < 280$ nm) [138].

In general, the photo-degradation pathway of chlorpromazine appears to be strongly dependent on the reaction medium. In the absence of molecular oxygen, the light induced products of the chlorpromazine transformation are different from those formed in the presence of O_2 [19]. Under UV irradiation of an aerated aqueous solution of chlorpromazine, the corresponding sulfoxide is reported to be the main photo-product [134,139,141], while no evidence for its formation is found in the absence of O_2. According to Huang and Sands, in a deoxygenated atmosphere, chlorpromazine photolysis under UV light leads to the formation of its dimers or polymers. They suggested that after the cleavage of the C-Cl bond, radicals are formed which promote the dimerization or polymerization processes (**Figure 1-14**) [127].
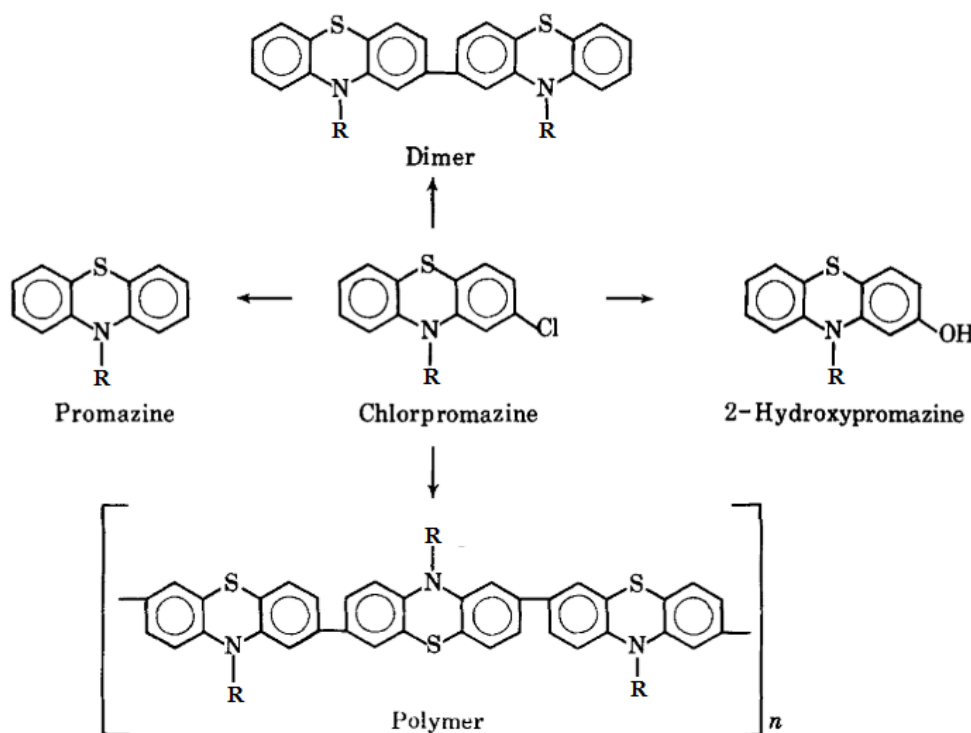
Figure 1-14. Proposed structures of UV light-induced reaction products of chlorpromazine under anaerobic conditions [127]; Adapted from Ref. [127], Copyright (1967), with permission from Elsevier.

A similar behavior under anaerobic conditions has also been observed by Davies and Navaratnam [140]. It was moreover reported by Grant and Greene that the solar photolytic

conversion of chlorpromazine under anaerobic conditions results in its conversion to promazine and 2-hydroxypromazine within minutes [142].

1.5. Analytical Methods

1.5.1. High performance liquid chromatography (HPLC-MS)

Other than the unstable free radical intermediates, some relatively stable intermediates are also formed during the photolysis of chlorpromazine. These are usually metabolites of the parent compound with some differences in their functional groups. These species are commonly detected through liquid chromatographic methods and identified *via* mass spectroscopic measurements. High performance liquid chromatography (HPLC)-based methods have been long employed in the pharmaceutical industries to detect the different metabolites of specific materials [143,144]. In this technique, complex mixtures are initially separated into individual components through a column filled with an adsorbent material. Then a detector (such as a UV-Vis detector in case of light absorbing compounds) generates signals proportional to the amount of the emerging sample components. Thus, an output chromatogram is obtained in which each peak is associated with a specific component based on its retention time (the time at which the component emerges from the column) [145,146].

Boehme and Strobel have employed HPLC method to study the in vitro metabolism of chlorpromazine and were able to detect chlorpromazine and five of its metabolites at 254 nm [147]. Nałecz-Jawecki *et al.* have investigated the photo-degradation of chlorpromazine under UV(A) and visible light irradiation using HPLC analysis. They have reported that after 7 days of irradiation with visible light, only 25% of the chlorpromazine concentration was decreased, while upon UV(A) irradiation, it was completely converted in a few hours. During the experiments performed under visible light irradiation, at least two photoproducts were detected, one of which also appeared as an unstable intermediate after 2 h of UV(A) irradiation [36].

In another study performed by Chagonda and Millership, the ability of the HPLC technique to qualitatively analyze chlorpromazine and its degradation products was evaluated. By utilizing reversed-phase chromatography with selective fluorescence detection and internal calibration techniques, chlorpromazine and two of its metabolites, namely, chlorpromazine

sulfoxide and chlorpromazine sulfone were successfully identified. This method showed fluorescence selectivity for chlorpromazine sulfoxide and chlorpromazine sulfone (**Figure 1-15**) at 385 nm, since the corresponding signals of these two products at 385 nm did not interfere with that of chlorpromazine [148].
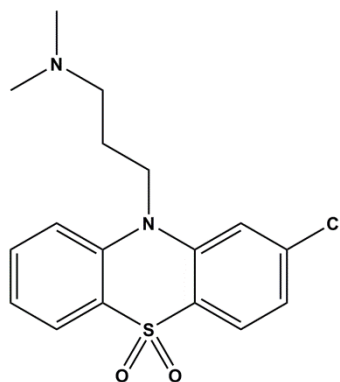
Figure 1-15. Chemical structure of chlorpromazine sulfone

A drawback of the HPLC method is that, to estimate the components of a mixture, the retention times of all desired components are needed to be known. However, based on the type of column, mobile phase, temperature, *etc.*, the retention time might be varying between different measurements. Therefore, a precise determination of the components is rather unlikely, especially for mixtures containing unknown components.

An alternative analytical method through which the elemental composition of the molecular structure of an analyte can be determined is mass spectroscopy (MS) [149]. In mass spectroscopy, the mass of the elemental isotopes is the focus of the measurement, rather than the elements atomic mass (the average weight of the naturally occurring stable isotopes of an element). Thus, in this method, the mass-to-charge ratio (m/z) of ions is determined. This value is defined as "the mass of the ion on the atomic scale divided by the number of charges that the ion possesses" [149]. In a mass analyzer, for the fragmentation, separation and detection of ions according to their individual m/z ratios, solid, liquid, or gases have to be ionized and the ions have to be in the gas phase before the separation. Once the desired atom or molecule is ionized in the gas phase, the MS technique can be employed to verify its accurate atomic or molecular weight [149,150].

The combination of liquid chromatography and mass spectroscopy, developed as the HPLC-MS method, has become a useful tool for the analysis and characterization of

pharmaceuticals and their metabolites [143,144]. Utilizing the MS technique together with HPLC measurements facilitates the analytical processes; since in addition to the separation process, the components will be fragmented and identified based on the distribution of the fragmental m/z ratios [151].

The HPLC-MS technique was employed by Kigondu *et al.* to analyze the antimycobacterial activities of chlorpromazine and its metabolites alone and in combination with antitubercular drugs in which chlorpromazine metabolites with m/z values of 335, 351, 305, and 321 were successfully identified [152]. In another study, Alexandru *et al.* carried out an investigation regarding the photoproducts of chlorpromazine in aqueous solution after exposure to a UV laser beam (266 nm). Utilizing the HPLC-MS method, they were able to identify chlorpromazine metabolites with m/z values of 285, 292, 301, 308, 317, and 335 [153].

Trautwein and Kümmerer have also applied high performance liquid chromatography coupled with multiple stage-mass spectrometry (HPLC–MS^{n}) for the evaluation of chlorpromazine and its metabolites over abiotic photolysis under illumination by a xenon arc lamp simulating the natural sunlight (300–800 nm). They were able to identify three main metabolites of chlorpromazine over its photolytic process having approximate m/z values of 301, 317 and 335 (**Figure 1-16**) and have reported the complete elimination of chlorpromazine after 4 h of illumination by the xenon lamp [41].
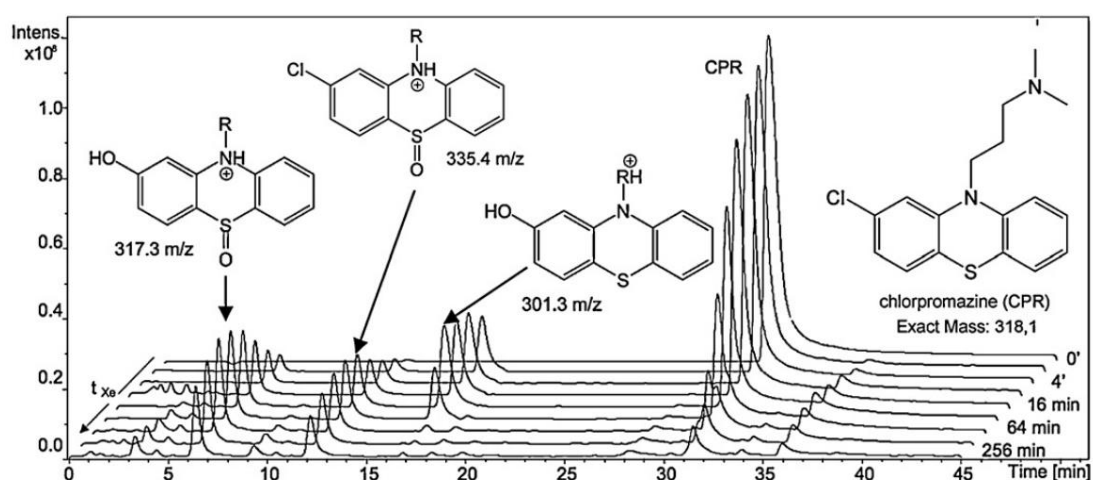
Figure 1-16. Total ion currents (TICs) of samples taken during the course of the photodegradation test and structures of chlorpromazine and its three main photolysis products; t_{Xe} = irradiation time with xenon lamp [41]. Reprinted from Ref. [41] Copyright (2012), with permission from Elsevier.

1.5.2. Laser Flash Photolysis Spectroscopy

In order to gain a better insight into the fundamental processes of a photocatalytic reaction, laser flash photolysis spectroscopy can be applied. This technique is a viable method to detect, for example photogenerated charge carriers in photocatalysts and to analyze their recombination pattern [64,154,155].

This method proceeds through the bandgap excitation of the photocatalyst by a pulsed laser leading to the formation of photogenerated electron-hole pairs (**Equation 1-26**) [52]. These are active species which are in charge of the photocatalytic activity of the photocatalyst [156,157]. The life-time of the photogenerated electron-hole pairs as well as their decays can be determined based on the analysis of their respective transient absorption signals [156–159].

$$\text{Photocatalyst} + h\nu \longrightarrow \text{Photocatalyst} (e^-_{CB} + h^+_{VB}) \tag{1-26}$$
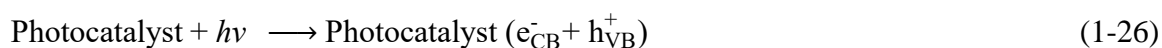
The electrons and holes generated within the short light pulse might either recombine directly in the bulk [160,161] or migrate to the surface of the photocatalyst and get rapidly trapped in the photocatalysts subsurface/surface states [64,162].

Bahnemann *et al.* have found experimental evidence revealing that in TiO_2 a short and a long wavelength transient absorption signal can be correlated to the absorption of trapped holes and trapped electrons, respectively [163,164]. These authors were able to observe a broad transient absorption spectrum between 400 nm to 800 nm, right after the laser pulse excitation of TiO_2 at $\leq$ 390 nm [163].

At around 650 nm, the trapped electron reveals a transient absorption signal, while the absorption of trapped hole is centered at shorter wavelengths (around 430 nm) [53]. The values of extinction coefficient for the electrons in TiO_2 is reported to vary between ε = 800-2600 $M^{-1} \cdot cm^{-1}$ (in the region of 700–800 nm) [165–167]. These values depend significantly on the electrolyte, the conditions and the material preparation methods. The extinction coefficient of holes in TiO_2 is estimated to be ε = 2930 $M^{-1} \cdot cm^{-1}$ (at 460 nm) [168].

In a recent review article, Schneider *et al.* have summarized the respective reports from various laboratories to correlate the observed transient absorption signals in TiO_2 with the assigned charge carriers. These authors have concluded that the photogenerated trapped electrons are mostly observed at wavelengths between 620 to 800 nm, while the photogenerated trapped holes correspond to signals at around 400 to 550 nm (as shown in **Figure 1-17**) [169].
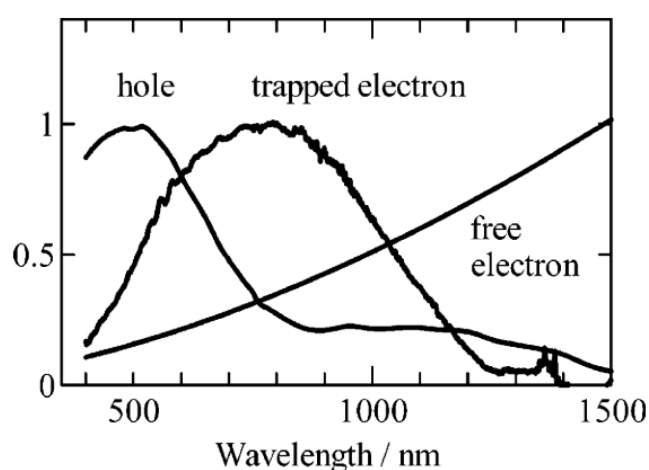
Figure 1-17. Transient absorption spectra of photo-generated electrons and holes in TiO_2 [170]. Adapted with permission from Ref [170], Copyright (2004), American Chemical Society.

Although the process of electron or hole trapping is extremely fast, the lifetime of the these trapped charge carriers might be rather long [171–173]. For instance, the trapping of conduction band electrons has been reported by Serpone *et al.* to occur in less than 20 ps, whereas, the valence band holes trapping process has been found to be much slower (in the ns scale) [155].

In order to study the role of photo-generated electrons or photogenerated holes individually, electron or hole scavenger molecules can be employed. These molecules are able to react selectively with either the electron or the hole, resulting in a slower charge carrier recombination. Molecular oxygen is commonly used as an electron scavenger and methanol is employed as a typical hole scavenger, while nitrogen or argon atmospheres are considered as inert standard or reference conditions [64,163,169,170,174].

For instance, to detect the photogenerated electrons in TiO_2, the oxidation reaction between methanol (as a hole scavenger), and the photogenerated holes on the surface of TiO_2 can be monitored (**Equation 1-27**) [175].

$$CH_3OH + h^+(TiO_2) \rightarrow {}^{\bullet}CH_2OH + H^+ \tag{1-27}$$

In the presence of methanol, it will react quickly with the photogenerated holes, and hence, the recombination of electrons and holes will be prevented. Thus, the photogenerated electrons will remain in the TiO_2 particles and result in a blue coloration in the TiO_2 powder. In this case, an initial decay in the transient absorption signal can be correlated with the reaction of methanol with the trapped holes, while a long-lived absorption could represent deeply trapped electrons. Accordingly, an observed difference between the transient absorption spectra measured in an inert atmosphere and those measured in the presence of methanol can be contributed to the trapped electrons.

The produced α-hydroxy radical (${}^{\bullet}CH_2OH$) can react further by injecting an electron into the conduction band of TiO_2 (**Equation 1-28**). This effect is known as the current doubling effect in which two electrons are formed by absorption of only one photon.

$$^{\bullet}CH_2OH \rightarrow e_{CB}^- + CH_2O + H^+ \tag{1-28}$$

Laser flash photolysis spectroscopy is also a strong tool to evaluate the photocatalytic activity of newly designed semiconductors. In this regard, Schneider *et al.* have employed this technique to investigate the improved photocatalytic activity of barium tantalate composites and compared it to that of pure tantalate and TiO_2 [176]. These authors were able to show that in the tantalate composite, due to the possibility for the electron to be stored in the system and the injection of an electron into the composite material by a ${}^{\bullet}CH_2OH$ radical, the electrons can be available for a longer period resulting in an extended reduction capability of the composite system [176].
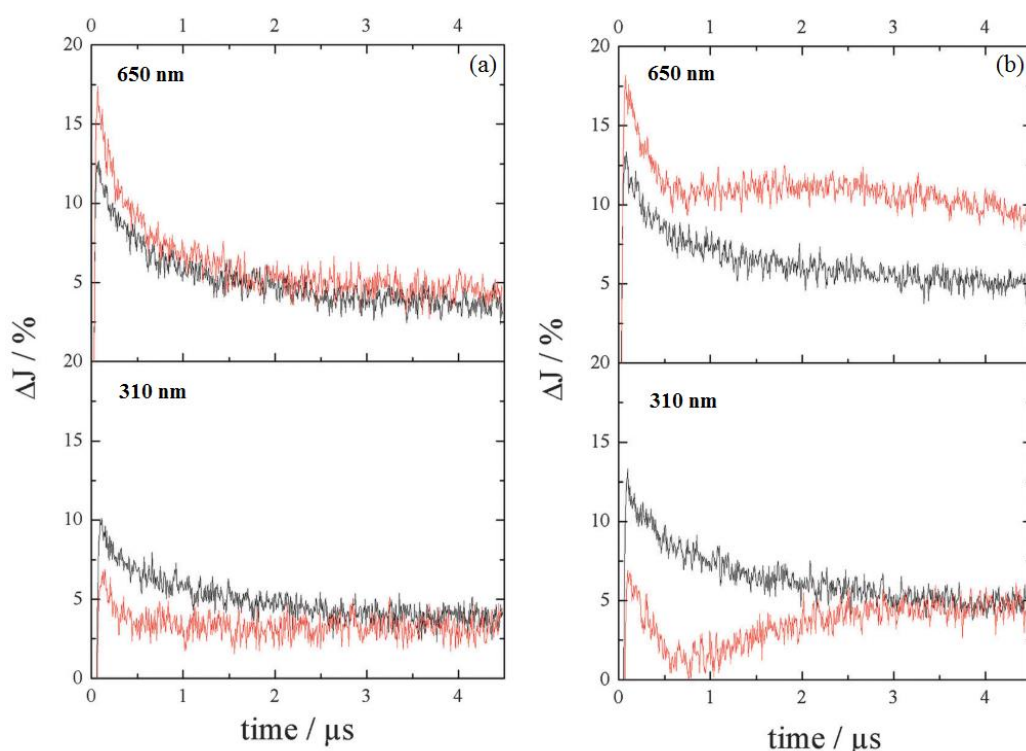
Figure 1-18. Transient absorption *vs.* time curves of (a) phase-pure $Ba_5Ta_4O_{15}$ and (b) $Ba_5Ta_4O_{15}$–$Ba_3Ta_5O_{15}$ composite powders, in a N_2 (black) and a N_2–methanol (red) atmosphere, $\lambda_{ex} = 248$ nm, observed at 650 nm and 310 nm [176]. Adapted from Ref. [176], copyright (2016), with permission from the PCCP Owner Societies.

As can be seen by comparing the transient absorption decays at 650 nm and 310 nm for pure barium tantalate, in the presence of methanol (red line in **Figure 1-18(a)**) the decay at 310 nm shows a shorter life time compared to that in the inert atmosphere (black line). This effect confirms the reaction of methanol with trapped holes which results in a fast decay of the transient absorption signal [176]. On the other hand, in the composite powders the transient absorption decay at 650 nm considerably changes in the presence of methanol (red line in **Figure 1-18(b)**), being always much higher than the signal measured in the inert atmosphere (black line). Also here, the rapid decay of the transient absorption observed at 310 nm correlates with the reaction of the trapped holes with methanol. Thus, it could be observed that in contrast to the phase pure barium tantalate (**Figure 1-18(a)** at 650 nm) (in which the lifetime of electrons was only slightly decreased), in the composite powder the charge carrier recombination in the presence of methanol could be sufficiently reduced [176]. In another study performed by Nie *et al.*, visible light photocatalytic activity of Au-modified anatase TiO_2 for hydrogen evolution was investigated using laser flash photolysis

spectroscopy. The authors have provided experimental evidence revealing that bare anatase TiO$_2$ can be excited by visible irradiation (420 nm laser light) and that the excited-state electrons can migrate to the Au nanoparticles loaded on the surface of the photocatalyst [177]. The same technique was utilized by Lim *et al.*, to evaluate the improvement of visible light activity of TiO$_2$ for the activation of Peroxymonosulfate (PMS), through sensitization of amino acids on the photocatalyst surface and to demonstrate the visible light-induced charge transfer characteristics of the amino acid-TiO$_2$ complexes [178]. Considering that both, PMS and amino acids are unable to absorb visible light, it was proposed by the authors that the formation of charge-transfer complexes resulting from the adsorption of amino acids on the surface of TiO$_2$ leads to a visible light absorption at wavelengths higher than 420 nm. By means of the data obtained with time-resolved laser spectroscopic measurements, they proposed that the ligand-to-metal charge transfer between the surface sensitizers and TiO$_2$ is responsible for the visible light activity [178].

Transient absorption spectroscopy can also be applied to monitor the photochemistry of complex molecules such as phenothiazine and its derivatives and the mechanism of their photoionization. For instance, this technique has been applied by Iwaoka and Kondo to investigate the photoionization of chlorpromazine hydrochloride in mixed solvent systems [179].
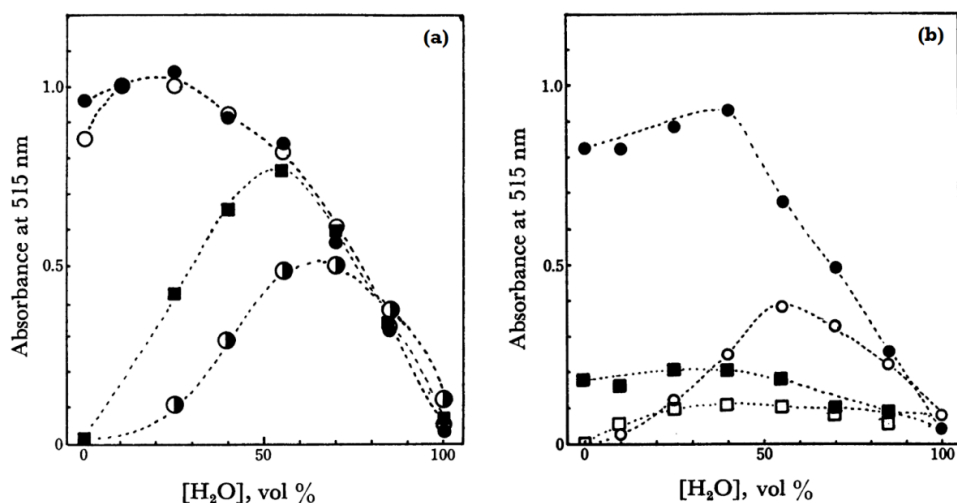
Figure 1-19. CPZ$^{\cdot+}$ absorbance at 515 nm (a) in the degassed (●), argon bubbled (○), air saturated (■), and oxygen bubbled (◑) mixed solvents of methanol and water; and (b) in argon bubbled (●), and oxygen bubbled (○) dioxane-water mixtures, and in argon bubbled (■) and air saturated (□) acetonitrile-water mixtures. [CPZ] = 2×10^{-4} M. Adapted from Ref. [179], copyright (1977) with permission from the Chemical Society of Japan.

These authors were able to show that the impact of the presence of oxygen on the photoionization in aqueous solutions is different than that in organic solutions. So that, in the absence of oxygen, no photoionization was found in water, while in organic solvents, efficient ionization proceeded (**Figure 1-19**). By employing flash photolytic measurements, through the detection of chlorpromazine radical cation, it was observed that the photoionization proceeds monomolecular *via* an excited state (an intermediate transient species such as a half-ionized state) which has a life-time much shorter than that of the lowest excited (π-π^*) triplet state [179].

Sub-nanosecond relaxation dynamics of the chlorpromazine cation ($CPZ(+H^+)$) were investigated by Maruthamuthu *et al.* [180] through a picosecond laser spectroscopic technique with an excitation wavelength of 335 nm in the presence and absence of TiO_2 colloids to assess chlorpromazine photosensitization of wide bandgap metal oxide semiconductors. Pulsed laser photolysis at 355 nm for ($CPZ(+H^+)$) revealed two transient absorption bands for this compound (**Figure 1-20(a)**); one centered in the range 480-565 nm and the second in the 580-675-nm region. The latter absorption band was found to be completely quenched in the presence of nitrate anions, so that an individual absorption with an absorption maximum at 525 nm was remained (**Figure 1-20(b)**) [180].
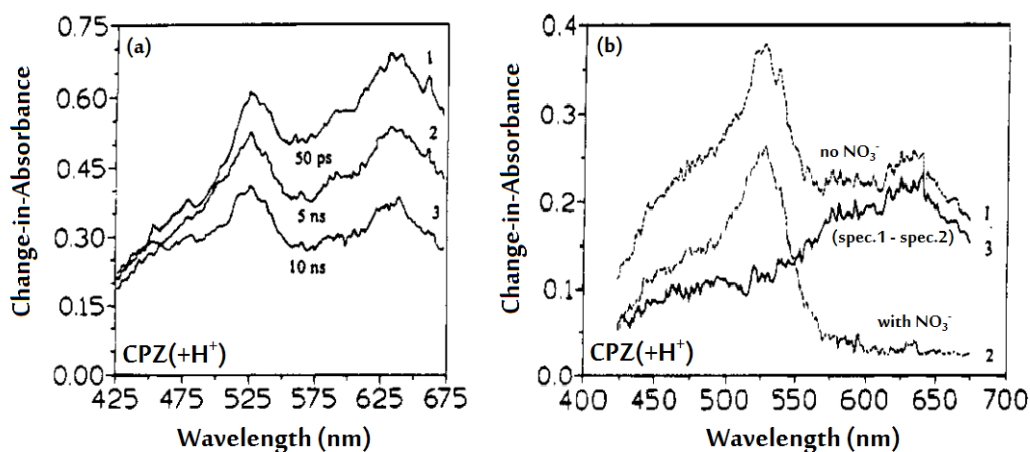
Figure 1-20. Picosecond laser transient absorption spectra: $[CPZ(+H^+)]=1 \times 10^{-3}$ M (a) laser pulse energy ~2.5 mj; (1) 50 ps, (2) 5 ns, and (3) 10 ns; and (b) laser pulse energy ~0.9 mJ; delay time 10 ns; (1) without NO_3^-, (2) with 1×10^{-4} M NO_3^-, and (3) difference spectrum (spectrum (1) minus spectrum (2)); solutions were degassed with argon [180]. Adapted with permission from Ref. [180], Copyright (1995) American Chemical Society.

As reported by Grätzel *et al.*, since solvated electrons are highly reductive and could react quickly with nitrate anions, no attribution of these electrons to the transient absorption will be observed in the presence of NO_3^- [181]. A similar effect has been observed by Mohamed *et al.*, revealing that one-electron reduction of nitrate ions by electrons (in photocatalytic systems) is possible [182].

Thus, it was concluded from these observations that upon 355 nm laser photolysis, the chlorpromazine cation transforms into its radical cation and a solvated electron (**Equation 1-29**) [180].

$$\left(CPZ\left(+H^+\right)\right) \xrightarrow{\lambda=335\ nm} \left(CPZ^{\bullet+}\left(+H^+\right)\right) + e_{aq}^- \tag{1-29}$$
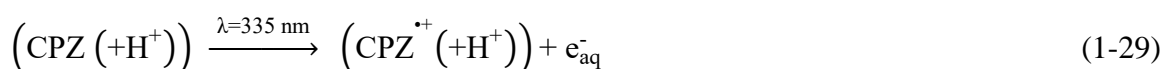
Accordingly, the transient absorption observed in the range of 480-565 nm with a maximum at 525 nm was attributed to $CPZ^{\bullet+}(+H^+)$, while the transient absorption detected in the range of 580-675 nm was ascribed to the ejected aqueous electron (e_{aq}^-). The observed absorption was reduced at longer delay times (**Figure 1-20(a)**) which revealed that the parent compound ($CPZ(+H^+)$) could be regenerated in the absence of other additives, as a result of the following recombination reaction [180]:

$$\left(CPZ^{\bullet+}\left(+H^+\right)\right) + e_{aq}^- \rightarrow \left(CPZ\left(+H^+\right)\right) \tag{1-30}$$
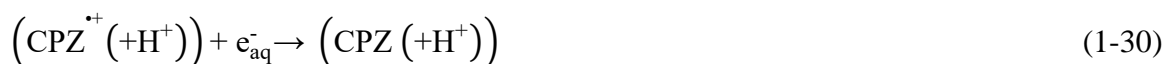
The formation of the chlorpromazine radical cation was found to be pulse-width limited (that is, if occurred in less than about 30 ps) and therefore, the formation of the excited singlet state species in aqueous media was too fast to be detected. However, in methanol and upon excitation with lower energy laser pulses, a transient absorption with a maximum at 470 nm attributable to the excited singlet state could be obtained. Interestingly, in the presence of colloidal TiO_2, the recorded transient absorption spectra were just about equal to those obtained for the photolysis of ($CPZ(+H^+)$). In the presence of TiO_2, the band attributed to $CPZ^{\bullet+}(+H^+)$ was found to be more intense. It was suggested by the authors that the TiO_2 colloids scavenge the electrons withdrawing the recombination reaction shown in **Equation 1-30** [180].

In a similar study, García *et al.* employed both nanosecond and picoseconds laser flash photolysis to determine the photoionization mechanism of two phenothiazine derivatives,

namely, chlorpromazine and promazine, as a function of solvent and excitation conditions [183]. In **Figure 1-21** the time-dependent transient absorption spectra obtained by these authors for chlorpromazine excitation at 355 nm in aqueous and methanol solutions are shown [183].
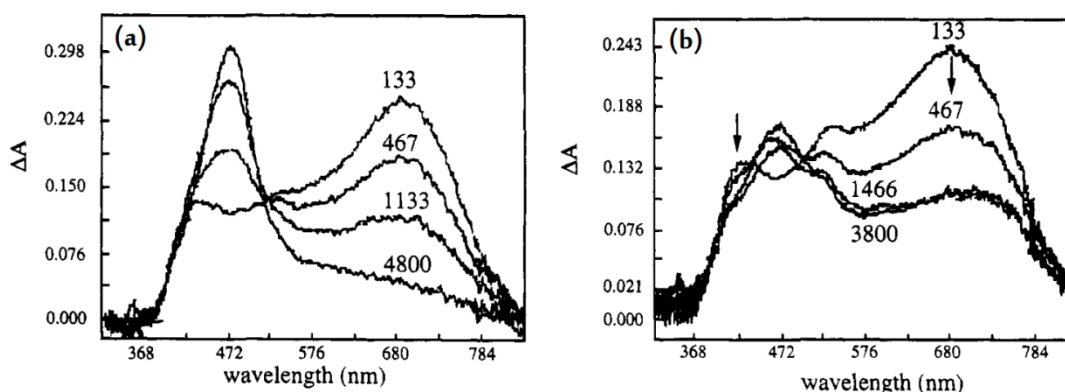
Figure 1-21. Time-dependent transient absorption spectra obtained on 355 nm picosecond laser flash photolysis of (a) chlorpromazine in aerated methanol and (b) chlorpromazine in aerated water. Delay times (in ps) are indicated [183]. Adapted with permission from Ref. [183], Copyright (1995) American Chemical Society.

As can be observed, in methanol two absorption maxima at approximately 430 and 680 nm were detected in the spectrum right after the laser pulse (**Figure 1-21(a)**). The authors have assigned these absorptions to the singlet state of chlorpromazine. They also suggested that the spectrum detected at the longest decay consists of the chlorpromazine triplet state (determined with nanosecond measurements) as well as a broad absorption due to the solvated electron in methanol. Also a small shoulder corresponding to the chlorpromazine radical cation ($CPZ^{\bullet+}$) at around 520 nm could also be observed. However, the situation was found to be completely different in the aqueous solution. In the aqueous solution of chlorpromazine, besides the absorption of its singlet and triplet states, also a long-lived absorption at about 700 nm (attributed to e^-_{aq}) and a significant shoulder at 520 nm ($CPZ^{\bullet+}$) were observed (**Figure 1-21(b)**) [183].

In addition, these authors pointed out that during single wavelength pulsed irradiation of chlorpromazine, in principle, the second photon is absorbed by the lowest excited singlet state rather than the lowest excited triplet state. The experimental results demonstrated that in aqueous solutions at excitation wavelengths larger than 308 nm, the photoionization process is biphotonic and that the excitation of both lowest singlet and triplet states can lead

to photoionization in aqueous solutions. However, in methanol (or other alcohols), biphotonic photoionization could only be induced by intense single wavelength excitation at ≤ 355 nm wavelengths [183].

Nevertheless, despite the vast number of investigations regarding the photolytic degradation of chlorpromazine and the determination of photo-induced intermediates or products of its transformation, yet, not much is known about its photocatalytic conversion. In this regard, Khataee *et al.* have investigated the photocatalytic activity of TiO_2 nanoparticles (PC-500) immobilized on ceramic plates to degrade a mixture of chlorpromazine and two other pharmaceuticals under UV irradiation (254 nm) and they were able to observe 90% removal of chlorpromazine in the mixture after 150 minutes exposure to UV irradiation [184]. However, since under UV light irradiation chlorpromazine is able to absorb light and will be photo-degraded directly, the undergoing mechanism is not clear; as it cannot be determined whether the observed degradation under UV light irradiation is a photocatalytic or a photolytic effect.

1.6. Objectives and Purpose of this Study

The particular focus of this work was directed towards the assessment of visible light activity of different semiconductors, namely, zinc ferrites prepared through various synthetic procedures, pure titanium dioxide, and carbon-modified titanium dioxide. Regarding this purpose, two important members of the phenothiazine group of antipsychotic medications (namely chlorpromazine and MB) were chosen as model pollutants. Accordingly, the photocatalytic removals of the model pollutants as well as the role of the formed intermediates throughout the photocatalytic reactions were investigated. Most importantly, the mechanisms behind the visible light-driven photocatalytic reactions under different experimental conditions were studied within the frames of this doctoral thesis.

The topics of this doctoral dissertation are presented in the following chapters. At first, an introduction is presented in this chapter (**Chapter 1**) on basic principles of the issues related to this scientific study. These issues include generally the necessity of pharmaceuticals removal from water and wastewater, photocatalysis, the target investigated group of pharmaceuticals, the utilized photocatalysts in this work, and the applied analytical methods.

In this study, the group of phenothiazines, one of the mostly consumed antipsychotic groups of medications was chosen as the target category of pharmaceuticals. Initially, MB, the pioneering member of the phenothiazine group also known as an organic dye molecule was selected as a model compound. Zinc ferrite was the first photocatalyst studied in the current work. Since different photocatalytic activities have been reported so far for this semiconducting material, it was of great interest to figure out an explanation for this behavior. Considering the impact of the synthetic procedure on the physiochemical properties of zinc ferrite, various zinc ferrite samples were prepared through different reported synthetic methods. Besides a detailed characterization analysis, the energetic positions of the conduction band and the valence band in differently prepared zinc ferrite samples had to be determined. Accordingly, a series of wavelength dependent photocatalytic measurements were carried out through which the photocatalytic activities of the zinc ferrite samples were studied. Moreover, the ability of zinc ferrite as a visible light-absorbing photocatalyst for the degradation of MB under visible light irradiation was evaluated. These investigations were able to determine whether the visible light-induced bleaching of MB observed in the presence of zinc ferrite was actually a photocatalytic effect or if another mechanism laid behind this observation. This topic is discussed in detail in **Chapter 2,** in an article entitled "Visible-Light Photocatalytic Activity of Zinc Ferrites" published in the Journal of Photochemistry and Photobiology A: Chemistry (doi:10.1016/j.jphotochem.2018.03.014).

Chlorpromazine is another member of the phenothiazine group of pharmaceuticals which was chosen as a model compound within the objectives of this work. Upon UV light irradiation, a system containing a photocatalyst and chlorpromazine is an ambiguous one, since the differentiation between the photolytic reaction of chlorpromazine and the photocatalytic procedure is rather unfeasible. Although under UV light irradiation chlorpromazine is able to absorb light and undergo degradation, it is reported to be persistent upon visible light irradiation. Hence, for the successful conversion of this compound upon visible light irradiation, a visible-light active photocatalyst is required. In order to evaluate the possibility of photocatalytic removal of chlorpromazine, its behavior in the presence of a visible light-active photocatalyst, K-7000, which is a commercially available carbon-modified anatase titanium dioxide, was investigated. Accordingly, the effect of the presence or absence of oxygen, the photocatalytically produced intermediates

throughout its conversion, as well as the potential similarities and differences between the photolytic and photocatalytic pathways under both UV and visible light irradiation in the presence of K-7000 were analyzed. These aspects were evaluated and discussed in **Chapter 3**, in an article entitled "Light-Induced Reactions of Chlorpromazine in the Presence of a Heterogeneous Photocatalyst: Formation of a Long-Lasting Sulfoxide" published in Catalysts (doi:10.3390/catal9070627).

Due to the lack of a presented mechanistic study, the photocatalytic reaction pathway of chlorpromazine remains yet unclarified. Thus, for a better understanding of the mechanism of photocatalytic conversion of this compound upon visible light irradiation, first, the fundamental processes regarding the promoted visible light activity of the utilized titanium dioxide photocatalyst, K-7000, are required to be known. For this purpose, K-7000 was considered as titanium dioxide sensitized with a carbon-based layer. Employing diffuse reflectance transient absorption spectroscopy, the nature of charge carriers formed by UV or visible light laser excitation at different atmospheres was studied. Furthermore, photocatalytic conversions of chlorpromazine and methanol under aerobic conditions upon visible light irradiation in the presence of K-7000 were also monitored and the obtained data were compared with those of the transient absorption measurements. These observations led to the conclusion that the excitation of K-7000 with UV light was able to generate electron-hole pairs in the anatase particles as well as in the carbon-based sensitizer layer, while under visible light irradiation, only the sensitizer layer was excited. Accordingly, a mechanism including the processes taking place after excitation of K-7000 with UV and visible light was proposed in **Chapter 4** which includes the article entitled "Regarding the Nature of Charge Carriers formed by UV or Visible Light Excitation of carbon-modified Titanium Dioxide" published in Catalysts (doi:10.3390/catal9080697). After all, in the last chapter (**Chapter 5**), a summarizing discussion about all the obtained experimental results is presented.

1.7. References

1.   Klavarioti, M.; Mantzavinos, D.; Kassinos, D. Removal of residual pharmaceuticals from aqueous systems by advanced oxidation processes. *Environ. Int.* **2009**, *35*, 402–417.

2.   Bruce, G.M.; Pleus, R.C.; Snyder, S.A. Toxicological relevance of pharmaceuticals

in drinking water. *Environ. Sci. Technol.* **2010**, *44*, 5619–5626.

3.   Benotti, M.J.; Trenholm, R.A.; Vanderford, B.J.; Holady, J.C.; Stanford, B.D.; Snyder, S.A. Pharmaceuticals and endocrine disrupting compounds in U.S. drinking water. *Environ. Sci. Technol.* **2009**, *43*, 597–603.

4.   Guo, Y.C.; Krasner, S.W. Occurrence of primidone, carbamazepine, caffeine, and precursors for N-Nitrosodimethylamine in drinking water sources impacted by wastewater. *JAWRA J. Am. Water Resour. Assoc.* **2009**, *45*, 58–67.

5.   Buser, H.R.; Poiger, T.; Müller, M.D. Occurrence and fate of the pharmaceutical drug diclofenac in surface waters: Rapid photodegradation in a lake. *Environ. Sci. Technol.* **1998**, *32*, 3449–3456.

6.   Saccà, M.L.; Accinelli, C.; Fick, J.; Lindberg, R.; Olsen, B. Environmental fate of the antiviral drug Tamiflu in two aquatic ecosystems. *Chemosphere* **2009**, *75*, 28–33.

7.   Kasprzyk-Hordern, B.; Dinsdale, R.M.; Guwy, A.J. The occurrence of pharmaceuticals, personal care products, endocrine disruptors and illicit drugs in surface water in South Wales, UK. *Water Res.* **2008**, *42*, 3498–3518.

8.   Ternes, T.A. Occurrence of drugs in German sewage treatment plants and rivers. *Water Res.* **1998**, *32*, 3245–3260.

9.   Kanda, R.; Griffin, P.; James, H.A.; Fothergill, J. Pharmaceutical and personal care products in sewage treatment works. *J. Environ. Monit.* **2003**, *5*, 823–830.

10.   Nakada, N.; Tanishima, T.; Shinohara, H.; Kiri, K.; Takada, H. Pharmaceutical chemicals and endocrine disrupters in municipal wastewater in Tokyo and their removal during activated sludge treatment. *Water Res.* **2006**, *40*, 3297–3303.

11.   Kim, S.D.; Cho, J.; Kim, I.S.; Vanderford, B.J.; Snyder, S.A. Occurrence and removal of pharmaceuticals and endocrine disruptors in South Korean surface, drinking, and waste waters. *Water Res.* **2007**, *41*, 1013–1021.

12.   Camacho-Muñoz, D.; Martín, J.; Santos, J.L.; Aparicio, I.; Alonso, E. Occurrence, temporal evolution and risk assessment of pharmaceutically active compounds in Doñana Park (Spain). *J. Hazard. Mater.* **2010**, *183*, 602–608.

13.   Bound, J.P.; Voulvoulis, N. Household disposal of pharmaceuticals as a pathway for aquatic contamination in the United kingdom. *Environ. Health Perspect.* **2005**, *113*, 1705–1711.

14. Tong, A.Y.C.; Peake, B.M.; Braund, R. Disposal practices for unused medications around the world. *Environ. Int.* **2011**, *37*, 292–298.

15. Vieno, N.; Tuhkanen, T.; Kronberg, L. Elimination of pharmaceuticals in sewage treatment plants in Finland. *Water Res.* **2007**, *41*, 1001–1012.

16. Mirzaei, A.; Chen, Z.; Haghighat, F.; Yerushalmi, L. Removal of pharmaceuticals and endocrine disrupting compounds from water by zinc oxide-based photocatalytic degradation: A review. *Sustain. Cities Soc.* **2016**, *27*, 407–418.

17. Rioja, N.; Benguria, P.; Peñas, F.J.; Zorita, S. Competitive removal of pharmaceuticals from environmental waters by adsorption and photocatalytic degradation. *Environ. Sci. Pollut. Res.* **2014**, *21*, 11168–11177.

18. Silva, B.; Costa, F.; Neves, I.C.; Tavares, T. *Psychiatric Pharmaceuticals as Emerging Contaminants in Wastewater*; SpringerBriefs in Molecular Science; Springer International Publishing: Cham, 2015; ISBN 978-3-319-20492-5.

19. Trawiński, J.; Skibiński, R. Studies on photodegradation process of psychotropic drugs: a review. *Environ. Sci. Pollut. Res.* **2017**, *24*, 1152–1199.

20. Sheng, L.-H.; Chen, H.-R.; Huo, Y.-B.; Wang, J.; Zhang, Y.; Yang, M.; Zhang, H.-X. Simultaneous determination of 24 antidepressant drugs and their metabolites in wastewater by ultra-high performance liquid chromatography–tandem mass spectrometry. *Molecules* **2014**, *19*, 1212–1222.

21. Yuan, S.; Jiang, X.; Xia, X.; Zhang, H.; Zheng, S. Detection, occurrence and fate of 22 psychiatric pharmaceuticals in psychiatric hospital and municipal wastewater treatment plants in Beijing, China. *Chemosphere* **2013**, *90*, 2520–2525.

22. Logarinho, F.; Rosado, T.; Lourenço, C.; Barroso, M.; Araujo, A.R.T.S.; Gallardo, E. Determination of antipsychotic drugs in hospital and wastewater treatment plant samples by gas chromatography/tandem mass spectrometry. *J. Chromatogr. B* **2016**, *1038*, 127–135.

23. Asimakopoulos, A.G.; Kannan, P.; Higgins, S.; Kannan, K. Determination of 89 drugs and other micropollutants in unfiltered wastewater and freshwater by LC-MS/MS: an alternative sample preparation approach. *Anal. Bioanal. Chem.* **2017**, *409*, 6205–6225.

24. The National Institute of Mental Health Information Resource Center -Mental Health Medications - Available online:

https://www.nimh.nih.gov/health/topics/mental-health-medications/index.shtml#part_149866 (accessed on Jun 7, 2019).

25. Garbis, H.; McElhatton, P.R. Psychotropic drugs. In *Drugs During Pregnancy and Lactation*; Elsevier Ltd., 2007; pp. 288–320 ISBN 978-0-444-52072-2.

26. Vardanyan, R.; Hruby, V. Antipsychotics. In *Synthesis of Best-Seller Drugs*; Elsevier, 2016; pp. 87–110 ISBN 978-0-12-411492-0.

27. Fourrier, A.; Gasquet, I.; Allicar, M.P.; Bouhassira, M.; Lépine, J.P.; Bégaud, B. Patterns of neuroleptic drug prescription: a national cross-sectional survey of a random sample of French psychiatrists. *Br. J. Clin. Pharmacol.* **2001**, *49*, 80–86.

28. Hudepohl, N.S.; Nasrallah, H.A. Antipsychotic drugs. In *Handbook of Clinical Neurology*; Elsevier, 2012; Vol. 106, pp. 657–667 ISBN 9780444520029.

29. Sudeshna, G.; Parimal, K. Multiple non-psychiatric effects of phenothiazines: A review. *Eur. J. Pharmacol.* **2010**, *648*, 6–14.

30. Shen, W.W. A history of antipsychotic drug development. *Compr. Psychiatry* **1999**, *40*, 407–14.

31. Frankenburg, F.R.; Baldessarini, R.J. Neurosyphilis, malaria, and the discovery of antipsychotic agents. *Harv. Rev. Psychiatry* **2008**, *16*, 299–307.

32. Wainwright, M.; Crossley, K.B. Methylene blue-a therapeutic dye for all seasons? *J. Chemother.* **2002**, *14*, 431–443.

33. Oz, M.; Lorke, D.E.; Petroianu, G.A. Methylene blue and Alzheimer's disease. *Biochem. Pharmacol.* **2009**, *78*, 927–932.

34. Mills, A. An overview of the methylene blue ISO test for assessing the activities of photocatalytic films. *Appl. Catal. B Environ.* **2012**, *128*, 144–149.

35. López-Muñoz, F.; Alamo, C.; Cuenca, E.; Shen, W.W.; Clervoy, P.; Rubio, G. History of the discovery and clinical introduction of chlorpromazine. *Ann. Clin. Psychiatry* **2005**, *17*, 113–135.

36. Nałecz-Jawecki, G.; Hajnas, A.; Sawicki, J. Photodegradation and phototoxicity of thioridazine and chlorpromazine evaluated with chemical analysis and aquatic organisms. *Ecotoxicology* **2008**, *17*, 13–20.

37. Bahnemann, D.; Asmus, K.-D.; Willson, R.L. Free radical induced one-electron oxidation of the phenothiazines chlorpromazine and promethazine. *J. Chem. Soc. Perkin Trans.* **1983**, *2*, 1661–1668.

38. Gocke, E. Review of the genotoxic properties of chlorpromazine and related phenothiazines. *Mutat. Res. Genet. Toxicol.* **1996**, *366*, 9–21.

39. Boreen, A.L.; Arnold, W.A.; McNeill, K. Photodegradation of pharmaceuticals in the aquatic environment: A review. *Aquat. Sci. - Res. Across Boundaries* **2003**, *65*, 320–341.

40. Andreozzi, R.; Raffaele, M.; Nicklas, P. Pharmaceuticals in STP effluents and their solar photodegradation in aquatic environment. *Chemosphere* **2003**, *50*, 1319–1330.

41. Trautwein, C.; Kümmerer, K. Degradation of the tricyclic antipsychotic drug chlorpromazine under environmental conditions, identification of its main aquatic biotic and abiotic transformation products by LC-MS^n and their effects on environmental bacteria. *J. Chromatogr. B Anal. Technol. Biomed. Life Sci.* **2012**, *889–890*, 24–38.

42. Wilde, M.L.; Schneider, M.; Kümmerer, K. Fenton process on single and mixture components of phenothiazine pharmaceuticals: Assessment of intermediaries, fate, and preliminary ecotoxicity. *Sci. Total Environ.* **2017**, *583*, 36–52.

43. Jiménez, J.J.; Muñoz, B.E.; Sánchez, M.I.; Pardo, R.; Vega, M.S. Fate of the drug chlorpromazine in river water according to laboratory assays. Identification and evolution over time of degradation products. Sorption to sediment. *Chemosphere* **2016**, *162*, 285–292.

44. Prieto-Rodriguez, L.; Miralles-Cuevas, S.; Oller, I.; Agüera, A.; Puma, G.L.; Malato, S. Treatment of emerging contaminants in wastewater treatment plants (WWTP) effluents by solar photocatalysis using low TiO_2 concentrations. *J. Hazard. Mater.* **2012**, *211–212*, 131–137.

45. Braslavsky, S.E.; Braun, A.M.; Cassano, A.E.; Emeline, A. V.; Litter, M.I.; Palmisano, L.; Parmon, V.N.; Serpone, N. Glossary of terms used in photocatalysis and radiation catalysis (IUPAC Recommendations 2011). *Pure Appl. Chem.* **2011**, *83*, 931–1014.

46. Fujishima, A.; Honda, K. Electrochemical photolysis of water at a semiconductor electrode. *Nature* **1972**, *238*, 37–38.

47. Herrmann, J.-M. Heterogeneous photocatalysis: fundamentals and applications to the removal of various types of aqueous pollutants. *Catal. Today* **1999**, *53*, 115–129.

48. Spasiano, D.; Marotta, R.; Malato, S.; Fernandez-Ibañez, P.; Di Somma, I. Solar

photocatalysis: Materials, reactors, some commercial, and pre-industrialized applications. A comprehensive approach. *Appl. Catal. B Environ.* **2015**, *170–171*, 90–123.

49.   Robertson, P.K.J.; Bahnemann, D.W.; Robertson, J.M.C.; Wood, F. Photocatalytic detoxification of water and air. *Environ. Photochem. Part II* **2005**, *2*, 367–423.

50.   Malato, S.; Fernández-Ibáñez, P.; Maldonado, M.I.; Blanco, J.; Gernjak, W. Decontamination and disinfection of water by solar photocatalysis: Recent overview and trends. *Catal. Today* **2009**, *147*, 1–59.

51.   Mills, A.; Hunte, S. Le An overview of semiconductor photocatalysis. *J. Photochem. Photobiol. A Chem.* **1997**, *108*, 1–35.

52.   Hoffmann, M.R.; Martin, S.T.; Choi, W.; Bahnemann, D.W. Environmental applications of semiconductor photocatalysis. *Chem. Rev.* **1995**, *95*, 69–96.

53.   Bahnemann, D. Photocatalytic water treatment: Solar energy applications. *Sol. Energy* **2004**, *77*, 445–459.

54.   Augugliaro, V.; Palmisano, G.; Soria, J.; Palmisano, L. Heterogeneous photocatalysis and catalysis: An overview of their distinctive features. In *Heterogeneous Photocatalysis*; Elsevier, 2019; pp. 1–24 ISBN 9780444640154.

55.   Fujishima, A.; Hashimoto, K.; Watanabe, T. *TiO$_2$ photocatalysis: Fundamentals and applications*; BKC, 1999; ISBN 493905103X.

56.   Hashimoto, K.; Irie, H.; Fujishima, A. TiO$_2$ photocatalysis: A historical overview and future prospects. *Jpn. J. Appl. Phys.* **2005**, *44*, 8269–8285.

57.   Fujishima, A.; Hashimoto, K.; Iyoda, T.; Fukayama, S.; Yoshimoto, T.; Saitoh, T. Patent: Titanium dioxide photocatalyst 2002, 1–33.

58.   Augugliaro, V.; Loddo, V.; Pagliaro, M.; Palmisano, G.; Palmisano, L. *Clean by light irradiation: Practical applications of supported TiO$_2$*; Royal Society of Chemistry: Cambridge, 2010; ISBN 978-1-84755-870-1.

59.   Gupta, S.M.; Tripathi, M. A review of TiO$_2$ nanoparticles. *Chinese Sci. Bull.* **2011**, *56*, 1639–1657.

60.   Ismail, A.A.; Bahnemann, D.W. Photochemical splitting of water for hydrogen production by photocatalysis: A review. *Sol. Energy Mater. Sol. Cells* **2014**, *128*, 85–101.

61.   Carp, O.; Huisman, C.L.; Reller, A. Photoinduced reactivity of titanium dioxide.

Prog. Solid State Chem. **2004**, *32*, 33–177.

62. Zhang, J.; Zhou, P.; Liu, J.; Yu, J. New understanding of the difference of photocatalytic activity among anatase, rutile and brookite TiO_2. *Phys. Chem. Chem. Phys.* **2014**, *16*, 20382–20386.

63. Mendive, C.B.; Curti, M.; Bahnemann, D. Current issues concerning the mechanism of pristine TiO_2 photocatalysis and the effects on photonic crystal nanostructures. In *Photocatalysis: Fundamentals and Perspectives*; Royal Society of Chemistry, 2016; pp. 51–79.

64. Bahnemann, D.W.; Marcus Hilgendorff; Memming, R.; Hilgendorff, M.; Memming, R. Charge carrier dynamics at TiO_2 particles: Reactivity of free and trapped holes. *J. Phys. Chem. B* **1997**, *101*, 4265–4275.

65. Montoya, J.F.; Atitar, M.F.; Bahnemann, D.W.; Peral, J.; Salvador, P. Comprehensive kinetic and mechanistic analysis of TiO_2 photocatalytic reactions according to the direct–indirect model: (II) Experimental validation. *J. Phys. Chem. C* **2014**, *118*, 14276–14290.

66. Ohtani, B. Photocatalysis A to Z—What we know and what we do not know in a scientific sense. *J. Photochem. Photobiol. C Photochem. Rev.* **2010**, *11*, 157–178.

67. Ohtani, B. Revisiting the fundamental physical chemistry in heterogeneous photocatalysis: its thermodynamics and kinetics. *Phys. Chem. Chem. Phys.* **2014**, *16*, 1788–1797.

68. Beranek, R. (Photo)electrochemical methods for the determination of the band edge positions of TiO_2-based nanomaterials. *Adv. Phys. Chem.* **2011**, *2011*, 80–99.

69. Memming, R. Principles of semiconductor physics. In *Semiconductor Electrochemistry*; Wiley-VCH Verlag GmbH: Weinheim, Germany, 2001; pp. 1–21.

70. Peter, L.M. Photoelectrochemistry: From basic principles to photocatalysis. In *Photocatalysis Fundamentals and perspectives*; Schneider, J., Bahnemann, D., Ye, J., Puma, G.L., Dionysiou, D.D., Eds.; The Royal Society of Chemistry: Cambridge, UK, 2016; pp. 1–28.

71. Rabek, J.F. *Photochemistry and photophysics*; 3rd ed.; CRC Press: Florida, United States, 1991; ISBN 9780849340437.

72. Grätzel, M.; Rotzinger, F.P. The influence of the crystal lattice structure on the

conduction band energy of oxides of titanium(IV). *Chem. Phys. Lett.* **1985**, *118*, 474–477.

73. ASTM International. *ASTM G173-03(2012): Standard tables for reference solar spectral irradiances: Direct normal and hemispherical on 37° tilted surface*; West Conshohocken, PA, 2012.

74. García-López, E.I. Photocatalytic and catalytic reactions in gas–solid and in liquid–solid systems. In *Heterogeneous Photocatalysis*; Elsevier, 2019; pp. 153–176 ISBN 9780444640154.

75. Dillert, R.; Taffa, D.H.; Wark, M.; Bredow, T.; Bahnemann, D.W. Research Update: Photoelectrochemical water splitting and photocatalytic hydrogen production using ferrites (MFe_2O_4) under visible light irradiation. *APL Mater.* **2015**, *3*, 104001-1–15.

76. Kim, J.H.; Kim, J.H.; Jang, J.-W.; Kim, J.Y.; Choi, S.H.; Magesh, G.; Lee, J.; Lee, J.S. Awakening solar water-splitting activity of $ZnFe_2O_4$ nanorods by hybrid microwave annealing. *Adv. Energy Mater.* **2015**, *5*, 1401933.

77. Tahir, A.A.; Wijayantha, K.G.U. Photoelectrochemical water splitting at nanostructured $ZnFe_2O_4$ electrodes. *J. Photochem. Photobiol. A Chem.* **2010**, *216*, 119–125.

78. Boumaza, S.; Boudjemaa, A.; Bouguelia, A.; Bouarab, R.; Trari, M. Visible light induced hydrogen evolution on new hetero-system $ZnFe_2O_4/SrTiO_3$. *Appl. Energy* **2010**, *87*, 2230–2236.

79. Taffa, D.H.; Dillert, R.; Ulpe, A.C.; Bauerfeind, K.; Bredow, T.; Bahnemann, D.; Wark, M. Photoelectrochemical and theoretical investigations of spinel type ferrites ($M_xFe_{3-x}O_4$) for water splitting: a mini-review. *J. Photonics Energy* **2016**, *7*, 1–24.

80. Song, G.; Xin, F.; Yin, X. Photocatalytic reduction of carbon dioxide over $ZnFe_2O_4/TiO_2$ nanobelts heterostructure in cyclohexanol. *J. Colloid Interface Sci.* **2015**, *442*, 60–66.

81. Casbeer, E.; Sharma, V.K.; Li, X. Synthesis and photocatalytic activity of ferrites under visible light : A review. *Sep. Purif. Technol.* **2012**, *87*, 1–14.

82. Valenzuela, M.A.; Bosch, P.; Jiménez-Becerrill, J.; Quiroz, O.; Páez, A.I. Preparation, characterization and photocatalytic activity of ZnO, Fe_2O_3 and $ZnFe_2O_4$. *J. Photochem. Photobiol. A Chem.* **2002**, *148*, 177–182.

83. Dom, R.; Subasri, R.; Hebalkar, N.Y.; Chary, A.S.; Borse, P.H. Synthesis of a

hydrogen producing nanocrystalline $ZnFe_2O_4$ visible light photocatalyst using a rapid microwave irradiation method. *RSC Adv.* **2012**, *2*, 12782–12791.

84. Sato, T.; Haneda, K.; Seki, M.; Iijima, T. Morphology and magnetic properties of ultrafine $ZnFe_2O_4$ particles. *Appl. Phys. A Solids Surfaces* **1990**, *50*, 13–16.

85. Granone, L.I. An Iron-Based Photoelectrode, Gottfried Wilhelm Leibniz Universität Hannover, 2019.

86. Alsayed, Z.; Badawi, M.S.; Awad, R. Characterization of zinc ferrite nanoparticles capped with different PVP concentrations. *J. Electron. Mater.* **2019**, *48*, 4925–4933.

87. Chuan, L.K.; Zaid, H.M.; Chuan, L.K.; Zaid, H.M. Zinc Composition and its Effect on Magnetic Properties of Nickel-Zinc Ferrite Prepared Via Sol-gel Technique. *Am. J. Appl. Sci.* **2018**, *15*, 121–123.

88. Mousa, M.A.; A Gomaa, E.; Khairy, M.; Eltanany, M.E. Thermodynamic and thermal properties of solvation for nano nickel ferrite and nano zinc ferrite prepared by the sol–gel method in different CH_3COOH concentrations at different temperatures. *J. Inorg. Organomet. Polym. Mater.* **2019**, *19*, 1–10.

89. Diodati, S.; Pandolfo, L.; Caneschi, A.; Gialanella, S.; Gross, S. Green and low temperature synthesis of nanocrystalline transition metal ferrites by simple wet chemistry routes. *Nano Res.* **2014**, *7*, 1027–1042.

90. Jang, J.-S.; Borse, P.H.; Lee, J.-S.; Jung, O.-S.; Cho, C.-R.; Jeong, E.-D.; Ha, M.-G.; Won, M.-S.; Kim, H.-G. Synthesis of nanocrystalline $ZnFe_2O_4$ by polymerized complex method for its visible light photocatalytic application: An efficient photo-oxidant. *Bull. Korean Chem. Soc.* **2009**, *30*, 1738–1742.

91. Sarkar, J.; Bhattacharyya, S. Operating characteristics of transcritical CO_2 heat pump for simultaneous water cooling and heating. *Arch. Thermodyn.* **2013**, *33*, 23–40.

92. Šutka, A.; Pärna, R.; Kleperis, J.; Käämbre, T.; Pavlovska, I.; Korsaks, V.; Malnieks, K.; Grinberga, L.; Kisand, V. Photocatalytic activity of non-stoichiometric $ZnFe_2O_4$ under visible light irradiation. *Phys. Scr.* **2014**, *89*, 1–8.

93. Arimi, A.; Megatif, L.; Granone, L.I.; Dillert, R.; Bahnemann, D.W. Visible-light photocatalytic activity of zinc ferrites. *J. Photochem. Photobiol. A Chem.* **2018**, *366*, 118–126.

94. Granone, L.I.; Ulpe, A.C.; Robben, L.; Klimke, S.; Jahns, M.; Renz, F.; Gesing, T.M.; Bredow, T.; Dillert, R.; Bahnemann, D.W. Effect of the degree of inversion

on optical properties of spinel $ZnFe_2O_4$. *Phys. Chem. Chem. Phys.* **2018**, *20*, 28267–28278.

95.   Dolcet, P.; Kirchberg, K.; Antonello, A.; Suchomski, C.; Marschall, R.; Diodati, S.; Muñoz-Espí, R.; Landfester, K.; Gross, S. Exploring wet chemistry approaches to $ZnFe_2O_4$ spinel ferrite nanoparticles with different inversion degrees: a comparative study. *Inorg. Chem. Front.* **2019**, *6*, 1527–1534.

96.   Meng, W.; Li, F.; Evans, D.G.; Duan, X. Photocatalytic activity of highly porous zinc ferrite prepared from a zinc-iron(III)-sulfate layered double hydroxide precursor. *J. Porous Mater.* **2004**, *11*, 97–105.

97.   Fan, G.; Gu, Z.; Yang, L.; Li, F. Nanocrystalline zinc ferrite photocatalysts formed using the colloid mill and hydrothermal technique. *Chem. Eng. J.* **2009**, *155*, 534–541.

98.   Su, M.; He, C.; Sharma, V.K.; Abou Asi, M.; Xia, D.; Li, X.; Deng, H.; Xiong, Y. Mesoporous zinc ferrite: Synthesis, characterization, and photocatalytic activity with H_2O_2/visible light. *J. Hazard. Mater.* **2012**, *211–212*, 95–103.

99.   Patil, S.B.; Bhojya Naik, H.S.; Nagaraju, G.; Viswanath, R.; Rashmi, S.K.; Vijay kumar, M. Sugarcane juice mediated eco-friendly synthesis of visible light active zinc ferrite nanoparticles: Application to degradation of mixed dyes and antibacterial activities. *Mater. Chem. Phys.* **2018**, *212*, 351–362.

100.   Qiu, J.; Wang, C.; Gu, M. Photocatalytic properties and optical absorption of zinc ferrite nanometer films. *Mater. Sci. Eng. B* **2004**, *112*, 1–4.

101.   Sharma, R.; Singhal, S. Structural, magnetic and electrical properties of zinc doped nickel ferrite and their application in photo catalytic degradation of methylene blue. *Phys. B Condens. Matter* **2013**, *414*, 83–90.

102.   Curti, M.; Kirsch, A.; Granone, L.I.; Tarasi, F.; López-Robledo, G.; Bahnemann, D.W.; Murshed, M.M.; Gesing, T.M.; Mendive, C.B. Visible-light photocatalysis with mullite-type $Bi_2(Al_{1-x}Fe_x)_4O_9$: Striking the balance between bandgap narrowing and conduction band lowering. *ACS Catal.* **2018**, *8*, 8844–8855.

103.   Xu, A.; Gao, Y.; Liu, H. The preparation, characterization, and their photocatalytic activities of rare-earth-doped TiO_2 nanoparticles. *J. Catal.* **2002**, *207*, 151–157.

104.   Klosek, S.; Raftery, D. Visible light driven V-doped TiO_2 photocatalyst and its photooxidation of ethanol. *J. Phys. Chem. B* **2001**, *105*, 2815–2819.

105. Ehret, A.; Stuhl, L.; Spitler, M.T. Spectral sensitization of TiO_2 nanocrystalline electrodes with aggregated cyanine dyes. *J. Phys. Chem. B* **2001**, *105*, 9960–9965.

106. O'Regan, B.; Grätzel, M. A low-cost, high-efficiency solar cell based on dye-sensitized colloidal TiO_2 films. *Nature* **1991**, *353*, 737–740.

107. Cho, Y.; Choi, W.; Lee, C.; Hyeon, T.; Lee, H. Visible light-induced degradation of carbon tetrachloride on dye-sensitized TiO_2. *Environ. Sci. Technol.* **2001**, *35*, 966–970.

108. Chowdhury, P.; Moreira, J.; Gomaa, H.; Ray, A.K. Visible-solar-light-driven photocatalytic degradation of phenol with dye-sensitized TiO_2: Parametric and kinetic study. *Ind. Eng. Chem. Res.* **2012**, *51*, 4523–4532.

109. Ząbek, P.; Eberl, J.; Kisch, H. On the origin of visible light activity in carbon-modified titania. *Photochem. Photobiol. Sci.* **2009**, *8*, 264–269.

110. Tobaldi, D.M.; Seabra, M.P.; Otero-Irurueta, G.; de Miguel, Y.R.; Ball, R.J.; Singh, M.K.; Pullar, R.C.; Labrincha, J.A. Quantitative XRD characterisation and gas-phase photocatalytic activity testing for visible-light (indoor applications) of KRONOClean 7000®. *RSC Adv.* **2015**, *5*, 102911–102918.

111. Sankova, N.; Semeykina, V.; Selishchev, D.; Glazneva, T.; Parkhomchuk, E.; Larichev, Y.; Uvarov, N. Influence of tetraalkylammonium compounds on photocatalytic and physical properties of TiO_2. *Catal. Letters* **2018**, *148*, 2391–2407.

112. Mills, A.; Wang, J. Photobleaching of methylene blue sensitised by TiO_2: an ambiguous system? *J. Photochem. Photobiol. A Chem.* **1999**, *127*, 123–134.

113. *ISO 10678:2010 - Fine ceramics (advanced ceramics, advanced technical ceramics) -- Determination of photocatalytic activity of surfaces in an aqueous medium by degradation of methylene blue*; Geneva, 2010.

114. Tschirch, J.; Dillert, R.; Bahnemann, D. Photocatalytic degradation of methylene blue on fixed powder layers: Which limitations are to be considered? *J. Adv. Oxid. Technol.* **2008**, *11*, 193–198.

115. Nowotny, M.K.; Bahnemann, D.W. Improved photocatalytic performance of rutile TiO_2. *Phys. status solidi - Rapid Res. Lett.* **2011**, *5*, 92–94.

116. Burek, B.O.; Sutor, A.; Bahnemann, D.W.; Bloh, J.Z. Completely integrated wirelessly-powered photocatalyst-coated spheres as a novel means to perform heterogeneous photocatalytic reactions. *Catal. Sci. Technol.* **2017**, *7*, 4977–4983.

117. Senthilraja, A.; Subash, B.; Krishnakumar, B.; Rajamanickam, D.; Swaminathan, M.; Shanthi, M. Synthesis, characterization and catalytic activity of co-doped Ag–Au–ZnO for MB dye degradation under UV-A light. *Mater. Sci. Semicond. Process.* **2014**, *22*, 83–91.

118. Yang, M.; Liu, X.; Chen, J.; Meng, F.; Zhang, Y.; Brandl, H.; Lippert, T.; Chen, N. Photocatalytic and electrochemical degradation of methylene blue by titanium dioxide. *Chinese Sci. Bull.* **2014**, *59*, 1964–1967.

119. Lachheb, H.; Puzenat, E.; Houas, A.; Ksibi, M.; Elaloui, E.; Guillard, C.; Herrmann, J.-M. Photocatalytic degradation of various types of dyes (Alizarin S, Crocein Orange G, Methyl Red, Congo Red, Methylene Blue) in water by UV-irradiated titania. *Appl. Catal. B Environ.* **2002**, *39*, 75–90.

120. Kuo, W.S.; Ho, P.H. Solar photocatalytic decolorization of methylene blue in water. *Chemosphere* **2001**, *45*, 77–83.

121. Lakshmi, S.; Renganathan, R.; Fujita, S. Study on TiO$_2$-mediated photocatalytic degradation of methylene blue. *J. Photochem. Photobiol. A Chem.* **1995**, *88*, 163–167.

122. de Tacconi, N.R.; Carmona, J.; Rajeshwar, K. Reversibility of photoelectrochromism at the TiO$_2$/methylene blue interface. *J. Electrochem. Soc.* **1997**, *144*, 2486.

123. Bauldreay, J.M.; Archer, M.D. Dye-modified electrodes for photogalvanic cells. *Electrochim. Acta* **1983**, *28*, 1515–1522.

124. Karyakin, A.A.; Strakhova, A.K.; Karyakina, E.E.; Varfolomeyev, S.D.; Yatsimirsky, A.K. The electrochemical polymerization of methylene blue and bioelectrochemical activity of the resulting film. *Bioelectrochemistry Bioenerg.* **1993**, *32*, 35–43.

125. Yan, X.; Ohno, T.; Nishijima, K.; Abe, R.; Ohtani, B. Is methylene blue an appropriate substrate for a photocatalytic activity test? A study with visible-light responsive titania. *Chem. Phys. Lett.* **2006**, *429*, 606–610.

126. Lang, X.; Chen, X.; Zhao, J. Heterogeneous visible light photocatalysis for selective organic transformations. *Chem. Soc. Rev.* **2014**, *43*, 473–486.

127. Huang, C.L.; Sands, F.L. Effect of ultraviolet irradiation on chlorpromazine II: Anaerobic condition. *J. Pharm. Sci.* **1967**, *56*, 259–264.

128. Ljunggren, B.; Moller, H. Phenothiazine phototoxicity: an experimental study on chlorpromazine and related tricyclic drugs. *Acta Derm. Venereol.* **1977**, *57*, 325–329.

129. Saucin, M.; Van de Vorst, A. Photodynamic potentialities of some phenothiazine derivatives. *Radiat. Environ. Biophys.* **1980**, *17*, 159–168.

130. Kochevar, I.E. Phototoxicity mechanisms: Chlorpromazine photosensitized damage to DNA and cell membranes. *J. Invest. Dermatol.* **1981**, *77*, 59–64.

131. Davies, A.K.; Land, E.J.; Navaratnam, S.; Parsons, B.J.; Phillips, G.O. Pulse radiolysis study of chlorpromazine and promazine free radicals in aqueous solution. *J. Chem. Soc. Faraday Trans. 1 Phys. Chem. Condens. Phases* **1979**, *75*, 22.

132. Bahnemann, D.; Asmus, K.-D.; Willson, R.L. Phenothiazine radical-cations: Electron transfer equilibria with iodide ions and the determination of one-electron redox potentials by pulse radiolysis. *J. Chem. Soc. Perkin Trans. II* **1983**, 1669–1673.

133. Ateş, S.; Somer, G. Photodegradation of chlorpromazine in aqueous solutions as studied by ultraviolet-visible spectrophotometry and voltammetry. *J. Chem. Soc. Faraday Trans. 1* **1981**, *77*, 859–867.

134. Felmeister, A.; Discher, C.A. Photodegradation of chlorpromazine hydrochloride. *J. Pharm. Sci.* **1964**, *53*, 756–762.

135. Borg, D.C.; Cotzias, G.C. Interaction of trace metals with phenothiazine drug derivatives. III. Theoretical part. *Proc. Natl. Acad. Sci. U. S. A.* **1962**, *48*, 643–52.

136. Merkle, F.H.; Discher, C.A. Electrochemical oxidation of chlorpromazine hydrochloride. *J. Pharm. Sci.* **1963**, *53*, 620–623.

137. Cheng, H.Y.; Sackett, P.H.; Mccreery, R.L. Kinetics of chlorpromazine cation radical decomposition in aqueous buffers. *J. Am. Chem. Soc.* **1978**, *100*, 962–967.

138. Motten, A.G.; Buettner, G.R.; Chignell, C.F. Spectroscopic studies of cutaneous photosensitizing agents--VIII. A spin-trapping study of light induced free radicals from chlorpromazine and promazine. *Photochem. Photobiol.* **1985**, *42*, 9–15.

139. Iwaoka, T.; Kondo, M. Mechanistic studies on the photooxidation of chlorpromazine in water and ethanol. *Bull. Chem. Soc. Jpn.* **1974**, *47*, 980–986.

140. Davies, A.K.; Navaratnam, S.; Phillips, G.O. Photochemistry of chlorpromazine [2-chloro-N-(3-dimethylaminopropyl)phenothiazine] in propan-2-ol solution. *J. Chem.*

Soc. Perkin Trans. 2 **1976**, 25–29.

141. Huang, C.L.; Sands, F.L. The effect of ultraviolet irradiation on chlorpromazine : I. Aerobic condition. *J. Chromatogr. A* **1964**, *13*, 246–249.

142. Grant, F.W.; Greene, J. Phototoxicity and photonucleophilic aromatic substitution in chlorpromazine. *Toxicol. Appl. Pharmacol.* **1972**, *23*, 71–74.

143. S.Lee, M.; Edward H.Kerns LC/MS applications in drug development. *Mass Spectrom. Rev.* **1999**, *18*, 187–279.

144. Xu, L.; Klunk, L.J.; Prakash, C. Common liquid chromatography-mass spectrometry (LC-MS) methodology for metabolite identification. In *Mass Spectrometry in Drug Metabolism and Disposition: Basic Principles and Applications*; Lee, M.S., Zhu, M., Eds.; John Wiley & Sons, Inc.: Hoboken, New Jersey, 2011; pp. 291–319.

145. Mascher, H. *HPLC methods for clinical pharmaceutical analysis : a user's guide*; 1st ed.; Wiley-VCH: Weinheim, Germany, 2012; ISBN 9783527331291.

146. Snyder, L.R.; Kirkland, J.J.; Glajch, J.L. *Practical HPLC method development*; 2nd ed.; John Wiley & Sons, Inc.: Hoboken, NJ, USA, 1997; ISBN 9781118592014.

147. Boehme, C.L.; Strobel, H.W. High-performance liquid chromatographic methods for the analysis of haloperidol and chlorpromazine metabolism in vitro by purified cytochrome P450 isoforms. *J. Chromatogr. B Biomed. Sci. Appl.* **1998**, *718*, 259–266.

148. Chagonda, L.F.S.; Millership, J.S. High-performance liquid chromatographic determination of chlorpromazine and its degradation products in pharmaceutical dosage forms: A stability-indicating assay. *Analyst* **1988**, *113*, 233–237.

149. Watson, J.T.; Sparkman, O.D. Introduction. In *Introduction to Mass Spectrometry: Instrumentation, Applications and Strategies for Data Interpretation*; John Wiley & Sons, Ltd.: The Atrium, Southern Gate, Chichester, West Sussex, England, 2007; pp. 1–52 ISBN 9780470516348.

150. Hopfgartner, G.R. Theory and instrumentation of mass spectrometry. In *Mass Spectrometry in Drug Metabolism and Disposition: Basic Principles and Applications*; Lee, M.S., Zhu, M., Eds.; John Wiley & Sons, Inc.: Hoboken, New Jersey, 2011; pp. 257–290.

151. Smyth, W.F. Electrospray ionisation mass spectrometric behaviour of selected drugs and their metabolites. *Anal. Chim. Acta* **2003**, *492*, 1–16.

152. Kigondu, E.M.; Njoroge, M.; Singh, K.; Njuguna, N.; Warner, D.F.; Chibale, K. Synthesis and synergistic antimycobacterial screening of chlorpromazine and its metabolites. *Med. Chem. Commun.* **2014**, *5*, 502–506.

153. Alexandru, T.; Staicu, A.; Pascu, A.; Radu, E.; Stoicu, A.; Nastasa, V.; Dinache, A.; Boni, M.; Amaral, L.; Pascu, M.L. Characterization of mixtures of compounds produced in chlorpromazine aqueous solutions by ultraviolet laser irradiation: their applications in antimicrobial assays. *J. Biomed. Opt.* **2014**, *20*, 051002-1–11.

154. Colombo, D.P.; Bowman, R.M. Femtosecond diffuse reflectance spectroscopy of TiO_2 powders. *J. Phys. Chem.* **1995**, *99*, 11752–11756.

155. Serpone, N.; Lawless, D.; Khairutdinov, R.; Pelizzetti, E. Subnanosecond relaxation dynamics in TiO_2 colloidal sols (particle sizes R_p = 1.0-13.4 nm). Relevance to heterogeneous photocatalysis. *J. Phys. Chem.* **1995**, *99*, 16655–16661.

156. Willsher, C.J. The study of transient absorptions in optically dense materials by diffuse reflectance laser flash photolysis. *J. Photochem.* **1985**, *28*, 229–236.

157. Wilkinson, F.; Willsher, C.J. The use of diffuse reflectance laser flash photolysis to study primary photoprocesses in anisotropic media. *Tetrahedron* **1987**, *43*, 1197–1209.

158. Wilkinson, F.; Kelly, G.P. Laser flash photolysis on solid surfaces. *Stud. Surf. Sci. Catal.* **1989**, *47*, 30–47.

159. Schneider, J.; Nikitin, K.; Dillert, R.; Bahnemann, D.W. Laser-flash-photolysis-spectroscopy: a nondestructive method? *Faraday Discuss.* **2017**, *197*, 505–516.

160. Szczepankiewicz, S.H.; Moss, J.A.; Hoffmann, M.R. Electron traps and the stark effect on hydroxylated titania photocatalysts. *J. Phys. Chem. B* **2002**, *106*, 7654–7658.

161. Kumar, C.P.; Gopal, N.O.; Wang, T.C.; Wong, M.-S.; Ke, S.C. EPR investigation of TiO_2 nanoparticles with temperature-dependent properties. *J. Phys. Chem. B* **2006**, *110*, 5223–5229.

162. Szczepankiewicz, S.H.; Moss, J.A.; Hoffmann, M.R. Slow surface charge trapping kinetics on irradiated TiO_2. *J. Phys. Chem. B* **2002**, *106*, 2922–2927.

163. Bahnemann, D.; Henglein, A.; Lilie, J.; Spanhel, L. Flash photolysis observation of the absorption spectra of trapped positive holes and electrons in colloidal titanium dioxide. *J. Phys. Chem.* **1984**, *88*, 709–711.

164. Bahnemann, D.; Henglein, A.; Spanhel, L. Detection of the intermediates of colloidal TiO$_2$-catalysed photoreactions. *Faraday Discuss. Chem. Soc.* **1984**, *78*, 151.

165. Boschloo, G.; Fitzmaurice, D. Spectroelectrochemical investigation of surface states in nanostructured TiO$_2$ electrodes. *J. Phys. Chem. B* **1999**, *103*, 2228–2231.

166. Boschloo, G.; Fitzmaurice, D. Electron accumulation in nanostructured TiO$_2$ (Anatase) electrodes. *J. Phys. Chem. B* **1999**, *103*, 7860–7868.

167. Koelle, U.; Moser, J.; Graetzel, M. Dynamics of interfacial charge-transfer reactions in semiconductor dispersions. Reduction of cobaltoceniumdicarboxylate in colloidal titania. *Inorg. Chem.* **1985**, *24*, 2253–2258.

168. Cowan, A.J.; Leng, W.; Barnes, P.R.F.; Klug, D.R.; Durrant, J.R. Charge carrier separation in nanostructured TiO$_2$ photoelectrodes for water splitting. *Phys. Chem. Chem. Phys.* **2013**, *15*, 8772.

169. Schneider, J.; Matsuoka, M.; Takeuchi, M.; Zhang, J.; Horiuchi, Y.; Anpo, M.; Bahnemann, D.W. Understanding TiO$_2$ Photocatalysis: Mechanisms and Materials. *Chem. Rev.* **2014**, *114*, 9919–9986.

170. Yoshihara, T.; Katoh, R.; Furube, A.; Tamaki, Y.; Murai, M.; Hara, K.; Murata, S.; Arakawa, H.; Tachiya, M. Identification of reactive species in photoexcited nanocrystalline TiO$_2$ films by wide-wavelength-range (400−2500 nm) transient absorption spectroscopy. *J. Phys. Chem. B* **2004**, *108*, 3817–3823.

171. Kuznetsov, A.I.; Kameneva, O.; Alexandrov, A.; Bityurin, N.; Marteau, P.; Chhor, K.; Sanchez, C.; Kanaev, A. Light-induced charge separation and storage in titanium oxide gels. *Phys. Rev. E* **2005**, *71*, 021403.

172. Shen, Q.; Katayama, K.; Sawada, T.; Yamaguchi, M.; Kumagai, Y.; Toyoda, T. Photoexcited hole dynamics in TiO$_2$ nanocrystalline films characterized using a lens-free heterodyne detection transient grating technique. *Chem. Phys. Lett.* **2006**, *419*, 464–468.

173. Ikeda, S.; Sugiyama, N.; Murakami, S.; Kominami, H.; Kera, Y.; Noguchi, H.; Uosaki, K.; Torimoto, T.; Ohtani, B. Quantitative analysis of defective sites in titanium(IV) oxide photocatalyst powders. *Phys. Chem. Chem. Phys.* **2003**, *5*, 778–783.

174. Furube, A.; Asahi, T.; Masuhara, H.; Yamashita, H.; Anpo, M. Charge carrier

dynamics of standard TiO_2 catalysts revealed by femtosecond diffuse reflectance spectroscopy. *J. Phys. Chem. B* **1999**, *103*, 3120–3127.

175. Feng, H.; Tan, S.; Tang, H.; Zheng, Q.; Shi, Y.; Cui, X.; Shao, X.; Zhao, A.; Zhao, J.; Wang, B. Temperature- and coverage-dependent kinetics of photocatalytic reaction of methanol on TiO_2 (110)-(1 × 1) surface. *J. Phys. Chem. C* **2016**, *120*, 5503–5514.

176. Schneider, J.; Nikitin, K.; Wark, M.; Bahnemann, D.W.; Marschall, R. Improved charge carrier separation in barium tantalate composites investigated by laser flash photolysis. *Phys. Chem. Chem. Phys.* **2016**, *18*, 10719–10726.

177. Nie, J.; Schneider, J.; Sieland, F.; Xia, S. The role of Au loading for visible-light photocatalytic activity of Au-TiO_2 (anatase). *J. Photochem. Photobiol. A Chem.* **2018**, *366*, 111–117.

178. Lim, J.; Kwak, D.; Sieland, F.; Kim, C.; Bahnemann, D.W.; Choi, W. Visible light-induced catalytic activation of peroxymonosulfate using heterogeneous surface complexes of amino acids on TiO_2. *Appl. Catal. B Environ.* **2018**, *225*, 406–414.

179. Iwaoka, T.; Kondo, M. Photoionization of chlorpromazine hydrochloride in binary mixed solvent systems. *Bull. Chem. Soc. Jpn.* **1977**, *50*, 1–5.

180. Maruthamuthu, P.; Sharma, D.K.; Serpone, N. Subnanosecond relaxation dynamics of 2,2'-Azinobis(3-ethylbenzothiazoline-6-sulfonate) and chlorpromazine. Assessment of photosensitization of a wide band gap metal oxide semiconductor TiO_2. *J. Phys. Chem.* **1995**, *99*, 3636–3642.

181. Alkaitis, S.A.; Beck, G.; Graetzel, M. Laser photoionization of phenothiazine in alcoholic and aqueous micellar solution. Electron transfer from triplet states to metal ion acceptors. *J. Am. Chem. Soc.* **1975**, *97*, 5723–5729.

182. Mohamed, H.H.; Mendive, C.B.; Dillert, R.; Bahnemann, D.W. Kinetic and mechanistic investigations of multielectron transfer reactions induced by stored electrons in TiO_2 nanoparticles: A stopped flow study. *J. Phys. Chem. A* **2011**, *115*, 2139–2147.

183. García, C.; Smith, G.A.; Mcgimpsey, W.G.; Kochevar, I.E.; Redmond, R.W. Mechanism and solvent dependence for photoionization of promazine and chlorpromazine. *J. Am. Chem. Soc* **1995**, *117*, 10871–10878.

184. Khataee, A.R.; Fathinia, M.; Joo, S.W. Simultaneous monitoring of photocatalysis

of three pharmaceuticals by immobilized TiO_2 nanoparticles: Chemometric assessment, intermediates identification and ecotoxicological evaluation. *Spectrochim. Acta - Part A Mol. Biomol. Spectrosc.* **2013**, *112*, 33–45.

Chapter 2: Visible-Light Photocatalytic Activity of Zinc Ferrites

2.1. Forewords

Despite the comprehensive investigations on photocatalytic reactions utilizing UV light, recently a lot of attention has been focused towards the solar- or visible light-driven photocatalytic processes and visible light-absorbing materials such as metal oxides. Zinc ferrite is among the semiconducting materials considered as one of the potential candidates for visible light-driven photocatalytic purposes. Nevertheless, the preparation procedure seems to have an important impact on the physiochemical properties and consequently, on the energetic position of the conduction band and the valence band in zinc ferrite. Hence, different photocatalytic activities have been reported for zinc ferrites prepared through varying synthetic methods. In most of the scientific studies, organic dyes, such as MB, are used as model compounds to confirm the reported visible light activity of zinc ferrite. However, it is commonly neglected that the possible photo-reduction of the dye molecule might be the reason of the observed bleaching of the dye. In addition, in some cases, the visible light emission and the dye's absorption spectra might overlap with each other and the photobleaching of the dye molecule is mistaken with its photocatalytic degradation. Thus, in this chapter, the degradation of MB, a member of the phenothiazine group, under visible light irradiation in the presence of zinc ferrite was evaluated.

This chapter contains the article "Visible-Light Photocatalytic Activity of Zinc Ferrites" by Arsou Arimi, Lena Megatif, Luis I. Granone, Ralf Dillert, and Detlef W. Bahnemann, published in the Journal of Photochemistry and Photobiology A: Chemistry (doi:10.1016/j.jphotochem.2018.03.014). Herein, seven zinc ferrite samples were prepared through different synthetic methods. The crystalline size and purity, the surface area, the flat band potentials and the bandgap energies of the prepared zinc ferrite samples were determined in order to understand the effect of synthetic method on the photocatalytic activity of the material. Accordingly, a series of detailed wavelength dependent measurements at wavelengths of 365, 455, 505, and 660 nm for the photocatalytic degradation of MB were performed. Despite the observed photobleaching of MB under visible light irradiation, this effect was not found to be initiated by hole or •OH mediated

oxidation. It was rather contributed to the electron transfer from photo-excited methylene blue molecules attached to the zinc ferrite surface into the conduction band of the semiconducting ferrite.

2.2. Abstract

Zinc ferrite samples were prepared at temperatures between 75°C and 1100°C employing published synthetic methods. Phase pure zinc ferrites were, however, only obtained through high-temperature methods (more than 800°C) as revealed by XRD and Raman analysis. Photocatalytic experiments under UV and visible light irradiation as well as a series of detailed wavelength dependent measurements applying monochromatic light sources emitting at wavelengths of 365, 455, 505, and 660 nm were performed. Visible light-induced bleaching of methylene blue in aqueous suspensions of zinc ferrites was observed. However, no photocatalytic formation of OH radicals was detected. The results of flat band potential measurements revealed the interfacial electron transfer from an excited methylene blue molecule into the conduction band of zinc ferrite to be thermodynamically possible. The bleaching of methylene blue containing suspensions under visible light irradiation is, therefore, assumed to be initiated by an interfacial electron transfer from photo-excited methylene blue molecules adsorbed on the ferrite surface into the conduction band of the semiconducting zinc ferrite.

Keywords: Photocatalysis; spinel ferrite; zinc ferrite; dye photobleaching; methylene blue; wavelength dependent measurements.

2.3. Introduction

During the past decades, heterogeneous photocatalysis has exhibited great potential as a suitable tool for environmental remediation [1,2] as well as clean and renewable energy generation [3]. Although the pioneering investigations in this field have been carried out using UV-light-absorbing photocatalysts [4], the current demand for efficient solar light harvesting systems has directed the interests to visible light-absorbing semiconductors. In this sense, ferrites with the general formula of MFe_2O_4 have been reported to be promising compounds for water splitting [5,6] and water treatment [7] due to their low cost, chemical and thermal stability, and narrow bandgap (ca. 1.9 eV [5]). Most ferrites of this stoichiometry crystallize in the spinel structure with oxide anions arranged in a cubic close-packed lattice and M and Fe cations occupying tetrahedral and/or octahedral sites [5]. Zinc

ferrite, $ZnFe_2O_4$, one of the most widely studied ferrites for photocatalytic and photoelectrocatalytic applications, has been reported to exhibit a normal spinel structure, with Zn^{2+} and Fe^{3+} cations in tetrahedral and octahedral sites, respectively [8–10].

Several authors have reported photocatalytic hydrogen evolution from aqueous zinc ferrite suspensions containing sacrificial reagents under visible light illumination [10–12]. However, in most cases the photocatalytic activity was determined via the degradation of organic dyes, such as methyl orange [13,14], rhodamine B [15], and methylene blue (MB) [16,17]. Organic dyes are usually chosen as the probe molecule due to facile quantification of their concentration employing spectrophotometric techniques. However, the suitability of dyes as probe molecules to determine the activity of a photocatalyst has already been questioned by some authors. Mills and Wang [18] have shown that photo-bleaching of MB in a TiO_2 aqueous suspension under UV-light irradiation can be an ambiguous system. The observed bleaching may not necessarily be due to photocatalytic dye oxidation, since other processes such as dye reduction can result in the same effect. The situation might even become more complicated when using a radiation source emitting visible light, since the light emission and the MB absorption spectra can overlap with each other yielding excited MB molecules. Subsequent reactions of excited MB may lead to the wrong conclusion that a semiconductor has a visible light photocatalytic activity as have been demonstrated by Yan *et al.* [19].

Accordingly, the question arises whether the reported photocatalytic activities of zinc ferrites have been overestimated due to employing organic dyes as model compounds. To answer this question, zinc ferrite samples were synthesized via different synthetic routes, and diverse photocatalytic activity tests were employed to investigate the behavior of these samples as visible light-absorbing photocatalysts.

2.4. Materials and Methods

2.4.1. Materials

For the synthesis of different zinc ferrite (ZFO) samples, zinc nitrate hexahydrate (98%), iron nitrate nonahydrate (98%), zinc oxide (≥99%), iron oxide (nano-powder < 50 nm), oxalic acid (≥99%), citric acid (99.5%), ethylene glycol (99.8%), and tetrabutyl ammonium hydroxide (40% in water) were used. NaOH (pellets, 99%) was employed in order to adjust the pH. Commercial zinc ferrite (nano-powder < 100 nm) and all other chemicals in the

present study were purchased from Sigma-Aldrich (if no additional notation is made) and were used without further purification. Titanium dioxide (anatase-rutile mixture, Aeroxide® TiO$_2$ P25) was purchased from Evonik Industries.

2.4.2. Synthesis of ZFOs

Four different synthetic methods reported to yield photocatalytically active ZFO, i.e., reflux [20], hydrothermal [20], solid-state reaction [21,22], and polymer complex method [21,22], were applied in order to produce different ZFO samples.

For the reflux synthesis (RF-75), Zn(NO$_3$)$_2$·6H$_2$O and Fe(NO$_3$)$_3$·9H$_2$O were dissolved in deionized water under constant stirring. Oxalic acid was then added as chelating precipitant (Zn:Fe:acid = 1:2:4) and a 20% w/w aqueous tetrabuthyl ammonium hydroxide solution was used as peptizing agent. The pH of the resulting solution was raised to 10 with a 10 M sodium hydroxide solution at room temperature in order to deprotonate the oxalic acid and cause the co-precipitation of metal oxalates. The flask containing the resulting suspension was fitted with a condenser and kept for 24 h at 75°C and then it was left to be cooled to room temperature [20].

For the hydrothermal synthesis, the same procedure was followed and after adjusting the pH, the resulting suspension was sealed in a PTFE cup, placed in a stainless steel autoclave, heated at 135°C (HT-135) and 175°C (HT-175) separately for 24 h and then allowed to cool down to room temperature. In both cases, the resulting solid powder was isolated by centrifugation, washed with deionized water and ethanol (two times each), and dried in an open-air oven at 60°C [20].

For the polymer complex route (PC-1100), Zn(NO$_3$)$_2$·6H$_2$O, and Fe(NO$_3$)$_3$·9H$_2$O were used as precursors in the required stoichiometric ratio. Citric acid was dissolved in water under constant agitation at 70°C. The salts of Zn(NO$_3$)$_2$·6H$_2$O and Fe(NO$_3$)$_3$.9H$_2$O were then dissolved in the citric acid solution. Finally, ethylene glycol was added to the mixture and it was kept at 24°C until it became a transparent solution. The solution was then heated at 130 °C for several hours until a polymeric gel was obtained. The viscous polymeric product was pyrolyzed at 400 °C for 2 h to form the precursor powder which was grounded and calcined at 1100 °C for 2 h to obtain the nano-crystalline ZFO [21,22].

For the synthesis through solid-state reaction, two routes were approached. In the first route (SO-1100), stoichiometric amounts of ZnO and Fe$_2$O$_3$ were mixed and grounded in

methanol. The pelletized powder was calcined at 1100 °C for 4 h to obtain the desired crystalline phase. In the second route, stoichiometric amounts of $Zn(NO_3)_2.6H_2O$ and $Fe(NO_3)_3.9H_2O$ were dissolved in distilled water and the solution was dehydrated in an oil bath until dryness. The amorphous powder was separated into two parts which were calcined at 800°C (SN-800) and 1100°C (SN-1100) separately in a furnace to obtain the desired crystalline phase [21,22].

2.4.3. Characterization

The synthesized ZFO powders were characterized by X-ray diffraction (XRD) using Cu Kα radiation ($\lambda = 0.154178$ nm) with a Bruker D8 Advanced Diffractometer. The patterns were recorded in the 2θ range between 20° and 80° in steps of 0.011°. The particle sizes were estimated using the Debye–Scherrer formula. Raman spectra were recorded employing a confocal Raman microscope (Senterra Bruker Optik GmbH). All spectra were obtained in backscattering geometry using a microscope device that allows the incident light (633 nm He-Ne laser with a maximal power of 20 mW) to be focused on the sample as a spot of about 2 μm in diameter.

The specific surface area of the samples was determined employing the Brunauer-Emmett-Teller (BET) method by nitrogen adsorption using a Micromeritics BET analyzer. The samples were degassed at 150°C prior to the specific surface area measurements.

The bandgap energies of the synthesized photocatalyst powders were determined by means of the diffuse reflectance technique employing a UV-visible Cary-100 spectrophotometer.

2.4.4. Photocatalytic Experiments

Photocatalytic experiments were carried out employing methylene blue (MB) as the probe molecule. These studies were performed under both UV and visible light irradiation using a UV setup (16 Philips 40W UV lamps) and a xenon lamp (450 W, Mueller Elektronik-Optik, $\lambda \geq 360$ nm by means of a cut-off filter). For these initial experiments, a quartz batch reactor (100 ml) with a cooling water circulation jacket was employed.

The wavelength dependent measurements were carried out in a 50 ml glass reactor covered in a black polymer shell connected at the top with a monochromatic LED light source (Thorlabs) emitting at 365, 455, 505 or 660 nm. This reactor was designed similar to a black

body reactor [23] in which the light entrance is small. Therefore, it is assumed that the light loss due to the back reflection or transmission is negligible and nearly all of the incoming light is absorbed by the photocatalyst. The spectral irradiance of the lamps was measured by means of a SpectraRad® Xpress (B&W Tek) spectral irradiance meter.

In all experimental runs, aqueous suspensions containing 20 µM MB and 1 g l^{-1} photocatalyst were used. Before irradiation, the suspensions were stirred in the dark for 60 min in order to ensure adsorption equilibrium. Subsequently, the suspensions were irradiated for 240 minutes. Samples were taken from the reactor at given time intervals. After being centrifuged, the obtained supernatant was analyzed using a UV-visible Cary-100 spectrophotometer. The fractional conversion at time t was calculated with $X_t = (A_0 - A_t)/A_0$ using the absorbance of MB at 664 nm for each sample. A_0 and A_t are the initial absorbance and the absorbance at time t, respectively. Accordingly, the fractional conversion of MB during irradiation was calculated by $X_{irr} = (A_{60} - A_{300})/A_{60}$ with A_{60} and A_{300} being the absorbance measured 60 min and 300 min after the start of the experimental run, respectively.

These experiments were also performed using two other model compounds, namely, formic acid ($\geq$ 96%) and ammonium formate ($\geq$99.99%). Moreover, the same experiments were performed with P25 as a photocatalyst for the purpose of comparison.

2.4.5. Determination of OH radicals

The terephthalic acid (TA) test [24] and the coumarin test [25] were carried out to detect photocatalytic hydroxyl radical generation. The TA test was performed for all the ZFO photocatalysts synthesized through different synthetic methods. Initially, a calibration curve with the known concentrations of 2-hydroxyterephthalic acid (97%) was prepared. For the •OH measurements, the ZFO photocatalysts were added to solutions containing 0.2 and 0.4 mM TA (99%) and 1 mM NaOH to get final catalyst concentrations of 1 and 2 g l^{-1}, respectively. After ultrasonic dispersion for 30 min, the suspension was then left under continuous stirring in the dark for 1 h. For the coumarin test, the ZFO photocatalyst was added to a 1 mM coumarin (99%) solution to get a final concentration of 1 g l^{-1} and then the same procedure was performed.

Afterwards, in both cases, the suspensions were irradiated with UV light. Samples were taken in the desired time intervals. These samples were centrifuged at 2000 rpm in order to

separate the catalyst from the liquid. The supernatant was analyzed using a Hitachi fluorescence spectrophotometer model F-700 recording the emission in the range of 400 to 600 nm (excitation wavelength = 315 nm).

2.4.6. Capacitance Measurements

Electrochemical measurements were performed in a Teflon-made three-electrode electrochemical cell with a Pt counter electrode and an Ag/AgCl/KCl (3M) reference electrode. As working electrodes, ferrite films on fluorine-doped tin oxide (FTO) glasses (Sigma-Aldrich) were prepared using the doctor blade technique. The paste used for the coating process consisted in 200 mg of ferrite powder which was treated in a mortar along with 100 μl of Triton X-100, 100 mg of polyethylene glycol 1000 (Merck) and 400 μl of deionized water. Capacitance measurements were carried out employing a ZENNIUM Electrochemical Workstation (ZAHNER-elektrik) using a 1.00 molar NaOH solution as the electrolyte and a frequency of 10 kHz.

2.5. Results

In the current study, seven zinc iron oxide (ZFO) samples were synthesized for photocatalytic application via reflux, hydrothermal, polymer complex, and solid-state methods by applying diverse precursors and reaction temperatures. The different synthetic methods yielded solids with colors varying from light brown to dark brown. Moreover, the magnetic properties of the products obtained via the different synthetic methods were found to be different (data not shown).

The XRD patterns of the synthesized ZFO samples as well as the XRD pattern of a commercially available zinc ferrite are presented in **Figure 2-1**. For the purpose of comparison, the standard data of the cubic spinel zinc ferrite phase with the Fd3m space group (JCPDS card No. 74-2397) is presented as well (vertical lines). All positions and intensities of the ZFO nanocrystals could be indexed to the standard PDF. This indicates that the as-prepared samples have mainly the cubic spinel phase structure of ZFO. The XRD patterns of all samples show peaks at 2θ values of 29.9°, 35.3°, 36.9°, 42.8°, 53.1°, 56.6°, and 62.2° which correspond to the (220), (311), (222), (400), (422), (511), and (440) crystal planes of cubic $ZnFe_2O_4$ with spinel structure [26].
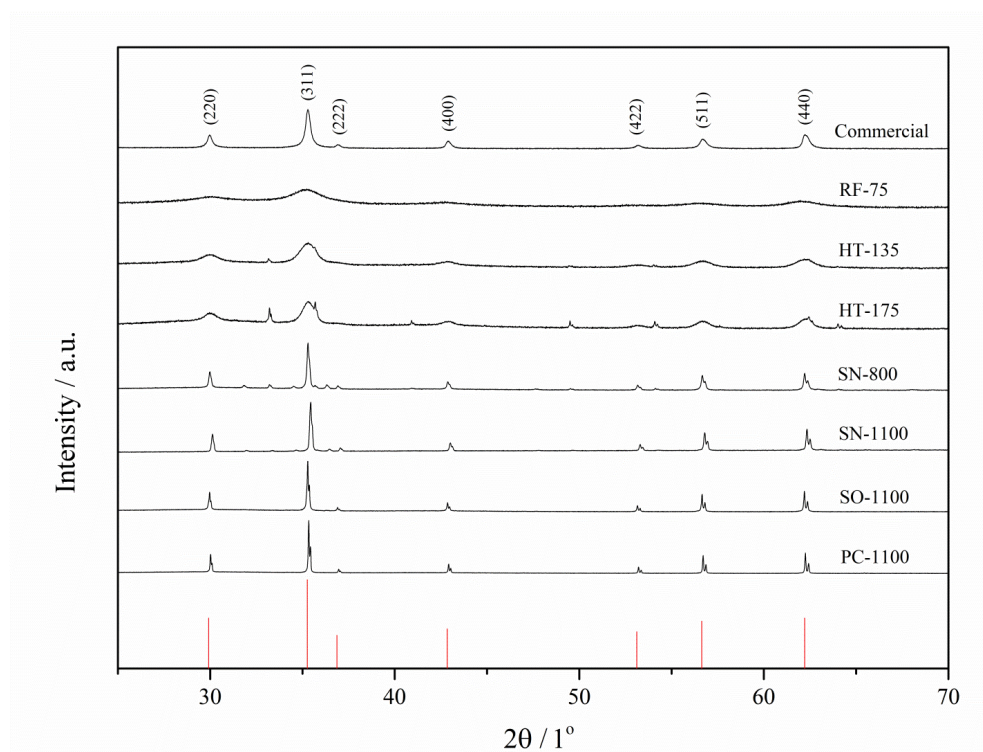
Figure 2-1. XRD spectra of the commercial zinc ferrite and the synthesized ZFO samples.

The average crystallite sizes of the samples synthesized through different methods were estimated by the Debye–Scherrer formula and from the measured BET surface areas (**Table 2-1**). The synthesized ZFO nanoparticles were found to have a particle size between 5 and 130 nm and a surface area between 7 and 210 m^2g^{-1} depending on the synthetic method. It becomes obvious from these data that zinc ferrites with high particle size and low surface area were specifically obtained at reaction temperatures higher than 800°C.

Due to the similarity between the structures of $ZnFe_2O_4$ and γ-Fe_2O_3 [27], XRD measurements may not be appropriate to determine the purity of the synthesized ZFO. Because of the high intensity of two of the Raman absorption modes of α-Fe_2O_3 [28], small impurities of this compound that may not identified by XRD can be detected. Therefore, Raman studies were carried out in order to characterize the samples. The Raman spectra of a commercial $ZnFe_2O_4$ and the different synthesized samples are given in **Figure 2-2**.
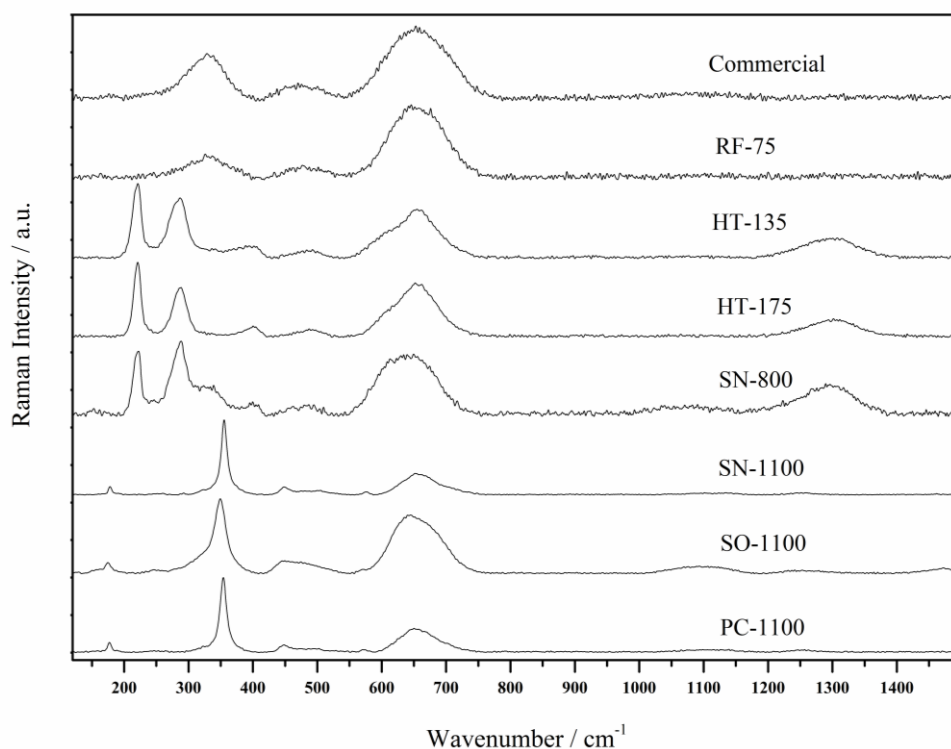
Figure 2-2. Raman spectra of the commercial zinc ferrite and the synthesized ZFO samples.

The observed Raman bands of the ZFO samples and some values extracted from the literature are presented in **Table 2-2**. HT-135, HT-175, and SN-800 samples show the two characteristic $\alpha\text{-}Fe_2O_3$ Raman bands at 220 and 288 cm^{-1} [23]. These characteristic bands for $\alpha\text{-}Fe_2O_3$ are not observed in the spectra of commercial zinc ferrite as well as in the spectra of the RF-75, SN-1100, SO-1100, and PC-1100 sample. No Raman bands are detected at around 381 and 718 cm^{-1} being characteristic for $\gamma\text{-}Fe_2O_3$ [29] are detected thus confirming the absence of this oxide in all samples.

Table 2-1. Measured physico-chemical properties of the ZFO samples

No.	ZFO Sample	Synthetic Method	Crystallite Size / nm	BET Surface Area / m^2g^{-1}	Band Gap Energy / eV	Flat Band Potential at pH 0 vs. NHE / V	Donor Density / 10^{19} cm^{-3}	X_{irr} (UV)	X_{irr} (VIS)
1	Commercial		27	43	1.87	0.54	5.79	~ 0	0.43
2	RF-75	Reflux at 75°C	5	210	1.86	0.26	6.84	~ 0	0.46
3	HT-135	Hydrothermal at 135°C	8	120	1.88	0.23	9.12	~ 0	0.45
4	HT-175	Hydrothermal at 175°C	10	95	1.91	0.31	9.26	~ 0	0.43
5	SN-800	Solid State Reaction at 800°C	50	20	1.95	-0.15	1.07	0.1	0.61
6	SN-1100	Solid State Reaction at 1100°C	100	11	1.89	-0.15	4.7	0.26	0.9
7	SO-1100	Solid State Reaction at 1100°C	110	7.8	1.89	-0.14	1.03	0.17	0.99
8	PC-1100	Polymer Complex at 1100°C	130	8.6	1.88	0.18	9.52	0.09	0.8
9	[photolysis]							~ 0	0.2

Note: X_{irr} (UV) and X_{irr} (VIS) are the fractional conversion under UV and visible light illumination, respectively.

Table 2-2. Raman absorption bands observed for ZFO samples and values extracted from the literature

Sample	Raman absorption band / cm^{-1}											
Commercial	1315 vw, br		1087 vw, br	652 s		472 w		333 m				
RF-75	1301 vw, br		1100 vw, br	648 s		476 w		329 m				
HT-135		1300 m		657 s		486 w	395 w	338 vw	288 vs		220 vs	
HT-175		1300 m		657 s		490 w	400 w	338 sh	288 vs		220 vs	
SN-800		1300 m	1068 w	640 s		490 w	400 w	338 Sh	288 vs		220 s	152 vw
SN-1100	1257 vw, br		1112 vw, br	655 m	576 w	447 w		355 Vs		249 vw		178 w
SO-1100	1250 w		1100 w	643 s	576 sh	447 w		350 vs		249 vw		174 w
PC-1100	1250 w		1110 w	655 m	576 vw	448 w		355 vs		250 vw		178 w
Wang et al.[30]	Raman spectrum measured up to 900 cm^{-1}			647 (A$_{1g}$) m		451 (F$_{2g}$) m		355 (F$_{2g}$) s		246 (E$_g$) vw	221 (F$_{2g}$) vw	
Sousa et al.[31]	1350 vbr		1160 vw	676 s, vbr		495 m, br		361 m, br				
Singh et al.[32]	1580 w, br	1288	1101	656		491		344				

Note: w = weak, m = medium, s = strong, v= very, br = broad, and sh = shoulder

The photocatalytic activities of the ZFO nanocrystals synthesized through different methods were investigated via the bleaching reaction of MB under UV and visible light irradiation. The graphs of the calculated fractional conversion of aqueous MB in the presence of ZFO as well as TiO$_2$ P25 versus time are shown in **Figure 2-3** and **Figure 2-4**. In these graphs, the first 60 minutes correspond to the dark period.

Figure 2-3. Photobleaching of MB as a function of UV light exposure time for an initial concentration of 20 μM and with and without ZFO (1 g l^{-1}). The first 60 minutes correspond to the dark period.

As can be seen from **Figure 2-3** no significant decrease of the dye concentration was observed under UV light irradiation in the presence of ZFO. The fractional conversion of MB under UV irradiation was relatively low with most of the ZFO samples employed here. The SN-1100, SO-1100, PC-1100, and SN-800 samples show conversions X_{irr}(UV) of 0.26, 0.17, 0.09, and 0.10, respectively (**Table 1-1**). All ZFOs synthesized at reaction temperatures lower than 800°C showed almost no activity. The bleaching of a homogeneous solution of MB was found to be negligible under these experimental conditions.

The photocatalytic assisted degradation of formic acid and ammonium formate, two model molecules that do absorb neither visible nor UV light irradiation within the wavelength range used for the excitation of the solids were also investigated. Experimental runs were

carried out with these two compounds under UV light using 1g l^{-1} of ZFO nanocrystals. Only about 9 % and 8 % of formic acid and ammonium formate (initial concentration = 50 mM) were converted during 180 min of UV irradiation.
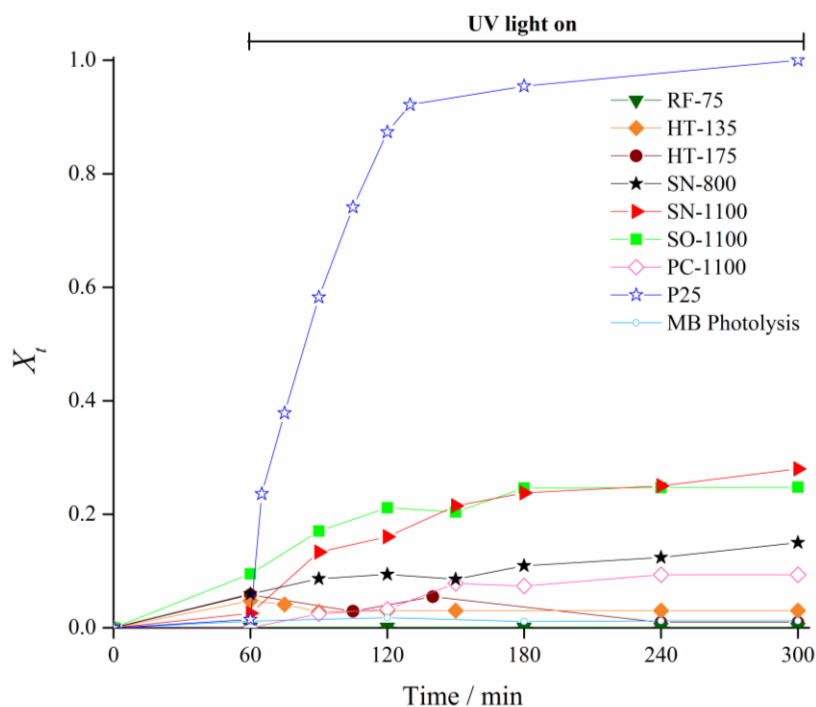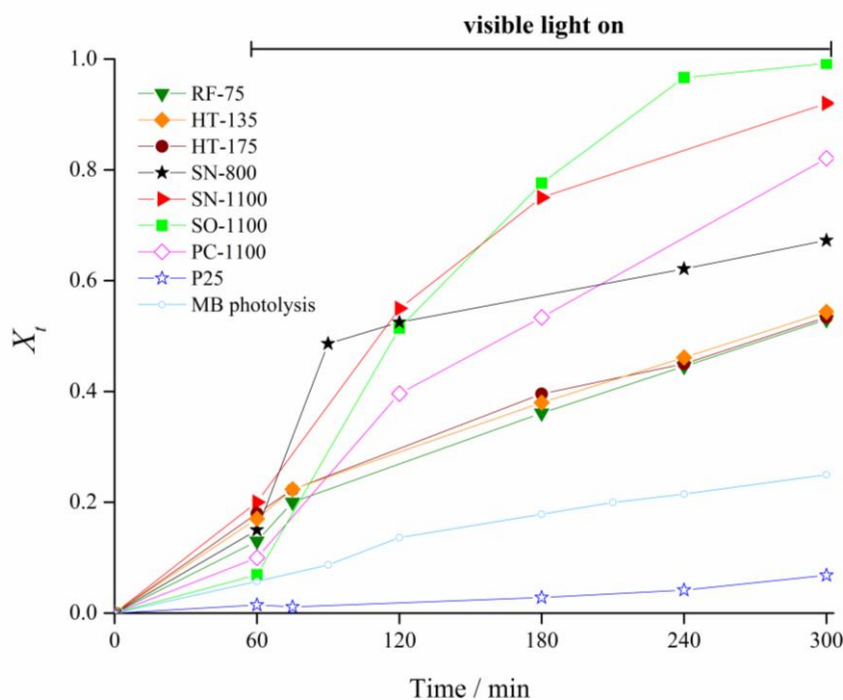

Figure 2-4. Photobleaching of MB as a function of visible light exposure time for an initial concentration of 20 μM and with and without ZFO (1 g l^{-1}). The first 60 minutes correspond to the dark period.

Photo-bleaching of MB was also conducted under visible light irradiation (**Figure 2-4**). As becomes obvious from data presented in **Table 2-1** and the graphs given in **Figure 2-4**, among all the ZFOs, SO-1100 shows the highest conversion during irradiation with visible light (X_{irr}(VIS) = 0.99), followed by SN-1100 (0.90), PC-1100 (0.80), SN-800 (0.61), and RF-75 (0.46). For the purpose of comparison an experimental run was performed with a homogeneous MB solution under visible light irradiation. A fractional conversion of 0.20 was observed within 240 minutes.

To get a deeper insight into the wavelength dependence of the photocatalytic activity of zinc ferrite the light-induced bleaching of MB in the presence of a ZFO semiconductor (SO-1100) was investigated employing four nearly monochromatic light sources with λ_{max} at 365, 455, 505 and 660 nm. The results of this set of experimental runs are gathered in **Figure 2-5**.
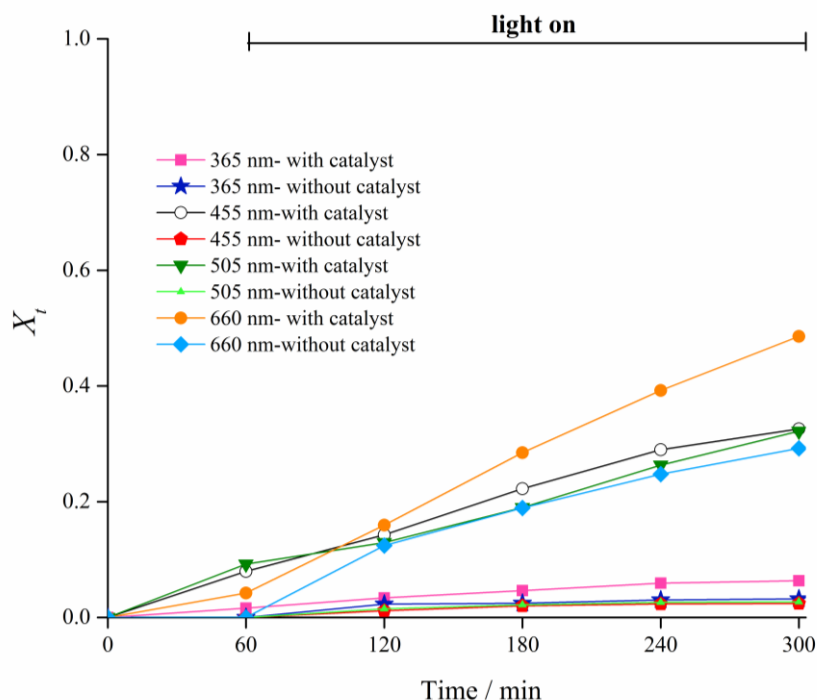
Figure 2-5. Light-induced conversion of MB in the presence of SO-1100 at different irradiation wavelengths

However, since these four lamps did not have the same intensity, the obtained fractional conversion after 240 min of irradiation, X_{irr}, had to be processed. Thus, the normalized photocatalytic conversion (X_{norm}) for an equal number of photons (N) was calculated. The number of photons (s^{-1} cm^{-2}) was calculated with:

$$N = \int_{\lambda_1}^{\lambda_2} \frac{I}{E} \, d\lambda \tag{2-1}$$

The spectral irradiance, I (mW cm^{-2} nm^{-1}) was measured using a spectral irradiance meter. The energy of a photon E with wavelength λ was calculated by the Planck–Einstein relation $E = hc/\lambda$, where h is the Planck constant equal to $6.62607004 \times 10^{-34}$ m^2 kg s^{-1} and c is the speed of light equal to 299 792 458 m s^{-1}. Since the lamp with 365 nm irradiation wavelength emitted the lowest photon flux (**Table 2-3**) a normalized photocatalytic conversion X_{norm} was defined as the photocatalytic conversion of each experimental run divided by the relative number of photons $N/N_{365\ nm}$. The calculated data are presented in **Table 2-3.**

Table 2-3. Normalized photocatalytic conversion data for degradation of MB in the presence of SO-1100 as a function of irradiation wavelength

Wavelength / nm	N = Number of photons / s^{-1} cm^{-2}	X_{irr}	$X_{norm}= X_{irr} \times N_{365\ nm}$ / N
365	1.12×10^{16}	0.05	0.05
455	7.47×10^{16}	0.27	0.04
505	3.36×10^{16}	0.25	0.08
660	10.9×10^{16}	0.46	0.05

The normalized fractional conversion of MB in the presence of SO-1100, commercial zinc ferrite and TiO$_2$ P25 (being a well-known UV active photocatalyst) as well as the normalized fractional conversion during MB photolysis are presented in **Figure 2-6**. According to these data, the highest MB bleaching rate was found under irradiation with a 505 nm light source; however, the conversion was only about 8%.
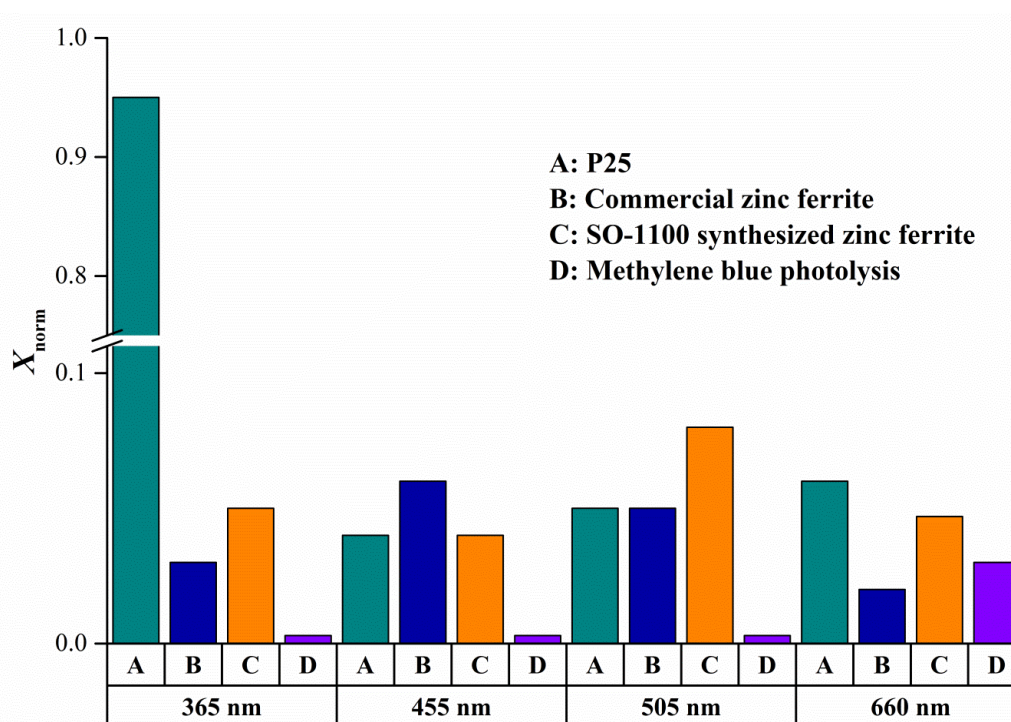
Figure 2-6. Methylene blue conversion in the presence of TiO$_2$ P25, synthesized zinc ferrite SO-1100, and commercial zinc ferrite as well as in the absence of a semiconducting oxide after irradiation with different wavelengths for 240 min.

The hydroxyl radical is assumed to be the major reactant responsible for the oxidation of chemical compounds through photocatalytic processes [33]. By measuring the amount of hydroxyl radicals formed on the catalyst surface exposed to UV light in aqueous

suspension, the photocatalytic degradation of MB with hydroxyl radicals generated by photoexcitation of photocatalyst nanoparticles can be examined and correlated. For the detection (and quantitative measurement) of OH radicals produced by photoexcitation of the electrons inside the photocatalyst under UV irradiation, fluorescence spectroscopy was applied using terephthalic acid as the probe molecule. This acid is known to yield the fluorescent 2-hydroxyterephthalic acid via reaction with a hydroxyl radical [34].

Figure 2-7 reveals the fluorescence intensity of the TA samples after UV irradiation in the presence of different synthesized ZFOs. In this figure (small graph on the right) also the calibration curve based on the measured fluorescence intensity of aqueous solutions having different known 2-hydroxyterephthalic acid concentrations at 427 nm irradiation wavelength is included.
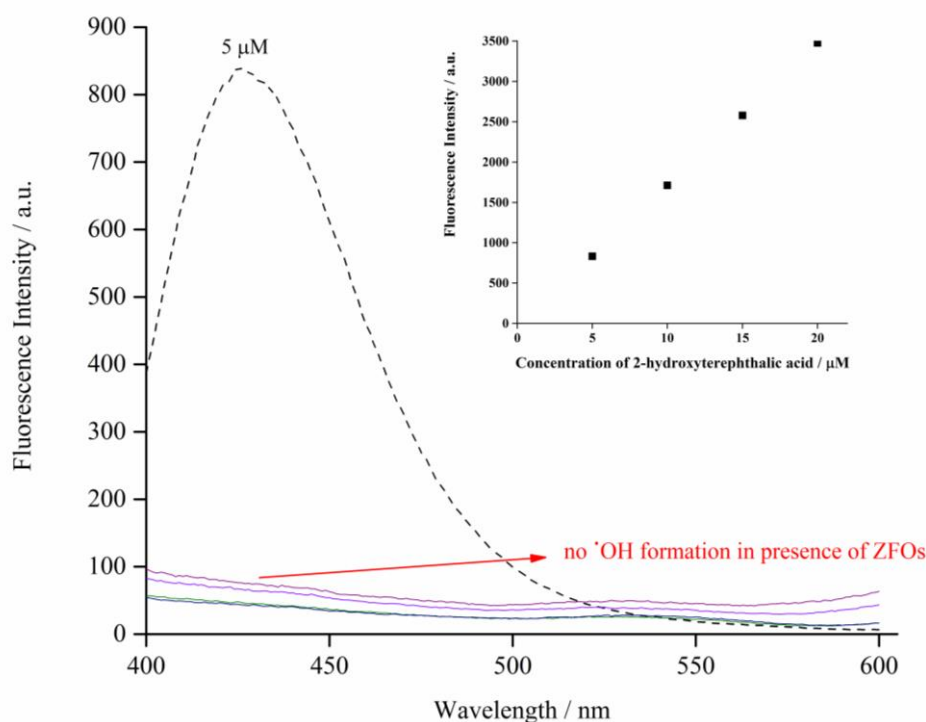
Figure 2-7. Fluorescence of UV-irradiated suspensions containing ZFO and terephthalic acid. The dashed line shows the fluorescence intensity of a solution containing 5 µmol l^{-1} TA. The calibration curve obtained with solutions with different concentrations of 2-hydroxyterephthalic acid is given in the insert.

Usually, the fluorescence intensity is proportional to the amount of produced hydroxyl radicals which reveals that this intensity has a positive relation with the photocatalytic activity of a semiconductor [24]. However, no increase of the fluorescence intensity was observed under UV irradiation for any of the prepared ZFO samples (**Figure 2-7**). The

same procedure was performed with coumarin being another model compound which forms a fluorescent product upon reaction with an OH radical [25]. Again no hydroxylated coumarin was detected (data not shown). These observations suggest that no OH radicals are formed at the zinc ferrite/water interface under UV irradiation.

Capacitance measurements and subsequent analysis were performed to determine the flat band potential, the donor density, and the conductivity type of ZFO samples. Mott-Schottky plots were obtained according to the following equation:

$$ 1/C_{SC}^2 = 2/{N_D\,\varepsilon_0\varepsilon_{SC}e_0 S^2}\ \left[V - V_{fb} - kT/e_0\right] \tag{2-2} $$

where C_{SC}^2 is the capacitance of the space charge layer in the semiconductor, N_D the donor density, ε_0 the vacuum permittivity, ε_{SC} the dielectric constant of the semiconductor, S the surface of the electrode, k the Boltzmann's constant, T the temperature, and e_0 the elementary charge. For all determinations, the temperature was 20°C and ε_{SC} was supposed to be equal to 100.

Table 2-1 shows the results obtained for the flat band potentials and donor densities of the ZFO samples. The experimentally obtained values were recalculated to pH 0 according to:

$$ V_{fb}(\text{pH }0) = V_{fb}(\text{pH x}) + 0.059\ x \tag{2-3} $$

Using the obtained values of the flat band potential and the bandgap energies of the synthesized ZFO samples (**Table 2-1**), the energetic positions of the conduction and valence bands were calculated assuming $V_{fb} \approx E_{CB}$. **Figure 2-8** shows the energetic position of the band edges for the different ZFO samples and for TiO_2 P25 together with the one-electron reduction potentials of oxidized methylene blue ($MB^{\bullet+}$).
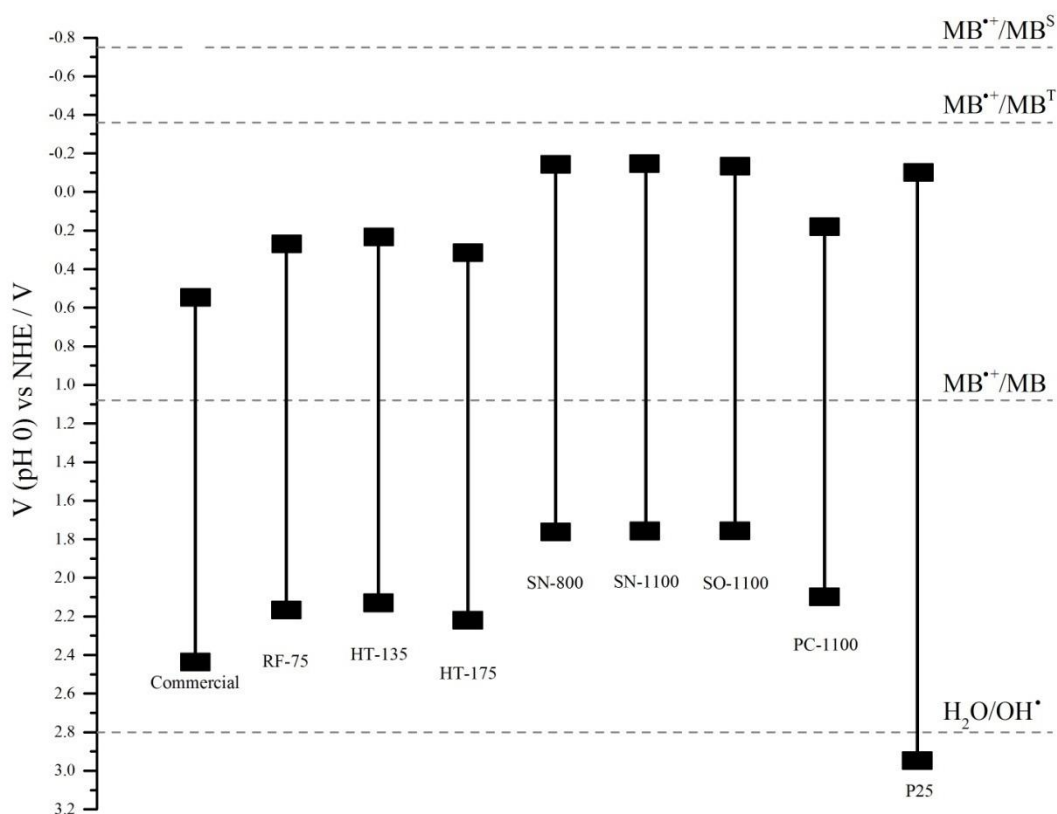
Figure 2-8. Energetic positions of the valance and the conduction band of different zinc ferrite samples and TiO$_2$ P25. MB, MB^T and MB^S denote the MB ground state, the excited triplet state and the excited singlet state of MB, respectively. The one electron reduction potentials have been calculated with data given in ref.[18].

2.6. Discussion

According to the XRD results, the ZFO samples prepared at temperatures lower than 1000°C (RF-75, HT-135, HT-175, and SN-800) contain some impurities. This could be related to the low synthetic temperature which is not high enough to ensure the formation of the bare spinel zinc ferrite structure.

The diffraction peaks of ZFO nanocrystals reveal considerable differences in the crystallinity. It can be observed that the ZFO particles synthesized through high-temperature methods (≥1000 °C), i.e., SO-1100, SN-1100, and PC-1100, exhibit high crystallinity compared to the other synthetic methods. Therefore, it is concluded that the phase pure zinc ferrite could only be achieved through high-temperature methods.

Some valuable information can also be extracted from the Raman measurements. According to the factor group analysis for the structure of a normal spinel (y = 0, space

group Fd3m), five Raman active bands are predicted [35]. Three of these bands correspond to T_{2g} modes and the others to A_{1g} and E_g modes. Broader peaks for the commercial and RF-75 samples evidence a poor degree of crystallinity. More narrow peaks are observed for the SN-1100, SN-1100, and PC-1100 samples, revealing an increasing degree of crystallinity with the temperature of synthesis. These results are in agreement with the obtained XRD data.

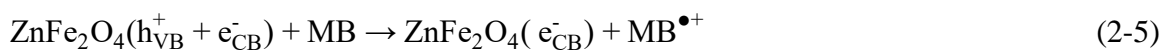The products obtained by hydrothermal synthesis at 135°C and 175°C, as well as by a solid-state reaction at 800°C show strong α-Fe_2O_3 characteristic Raman absorptions. According to Shim *et al.*, the absorption bands at 220, 288, 400, 490, and 1300 cm^{-1} can be assigned to the presence of this phase of iron oxide [28]. As mentioned before, the ZFO phase was not completely formed due to the low temperatures employed and some hematite impurities remain in the sample. The polymer complex and the solid-state reaction at 1100°C proved to be the best synthetic pathways to obtain phase-pure ZFO. These samples show the narrowest absorption bands being in good agreement with the values reported in the literature.

According to the average crystallite sizes estimated by the Debye–Scherrer formula and the BET surface areas, zinc ferrites with bigger crystallite sizes, and lower specific surface areas were obtained at higher reaction temperatures. The RF-75 method yielded crystallites with a minimum size of 5.3 nm. However, solid state methods employed for the synthesis of PC-1100, SN-1100 and SO-1100 yielded products with crystallite sizes of 130, 100 and 110 nm, respectively.

According to the literature [7], zinc ferrite is an effective photocatalyst to utilize visible light to perform oxidation processes. Zinc ferrite has been reported to be able to efficiently degrade the dyes rhodamine B and methyl orange [10,13,15,17,36–39]. For example, zinc ferrite prepared as nanospheres was able to photodegrade 100% of the rhodamine B under visible light within 300 min [15]. The photocatalytic activity of the synthesized ZFO photocatalysts obtained by different preparation methods seems to be affected by the particle size, the surface area, the crystallinity, the bandgap energy, the morphology and the overall structure [36]. MB dye tends to show relatively high degradation potential in the presence of ferrites [37].

But as observed in the current study, the prepared zinc ferrite samples were not able to bleach significant amounts of MB under UV irradiation. However, bleaching of MB in the presence of zinc ferrite under visible light irradiation using a xenon lamp as the light source was a relatively fast process. However, no formation of OH radical was detected indicating that the observed bleaching of MB is not resulting from a reaction between the dye molecule and a photocatalytically generated OH radical. This conclusion is in agreement with the calculated positions of the conduction and valence band of the ZFO samples (**Figure 2-8**). The data given in this figure clearly reveal that the energetic position of the valence band of all zinc ferrite samples investigated here is less positive (*vs.* NHE) than $E(H_2O/\bullet OH)$, thus preventing the formation of OH radicals by hole oxidation of water.

Consequently, it seems to be unlikely that the observed MB bleaching is due to a reaction between photocatalytically generated reactive oxygen species such as the OH radical and the probe molecule. However, the standard reduction potential for the couple $MB^{\bullet+}/MB$ lies within the bandgap of ZFO [18]. Therefore, the oxidation of MB molecules by light-generated valance band holes according to

$$ZnFe_2O_4 + hv \rightarrow ZnFe_2O_4(h_{VB}^+ + e_{CB}^-) \tag{2-4}$$

$$ZnFe_2O_4(h_{VB}^+ + e_{CB}^-) + MB \rightarrow ZnFe_2O_4(\,e_{CB}^-) + MB^{\bullet+} \tag{2-5}$$

may occur in the presence of suitable acceptors for the conduction band electrons.
MB has a light absorption maximum at 664 nm. It is, therefore, very likely that a significant concentration of excited MB is generated in the suspensions during visible light irradiation. Furthermore, MB might be adsorbed on the ZFO surface in an energetically favourable position which allows an interaction between the orbitals of the excited MB and ZFO. This could lead to an interfacial electron transfer from an excited surface-bound MB molecule (MB*) to the semiconductor according to

$$MB + hv \rightarrow MB^* \tag{2-6}$$

$$MB^* + ZnFe_2O_4 \rightarrow MB^{\bullet+} + ZnFe_2O_4(e_{CB}^-) \tag{2-7}$$
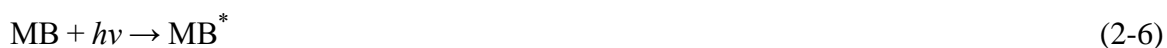
and a subsequent reaction of $MB^{\bullet+}$ with dissolved molecular oxygen must be taken into account. Such electron injection from photo-excited MB into the conduction band of a semiconductor has already been suggested by several authors [18,19].

The suggestion that the observed light-induced bleaching of MB is due to an electron transfer from the excited dye molecule to the semiconducting zinc ferrite is supported by the experimental data. Methylene blue has only small absorption coefficients in the UV(A) region of the spectrum. Consequently, only a small fraction of the dye molecules present in the suspension are excited resulting in a low electron transfer and, thus, in a low bleaching rate.

On the other hand, in the visible range, MB absorbs a significant portion of the light entering the suspension resulting in a higher concentration of excited molecules, faster electron transfer rates, and faster bleaching rates. These considerations lead one to expect that the bleaching rate has its highest value at the wavelength of the absorption maximum of MB (i.e., 664 nm). This, however, was not observed. As the data given in **Table 2-3** show, the maximum of the reaction rate is observed at 505 nm. This leads to the further assumption that the adsorbed MB molecule, whose presence must be presupposed for efficient electron transfer, has a different adsorption maximum than the dissolved MB.

The results obtained for the photocatalytic activity of the ZFO obtained under UV and visible light irradiation could thus be explained by a simple mechanism. Under visible light irradiation, the absorption by the dye molecule and a consequent electron injection from photoexcited MB molecules to the conduction band of the catalyst possibly results in the reduction of Fe^{3+} to Fe^{2+} within the semiconductor. This process results in the formation of an unstable dye cation radical which is able to decompose to form bleached products [40]. Since MB does not absorb strongly in the UV, this dye-sensitized process is most easily and usually demonstrated using an intense visible light [18].

Although the photocatalytic activity of ferrites plays no role in this photoreaction, the nature of the catalyst particles and their physical properties might influence the rate of this photoreaction. That is mainly because the MB photoreaction may proceed through adsorption and electron injection [19]. As mentioned before, the electrons transferred to the semiconductor might possibly reduce Fe^{3+} centers, thus, resulting in some degradation of

the solid due to leaching of soluble Fe^{2+} in parallel to the degradation of the dye. This undesired process becomes more important at low concentrations of the catalyst [40].

2.7. Conclusions

The rate of the light-induced bleaching of methylene blue in the presence of zinc ferrite was found to be wavelength dependent with a low rate in the UV region and a maximum rate at about 505 nm. No hydroxyl radicals were photocatalytically produced in the presence of irradiated zinc ferrite. The experimental observations suggest that the light-induced transformation of methylene blue in the presence of zinc ferrite is not initiated by hole or •OH mediated oxidation of the probe molecules. The observed bleaching of methylene blue containing suspensions under visible light irradiation is possibly initiated by an electron transfer from photo-excited methylene blue molecules being attached to the zinc ferrite surface into the conduction band of the semiconducting ferrite.

2.8. Acknowledgement

2.9. References

1.   Bahnemann, D. Photocatalytic water treatment: Solar energy applications. *Sol. Energy* **2004**, *77*, 445–459.

2.   Chen, D.; Sivakumar, M.; Ray, A.K. Heterogeneous photocatalysis in environmental remediation. *Dev. Chem. Eng. Miner. Process* **2000**, *8*, 505–550.

3.   Fujishima, A.; Zhang, X.; Tryk, D.A. Heterogeneous photocatalysis: From water photolysis to applications in environmental cleanup. *Int. J. Hydrogen Energy* **2007**, *32*, 2664–2672.

4.   Fujishima, A.; Honda, K. Electrochemical photolysis of water at a semiconductor electrode. *Nature* **1972**, *238*, 37–38.

5.   Dillert, R.; Taffa, D.H.; Wark, M.; Bredow, T.; Bahnemann, D.W. Research Update: Photoelectrochemical water splitting and photocatalytic hydrogen production using ferrites (MFe_2O_4) under visible light irradiation. *APL Mater.* **2015**, *3*, 104001-1–15.

6. Taffa, D.H.; Dillert, R.; Ulpe, A.C.; Bauerfeind, K.; Bredow, T.; Bahnemann, D.; Wark, M. Photoelectrochemical and theoretical investigations of spinel type ferrites ($M_xFe_{3-x}O_4$) for water splitting: a mini-review. *J. Photonics Energy* **2016**, *7*, 1–24.

7. Casbeer, E.; Sharma, V.K.; Li, X. Synthesis and photocatalytic activity of ferrites under visible light : A review. *Sep. Purif. Technol.* **2012**, *87*, 1–14.

8. Sato, T.; Haneda, K.; Seki, M.; Iijima, T. Morphology and magnetic properties of ultrafine $ZnFe_2O_4$ particles. *Appl. Phys. A Solids Surfaces* **1990**, *50*, 13–16.

9. Boumaza, S.; Boudjemaa, A.; Bouguelia, A.; Bouarab, R.; Trari, M. Visible light induced hydrogen evolution on new hetero-system $ZnFe_2O_4$/$SrTiO_3$. *Appl. Energy* **2010**, *87*, 2230–2236.

10. Dom, R.; Subasri, R.; Hebalkar, N.Y.; Chary, A.S.; Borse, P.H. Synthesis of a hydrogen producing nanocrystalline $ZnFe_2O_4$ visible light photocatalyst using a rapid microwave irradiation method. *RSC Adv.* **2012**, *2*, 12782–12791.

11. Xu, X.; Azad, A.K.; Irvine, J.T.S. Photocatalytic H_2 generation from spinels $ZnFe_2O4$, $ZnFeGaO_4$ and $ZnGa_2O_4$. *Catal. Today* **2013**, *199*, 22–26.

12. Lv, H.; Ma, L.; Zeng, P.; Ke, D.; Peng, T. Synthesis of floriated $ZnFe_2O_4$ with porous nanorod structures and its photocatalytic hydrogen production under visible light. *J. Mater. Chem.* **2010**, *20*, 3665–3672.

13. Jadhav, S.D.; Hankare, P.P.; Patil, R.P.; Sasikala, R. Effect of sintering on photocatalytic degradation of methyl orange using zinc ferrite. *Mater. Lett.* **2011**, *65*, 371–373.

14. Qiu, J.; Wang, C.; Gu, M. Photocatalytic properties and optical absorption of zinc ferrite nanometer films. *Mater. Sci. Eng. B* **2004**, *112*, 1–4.

15. Li, X.; Hou, Y.; Zhao, Q.; Wang, L. A general, one-step and template-free synthesis of sphere-like zinc ferrite nanostructures with enhanced photocatalytic activity for dye degradation. *J. Colloid Interface Sci.* **2011**, *358*, 102–108.

16. Dom, R.; Sivakumar, G.; Hebalkar, N.Y.; Joshi, S. V.; Borse, P.H. Deposition of nanostructured photocatalytic zinc ferrite films using solution precursor plasma spraying. *Mater. Res. Bull.* **2012**, *47*, 562–570.

17. Dom, R.; Subasri, R.; Radha, K.; Borse, P.H. Synthesis of solar active nanocrystalline ferrite, MFe_2O_4 (M: Ca, Zn, Mg) photocatalyst by microwave irradiation. *Solid State Commun.* **2011**, *151*, 470–473.

18. Mills, A.; Wang, J. Photobleaching of methylene blue sensitised by TiO_2: an

ambiguous system? *J. Photochem. Photobiol. A Chem.* **1999**, *127*, 123–134.

19. Yan, X.; Ohno, T.; Nishijima, K.; Abe, R.; Ohtani, B. Is methylene blue an appropriate substrate for a photocatalytic activity test? A study with visible-light responsive titania. *Chem. Phys. Lett.* **2006**, *429*, 606–610.

20. Diodati, S.; Pandolfo, L.; Caneschi, A.; Gialanella, S.; Gross, S. Green and low temperature synthesis of nanocrystalline transition metal ferrites by simple wet chemistry routes. *Nano Res.* **2014**, *7*, 1027–1042.

21. Jang, J.S.; Borse, P.H.; Lee, J.S.; Jung, O.S.; Cho, C.R.; Jeong, E.D.; Ha, M.G.; Won, M.S.; Kim, H.G. Synthesis of nanocrystalline $ZnFe_2O_4$ by polymerized complex method for its visible light photocatalytic application: An efficient photo-oxidant. *Bull. Korean Chem. Soc.* **2009**, *30*, 1738–1742.

22. Sarkar, J.; Bhattacharyya, S. Operating characteristics of transcritical CO_2 heat pump for simultaneous water cooling and heating. *Arch. Thermodyn.* **2013**, *33*, 23–40.

23. Emeline, A. V.; Zhang, X.; Jin, M.; Murakami, T.; Fujishima, A. Application of a "black body" like reactor for measurements of quantum yields of photochemical reactions in heterogeneous systems. *J. Phys. Chem. B* **2006**, *110*, 7409–7413.

24. Yu, J.; Xiang, Q.; Zhou, M. Preparation, characterization and visible-light-driven photocatalytic activity of Fe-doped titania nanorods and first-principles study for electronic structures. *Appl. Catal. B Environ.* **2009**, *90*, 595–602.

25. Ishibashi, K.I.; Fujishima, A.; Watanabe, T.; Hashimoto, K. Detection of active oxidative species in TiO_2 photocatalysis using the fluorescence technique. *Electrochem. commun.* **2000**, *2*, 207–210.

26. Xue, H.; Li, Z.; Wang, X.; Fu, X. Facile synthesis of nanocrystalline zinc ferrite via a self-propagating combustion method. *Mater. Lett.* **2007**, *61*, 347–350.

27. Zhou, Z.H.; Xue, J.M.; Chan, H.S.O.; Wang, J. Transparent magnetic composites of $ZnFe_2O_4$ nanoparticles in silica. *J. Appl. Phys.* **2001**, *90*, 4169–4174.

28. Shim, S.-H.; Duffy, T.S. Raman spectroscopy of Fe_2O_3 to 62 GPa. *Am. Mineral.* **2001**, *87*, 318–326.

29. Oh, S.J.; Cook, D.C.; Townsend, H.E. Characterization of iron oxides commonly formed as corrosion products on steel. *Hyperfine Interact.* **1998**, *112*, 59–66.

30. Wang, Z.; Schiferl, D.; Zhao, Y.; O'Neill, H.S.C. High pressure Raman spectroscopy of spinel-type ferrite $ZnFe_2O_4$. *J. Phys. Chem. Solids* **2003**, *64*, 2517–2523.

31. Sousa, M.H.; Tourinho, F. a; Rubim, J.C. Use of Raman micro-spectroscopy in the

characterization of $M^{II}Fe_2O_4$ (M = Fe, Zn) electric double layer ferrofluids. *J. Raman Spectrosc.* **2000**, *31*, 185–191.

32. Singh, J.P.; Srivastava, R.C.; Agrawal, H.M.; Kumar, R. Micro-Raman investigation of nanosized zinc ferrite: Effect of crystallite size and fluence of irradiation. *J. Raman Spectrosc.* **2011**, *42*, 1510–1517.

33. Tang, J.; Zou, Z.; Yin, J.; Ye, J. Photocatalytic degradation of methylene blue on $CaIn_2O_4$ under visible light irradiation. *Chem. Phys. Lett.* **2003**, *382*, 175–179.

34. Shafaei, A.; Nikazar, M.; Arami, M. Photocatalytic degradation of terephthalic acid using titania and zinc oxide photocatalysts: Comparative study. *Desalination* **2010**, *252*, 8–16.

35. White, W.B.; DeAngelis, B.A. Interpretation of the vibrational spectra of spinels. *Spectrochim. Acta Part A Mol. Spectrosc.* **1967**, *23*, 985–995.

36. Dom, R.; Chary, A.S.; Subasri, R.; Hebalkar, N.Y.; Borse, P.H. Solar hydrogen generation from spinel $ZnFe_2O_4$ photocatalyst : Effect of synthesis methods. **2015**, 1378–1390.

37. Singhal, S.; Sharma, R.; Singh, C.; Bansal, S. Enhanced photocatalytic degradation of methylene blue using $ZnFe_2O_4$ / MWCNT composite synthesized by hydrothermal method. *Indian J. Mater. Sci.* **2013**, *2013*, 1–6.

38. Jia, Z.; Ren, D.; Liang, Y.; Zhu, R. A new strategy for the preparation of porous zinc ferrite nanorods with subsequently light-driven photocatalytic activity. *Mater. Lett.* **2011**, *65*, 3116–3119.

39. Cao, X.; Gu, L.; Lan, X.; Zhao, C.; Yao, D.; Sheng, W. Spinel $ZnFe_2O_4$ nanoplates embedded with Ag clusters: Preparation, characterization, and photocatalytic application. *Mater. Chem. Phys.* **2007**, *106*, 175–180.

40. Rochkind, M.; Pasternak, S.; Paz, Y. Using dyes for evaluating photocatalytic properties: A critical review. *Molecules* **2015**, *20*, 88–110.

Chapter 3: Light-Induced Reactions of Chlorpromazine in the Presence of a Heterogeneous Photocatalyst: Formation of a Long-Lasting Sulfoxide

3.1. Forewords

Besides MB as the pioneering associate of the phenothiazine group of antipsychotic pharmaceuticals, the major representative member, namely, chlorpromazine was selected as another target compound for photocatalytic conversion in this study. Chlorpromazine is known to undergo photodegradation under UV light irradiation. However, very little is known about its behavior under visible light irradiation. Also the possible reaction pathway and reaction intermediates of its conversion upon visible irradiation have to be analyzed. Most importantly, the fundamental processes of its photocatalytic conversion are barely identified and thus, poorly understood. One of the known approaches to increase the visible light absorption of titanium dioxide is the deposition of sensitizing materials on its surface. This method has been applied for preparation of K-7000 by sensitizing a carbon-based substrate on titanium dioxide surface. This modification leads to the enhanced ability of K-7000 to absorb incoming photons also in the visible region. Accordingly, it was of high interest to evaluate the photocatalytic activity of this visible light-absorbing semiconductor for the conversion of chlorpromazine and to determine the reaction pathway and intermediates of this conversion in the presence of K-7000.

This chapter includes the article "Light-Induced Reactions of Chlorpromazine in the Presence of a Heterogeneous Photocatalyst: Formation of a Long-Lasting Sulfoxide" by Arsou Arimi, Rafl Dillert, Gerald Dräger, and Detlef W. Bahnemann, published in Catalysts (doi:10.3390/catal9070627). In this chapter, a commercially available visible light-absorbing photocatalyst, namely K-7000, was evaluated for the photocatalytic conversion of chlorpromazine. Chlorpromazine was found to be a persistent compound under visible light irradiation. Within the objectives of this work, photocatalytic conversion of chlorpromazine in the presence of K-7000 was evaluated and compared under aerobic and anaerobic conditions, upon both UV and visible light irradiation. In this regard, by employing mainly the high performance liquid chromatography (HPLC-MS) technique, under UV and visible light irradiation, various reaction intermediates throughout the photolytic and photocatalytic conversion of chlorpromazine were observed which revealed

different reaction pathways under these conditions. Moreover, the main reaction intermediate of the visible light-driven photolytic and photocatalytic conversions of chlorpromazine under aerobic conditions, namely, chlorpromazine sulfoxide, was found to be highly persistent upon visible light irradiation even in the presence of K-7000 photocatalyst.

3.2. Abstract

A commercial carbon-modified titanium dioxide, KRONOClean 7000, was applied as a UV(A) and visible-light active photocatalyst to investigate the conversion of the antipsychotic pharmaceutical chlorpromazine in aqueous phase employing two monochromatic light sources emitting at wavelengths of 365 and 455 nm. Photocatalytic and photolytic conversion of chlorpromazine under both anaerobic and aerobic conditions was analyzed using a HPLC-MS technique. Depending on the irradiation wavelength and the presence of oxygen, varying conversion rates and intermediates revealing different reaction pathways were observed. Upon visible light irradiation under aerobic conditions, chlorpromazine was only converted in the presence of the photocatalyst. No photocatalytic conversion of this compound under anaerobic conditions upon visible light irradiation was observed. Upon UV(A) irradiation, chlorpromazine was successfully converted into its metabolites in both presence and absence of the photocatalyst. Most importantly, chlorpromazine sulfoxide, a very persistent metabolite of chlorpromazine, was produced throughout the photolytic and photocatalytic conversions of chlorpromazine under aerobic conditions. Chlorpromazine sulfoxide was found to be highly stable under visible light irradiation even in the presence of the photocatalyst. Heterogeneous photocatalysis under UV(A) irradiation resulted in a slow decrease of the sulfoxide concentration, however, the required irradiation time for its complete removal was found to be much longer compared to the removal of chlorpromazine at the same initial concentration.

Keywords: chlorpromazine; chlorpromazine sulfoxide; KRONOClean 7000; visible light-driven photocatalysis; HPLC-MS

3.3. Introduction

The presence of pharmaceutical residues is being reported globally in water and wastewater streams during the past few decades and this issue has become a big concern [1]. As many of these medicinal compounds are essential in remedial applications for human/animal

health, their consumption cannot be minimized or limited [2,3]. Despite the very low concentrations of these chemicals in aquatic systems, they result in serious problems in the environment for humans and for living organisms, since they are designed in a way to have specific physiological effects on living organisms [4–6]. Generally, these chemicals have structures which cannot be biologically degraded by conventional treatment methods [7,8] and therefore, some post-treatment steps are additionally required for their proper removal [9–11]. Nevertheless, these methods might not be adequate to remove the large variety of organic compounds present in wastewater. Thus, the effluents of conventional treatment plants are major sources of chemical discharges into the aquatic system [12].

One of the proposed methods to treat pharmaceutical-rich aquatic streams is the application of heterogeneous photocatalytic reactions [13,14]. Through this method, the structure of the drugs present in water and wastewater streams will be decomposed, and as a result, their negative effects on the environment, especially their toxicity, will be reduced [15]. Recently, solar light driven heterogeneous photocatalysis in the treatment of contaminated wastewater has been widely investigated [16–21]. TiO_2 is the most commonly used photocatalyst in heterogeneous photocatalytic processes. However, despite its high stability, low toxicity, and low cost, this photocatalyst is not able to absorb the sunlight efficiently. Only 5% of sunlight can be absorbed by bare TiO_2 and the visible part of the solar energy remains unutilized [22]. Thus, having a visible-light active photocatalyst allows effectively harvesting and utilizing the solar energy in wastewater treatment.

In order to increase the light absorption by TiO_2, some methods have been investigated such as doping with metal ions or adsorption of compounds acting as sensitizers on the surface of the photocatalyst. By doping the TiO_2 surface with metal ions, the absorption of this photocatalyst will be altered to higher wavelengths leading to its increased visible light absorption [23–26]. The latter approach using dyes as a sensitizer is commonly used in dye sensitized solar cells [27,28] as well as in photocatalytic applications [29–32]. However, due to the adsorption of the dye on the photocatalyst surface, the absorption spectrum of the photocatalyst will be changed [33]. This by-effect can be avoided when applying a carbon-based layer on the surface of the photocatalyst as applied for KRONOClean 7000, the commercially available carbon-modified TiO_2, also known as VLP or Kronos VLP 7000 in the literature [34–36]. KRONOClean 7000 (named in this work as K-7000) is a commercial carbon-modified TiO_2 with no pigmentary properties, produced by Kronos

International, Inc. K-7000 is one of the commercially available UV light active photocatalysts which also shows a high activity in response to visible light. This material is an ultra-fine carbon modified titanium dioxide with anatase crystal modification in which due to an aromatic carbon-based sensitizer layer, the visible light can be absorbed [35]. K-7000 is a bimodal anatase that is able to decompose organic pollutants as well as odors and NOx compounds [34,35]. As reported by the producer, this material has a BET surface area of 225 m^2 g^{-1} and an average crystallite size of about 15 nm [37]. Detailed characteristic and morphological studies on this photocatalyst have been reported before [34–36]. Zabek *et al.* have shown that by this modification the bandgap position of the photocatalyst did not change (compared to bare anatase TiO_2) while the visible light absorption was increased [35]. K-7000 has shown a stable photocatalytic activity after three consecutive experimental runs which confirmed its reusability for visible light-driven photocatalytic applications [36]. Furthermore, the photo-stability of the sensitizer layer on the TiO_2 upon visible irradiation was also proved through eighteen hours of photo-mineralization of 4-chlorophenol [35].

Antipsychotic drugs are frequently detected among the various categories of pharmaceuticals contaminating the water system. These drugs are used widely around the world, while their increased consumption leads to the enhanced release of these compounds and their metabolites into the environment [38]. One of the most commonly prescribed groups of psychotropic drugs in the world is called the phenothiazine group [39,40]. Phenothiazine drugs might end up in water or wastewater streams after their consumption, in the sewage treatment plant effluents, or as effluents of the pharmaceutical companies [41,42]. Residual traces of these drugs or their transformation products in aquatic environments with possible ecotoxicological properties have already been detected and reported [41,43,44]. Generally, the oxidation process of phenothiazines leads to one, two, or four-electron oxidation products and the two-electron oxidation product is reported to be the sulfoxide metabolite [45].

Chlorpromazine hydrochloride, [3-(2-chloro-10H-phenothiazin-10-yl) propyl] dimethylamine hydrochloride, the most popular compound from the phenothiazine group, is one of the first of its kind which was released to the pharmaceutical market in 1952 [46]. This compound is photosensitive in liquid or solid form and its negative effects upon exposure to sunlight in the human body are already identified [47]. The dechlorinated free

radicals produced from irradiation of this compound in the body react with the DNA and form singlet oxygen [48]. The formation of short-lived radicals causing genotoxic consequences was indicated as well [49]. Chlorpromazine is known to be converted into its metabolites upon UV irradiation through demethylation in the N-chain, oxidation of sulfur or nitrogen, or ring hydroxylation [43,50]. Chlorpromazine absorbs light more strongly at wavelengths shorter than 300 nm and the resulting excited singlet state easily converts into the triplet state. The excited states either fragment to form radicals or photo-ionize to form radical cations and electrons [51]. The main metabolite in photolytic transformation of chlorpromazine, namely, chlorpromazine sulfoxide (named in this work as SFX) is obtained by the direct reaction of chlorpromazine with molecular oxygen [52]. It is also likely to be produced through hydrolysis of the radical cation [53]. Trautwein and Kümmerer investigated the fate of chlorpromazine and its potential transformation through aerobic and anaerobic biodegradation as well as abiotic photolytic degradation by sunlight. They observed nearly complete elimination of chlorpromazine within 4 h of illumination by a xenon arc lamp. They determined the molecular structures of the three main photolysis products having m/z values of 301, 317, and 335, through an analysis by high performance liquid chromatography coupled to multiple stage mass-spectrometry (HPLC–MS^n) [43]. In another study, Kigondu *et al.* evaluated the antimycobacterial activities of chlorpromazine and its metabolites alone and in combination with antitubercular drugs in which intermediates with m/z values of 335 and 351 were detected [54]. These compounds were also reported in an analytical study by Boehme and Strobel in which two HPLC methods have been introduced to analyze the in vitro metabolism of chlorpromazine [55].

On the other hand, chlorpromazine was reported to show diverse behaviors upon UV irradiation under aerobic and anaerobic conditions. The photo-induced reaction of chlorpromazine under anaerobic conditions revealed that polymerization and dimerization processes predominated upon anaerobic UV photolysis and, interestingly, no evidence of the formation of SFX or other photolytic products of the aerobic conditions was observed. It was suggested that the free radicals of chlorpromazine resulted from cleavage of chloride function from the structure, promote these processes and the polymers were found to be the major products [56].

Despite the extended studies on photolytic degradation of chlorpromazine in aqueous solutions, to the best of the authors' knowledge, very little is known about the

photocatalytic conversion of this compound and its metabolites in aqueous systems and their possible removal from water streams. The photocatalytic conversion of chlorpromazine (in a mixture with two other pharmaceuticals) using immobilized TiO_2 nanoparticles (PC-500) upon UV irradiation was investigated by Khataee *et al.* [57]. They have reported 90% removal of chlorpromazine in the mixture after 150 min UV irradiation. However, a detailed mechanistic study was not presented by these authors.

In the current study, photocatalytic and photolytic conversions of chlorpromazine using K-7000 photocatalyst upon UV(A) and visible light irradiation at both anaerobic and aerobic conditions were studied. Furthermore, the photocatalytic and photolytic transformations of the highly stable metabolite, SFX, produced under aerobic conditions throughout a long-term irradiation period and its stability over this process were analyzed.

3.4. Results and Discussion

In the current study, the conversion of chlorpromazine under photocatalytic conditions as well as photolytic conditions upon both UV(A) (365 nm) and visible (455 nm) light irradiation was investigated. KronoClean 7000 (K-7000) was applied as a photocatalyst for conversion of chlorpromazine using UV(A) and visible light sources. The experimental runs were performed in the presence and absence of molecular oxygen at room temperature and natural pH of the suspension. Accordingly, the reaction intermediates at both photocatalytic and photolytic processes were detected and compared to figure out the possible reaction pathway for the photocatalytic reaction.

3.4.1. Photocatalytic and Photolytic Conversion of Chlorpromazine

The photocatalytic and photolytic conversions ($C/C_{0,e}$) of the probe compound (chlorpromazine) versus reaction time upon UV(A) and visible light irradiation at, respectively, 365 and 455 nm wavelengths using K-7000 as photocatalyst in aerobic conditions are presented in **Figure 3-1**. These experimental runs were performed for 180 min, however, in the following graph, only the first 60 min of irradiation are presented.
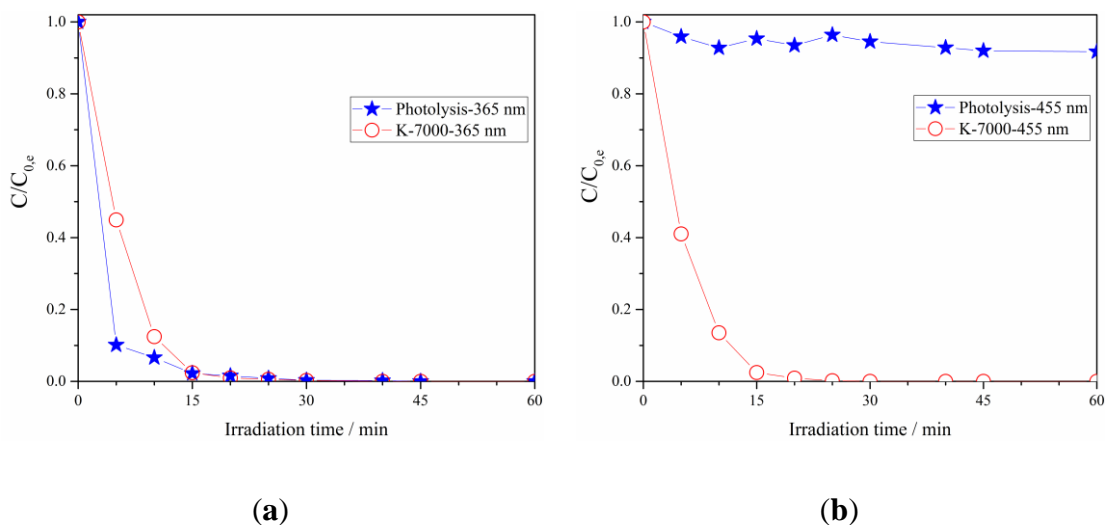
(**a**)   (**b**)

Figure 3-1. Photocatalytic and photolytic conversions of chlorpromazine upon (**a**) UV(A) and (**b**) visible light irradiation (C_0: 100 μM-Catalyst: K-7000 (1 g L^{-1}) -Irradiation wavelengths: 365 and 455 nm).

As can be seen in **Figure 3-1**, in the presence of K-7000 as photocatalyst upon both UV(A) and visible light irradiation, up to 90% of the chlorpromazine initially present in the aqueous phase was converted after only 10 min of irradiation and almost complete conversion was achieved within 30 min of irradiation. Upon UV(A) irradiation however, the photocatalytic reaction seems to be slower than the photolytic reaction. This suggests that during the photocatalytic reaction under UV(A) irradiation, most of the photons are absorbed by the photocatalyst itself; therefore, the contribution of the homogeneous reaction (photolytic excitation of the probe compound) is small compared to the photocatalytic reaction.

In comparison, in the photolytic procedure, after 30 min of irradiation with 455 nm wavelengths, only a slight decrease (5%) in the chlorpromazine concentration was observed (**Figure 3-1(b)**) indicating the high stability of this compound upon visible light irradiation. Nevertheless, after 30 min of UV(A) irradiation, up to 99% of the pharmaceutical was converted photolytically. It becomes obvious from **Figure 3-2** that the absorbance of chlorpromazine at 365 nm is significantly larger than at 455 nm. Consequently, less amount of photons are absorbed at 455 nm. Due to this low absorption, a significant part of photons will be lost by transmission through the suspension resulting in a weak photolysis of chlorpromazine at this wavelength.
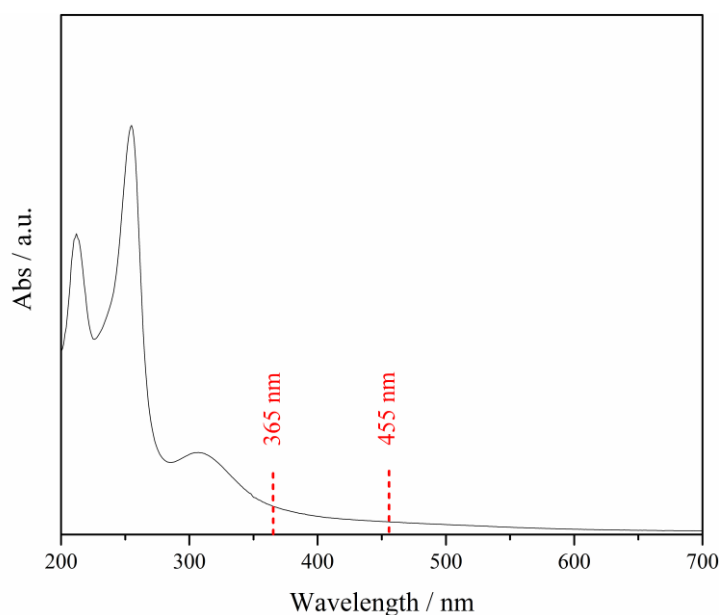
Figure 3-2. Absorption spectrum of a 100 μM chlorpromazine solution in water.

All the photocatalytic and photolytic experiments followed a first order kinetic behavior; except for photolysis upon visible light irradiation (455 nm) in which the conversion of the probe compound was negligible (5%). The rate constant values for UV(A)-photocatalysis, visible light-photocatalysis, and UV(A)-photolysis were calculated to be 0.21 ± 0.01, 0.24 ± 0.01, and 0.19 ± 0.01, respectively.

At first glance, no significant difference in the conversion rates of the photocatalytic reactions upon UV(A) and visible light irradiations is observed. However, the photon flux density, N, emitted by the UV(A) and the Visible light LED lamps were calculated to be 1.12×10^{16} s^{-1} cm^{-2} and 7.47×10^{16} s^{-1} cm^{-2}, respectively. This reveals that under identical experimental conditions, the amount of emitted photons from the visible light LED lamp was almost seven times higher compared to that of the UV(A) LED lamp. Therefore, even though the rate constant of the photocatalytic process seems to be a bit higher upon visible light irradiation, considering the much higher photon flux density of the visible light lamp, K-7000 was found to be less active upon visible light irradiation than upon UV(A) irradiation.

During the photolysis upon visible light irradiation, the chlorpromazine suspension reached a strong pink color after 5 min and it turned colorless after 15 min of irradiation. However, throughout the photolytic experiment upon UV(A) irradiation, the colorless suspension of chlorpromazine turned to pink and ruby. Nevertheless, no change of color was observed

during the photocatalytic experiments in the presence of K-7000. From these observations, a possible variety of intermediates throughout different reaction pathways seems to be likely.

Accordingly, some intermediates produced during the experimental runs were detected via HPLC-MS analysis. These compounds are named in this manuscript according to their detected molecular mass (or m/z value). The photocatalytic and photolytic transformation of chlorpromazine (m/z: 319) resulted in the formation of products having m/z values of 301, 317, 335, and 351.

Figure 3-3 demonstrates the time course of the products/intermediates formation during the photocatalytic and photolytic conversion of chlorpromazine upon both UV(A) and visible light irradiation. The main conversion products found during the first 60 min of the photocatalytic experimental runs upon UV(A) irradiation have m/z values of 335, 351, and 317 (**Figure 3-3(a)**); however, for the photocatalytic process upon visible light irradiation, only the intermediates with m/z values of 335 and 351 were detected (**Figure 3-3(b)**).

Interestingly, throughout the photocatalytic reaction upon both UV(A) and visible light irradiation, the intermediate giving the highest signal intensity (m/z = 335) was found to be highly stable over the reaction period.

Alternatively, during the photolytic reaction upon UV(A) irradiation (**Figure 3-3(c)**), compounds with m/z values of 301, 335, and 317 were observed and no intermediates for the photolytic reaction upon visible light irradiation (**Figure 3-3(d)**) were detected as the conversion of the probe compound was negligible.

(**a**)

(**b**)

(**c**)

(**d**)
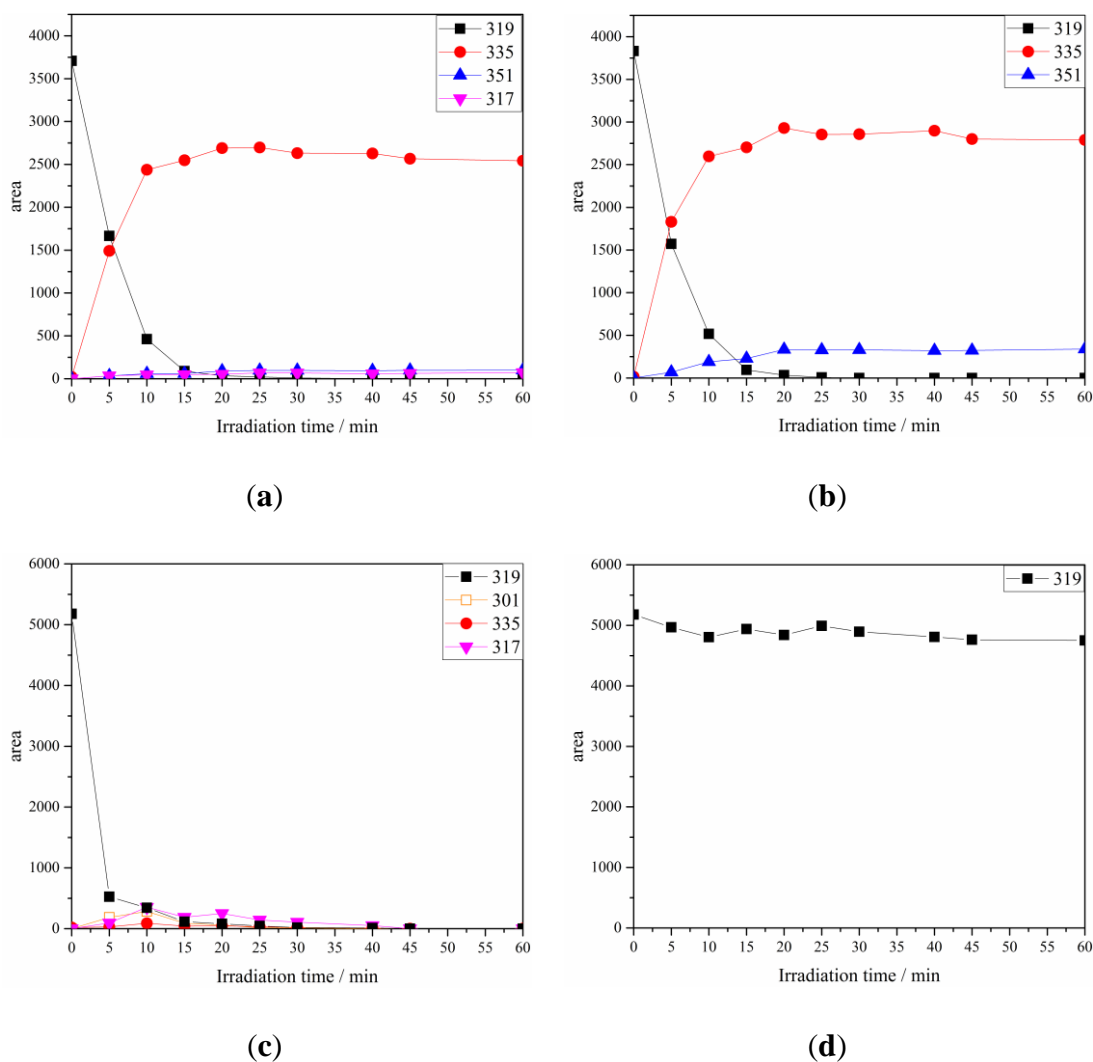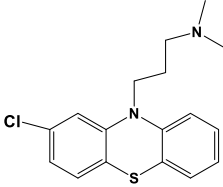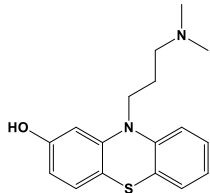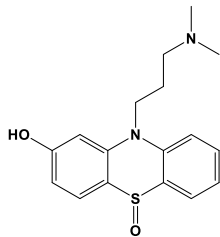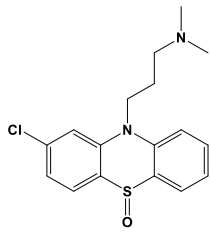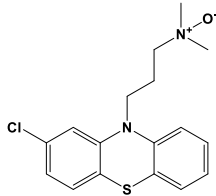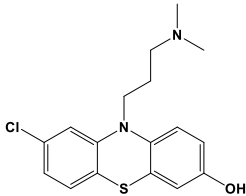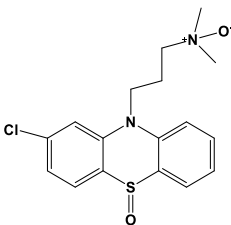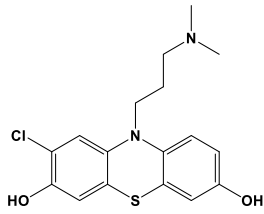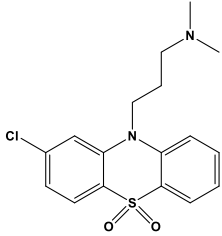
Figure 3-3. Time course of the intermediates formation during chlorpromazine conversion: (**a**) photocatalysis upon UV(A) irradiation, (**b**) photocatalysis upon visible light irradiation (K-7000 as photocatalyst (1 g L^{-1})), (**c**) photolysis upon UV(A) irradiation, and (**d**) photolysis upon visible light irradiation.

As revealed by the intermediates analysis, conversion rate of the probe compound as well as type and production rates of the intermediates varied upon UV(A) and visible light irradiation in the presence and absence of the photocatalyst. Three main detected products in photolysis upon UV(A) irradiation, having m/z values of 335, 317, and 301 were also reported for this reaction in similar analytical studies and for each of these compounds, one or more possible structures have been proposed [43,44,54,55]. Some of the intermediates with significant signal intensities detected throughout the photocatalytic and photolytic conversion of chlorpromazine under aerobic conditions, their retention times, masses, and reported structures are gathered in **Table 3-1**.

Table 3-1. Chlorpromazine and some of the reaction intermediates of its photocatalytic and photolytic conversion under aerobic conditions, their retention times, masses, and possible structures.

Retention Time/min	Mass (m/z)	Possible Structures (Found as [M + H]⁺)
19.2	319	
15.8	301	
11.7	317	
14.7	335	
15.2	351	

The molecular mass of the highly persistent intermediate giving the highest signal intensity with m/z value of 335 corresponds either to chlorpromazine sulfoxide (SFX) or to chlorpromazine -N-oxide [54]. Therefore, in order to identify this produced metabolite, a pure commercial SFX was analyzed by HPLC-MS and the obtained signal for the

commercial SFX matched 100% to that of the metabolite with m/z value of 335 in the experimental runs, confirming the identity of the produced metabolite to be the SFX.

3.4.2. Long Term Experiments with Chlorpromazine Sulfoxide

Chlorpromazine sulfoxide (SFX) was found to be a highly stable product of the photocatalytic conversion of chlorpromazine under aerobic conditions. Therefore, the stability and transformation of this compound was investigated in long-term experiments. The experimental runs were performed under aerobic photocatalytic and photolytic conditions upon UV(A) and visible light irradiation (**Figure 3-4**).
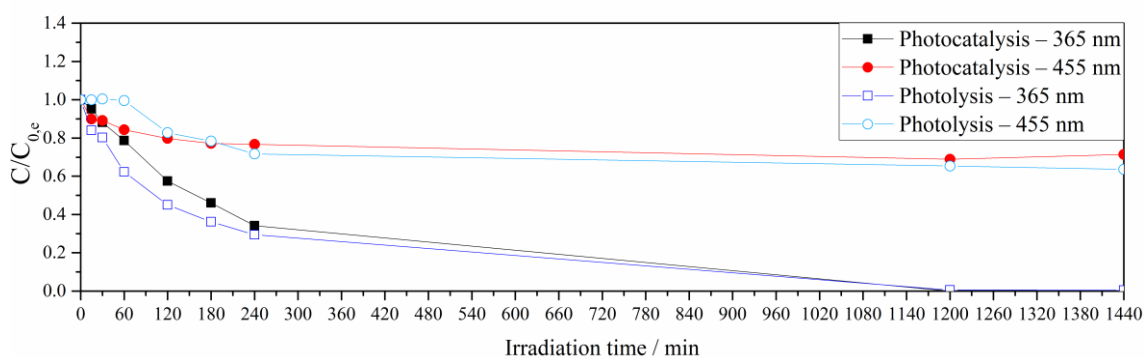
Figure 3-4. Long term photocatalytic and photolytic conversion of chlorpromazine sulfoxide (SFX) (100 μM) upon UV(A) and visible light irradiation using K-7000 as photocatalyst (1 g L^{-1}).

The long term photocatalytic experiments upon visible light irradiation revealed that SFX was converted only up to 20% during the first 2 h of irradiation; nevertheless, after this period it was highly stable even over the 24 h visible light irradiation (only 7% decrease). On the other hand, during the photocatalytic reaction upon UV(A) irradiation, SFX concentration was slowly reduced. However, the required irradiation time for its complete removal compared to the removal of chlorpromazine having the same initial concentration was found to be at least 20 times longer.

Furthermore, during the photolytic experiments upon visible light irradiation, SFX concentration decreased only up to 17% from 2 h to 24 h confirming the high stability of SFX upon visible light photolysis. However, SFX concentration was found to be slowly reduced under photolytic conditions upon UV(A) light irradiation.

Nevertheless, it seemed that upon UV(A) irradiation, the presence of the photocatalyst

inhibited the conversion reaction and that the photolytic reaction was faster than the photocatalytic one. Thus, possible differences in the conversion pathways are assumed. Accordingly, the intermediates of the photocatalytic and the photolytic reactions of SFX after 2 h and 24 h of UV(A) irradiation (**Figure 3-5**) were analyzed and compared.

(**a**)   (**b**)

Figure 3-5. Chromatograms of SFX under both photocatalytic and photolytic conditions upon irradiation with UV(A) light after: (**a**) 2 h and (**b**) 24 h.

Upon long term UV(A) irradiation, as assumed some differences between the photocatalytic and photolytic conversion pathways of SFX were observed. It was found that the product/intermediate distributions of these two reactions after 2 h and 24 h UV(A) irradiation were different (**Figure 3-5**). Significant differences in values and types of intermediates between photocatalytic and photolytic conversions of SFX after 2 h UV(A) irradiation were observed.

Furthermore, the comparison between **Figure 3-5(a)** and **Figure 3-5(b)** revealed that the produced intermediates throughout the photocatalytic reaction were completely degraded or converted after 24 h UV(A) irradiation, while in the photolytic reaction, not only were the produced intermediates not removed after 24 h UV(A) irradiation, but also some new ones were detected at the end of the reaction.

During the photolytic conversion of SFX upon UV(A) irradiation, the intermediate with the most intense signal (m/z = 317), was detected at 11.7 min retention time. This signal was increasingly produced from 15 min to 6 h irradiation and it remained stable until the end of the 24 h UV(A) irradiation. Another signal at retention time of 15.8 min, corresponding to

a combination of m/z = 301 and m/z = 318 was detected from 30 min until 4 h irradiation. Moreover, some new peaks (mainly low intensity signals) corresponding to m/z = 333, 303, 269, and 287 emerged along the UV(A) irradiation. However, during the photocatalytic reaction, other detected intermediates after 2 h irradiation corresponding to m/z = 321 and 250 were completely removed after 24 h UV(A) irradiation. The fact that, under photocatalytic conditions, much lower concentrations of intermediates were detected indicates that the photocatalytic process is superior in removal of the produced intermediates compared to the photolytic process. Analyzing these intermediates suggested different reaction pathways for photocatalytic and photolytic conversion of SFX over 24 h UV(A) irradiation.

Also upon irradiation with visible light, some differences between the photocatalytic and the photolytic reactions were observed. Therefore, the intermediates of the photocatalytic and the photolytic reactions of SFX after 2 h and 24 h of visible irradiation were analyzed and compared as well (**Figure 3-6**).
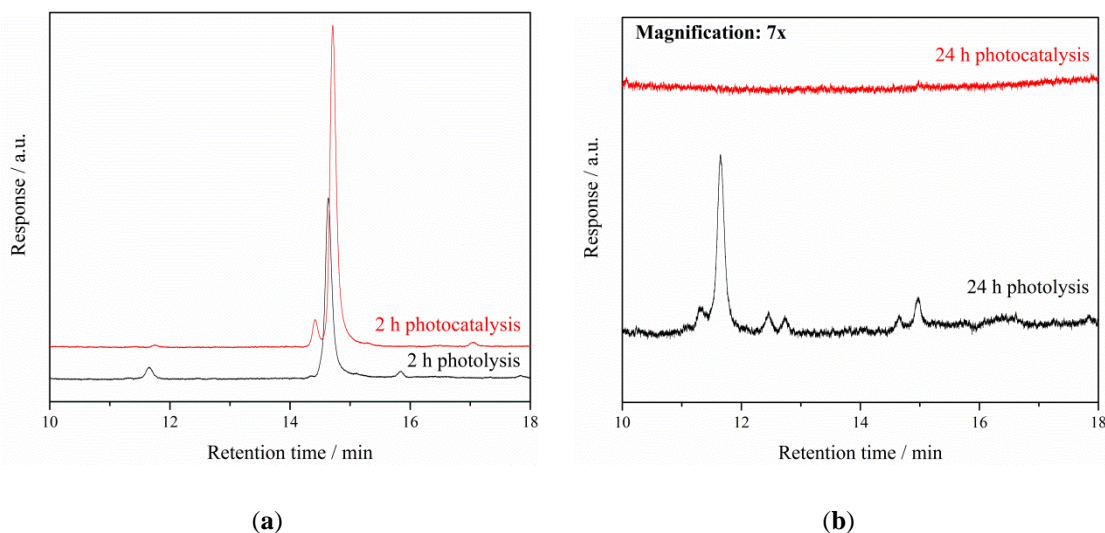

(**a**)   (**b**)
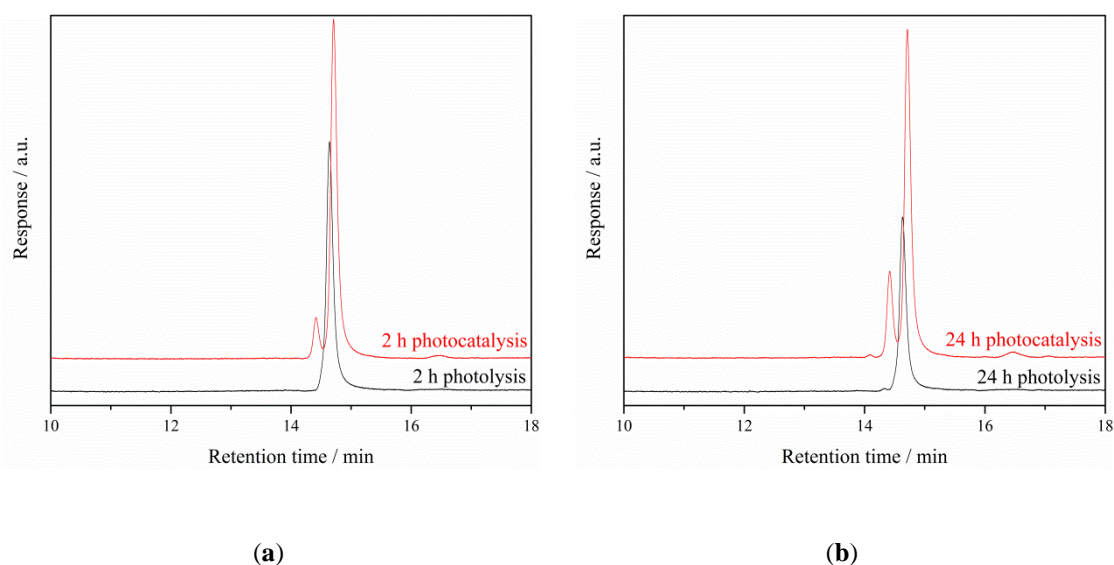
Figure 3-6. Chromatograms of SFX samples under both photocatalytic and photolytic conditions upon irradiation with visible light after: (**a**) 2 h and (**b**) 24 h.

As observed in **Figure 3-6**, throughout the photocatalytic reaction upon visible light irradiation, no significant difference in the signal intensity of SFX was detected from 2 h to 24 h (only 7% decrease); revealing that this compound was highly stable throughout the reaction period. During this process, an evolving small signal at retention time of about

14.4 min (attached to the SFX signal) corresponding to m/z value of 321 was observed. The intensity of this signal slightly increased over the 24 h visible light irradiation. Furthermore, throughout the photolytic experiments upon visible light irradiation, the signal intensity of SFX from 2 h to 24 h decreased up to 17%, while no other intermediates were detected, confirming that the SFX was highly stable during visible light photolysis.

3.4.3. Photocatalytic and Photolytic Conversion of Chlorpromazine under Anaerobic Conditions

In addition, the photo-induced intermediates of photolytic and photocatalytic conversions of chlorpromazine under anaerobic conditions were evaluated. The obtained results are presented in **Figure 3-7**. It was observed that upon UV(A) irradiation, the rate of chlorpromazine conversion as well as production rates and types of the intermediates under anaerobic conditions were completely different from aerobic conditions. However, chlorpromazine was not converted under anaerobic conditions upon visible light irradiation both in the presence and the absence of K-7000 and, therefore, no intermediates were detected for those experimental runs.

(**a**)   (**b**)
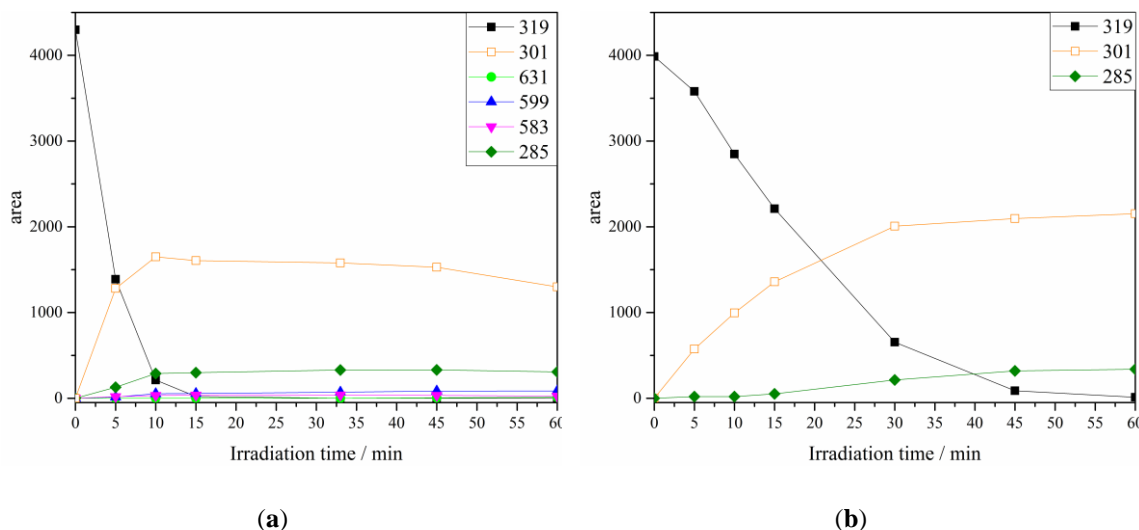
Figure 3-7. Conversion of chlorpromazine into its metabolites under anaerobic conditions: (**a**) photolysis upon UV(A) irradiation, (**b**) photocatalysis upon UV(A) irradiation with K-7000 as photocatalyst (1 g L^{-1}).

A simple comparison between the aerobic and anaerobic photolysis of chlorpromazine upon UV(A) irradiation clearly reveals their different reaction pathways. The reaction products/intermediates of the aerobic UV(A) photolytic reaction were found to have m/z values of 335, 301, and 317 (**Figure 3-3(c)**). However, throughout the anaerobic photolysis

of chlorpromazine upon UV(A) irradiation (**Figure 3-7(a)**), no traces of SFX (m/z: 335) were found and other products/intermediates, with m/z values of 301, 285, 631, 599, and 583 were detected. The compound with m/z value of 285 is most likely promazine which has been also identified under anaerobic conditions by Davies *et al.* via comparing the retention factor with that of an authentic sample. They have shown that in an oxygen-free system, the photo-excited chlorpromazine undergoes a dechlorination step to form free radicals which then react with the solvent and produce promazine and other products [58]. Detection of the products with large m/z values of 631, 599, and 583 is an evidence of formation of different chlorpromazine dimers during this reaction. Similar observations were reported by Huang and Sands confirming that under anaerobic UV photolysis of chlorpromazine, polymerization and dimerization processes take place and that the free radical of chlorpromazine resulted from cleavage of chloride function from the structure promotes these processes [56].

On the other hand, in the presence of the photocatalyst upon anaerobic conditions (**Figure 3-7(b)**), the conversion of chlorpromazine slowed down but it still happened, while only two products with m/z values of 301 and 285 were detected and no dimers or polymers were formed. In the photocatalytic system, the photocatalyst absorbs the main part of the incident photons. Consequently, the key step of the dimerization and polymerization process, namely, the formation of chlorpromazine free radicals will be limited.

Interestingly, during both anaerobic photolysis and photocatalysis of chlorpromazine, the products with m/z values of 301 and 285 were found to be the most stable ones among all other intermediates. These masses most probably correspond to the chemical structures proposed in **Figure 3-8**, in which the chlorine in the chlorpromazine structure is replaced with an OH or hydrogen.

m/z: 301   m/z: 285
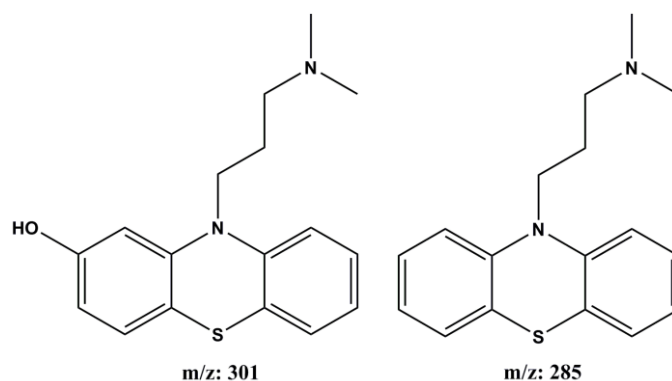
(**a**)   (**b**)

Figure 3-8. Possible structures of the two most stable products under anaerobic conditions.

During the photocatalytic reaction in the presence of oxygen, most of the photons are absorbed by the photocatalyst resulting into its excitation. In this case two reactions are likely to happen; either the photo-generated conduction band electrons react with the oxygen resulting into $O_2^{-\bullet}$ or they reduce the chlorpromazine and break the C-Cl bond, leaving Cl^- and the radical of chlorpromazine. The probability of the second path is rather low in the presence of oxygen as it is a highly strong electron scavenger. However, in oxygen-free conditions, the first reaction cannot occur, thus, chlorpromazine will be the only electron acceptor present in the system resulting in the dechlorination of this compound. Considering the possible structures of the two most stable products under anaerobic conditions (**Figure 3-8**), the C-Cl bond in the structure of chlorpromazine was replaced with a C-OH or a C-H bond. To yield these products, the dechlorinated chlorpromazine radical requires reaction with $^{\bullet}H$ or $^{\bullet}OH$. These radicals are suggested to result from the reaction of the chlorpromazine radical with water. Although the reactions between organic radicals and water are usually quite unlikely, such reactions have been reported before under anaerobic conditions [59]. Therefore, detection of the products with m/z values of 301 and 285 in the absence of oxygen proposes the possible reaction of electrons instead of hydroxyl radicals. It seems to be likely that these products are formed through the reduction reaction of chlorpromazine which is more expected to take place in the absence of oxygen.

3.4.4. Participation of OH Radicals in the Degradation Pathway of Chlorpromazine

To evaluate the role of hydroxyl radicals throughout the photocatalytic transformation or oxidation of chlorpromazine and formation of its intermediates or products, an analysis on the amount of produced hydroxyl radicals upon both UV(A) and visible light irradiation under aerobic conditions in the presence of K-7000 photocatalyst was performed. Hydroxyl radical is one of the major oxidants in photocatalytic processes. Throughout a photocatalytic reaction, the formation of hydroxyl radicals on the surface of the photocatalyst upon irradiation is correlated with photocatalytic conversion of the probe compound through these radicals generated from photoexcitation of the photocatalyst surface [60]. For this matter, terephthalic acid was applied as a probe molecule which is

known to react specifically with OH radicals transforming into a fluorescent product, 2-hydroxyterephthalic acid. This reaction product is intensely fluorescent whereas terephthalic acid itself is non-fluorescent [61]. Irradiating the terephthalic acid suspension at 315 nm wavelength results in generation of a strong fluorescent signal with a maximum at around 425 nm. The signal intensity which is directly detected and measured corresponds to the concentration of the product (2-hydroxyterephthalic acid) in the suspension. Thus, it is possible to identify the OH radical concentration in the suspension through this method [62].

Accordingly, a suspension of 0.4 mM TA (99%) and 1 mM NaOH with 1 g L^{-1} photocatalyst concentration was irradiated for 60 min with UV(A) and visible light. **Figure 3-9** presents the amount of produced 2-hydroxyterephthalic acid from this suspension upon UV(A) irradiation *vs.* irradiation time. Upon visible light irradiation no formation of hydroxyl radicals was observed.
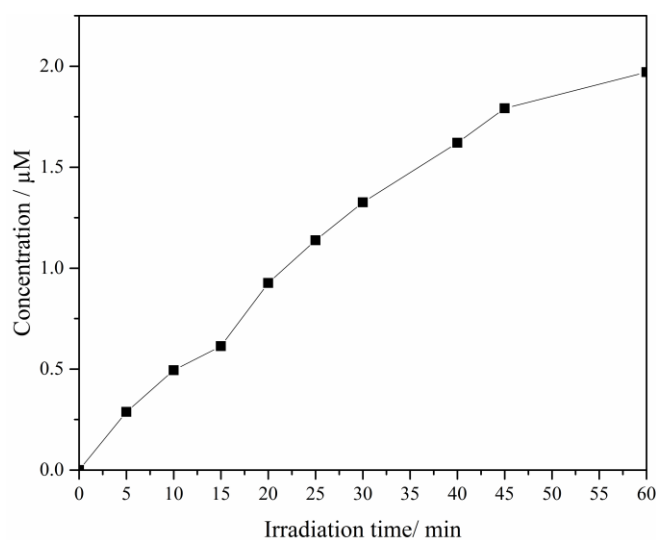
Figure 3-9. Amount of the produced 2-hydroxyterephthalic acid from the UV(A)-irradiated suspension of terephthalic acid and K-7000.

As can be seen, upon UV(A) irradiation at 365 nm wavelength, an increased production of 2-hydroxyterephthalic acid over the irradiation time was observed which was proportional to the amount of hydroxyl radicals. This revealed that hydroxyl radicals were produced at the surface of the photocatalyst. Wilde *et al.* have studied the degradation of different phenothiazines by hydroxyl radicals produced through a Fenton process. Based on their UHPLC-HRMS^n data, for the degradation of chlorpromazine by hydroxyl radicals, a

dechlorination step leading to products with m/z values of 301 and 285 was reported which is likely to result in a product with m/z value of 317, eventually after an extra hydroxylation step. Other transformation products with m/z values of 335 and 351 were also proposed to be formed after one or two aromatic hydroxylation steps instead of S-oxidation in the chlorpromazine structure [44]. In the current study, similar products with m/z values of 335, 351, and 317 were observed upon aerobic photocatalytic conversion of chlorpromazine. This indicates the degradation of chlorpromazine mainly by hydroxyl radicals produced upon UV(A) irradiation under aerobic conditions in the presence of K-7000 photocatalyst. However, the intermediates with m/z values of 285 and 301 were not detected, most likely due to the quick transformation of chlorpromazine to the other products.

Nevertheless, upon visible light irradiation under aerobic conditions no formation of hydroxyl radicals was observed indicating that the conversion of chlorpromazine in the presence of K-7000 photocatalyst did not result from the reaction between a photocatalytically generated OH radical and the chlorpromazine molecule and that the contribution of OH radicals in conversion of chlorpromazine upon visible light irradiation is almost negligible. Therefore, the photocatalytic conversion of chlorpromazine upon visible light irradiation is most likely approached through a direct mechanism. This means that the photogenerated electrons attack the chlorpromazine molecule and produce a free radical cation which then reacts with water or molecular oxygen in the system and results in the detected products with m/z values of 335, 351. Moreover, observation of these products upon visible light irradiation under aerobic conditions also confirms that in the absence of hydroxyl radicals, the dechlorination step does not take place.

Accordingly, the main detected intermediates in photocatalytic conversions of chlorpromazine under anaerobic and aerobic conditions upon both UV(A) and visible light irradiation are gathered and presented in **Figure 3-10**, proposing the reaction pathway for these procedures.

Figure 3-10. The proposed reaction pathway for photocatalytic conversion of chlorpromazine.

3.5. Materials and Methods

3.5.1. Materials

The commercial carbon-modified titanium dioxide powder (Kronos International, Inc., Leverkusen, NRW, Germany), KRONOClean 7000 (K-7000), was applied as the photocatalyst in this work. The commercial chlorpromazine sulfoxide (SFX) was purchased from LGC-Standards (Wesel, NRW, Germany). Acetonitrile (Rotisolv® HPLC Gradient) was purchased from Carl-Roth (Karlsruhe, BW, Germany). Chlorpromazine hydrochloride (≥98%), trifluoroacetic acid (spectroscopy Uvasol®), and all other chemicals in the present study were purchased from Sigma-Aldrich (Merck, Darmstadt, HE, Germany) (if no additional notation is made). All the chemicals were used as purchased without further

purification. Ultrapure water (≥18.2 MΩ cm) was applied in all the experiments.

3.5.2. Photocatalytic Procedure

The photocatalytic experiments of chlorpromazine conversion using K-7000 as photocatalyst, as well as photolysis of chlorpromazine under both UV(A) (365 nm) and visible (455 nm) light irradiation were performed. These experiments were carried out in a closed cylindrical borosilicate photoreactor (diameter: 6 cm, height: 3 cm) covered in a shell made of a black polymer which was connected from the top to one of the monochromatic LED light sources emitting at 365 nm (Thorlabs, M365L2, 190 mW, 700 mA) or 455 nm (Thorlabs, M455L3, 900 mW, 1000 mA) irradiation wavelengths. For each of the LED lamps the photon flux density, N (s^{-1} cm^{-2}) was calculated through the following equation:

$$N = \int_{\lambda_1}^{\lambda_2} \frac{I}{E} \, d\lambda \qquad (3\text{-}1)$$

The spectral irradiance, I (mW cm^{-2} nm^{-1}) was measured by a SpectraRad® Xpress (B&W Tek, Lübeck, SH, Germany)) spectral irradiance meter. E, the energy of a photon with wavelength λ was calculated by the Planck–Einstein relation [63]. The calculated N value was found to be 1.12×10^{16} s^{-1} cm^{-2} for the UV(A) LED lamp (365 nm) and 7.47×10^{16} s^{-1} cm^{-2} for the visible light LED lamp (455 nm). The UV/Vis spectrum of chlorpromazine was recorded employing a UV-visible Cary-100 spectrophotometer.

For each experimental run, an aqueous suspension containing 100 μM chlorpromazine (or SFX) and 1 g L^{-1} photocatalyst was prepared. The reactor was filled with 60 mL of reaction suspension which was first stirred in the dark for 60 min to ensure the adsorption equilibrium. Clearly, for the photolytic experiments, the dark period was not required. Subsequently, the suspension was irradiated for 180 min. In aerobic experiments the suspension was purged with oxygen and in anaerobic conditions the suspension was purged with argon throughout the reaction period. In the case of long-term experiments, the irradiation time was extended to 24 h. At certain time intervals, samples were taken from the sampling point provided on the reactor, centrifuged, filtered (PVDF, 0.2 μm pore size), and finally, the supernatant was obtained and analyzed through HPLC-MS analysis. The results of these experiments were reported as the conversion of the probe compound calculated from the ratio of its concentration at a desired reaction time to initial

concentration of this compound after equilibrium ($C/C_{0,e}$).

3.5.3. HPLC-MS Analysis

The product distribution was determined by HPLC-UV-MS (ESI) using an Alliance 2795-HT HPLC (Waters, UK) coupled with a 1050 UV-detector (type 79853C, detection wavelength =254 nm, HP, USA) and an LCT Premier ESI mass spectrometer (Waters, UK). The chromatography was performed on an Eurospher II C_{18} HPLC column (150 * 4 mm, Eurospher II 100-5 C18A, Knauer, Germany) using water (A) and acetonitril (B), each containing 0.1% trifluoroacetic acid, at a flow rate of 600 µL min^{-1} with a linear gradient (B%: 15% [0 min], 15% [6 min], 60% [20 min], 60% [23 min], 15% [26 min]; runtime =35 min). The following relevant MS settings were used: polarity = ESI +; capillary voltage =2700 V; desolvation temperature =350 °C; desolvation gas flow =650 L h^{-1} (nitrogen); source temperature =100 °C; sample cone voltage =30 V.

3.5.4. Determination of OH Radicals

In order to detect the possible photocatalytic formation of hydroxyl radicals, the terephthalic acid (TA) test [33] was performed upon both UV(A) and visible light irradiation wavelengths. Accordingly, a calibration curve using different concentrations of 2-hydroxyterephthalic acid (97%) was prepared. To measure the hydroxyl radical formation, a solution of 0.4 mM TA (99%) and 1 mM NaOH was prepared and the photocatalyst (K-7000) was added to reach a 1 g L^{-1} concentration in the suspension. This was followed by a 40 min ultrasonic dispersion step and the suspension was then left in the dark for 1 h under continuous stirring.

Afterwards, the suspension was divided into two parts which were irradiated separately with the same UV(A) and visible light sources used for the photocatalytic experiments. Accordingly, at desired time intervals, samples were taken from these suspensions, centrifuged, and analyzed via a Hitachi fluorescence spectrophotometer model F-700 recording the emission in the range of 400 to 600 nm (excitation wavelength =315 nm).

3.6. Conclusions

The experimental results of this work revealed that the conversion rate of the probe compound, chlorpromazine, as well as type and production rates of the reaction intermediates varies using different irradiation wavelengths. Although chlorpromazine was

converted directly upon UV(A) irradiation into its metabolites, for its conversion upon visible light irradiation, the presence of a visible-light active photocatalyst was necessary. Furthermore, observation of the products with m/z values of 301 and 285 under anaerobic conditions suggested the reduction of chlorpromazine through electrons and not the hydroxyl radicals.

A persistent intermediate, namely, chlorpromazine sulfoxide (SFX) was the main reaction intermediate of visible-light photolytic and photocatalytic conversions of chlorpromazine under aerobic conditions. Although chlorpromazine was completely converted upon visible-light photocatalysis within the first 30 min of irradiation, this persistent intermediate, SFX, was highly stable over the 24 h of constant visible light irradiation even in the presence of K-7000 photocatalyst. This long-lasting compound was converted extremely slowly over a long-term heterogeneous photocatalytic process under UV(A) irradiation, however, the required irradiation time for complete removal of SFX was found to be at least 20 times longer compared to the removal of chlorpromazine at the same initial concentration. Nevertheless, the photocatalytic and photolytic conversions of SFX were found to have different reaction pathways. Moreover, throughout the photocatalytic pathway, the reaction intermediates or metabolites were successfully removed from the reaction medium indicating the superior ability of the photocatalytic process in the removal of the produced intermediates compared to the photolytic process.

3.7. Acknowledgments

3.8. References

1. Radjenović, J.; Sirtori, C.; Petrović, M.; Barceló, D.; Malato, S. Solar photocatalytic degradation of persistent pharmaceuticals at pilot-scale: Kinetics and characterization of major intermediate products. *Appl. Catal. B Environ.* **2009**, *89*, 255–264.

2. Fatta-Kassinos, D.; Vasquez, M.I.; Kümmerer, K. Transformation products of

pharmaceuticals in surface waters and wastewater formed during photolysis and advanced oxidation processes – Degradation, elucidation of byproducts and assessment of their biological potency. *Chemosphere* **2011**, *85*, 693–709.

3. Jones, O.A.H.; Voulvoulis, N.; Lester, J.N. Human pharmaceuticals in wastewater treatment processes. *Crit. Rev. Environ. Sci. Technol.* **2005**, *35*, 401–427.

4. Taylor, D.; Senac, T. Human pharmaceutical products in the environment - The "problem" in perspective. *Chemosphere* **2014**, *115*, 95–99.

5. Mirzaei, A.; Chen, Z.; Haghighat, F.; Yerushalmi, L. Removal of pharmaceuticals and endocrine disrupting compounds from water by zinc oxide-based photocatalytic degradation: A review. *Sustain. Cities Soc.* **2016**, *27*, 407–418.

6. Zwiener, C.; Frimmel, F.H. Oxidative treatment of pharmaceuticals in water. *Water Res.* **2000**, *34*, 1881–1885.

7. Luo, Y.; Guo, W.; Ngo, H.H.; Nghiem, L.D.; Hai, F.I.; Zhang, J.; Liang, S.; Wang, X.C. A review on the occurrence of micropollutants in the aquatic environment and their fate and removal during wastewater treatment. *Sci. Total Environ.* **2014**, *473– 474*, 619–641.

8. Bolong, N.; Ismail, A.F.; Salim, M.R.; Matsuura, T. A review of the effects of emerging contaminants in wastewater and options for their removal. *Desalination* **2009**, *238*, 229–246.

9. Bernabeu, A.; Vercher, R.F.; Santos-Juanes, L.; Simón, P.J.; Lardín, C.; Martínez, M.A.; Vicente, J.A.; González, R.; Llosá, C.; Arques, A.; et al. Solar photocatalysis as a tertiary treatment to remove emerging pollutants from wastewater treatment plant effluents. *Catal. Today* **2011**, *161*, 235–240.

10. Ganiyu, S.O.; van Hullebusch, E.D.; Cretin, M.; Esposito, G.; Oturan, M.A. Coupling of membrane filtration and advanced oxidation processes for removal of pharmaceutical residues: A critical review. *Sep. Purif. Technol.* **2015**, *156*, 891–914.

11. de Jesus Gaffney, V.; Almeida, C.M.M.; Rodrigues, A.; Ferreira, E.; Benoliel, M.J.; Cardoso, V.V. Occurrence of pharmaceuticals in a water supply system and related human health risk assessment. *Water Res.* **2015**, *72*, 199–208.

12. Bollmann, A.F.; Seitz, W.; Prasse, C.; Lucke, T.; Schulz, W.; Ternes, T. Occurrence and fate of amisulpride, sulpiride, and lamotrigine in municipal wastewater treatment plants with biological treatment and ozonation. *J. Hazard. Mater.* **2016**, *320*, 204–215.

13. Prieto-Rodriguez, L.; Miralles-Cuevas, S.; Oller, I.; Agüera, A.; Puma, G.L.; Malato, S. Treatment of emerging contaminants in wastewater treatment plants (WWTP) effluents by solar photocatalysis using low TiO$_2$ concentrations. *J. Hazard. Mater.* **2012**, *211–212*, 131–137.

14. Klavarioti, M.; Mantzavinos, D.; Kassinos, D. Removal of residual pharmaceuticals from aqueous systems by advanced oxidation processes. *Environ. Int.* **2009**, *35*, 402–417.

15. Trawiński, J.; Skibiński, R. Studies on photodegradation process of psychotropic drugs: a review. *Environ. Sci. Pollut. Res.* **2017**, *24*, 1152–1199.

16. Spasiano, D.; Marotta, R.; Malato, S.; Fernandez-Ibañez, P.; Di Somma, I. Solar photocatalysis: Materials, reactors, some commercial, and pre-industrialized applications. A comprehensive approach. *Appl. Catal. B Environ.* **2015**, *170–171*, 90–123.

17. Robertson, P.K.J.; Bahnemann, D.W.; Robertson, J.M.C.; Wood, F. Photocatalytic detoxification of water and air. *Environ. Photochem. Part II* **2005**, *2*, 367–423.

18. Malato, S.; Fernández-Ibáñez, P.; Maldonado, M.I.; Blanco, J.; Gernjak, W. Decontamination and disinfection of water by solar photocatalysis: Recent overview and trends. *Catal. Today* **2009**, *147*, 1–59.

19. Mills, A.; Hunte, S. Le An overview of semiconductor photocatalysis. *J. Photochem. Photobiol. A Chem.* **1997**, *108*, 1–35.

20. Hoffmann, M.R.; Martin, S.T.; Choi, W.; Bahnemann, D.W. Environmental applications of semiconductor photocatalysis. *Chem. Rev.* **1995**, *95*, 69–96.

21. Bahnemann, D. Photocatalytic water treatment: Solar energy applications. *Sol. Energy* **2004**, *77*, 445–459.

22. Fagan, R.; McCormack, D.E.; Dionysiou, D.D.; Pillai, S.C. A review of solar and visible light active TiO$_2$ photocatalysis for treating bacteria, cyanotoxins and contaminants of emerging concern. *Mater. Sci. Semicond. Process.* **2016**, *42*, 2–14.

23. Xu, A.; Gao, Y.; Liu, H. The Preparation, characterization, and their photocatalytic activities of rare-earth-doped TiO$_2$ nanoparticles. *J. Catal.* **2002**, *207*, 151–157.

24. Klosek, S.; Raftery, D. Visible light driven V-doped TiO$_2$ photocatalyst and its photooxidation of ethanol. *J. Phys. Chem. B* **2001**, *105*, 2815–2819.

25. Lee, K.; Yoon, H.; Ahn, C.; Park, J.; Jeon, S. Strategies to improve the photocatalytic activity of TiO$_2$: 3D nanostructuring and heterostructuring with graphitic carbon

nanomaterials. *Nanoscale* **2019**, *11*, 7025–7040.

26. Cho, S.; Ahn, C.; Park, J.; Jeon, S. 3D nanostructured N-doped TiO_2 photocatalysts with enhanced visible absorption. *Nanoscale* **2018**, *10*, 9747–9751.

27. O'Regan, B.; Grätzel, M. A low-cost, high-efficiency solar cell based on dye-sensitized colloidal TiO_2 films. *Nature* **1991**, *353*, 737–740.

28. Freitag, M.; Teuscher, J.; Saygili, Y.; Zhang, X.; Giordano, F.; Liska, P.; Hua, J.; Zakeeruddin, S.M.; Moser, J.-E.; Grätzel, M.; et al. Dye-sensitized solar cells for efficient power generation under ambient lighting. *Nat. Photonics* **2017**, *11*, 372–378.

29. Cho, Y.; Choi, W.; Lee, C.; Hyeon, T.; Lee, H. Visible light-induced degradation of carbon tetrachloride on dye-sensitized TiO_2. *Environ. Sci. Technol.* **2001**, *35*, 966–970.

30. Chowdhury, P.; Moreira, J.; Gomaa, H.; Ray, A.K. Visible-solar-light-driven photocatalytic degradation of phenol with dye-sensitized TiO_2: Parametric and kinetic study. *Ind. Eng. Chem. Res.* **2012**, *51*, 4523–4532.

31. Li, X.; Shi, J.-L.; Hao, H.; Lang, X. Visible light-induced selective oxidation of alcohols with air by dye-sensitized TiO_2 photocatalysis. *Appl. Catal. B Environ.* **2018**, *232*, 260–267.

32. Lang, X.; Zhao, J.; Chen, X. Visible-light-induced photoredox catalysis of dye-sensitized titanium dioxide: Selective aerobic oxidation of organic sulfides. *Angew. Chemie Int. Ed.* **2016**, *55*, 4697–4700.

33. Ehret, A.; Stuhl, L.; Spitler, M.T. Spectral sensitization of TiO_2 nanocrystalline electrodes with aggregated cyanine dyes. *J. Phys. Chem. B* **2001**, *105*, 9960–9965.

34. Tobaldi, D.M.; Seabra, M.P.; Otero-Irurueta, G.; de Miguel, Y.R.; Ball, R.J.; Singh, M.K.; Pullar, R.C.; Labrincha, J.A. Quantitative XRD characterisation and gas-phase photocatalytic activity testing for visible-light (indoor applications) of KRONOClean 7000®. *RSC Adv.* **2015**, *5*, 102911–102918.

35. Ząbek, P.; Eberl, J.; Kisch, H. On the origin of visible light activity in carbon-modified titania. *Photochem. Photobiol. Sci.* **2009**, *8*, 264-269.

36. Quesada-Cabrera, R.; Mills, A.; O'Rourke, C. Action spectra of P25 TiO_2 and a visible light absorbing, carbon-modified titania in the photocatalytic degradation of stearic acid. *Appl. Catal. B Environ.* **2014**, *150–151*, 338–344.

37. KRONOS Specialties GmbH. *Kronos Information 2.2, KRONOClean ® 7000 TiO_2-*

photocatalyst; Leverkusen, NRW, Germany, DS2186EN/615EN, 2015.

38. Herrmann, M.; Menz, J.; Gassmann, M.; Olsson, O.; Kümmerer, K. Experimental and in silico assessment of fate and effects of the antipsychotic drug quetiapine and its bio- and phototransformation products in aquatic environments. *Environ. Pollut.* **2016**, *218*, 66–76.

39. Vardanyan, R.; Hruby, V. Antipsychotics. In *Synthesis of Best-Seller Drugs*; Elsevier, 2016; pp. 87–110 ISBN 978-0-12-411492-0.

40. Fourrier, A.; Gasquet, I.; Allicar, M.P.; Bouhassira, M.; Lépine, J.P.; Bégaud, B. Patterns of neuroleptic drug prescription: a national cross-sectional survey of a random sample of French psychiatrists. *Br. J. Clin. Pharmacol.* **2001**, *49*, 80–86.

41. Boreen, A.L.; Arnold, W.A.; McNeill, K. Photodegradation of pharmaceuticals in the aquatic environment: A review. *Aquat. Sci. - Res. Across Boundaries* **2003**, *65*, 320–341.

42. Andreozzi, R.; Raffaele, M.; Nicklas, P. Pharmaceuticals in STP effluents and their solar photodegradation in aquatic environment. *Chemosphere* **2003**, *50*, 1319–1330.

43. Trautwein, C.; Kümmerer, K. Degradation of the tricyclic antipsychotic drug chlorpromazine under environmental conditions, identification of its main aquatic biotic and abiotic transformation products by LC-MS^n and their effects on environmental bacteria. *J. Chromatogr. B Anal. Technol. Biomed. Life Sci.* **2012**, *889–890*, 24–38.

44. Wilde, M.L.; Schneider, M.; Kümmerer, K. Fenton process on single and mixture components of phenothiazine pharmaceuticals: Assessment of intermediaries, fate, and preliminary ecotoxicity. *Sci. Total Environ.* **2017**, *583*, 36–52.

45. Buettner, G.R.; Motten, A.G.; Hall, R.D.; Chignell, C.F. Free radical production by chlorpromazine sulfoxide, an ESR spin-trapping and flash photolysis study. *Photochem. Photobiol.* **1986**, *44*, 5–10.

46. López-Muñoz, F.; Alamo, C.; Cuenca, E.; Shen, W.W.; Clervoy, P.; Rubio, G. History of the discovery and clinical introduction of chlorpromazine. *Ann. Clin. Psychiatry* **2005**, *17*, 113–135.

47. Nałecz-Jawecki, G.; Hajnas, A.; Sawicki, J. Photodegradation and phototoxicity of thioridazine and chlorpromazine evaluated with chemical analysis and aquatic organisms. *Ecotoxicology* **2008**, *17*, 13–20.

48. Gocke, E. Review of the genotoxic properties of chlorpromazine and related

phenothiazines. *Mutat. Res. Genet. Toxicol.* **1996**, *366*, 9–21.

49.   Bahnemann, D.; Asmus, K.-D.; Willson, R.L. Free radical induced one-electron oxidation of the phenothiazines chlorpromazine and promethazine. *J. Chem. Soc. Perkin Trans.* **1983**, *2*, 1661–1668.

50.   Ljunggren, B.; Moller, H. Phenothiazine phototoxicity: an experimental study on chlorpromazine and related tricyclic drugs. *Acta Derm. Venereol.* **1977**, *57*, 325–329.

51.   Kochevar, I.E. Phototoxicity mechanisms: Chlorpromazine photosensitized damage to DNA and cell membranes. *J. Invest. Dermatol.* **1981**, *77*, 59–64.

52.   Motten, A.G.; Buettner, G.R.; Chignell, C.F. Spectroscopic studies of cutaneous photosensitizing agents--VIII. A spin-trapping study of light induced free radicals from chlorpromazine and promazine. *Photochem. Photobiol.* **1985**, *42*, 9–15.

53.   Cheng, H.Y.; Sackett, P.H.; Mccreery, R.L. Kinetics of chlorpromazine cation radical decomposition in aqueous buffers. *J. Am. Chem. Soc.* **1978**, *100*, 962–967.

54.   Kigondu, E.M.; Njoroge, M.; Singh, K.; Njuguna, N.; Warner, D.F.; Chibale, K. Synthesis and synergistic antimycobacterial screening of chlorpromazine and its metabolites. *Med. Chem. Commun.* **2014**, *5*, 502–506.

55.   Boehme, C.L.; Strobel, H.W. High-performance liquid chromatographic methods for the analysis of haloperidol and chlorpromazine metabolism in vitro by purified cytochrome P450 isoforms. *J. Chromatogr. B Biomed. Sci. Appl.* **1998**, *718*, 259–266.

56.   Huang, C.L.; Sands, F.L. Effect of ultraviolet irradiation on chlorpromazine II. Anaerobic condition. *J. Pharm. Sci.* **1967**, *56*, 259–264.

57.   Khataee, A.R.; Fathinia, M.; Joo, S.W. Simultaneous monitoring of photocatalysis of three pharmaceuticals by immobilized TiO_2 nanoparticles: Chemometric assessment, intermediates identification and ecotoxicological evaluation. *Spectrochim. Acta - Part A Mol. Biomol. Spectrosc.* **2013**, *112*, 33–45.

58.   Davies, A.K.; Navaratnam, S.; Phillips, G.O. Photochemistry of chlorpromazine [2-chloro-N-(3-dimethylaminopropyl)phenothiazine] in propan-2-ol solution. *J. Chem. Soc. Perkin Trans. 2* **1976**, 25–29.

59.   Hamid, S.; Ivanova, I.; Jeon, T.H.; Dillert, R.; Choi, W.; Bahnemann, D.W. Photocatalytic conversion of acetate into molecular hydrogen and hydrocarbons over Pt/TiO_2: pH dependent formation of Kolbe and Hofer-Moest products. *J. Catal.*

2017, *349*, 128–135.

60.   Shafaei, A.; Nikazar, M.; Arami, M. Photocatalytic degradation of terephthalic acid using titania and zinc oxide photocatalysts: Comparative study. *Desalination* **2010**, *252*, 8–16.

61.   Barreto, J.C.; Smith, G.S.; Strobel, N.H.P.; McQuillin, P.A.; Miller, T.A. Terephthalic acid: A dosimeter for the detection of hydroxyl radicals in vitro. *Life Sci.* **1994**, *56*, PL89–PL96.

62.   Li, S.; Timoshkin, I. V.; Maclean, M.; Macgregor, S.J.; Wilson, M.P.; Given, M.J.; Wang, T.; Anderson, J.G. Fluorescence detection of hydroxyl radicals in water produced by atmospheric pulsed discharges. *IEEE Trans. Dielectr. Electr. Insul.* **2015**, *22*, 1856–1865.

63.   Arimi, A.; Megatif, L.; Granone, L.I.; Dillert, R. Visible-light photocatalytic activity of zinc ferrites. *J. Photochem. Photobiol. A Chem.* **2018**, *366*, 118–126.

Chapter 4: Regarding the Nature of Charge Carriers Formed by UV or Visible Light Excitation of Carbon-Modified Titanium Dioxide

4.1. Forewords

Following the previous chapter, it was found that chlorpromazine, a visible light-persistent material, can be photocatalytically converted under aerobic conditions upon visible light irradiation in the presence of K-7000. However, its main reaction intermediate, chlorpromazine sulfoxide, remained stable under the same conditions. These observations pointed out some limitations in the visible light activity of K-7000. In addition, both the chlorpromazine and its sulfoxide could eventually be converted upon UV irradiation in the presence of K-7000. Thus the difference between the photocatalytic excitation of K-7000 under UV and visible irradiation had to be determined. Nevertheless, due to the lack of a fundamental study regarding the mechanism behind the visible light-driven photocatalytic conversion of chlorpromazine, a deeper analysis on the origin of the visible light activity of the employed photocatalyst was necessary. Hence, by considering K-7000 as a TiO_2-sensitizer assembly, the fate of photogenerated charge carriers in this photocatalyst under different excitation wavelengths was evaluated. Moreover, the differences between the redox potential of the radical cation of the carbon-based sensitizer and that of the molecule to be oxidized were studied. Accordingly, a mechanism was proposed through which the different visible light-driven photocatalytic activity of K-7000 for conversion of different organic molecules could be explained.

This chapter includes the article "Regarding the Nature of Charge Carriers formed by UV or Visible Light Excitation of carbon-modified Titanium Dioxide" by Arsou Arimi, Carsten Günnemann, Mariano Curti, and Detlef W. Bahnemann, published in Catalysts (doi:10.3390/catal9080697). Within the frames of this chapter, K-7000, an anatase titanium dioxide modified with a carbon-based sensitizer layer, was investigated through laser flash photolysis spectroscopy in argon, methanol and oxygen atmospheres. The transient absorption measurements were performed *via* both UV and visible light laser excitation and the nature of charge carriers formed by UV or visible light at different atmospheres was

evaluated. The data obtained through these experiments together with the results of the photocatalytic conversion of chlorpromazine and methanol upon UV and visible light irradiation paved the way for understanding the mechanism of visible light-driven conversion of chlorpromazine in the presence of K-7000.

4.2. Abstract

Although titanium dioxide gathers many of the required properties for its application in photocatalytic processes, its lack of activity in the visible range is a major hurdle yet to be overcome. Among different strategies, the post-synthesis modification of TiO_2 powders with organic compounds has already led to commercially available materials, such as KRONOClean 7000. In this work, we apply diffuse reflectance transient absorption spectroscopy on this visible-light active photocatalyst and study the dynamics of the charge carriers alternatively induced by UV or visible light laser irradiation, under inert or reactive atmospheres. Our results can be interpreted by considering the material as TiO_2 sensitized by an organic-based layer, in agreement with previous studies on it, and show that the oxidative power of the material is considerably diminished under visible light irradiation. By complementarily performing continuous visible light irradiation photocatalysis experiments in aerated aqueous suspensions, we show that, although the oxidation of methanol proceeds at a very slow rate, the oxidation of chlorpromazine occurs much faster thanks to its better suited redox potential.

Keywords: visible light driven photocatalysis; KRONOClean 7000; carbon-based modified TiO_2; transient absorption spectroscopy; chlorpromazine; carbon-doped materials.

4.3. Introduction

In 1972, Fujishima and Honda reported the photocatalytic splitting of water over titanium dioxide (TiO_2) photoelectrodes irradiated with UV light [1]. Since this discovery, much work has been done to understand the underlying processes in photocatalytic reactions [2] and develop new materials with activity in the visible range [3]. Despite these efforts, TiO_2 continues to be the most employed photocatalyst, in particular in its anatase polymorph, due to its higher activity in comparison with the thermodynamically stable form rutile [4,5].

However, anatase has a bandgap of 3.23 eV [6] and, thus, it can make use of not more than 3.5% of the energy emitted by the sun [7].

Different strategies have been considered to increase this fraction. One possibility is to replace the material altogether. For example, iron based photocatalysts generally show a strong absorption in the visible range; however, they are far less active under visible light irradiation than TiO_2 under UV irradiation [8,9]. Besides its replacement with other photocatalysts, a range of different approaches can be used to enhance the light absorption by TiO_2, such as doping or the adsorption of sensitizers on the surface. While doping of TiO_2 (either with metals or non-metals) typically leads to bandgap narrowing [10,11], dye-sensitization extends the visible-light response by coupling the semiconductor with a strongly absorbing molecule, finding applications not only in the field of solar cells [12], but also for photocatalysis [13,14].

These attempts can be considered successful after the commercial development of the KRONOClean 7000 photocatalyst from Kronos International, synthesized by the modification of TiO_2 with pentaerythritol [15]. Although initially it was thought to be carbon-doped TiO_2, it was later proven to consist of anatase particles with a carbon-based sensitizer layer around them [15]. By performing a set of simple but elegant experiments, Ząbek *et al.* were able to remove the layer around the particles and to reassemble it afterwards, while getting exactly the same properties as before the removal. Importantly, the material was shown to be superior to Evonik P25, both for the photocatalytic abatement of NO_x under white light excitation and for the degradation of acetone under visible light [16,17].

Nevertheless, to the best of our knowledge, the tradeoffs incurred by extending the photocatalytic activity of TiO_2 to the visible range, and the similarities or differences of this process compared to those initiated with UV light, remain so far unclarified.

With the goal of understanding the nature and reactivity of its photogenerated charge carriers, here we investigated KRONOClean 7000 by means of transient absorption spectroscopy using both UV (355 nm) and visible light (455 nm) laser excitation. Furthermore, we analyzed the influences of inert (argon), oxygen, and methanol atmospheres on the charge carrier dynamics. Complementarily, we studied the

photocatalytic oxidation of two organic compounds, chlorpromazine and methanol, using aerated KRONOClean 7000 suspensions under continuous visible light irradiation, from which we were able to establish boundaries on its photocatalytic activity under such conditions.

4.4. Results

4.4.1. Characterization of the Photocatalyst

We start the material characterization by analyzing the basic structural properties of KRONOClean 7000 (from here on, K-7000). As can be observed in **Figure 4-1**, the XRD pattern matches well with the standard data of anatase TiO_2 (JCPDS card No. 21-1272), indicating that the carbon modification does not significantly modify the crystalline structure of the parent material. The pattern precludes the presence of a significant fraction of the rutile or brookite TiO_2 polymorphs.
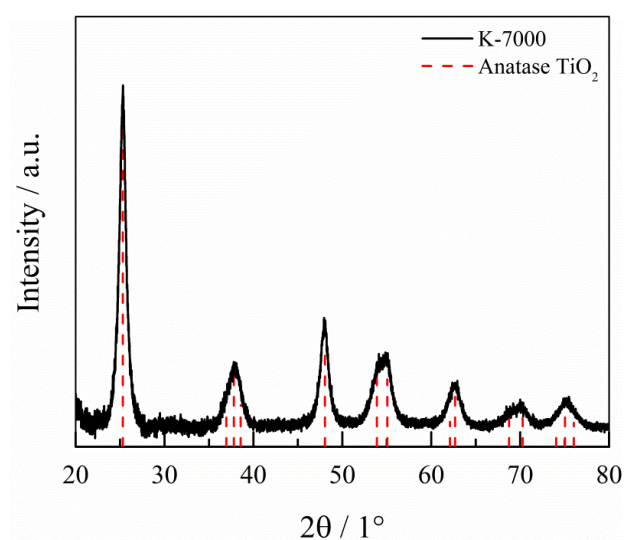
Figure 4-1. XRD pattern of K-7000 and the anatase reference JCPDS card No. 21-1272.

To determine the light absorbing properties of the photocatalyst, we measured its diffuse reflectance spectra in the spectral range from 300 to 800 nm (**Figure 4-2(a)**). As a comparison, the results for the pure-anatase photocatalyst Hombikat UV100 are also shown. From these spectra, we determined the Kubelka–Munk functions, shown in **Figure 4-2(b)**. A long-tailed absorption is clearly observed for K-7000, spanning the visible range from 400 nm to 550 nm. On the contrary, UV100 only absorbs in the ultraviolet range. By processing the spectra of K-7000 and Hombikat UV100 with the Tauc plot (**Figure 4-S1**)

we obtained bandgap values of 3.31 eV (corresponding to a wavelength of 374 nm) for K-7000 and 3.32 eV (~373 nm) for UV100.
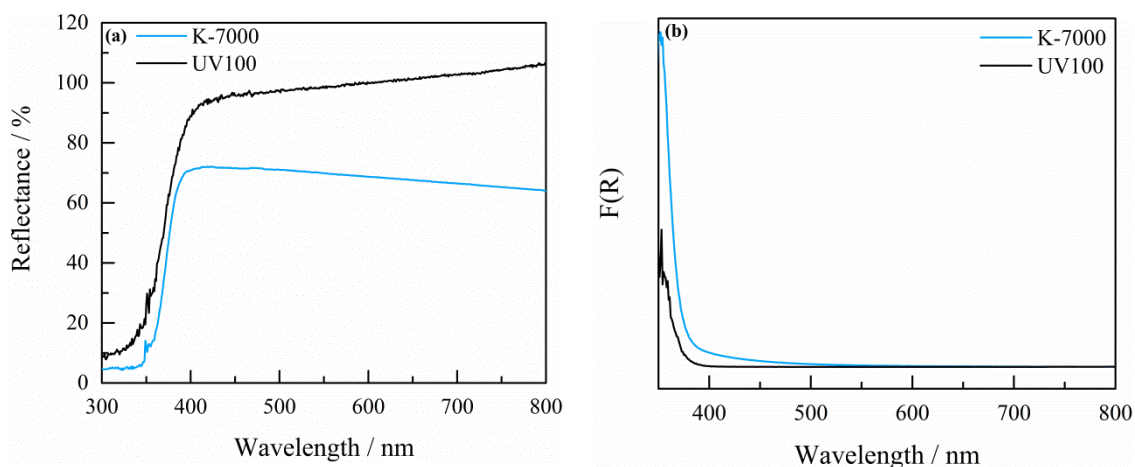
Figure 4-2. (**a**) Diffuse reflectance spectra (DRS) and (**b**) Kubelka–Munk functions of K-7000 and Hombikat UV100.

4.4.2. Mott–Schottky Measurements

In order to determine the flatband potential of K-7000 and Hombikat UV100, we performed electrochemical measurements. By plotting the inverse of the square of the measured capacitance versus the applied potential, the flatband potential can be obtained by a linear fit. As shown in **Figure 4-3**, this value was determined to be equal to −0.46 V *vs.* NHE and −0.51 V *vs.* NHE, for K-7000 and Hombikat UV100, respectively. The small difference is within experimental error.
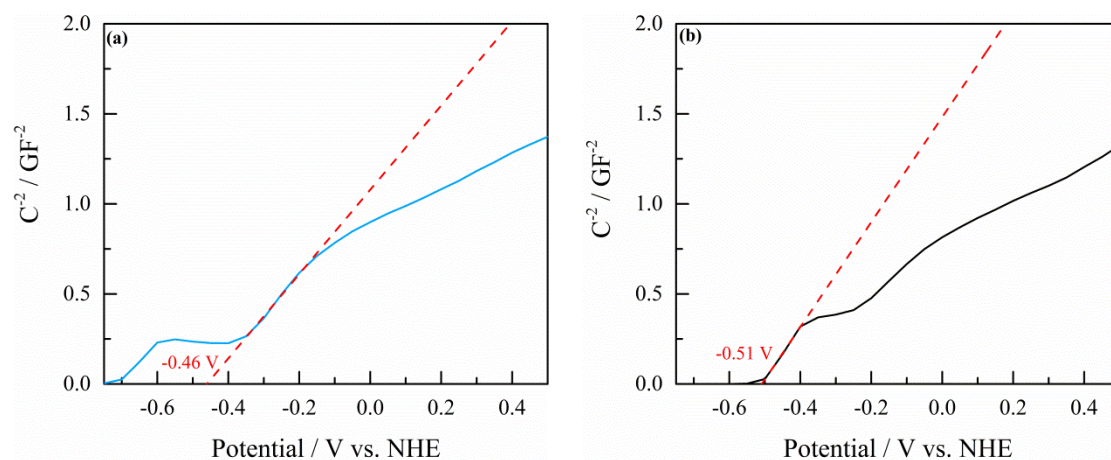
Figure 4-3. Mott–Schottky plot of (**a**) a K-7000 film and (**b**) a Hombikat UV100 film measured in a 0.1 M KNO₃ solution at a frequency of 100 Hz. The dashed red line shows the extrapolation of the linear part to the ordinate value of zero.

4.4.3. Transient Absorption Spectroscopy

To study the dynamics of the photogenerated charge carriers, we investigated K-7000 via diffuse reflectance transient absorption spectroscopy. **Figure 4-4** presents the transient absorption spectra of the K-7000 powder obtained after excitation with 355 nm (**Figure 4-4(a)**) and 455 nm (**Figure 4-4(b)**) at 100 ns after the laser excitation. The spectra were obtained at three different conditions, as follows: in the presence of oxygen (electron scavenger), of methanol (hole scavenger), and in the absence of electron scavengers or donors (Ar atmosphere). In the latter case, the photogenerated charge carriers can only react with each other (i.e., recombine).

As can be seen in **Figure 4-4(a)**, after excitation with 355 nm, there are no significant differences in the transient absorption spectra under Ar or O_2 atmospheres, while the experiments in Ar atmosphere and methanol atmosphere show a considerable difference. Moreover, this difference is larger at shorter wavelengths (~400 nm) than at the longer wavelength range (~650 nm). On the other hand, as revealed in **Figure 4-4(b)**, the transient absorption spectra obtained after excitation with 455 nm in all the atmospheres are, within experimental error, identical to each other.
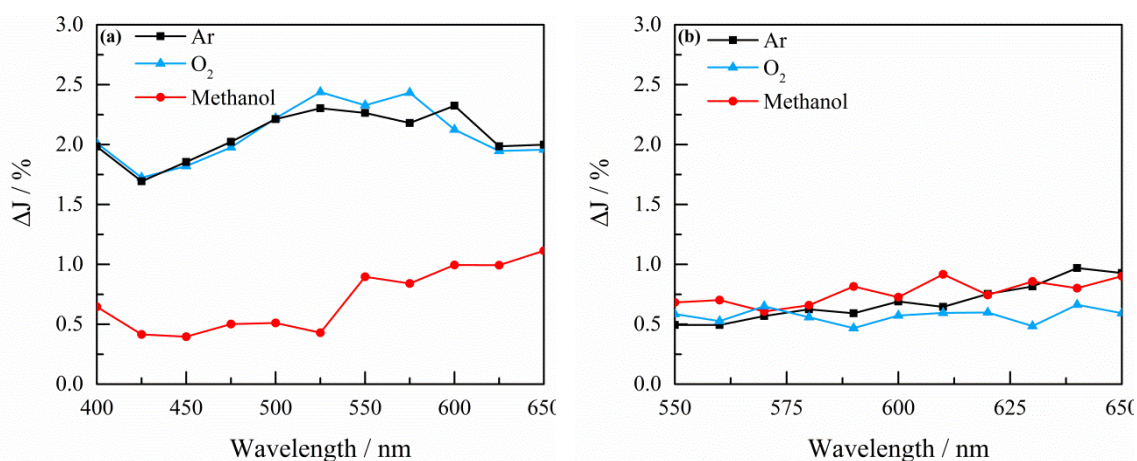
Figure 4-4. Transient absorption spectra of K-7000 measured 100 ns after excitation with a (**a**) 355 nm and (**b**) 455 nm laser in Ar (black), O_2 (blue), and methanol (red) atmospheres.

Figure 4-5 displays the transient absorption decays detected at 650 nm for the K-7000 powder in O_2, methanol and Ar atmospheres after excitation with 355 nm (left) and 455 nm (right). In the case of excitation with 355 nm (**Figure 4-5(a)**), both under Ar and O_2

atmospheres the transient absorption strongly increases right after the laser pulse and is followed by a rapid decrease down to ~15% of the initial value at 8 µs. In the case of the methanol atmosphere, however, the transient absorption is initially lower than the other two cases and increases with time in the investigated window. By comparing the transient absorption decays after excitation with 355 nm and 455 nm, **Figure 4-5(a)** and **Figure 4-5(b)**, it can be seen that the initial absorptions after excitation with 455 nm are much lower than those values after excitation with 355 nm. After excitation with 455 nm the decrease of the transient absorption is significantly slower and decreases only to ~60% of the initial value after 8 µs. Furthermore, at this excitation wavelength no significant difference was observed regarding the type of atmosphere.
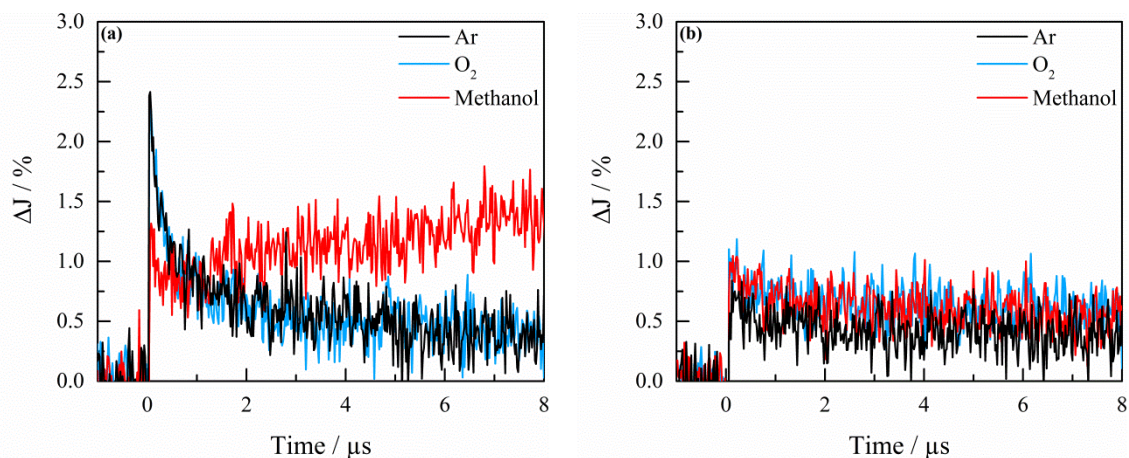
Figure 4-5. Transient absorption decays of K-7000 detected at 650 nm in an Ar (black), an O_2 (blue), and a methanol (red) atmosphere, after excitation with (**a**) 355 nm and (**b**) 455 nm.

The behavior of K-7000 under visible-light excitation was compared with that of Hombikat UV100 in Ar atmosphere. **Figure 4-6(a)** shows the transient absorption decays in K-7000 and UV100 powders detected at 650 nm, after excitation with 455 nm. While UV100 shows virtually no transient absorption, a significant signal with a long-lived component can be observed for K-7000. Similarly, the transient absorption spectrum of UV100 (**Figure 4-6(b)**) at 100 ns after the pulse is negligible with respect to that of K-7000.
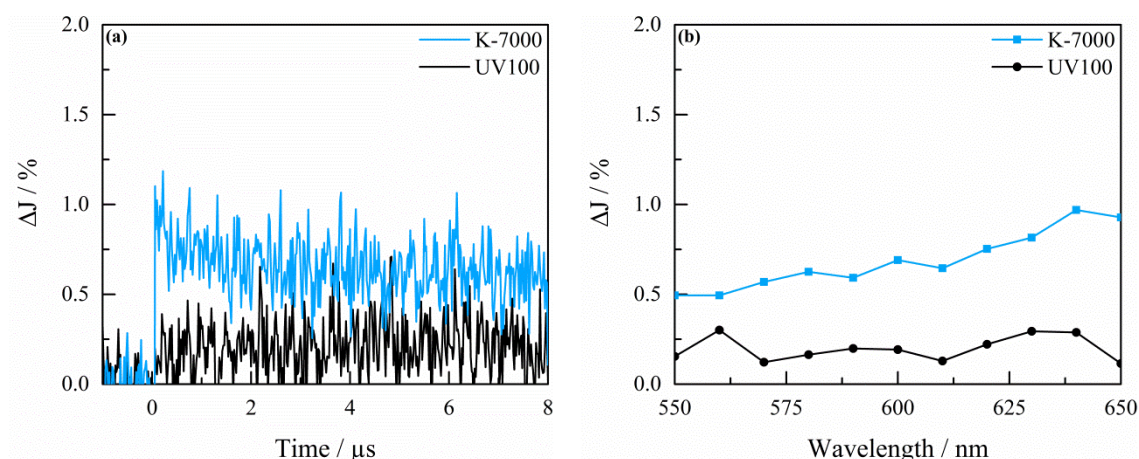
Figure 4-6. (**a**) Transient absorption decays of K-7000 (blue) and UV100 (black) observed at 650 nm in an
Ar atmosphere after excitation with 455 nm, (**b**) transient absorption spectra of K-7000 (blue) and UV100
(black) measured at 100 ns after the laser excitation.

4.4.4. Photocatalytic Experiments

In order to evaluate the visible-light activity of K-7000, we performed photocatalytic
experiments using methanol and chlorpromazine as organic model compounds. For that
matter, we analyzed their conversion in the presence of a K-7000 suspension upon
irradiation at 455 nm. The results of these experiments are shown in **Figure 4-7**.

Figure 4-7. Comparison of the conversion of methanol and chlorpromazine upon visible light irradiation
(455 nm) in the presence of K-7000.

The oxidation of methanol was monitored by assessing the production of formaldehyde
throughout the reaction period (**Figure 4-S2**). After 60 minutes of visible light irradiation
in the presence of K-7000, only a slight degradation of methanol was observed.

In the case of chlorpromazine, it was found to be stable in the absence of K-7000 throughout the photolytic reaction time (**Figure 4-S3**) under visible light irradiation (455 nm), as expected from the very low overlap between its absorption spectrum and the emission spectrum of the light source (**Figure 4-S4**). In the presence of K-7000, however, chlorpromazine is completely converted within the first 30 minutes of irradiation. The main product of this reaction is chlorpromazine sulfoxide, identified by comparing its retention time with a standard sample. The sulfoxide seems to be stable with respect to its photocatalytic conversion, since its concentration increases monotonically before reaching a constant value at ~30 minutes (**Figure 4-S5**). As a comparison, we have also investigated the photocatalytic conversion 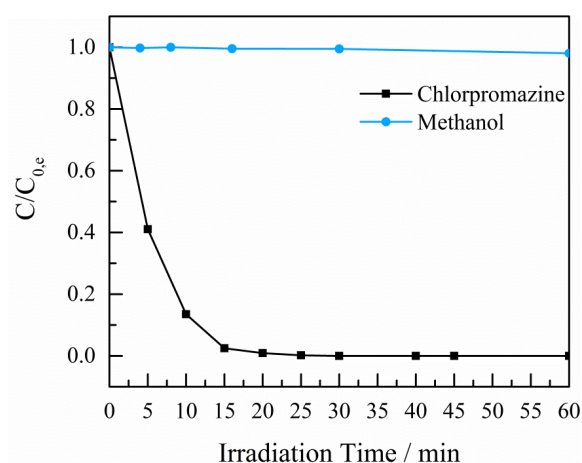of chlorpromazine in the presence of Hombikat UV100 under visible light irradiation under identical conditions. However, in this case, the conversion of chlorpromazine was negligible (**Figure 4-S6**).

4.5. Discussion

The XRD analysis of the K-7000 powder (**Figure 4-1**) confirms that anatase is the only crystalline phase significantly present, as also reported by Ząbek *et al.* [15]. Thus, no effect of the carbon-based layer on the crystalline structure of the titanium dioxide is observed. The anatase phase of the photocatalyst was further evinced by the UV-vis reflectance measurements (**Figure 4-2(a)**). From these, a bandgap value of 3.31 eV was found (**Figure 4-S1**), which was in good agreement with previous reports [15,17]. Moreover, the comparison of the absorption properties of K-7000 with those of UV100 (pure anatase) reveals a broad absorption band in the visible region for K-7000, not observed in anatase and, thus, ascribed to the carbon-based layer. The flatband potential of K-7000 was determined via Mott–Schottky measurements to be −0.46 V *vs.* NHE at pH 7 (**Figure 4-3(a)**), similar to a previously reported value for its quasi-Fermi level (−0.50 V *vs.* NHE at pH 7) [15]. Both values match very well with those measured for anatase TiO_2 (Hombikat UV100) and, therefore, it can be concluded that the modification performed on K-7000 does not significantly affect the position of its conduction band.

Transient absorption spectroscopy measurements were performed in different atmospheres using excitation with UV light (355 nm) and visible light (455 nm). In the Ar atmosphere the only possible fate of the photogenerated charge carriers is recombination with each other, since no other species are present to react with them. Since oxygen can act as an

electron scavenger, it would be expected for it to affect the transient absorption spectra and decays. However, no difference can be observed between inert and O_2 atmospheres in both transient absorption spectra and transient decays, irrespective of the excitation wavelength. The standard reduction potential of oxygen is -0.33 V *vs.* NHE [18], i.e., more positive than the flatband potential of K-7000 (-0.46 V *vs.* NHE in neutral solution). Therefore, from a thermodynamic point of view, the transfer of electrons from the conduction band of TiO_2 to oxygen molecules is expected to happen. The scavenging of photogenerated electrons in TiO_2 by O_2 molecules in the gas atmosphere has been studied by Yamakata *et al.*, who found a characteristic reaction time of tens of microseconds. Consequently, no significant reaction can be observed before 10 μs [19]. Accordingly, O_2 shall not affect the transient absorption spectra in the considered time scale. For longer time scales it would be possible to observe an effect of the O_2 atmosphere; however, our focus is on the oxidative half-reaction, and thus, for consistency, we limited ourselves to an 8 μs window.

Methanol is a well-known hole scavenger and reacts in a first step to form an α-hydroxyl radical (**Equation 4-1**) [20,21]. For this oxidation reaction, a potential of 1.03 V *vs.* NHE is required at pH 7 [22]. With the flatband potential of -0.46 V *vs.* NHE and the determined bandgap of 3.31 eV, the valence band edge can be calculated to be at 2.85 V *vs.* NHE. For the abstraction of an electron from a methanol molecule, the valence band edge and thus the potential of the photogenerated holes must be more positive compared to the redox potential of the methanol oxidation. Accordingly, this reaction is likely to take place. In general, a transient absorption spectrum contains contributions from both, photogenerated electrons and holes. Herein, methanol acts as a hole scavenger; therefore, only the spectrum of the remaining electrons can be detected. Furthermore, since there is no electron scavenger present, photogenerated electrons accumulate in the particles, a well-known phenomenon for TiO_2 [23]. It can be concluded from the spectrum (**Figure 4-4 (a)**) that the photogenerated electrons mainly absorb at higher wavelengths, as reported before [24]. This explains the observed differences in the spectra under Ar and methanol atmospheres.

$$CH_3OH \rightarrow {}^{\bullet}CH_2OH + H^+ + e^- \tag{4-1}$$

For completeness, we note that in the absence of oxygen, the formed α-hydroxyl radicals react in a further step to produce formaldehyde (**Equation 4-2**). This reaction possesses a

redox potential of -1.41 V *vs.* NHE at pH 7 [22]. According to this potential, which is more negative than the flatband potential of K-7000 (-0.46 V *vs.* NHE), the formation of formaldehyde can occur by the injection of an electron into the conduction band of TiO_2, known as the current doubling effect [21].

$$^\bullet CH_2OH \rightarrow CH_2O + e^- + H^+ \tag{4-2}$$

The transient absorption spectroscopy experiments using 455 nm light excitation offer a different picture. The photon energy (2.73 eV) is not sufficient for bandgap excitation in anatase TiO_2, as illustrated by the bandgap of K-7000 (3.31 eV). Accordingly, the pure anatase material UV100 shows no transient response after visible light excitation (**Figure 4-6**), with the exception of some experimental noise. On the contrary, a notable and long-lived signal can be detected in K-7000 under the same conditions, originated from its light absorption in the visible range, as described above. Regarding the physical origin of such absorption, we recall that investigations performed in the group of Prof. Kisch have determined that, in K-7000, carbon is not incorporated into the lattice, as originally thought, but is rather deposited on the surface in the form of a molecular sensitizer [15]. This important distinction may have a profound impact on the photocatalytic mechanism under visible light, since doping usually causes bandgap narrowing, as demonstrated, for instance, in N- and S-doped TiO_2 [25,26]. In agreement with the molecular sensitizer description, we found no bandgap narrowing for K-7000, but rather an absorption band in the visible range related to the sensitizer. Incidentally, the sensitizer–TiO_2 assembly can be treated akin to dye-sensitized solar cells, where the electronic structure of the former is characterized by defined HOMO (highest occupied molecular orbital) and LUMO (lowest unoccupied molecular orbital) levels [27]. Therefore, under excitation with visible light, the transition does not involve the valence band and the conduction band of TiO_2, but rather the HOMO and LUMO levels of the sensitizer.

In coincidence with the experiments using excitation with UV light, no difference in the spectra and decays in Ar and oxygen atmosphere was observed after visible light excitation of K-7000 (**Figure 4-4** and **Figure 4-5**). This indicates that no reaction takes place with oxygen in the considered time scale. A plausible explanation is that, after excitation of the carbon-based sensitizer, electrons are injected from the LUMO to the conduction band of

TiO_2, as known for dye-sensitized solar cells [27]. Therefore, under visible light irradiation, oxygen reduction is ultimately limited in the same way as for bandgap excitation [19].
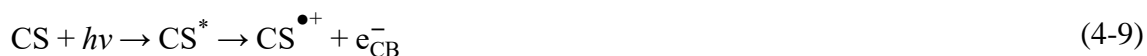
At odds with the transient absorption results using UV excitation, we observed no differences in the decays and spectra in methanol atmosphere with respect to inert atmosphere, indicating that no degradation of methanol takes place within the considered time scale under visible light excitation. Furthermore, the decays observed in all atmospheres after excitation with visible light were found to be rather long-lasting. This behavior is comparable to the decay obtained in methanol atmosphere after excitation with UV light (**Figure 4-5(a)**), where electrons accumulate in the TiO_2 particles. In the present case, electron transfer from the LUMO of the sensitizer to the conduction band of TiO_2 gives rise to their accumulation, since either no electron scavenger is present (Ar or methanol) or the rate of electron consumption is very low (O_2). Concomitantly, the radical cations of the sensitizer are produced after electron injection, which may lead to a bleaching of the sensitizer [28].

To obtain further insights into the oxidation of methanol over K-7000 under visible light irradiation (or the lack thereof), we performed photocatalytic experiments under continuous irradiation in aerated aqueous suspensions. After 60 minutes of irradiation in the presence of K-7000, less than 2% of a 100 μM methanol solution was transformed to formaldehyde (**Figure 4-7** and **Figure 4-S2**). These observations are in good agreement with the transient absorption spectroscopy results, revealing that, under visible light irradiation, the degradation of methanol is negligible or, at best, slow. To understand this behavior, the possible degradation mechanisms of methanol under irradiation with UV light as well as visible light in the presence of the photocatalyst must be discussed. Generally, after excitation with UV light, electron–hole pairs are generated in the TiO_2 particles (**Equation 4-3**). In this case, the carbon-based sensitizer is possibly excited as well. However, considering the smaller amount of the sensitizer layer compared to TiO_2, the excitation of the sensitizer can be neglected in the mechanism. The photogenerated electrons can react with oxygen molecules forming a superoxide radical ($O_2^{-\bullet}$) (**Equation 4-4**), while the photogenerated holes can be trapped either at terminal protonated bridging oxygen ions (OH_{br}^-) to form a hydroxyl radical ($-OH_{br}^\bullet$) (**Equation 4-5**) or at adsorbed methanol molecules (CH_3OH_{ads}) forming an α-hydroxyl radical ($^\bullet CH_2OH$) (**Equation 4-6**).

Methanol molecules in aqueous solution (CH_3OH_{aq}) can be oxidized via hydroxyl radicals yielding the same radical (**Equation 4-7**). In an aerated suspension, the produced α-hydroxyl radicals are further oxidized to formaldehyde through reaction with oxygen molecules (**Equation 4-8**) [29].

$$TiO_2 + h\nu \rightarrow e_{CB}^- + h_{VB}^+ \tag{4-3}$$

$$O_2 + e_{CB}^- \rightarrow O_2^{-\bullet} \tag{4-4}$$

$$OH_{br}^- + h_{VB}^+ \rightarrow \text{-}OH_{br}^\bullet \tag{4-5}$$

$$CH_3OH_{ads} + h_{VB}^+ \rightarrow {}^\bullet CH_2OH + H^+ \tag{4-6}$$

$$CH_3OH_{aq} + \text{-}OH_{br}^\bullet \rightarrow {}^\bullet CH_2OH + \text{-}OH_{2br} \tag{4-7}$$

$${}^\bullet CH_2OH + O_2 \rightarrow CH_2O + O_2^{-\bullet} + H^+ \tag{4-8}$$

On the other hand, after excitation with visible light the mechanism will be different, since the excitation energy is not enough to generate electron–hole pairs in TiO2. Thus, under visible light irradiation, only the carbon-based sensitizer layer (CS) can be excited (CS^*), after which an electron is transferred from the LUMO to the conduction band of the TiO2 (**Equation 4-9**), simultaneously forming the radical cation of the sensitizer ($CS^{\bullet+}$). Afterwards, the electron in the conduction band can react with molecular oxygen (**Equation 4-4**), while the sensitizer radical cation could react with methanol to form an α-hydroxyl radical (${}^\bullet CH_2OH$) (**Equation 4-10**). Exactly as after irradiation with UV light, this radical can react further with molecular oxygen, yielding formaldehyde (**Equation 4-8**).

$$CS + h\nu \rightarrow CS^* \rightarrow CS^{\bullet+} + e_{CB}^- \tag{4-9}$$

$$CS^{\bullet+} + CH_3OH \rightarrow CS + {}^\bullet CH_2OH + H^+ \tag{4-10}$$

However, the reaction shown in **Equation 4-10** does not occur at a significant rate, since neither the transient absorption spectroscopy measurements nor the photocatalytic experiments suggest a degradation of methanol. The reason for the lack of reaction is discussed below. In passing, we represent the different reactions and processes occurring after excitation with UV and visible light in **Scheme 4-1**.
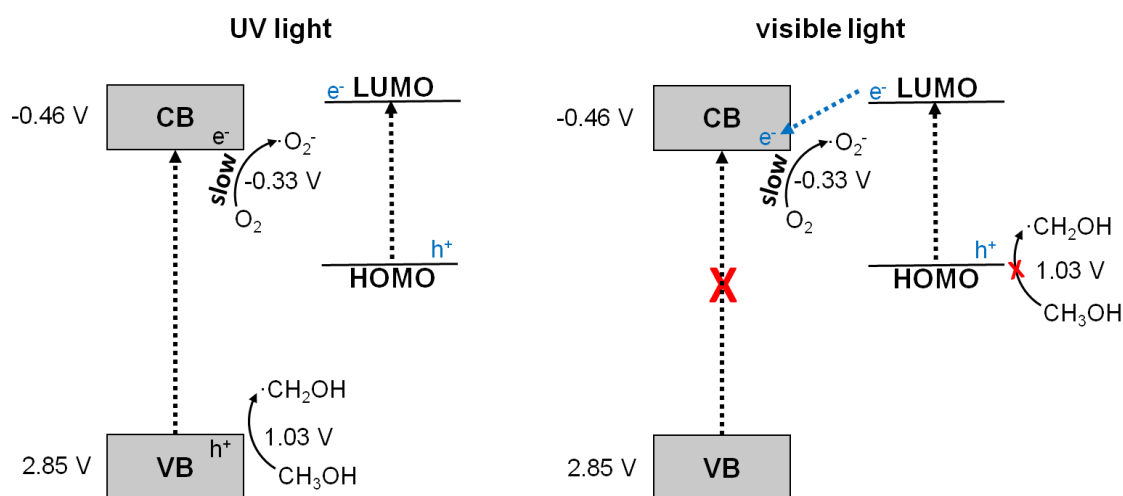
Scheme 4-1. Proposed processes taking place after excitation of K-7000 with UV light and visible light. The excitation with UV light leads to the generation of electron-hole pairs in the anatase particles and the carbon-based sensitizer as well, while visible light causes the excitation of the carbon-based sensitizer.

In contrast to methanol, chlorpromazine, which belongs to the phenothiazines group, could be completely degraded within the first 30 minutes of continuous visible light irradiation in the presence of K-7000 (**Figure 4-7**). In order to explain this difference, the mechanism of the visible light induced conversion of chlorpromazine must be taken into account. Upon visible light irradiation, excitation of the carbon-based sensitizer leads to electron transfer to the conduction band of TiO_2 (**Equation 4-9**). In the presence of oxygen, these electrons (slowly) reduce it, forming superoxide radicals (**Equation 4-4**). The sensitizer radical cation ($CS^{\bullet+}$) is able to oxidize chlorpromazine to form a chlorpromazine radical cation (**Equation 4-11**), simultaneously regenerating the sensitizer. As reported for similar compounds [30], the next step is most likely the reaction between the produced chlorpromazine radical cation and a superoxide radical to form a persulfoxide molecule (**Equation 4-12**). The persulfoxide molecule forms a thiadioxirane (**Equation 4-13**), which

reacts with a further chlorpromazine molecule yielding two chlorpromazine sulfoxide molecules (**Equation 4-14**), as expected from the mechanism proposed by Somasundaram and Srinivasan for the oxidation of aryl methyl sulfides in the presence of irradiated TiO_2 [30].

(4-11)

(4-12)

(4-13)

(4-14)
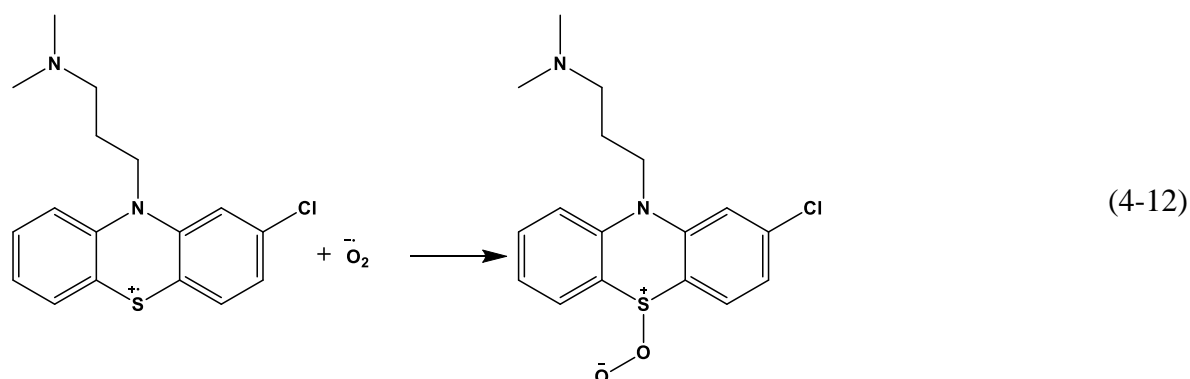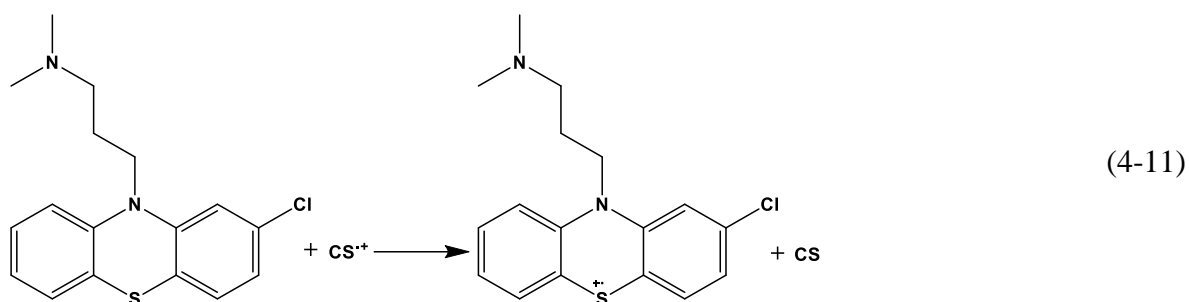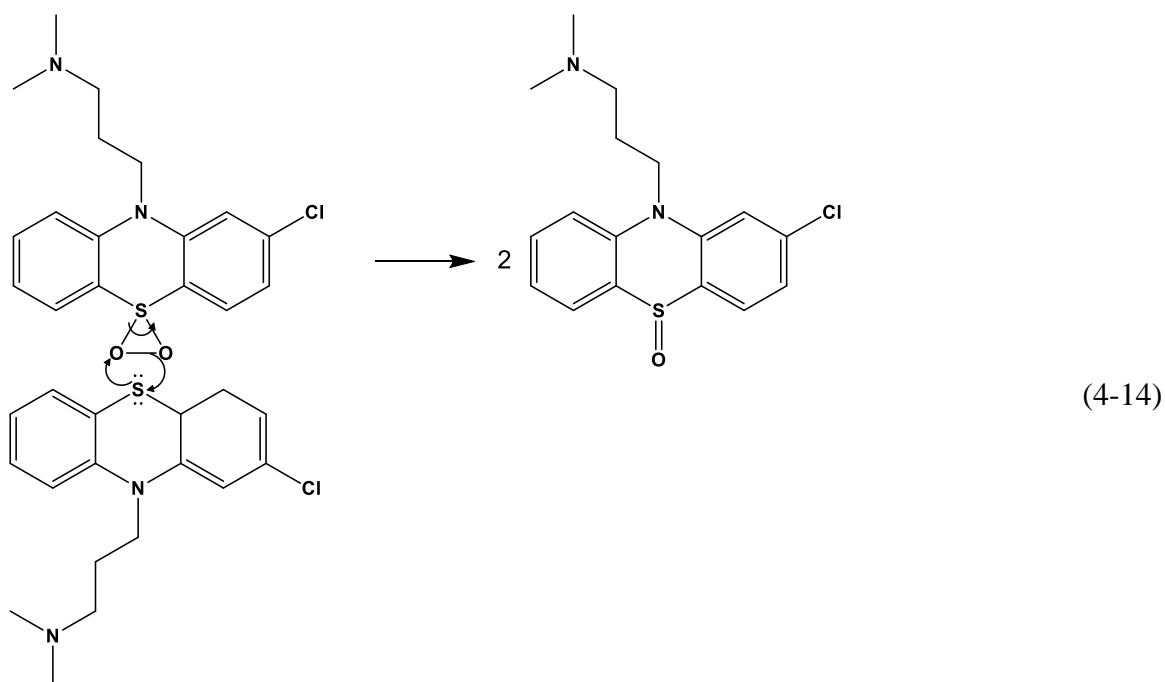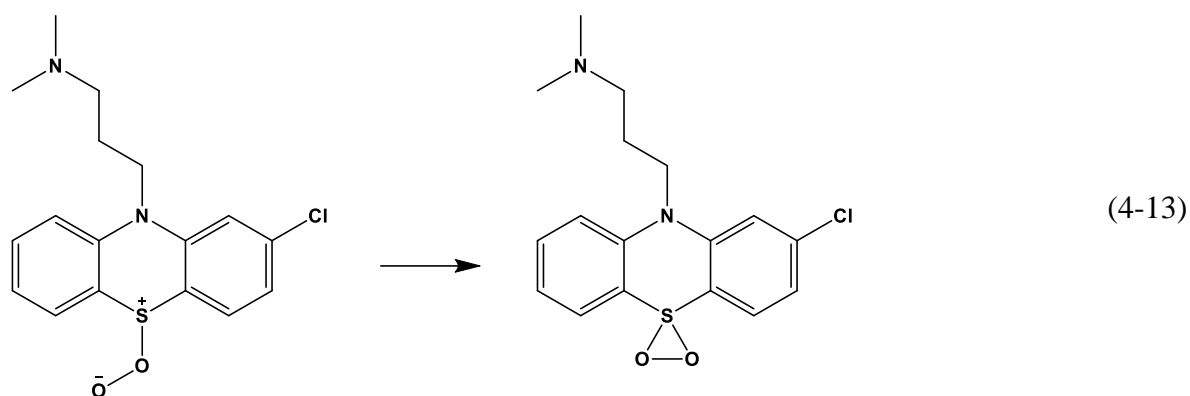
Contrary to methanol, which was not significantly oxidized upon visible light irradiation of K-7000, chlorpromazine is able to react with the sensitizer radical cation, yielding its sulfoxide. The reaction of the organic compound with the sensitizer radical cation is essential for the further photocatalytic reaction steps. If this initial reaction does not take place, the further steps will not occur as well. To explain the reason why this initial reaction only happens with chlorpromazine and not with methanol, the redox potentials for the corresponding reactions have to be considered. As mentioned before, the required potential

for the methanol oxidation (**Equation 4-1**) is 1.03 V *vs*. NHE at pH 7 [22]. The redox potential for the one-electron oxidation of chlorpromazine is 0.53 V *vs*. NHE at pH 7 and, thus, more negative [31,32]. From this information, it can be concluded that the redox potential of the sensitizer radical cation is more positive than that of the chlorpromazine oxidation and either more negative or close to that of the methanol oxidation, which hinders its reaction with the latter. We note that, being electron transfer reactions, their kinetics are governed by Marcus theory [33,34]. As such, even if the reaction is moderately exergonic, it still may occur at a reduced rate due to the influence of the solvent reorganization energy. Additionally, we can estimate that the position of the LUMO must be located at a more negative potential than the conduction band edge of TiO_2; otherwise, no electron transfer from the excited sensitizer to the conduction band of TiO_2 would be possible. However, it has to be mentioned that the exact position of the LUMO cannot be determined from these experiments. All relevant redox potentials, as well as the conduction band and valence band position of the photocatalyst, including the possible positions of the LUMO and HOMO, are gathered in **Scheme 4-2**.
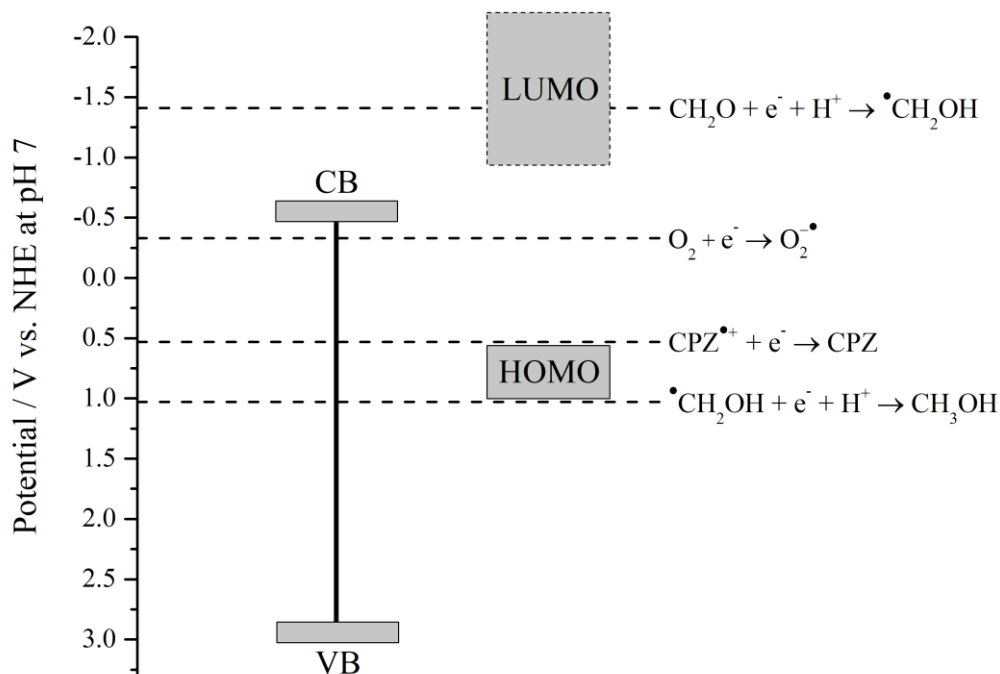
Scheme 4-2. Band positions of the anatase photocatalyst K-7000 with the corresponding redox potentials of the oxygen reduction, methanol oxidation, and chlorpromazine (CPZ) oxidation at pH 7 and the possible positions of the LUMO and the HOMO of the sensitizer [18,22].

To confirm the results of the photocatalytic experiments, we performed transient absorption spectroscopy measurements with the K-7000 powder in the presence of pre-adsorbed chlorpromazine. Unlike the case of methanol (**Figure 4-5(b)**), the transient absorption of bare K-7000 changes in the presence of chlorpromazine, giving rise to a signal attributable to the chlorpromazine radical cation [35] (**Figure 4-S7**). Thus, both the continuous irradiation experiments and the transient absorption spectroscopy measurements evince a prompt degradation of chlorpromazine and a negligible one for methanol. We note that chlorpromazine oxidation under UV irradiation of K-7000 has been the subject of a recent study [36] and, thus, we focused here on its visible light degradation.

Interestingly, the oxidation product of the chlorpromazine degradation, namely chlorpromazine sulfoxide, was found to be highly persistent throughout the visible light irradiation of K-7000 (**Figure 4-S5**). This product was found to be a long-lasting compound upon visible light driven photocatalysis as well, as previously reported [36]. This result can be understood on the same grounds as for methanol and chlorpromazine. Although the redox potential for the one-electron oxidation of chlorpromazine sulfoxide has not, to the best of our knowledge, been determined, potentials in the range of 2.5 V to 2.8 V have been reported for similar sulfoxides [30], i.e., very close to the valence band edge of K-7000. By assuming a potential for chlorpromazine sulfoxide in this range, no oxidation can be expected, since this value is located at a position even more positive than that for the methanol oxidation.

In summary, our results with the commercial photocatalyst K-7000 illustrate that photogenerated charge carriers in visible light active materials may have a limited ability to drive oxidation reactions, which is at odds with the general wisdom stating that photogenerated holes in TiO_2 possess a very high oxidizing power. Moreover, while this fact may be detrimental for the application of such materials in environmental remediation, it may however be exploited to increase the selectivity of the oxidation half-reaction in photocatalytic processes. Instead of complete mineralization, under the right conditions it might be possible to selectively oxidize an unwanted compound into a valuable one [37].

4.6. Materials and Methods

4.6.1. Chemicals

KRONOClean 7000, the carbon-modified TiO_2 powder, was provided by Kronos International, Inc. (Leverkusen, NRW, Germany). Hombikat UV100, a pure anatase TiO_2 photocatalyst, was provided by Sachtleben Chemie GmbH (Duisburg, NRW, Germany). Chlorpromazine sulfoxide was purchased from LGC-Standards (Wesel, NRW, Germany) and acetonitrile (Rotisolv® HPLC Gradient) was purchased from Carl-Roth (Karlsruhe, BW, Germany). Chlorpromazine hydrochloride (CPZ) ($\geq$98%), trifluoroacetic acid (Uvasol®, for spectroscopy), and all other chemicals in this work were purchased from Sigma-Aldrich (Merck, Darmstadt, HE, Germany) (unless noted) and were used as received. In all experiments ultrapure water ($\geq$18.2 MΩ cm) was employed.

4.6.2. Characterization of K-7000

X-ray diffraction (XRD) analysis was performed using Cu K_α radiation ($\lambda = 0.154178$ nm) with a Bruker D8 Advance diffractometer. The patterns were recorded at room temperature in the 2θ range between 20° and 80°, with steps of 0.011° in Bragg–Brentano geometry (θ–θ). The diffuse reflectance spectra of the photocatalysts powders were determined in the spectral range from 300 to 800 nm by means of a Varian Cary-100 UV–vis spectrophotometer equipped with an integrating sphere, with barium sulfate as a reflectance reference. The optical bandgap was determined using a Tauc plot analysis assuming indirect transitions (**Figure 4-S1**).

The flatband potential was determined through the Mott–Schottky method, performed using a ZENNIUM Electrochemical Workstation (ZAHNER-elektrik) with a 0.1 M KNO_3 solution as the electrolyte and a frequency of 100 Hz. For this measurement, a three-electrode electrochemical cell made of Teflon, with a Pt counter electrode and an Ag/AgCl/NaCl (3 M) reference electrode, was used. The screen-printing technique was applied to prepare the K-7000 and Hombikat UV100 films on a 3 cm × 3 cm fluorine-doped tin oxide (FTO) glass (Sigma-Aldrich) calcined at 450 °C, as the working electrode. The paste used to prepare the films was obtained following the procedure described by Ito *et al.* [38].

4.6.3. Transient Absorption Spectroscopy

The transient absorption spectroscopy measurements were performed with the catalyst powder inside a flat quartz cell. All samples were purged prior to the experiments with either argon, a mixture of nitrogen and methanol, or oxygen for 30 minutes. The experiments were performed in diffuse reflectance mode by means of an Applied Photophysics LKS 80 Laser Flash Photolysis Spectrometer with a pulsed Nd:YAG laser (Quantel, Brilliant B). For excitation of the samples, the third harmonic of the laser (355 nm, 6 ns pulses) or the third harmonic equipped with an optical parametric oscillator (OPO, 455 nm) was used with an average energy of 3 mJ·cm^{-2}. The laser light and the analyzing light (Xenon lamp, pulsed, Osram XBO, 150 W) were focused on the surface of the powder sample. The reflected light was guided to a detector (Hamamatsu PMT R928), which was connected with a 100 Ω resistance to an oscilloscope. The photomultiplier converted the incoming photons directly into a current. For every detection wavelength, a different voltage was applied to the photomultiplier to adjust the light level to a constant value. Absorbance values, Abs, were calculated from the reflected light before (J_0) and after the laser excitation (J). The values of the change of reflectance, ΔJ, were obtained by applying the following equation:

$$\Delta J = 1-10^{\text{-Abs}} = \frac{J_0 - J}{J_0} \tag{4-15}$$

For each detection wavelength, a time scale of 10 μs was considered, 25 shots were averaged and the data points were reduced to 200. The spectra were recorded from 400 nm to 650 nm in 25 nm steps for excitation with 355 nm and from 550 nm to 650 nm in 25 nm steps for the excitation with 455 nm.

4.6.4. Photocatalytic Procedure

For the photocatalytic experiments, chlorpromazine and methanol were chosen as probe organic molecules. The irradiation source was a monochromatic light emitting diode (LED) with an emission maximum at 455 nm (Thorlabs, M455L3, 339 W·m^{-2}; emission spectrum shown in **Figure 4-S5**). The photocatalytic setup included a barrel-shaped borosilicate photoreactor (diameter: 6 cm, height: 3 cm) covered with a black polymer case, which had

a connection on the top for the attachment of the LED light source. For these experiments, initially a 60 mL aqueous suspension of 100 μM chlorpromazine/methanol and 1 g·L^{-1} photocatalyst was prepared at its natural pH. The suspension was then stirred for 60 minutes under dark conditions in the photoreactor to reach the adsorption–desorption equilibrium. Afterwards, the LED light source began to irradiate the reaction medium for 60 minutes; throughout the reaction period, the suspension was purged with oxygen. At regular time intervals, samples were taken, centrifuged, and filtered (PVDF, 0.2 μm pore size). For the experiments with chlorpromazine, the samples were analyzed with a HPLC-UV-MS (ESI) device using an Alliance 2795-HT HPLC (Waters, UK) coupled with a 1050 UV-detector (type 79853C, detection wavelength: 254 nm, HP, USA) and an LCT Premier ESI mass spectrometer (Waters, UK). The resulting data of the conversion of chlorpromazine into its main product chlorpromazine sulfoxide were presented in terms of the change of their concentration (μM) versus irradiation time (min). For the methanol degradation, the production of formaldehyde was monitored by derivatizing it with Nash's reagent [39] and then following the colored product with a Varian Cary-100 UV–vis spectrophotometer. The conversion of methanol was compared with that of chlorpromazine in terms of the concentration at the sampling time divided by the initial concentration after the equilibrium (C/C$_{0,e}$). Photocatalytic experiments were performed at least twice to ensure reproducibility.

4.7. Conclusions

We studied the reactivity upon UV and visible light irradiation of the commercially available photocatalyst KRONOClean 7000. Its characterization revealed that its crystalline structure, flatband potential, and light absorption in the UV range closely match those of pure anatase TiO$_2$. Its visible light photocatalytic activity originates from a long-tailed absorption in this range, which is ascribed to the carbon modification employed for its preparation. By means of transient absorption spectroscopy, we investigated charge carrier generation and recombination in the material using Ar, O$_2$, and methanol atmospheres. Excitation with UV light did not show a significant reaction of photogenerated charge carriers with oxygen in the investigated time window, explained by a slow electron transfer. In the presence of methanol, we observed a gradual accumulation of electrons due to its fast reaction with photogenerated holes. Upon excitation with visible

light, all spectra and decays show similar features, indicating that neither with methanol nor with O_2 a reaction takes place to a significant degree. Complementarily, we performed photocatalytic reactions under visible light irradiation, after which we observed no methanol oxidation, but a fast degradation of chlorpromazine. We rationalized these results by considering K-7000 akin to a dye-sensitized system, in which the carbon-based layer acts as a molecular sensitizer. As such, excitation with UV light leads to the generation of electron-hole pairs in TiO_2, while visible light causes the excitation of the sensitizer followed by electron injection into TiO_2 and subsequent formation of the radical cation. Ultimately, the oxidation ability of the material depends on the difference between the redox potential of the radical cation and that of the molecule to be oxidized: while the oxidation potential of methanol is too negative for it to react, that of chlorpromazine allows the reaction to swiftly occur.

All in all, our results show that excitation of the photocatalyst with visible light leads to a lower reactivity than for UV light, limited by the redox potential of the radical cation of the sensitizer. Moreover, although photogenerated charge carriers in this visible light active material may have a limited ability to drive oxidation reactions, under the right circumstances this could be exploited to increase the selectivity of photocatalytic transformations.

4.8. Supplementary Materials
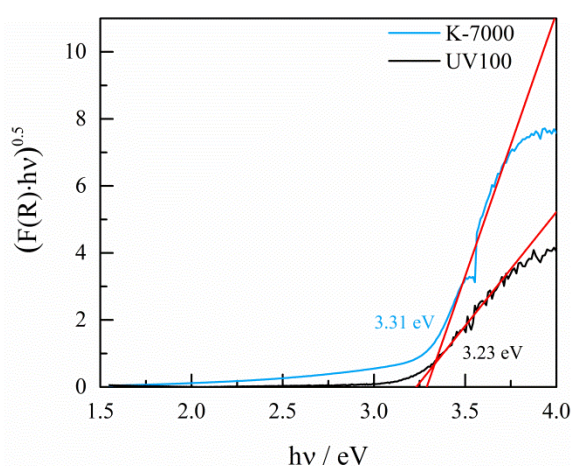
Figure 4-S1. Determination of the bandgap of K-7000 and UV100 *via* the Tauc plot.
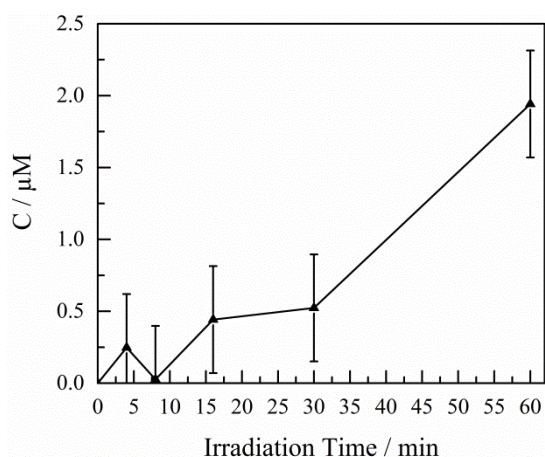
Figure 4-S2. Kinetic profile for the formation of formaldehyde upon the photocatalytic oxidation of methanol ($C_0 = 100$ µM) under visible light irradiation in the presence of K-7000.
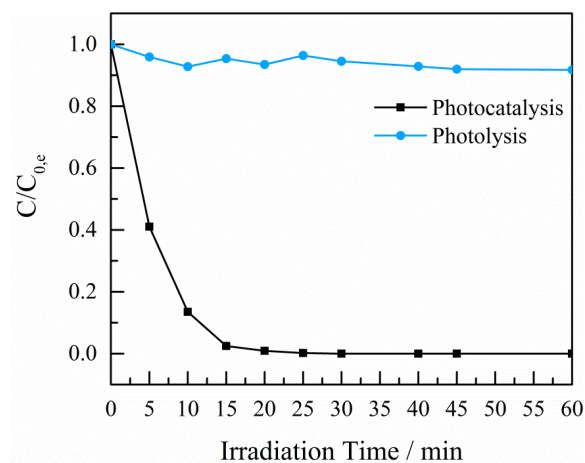
Figure 4-S3. Photolysis and photocatalytic conversion (in the presence of K-7000) of chlorpromazine under visible light irradiation.
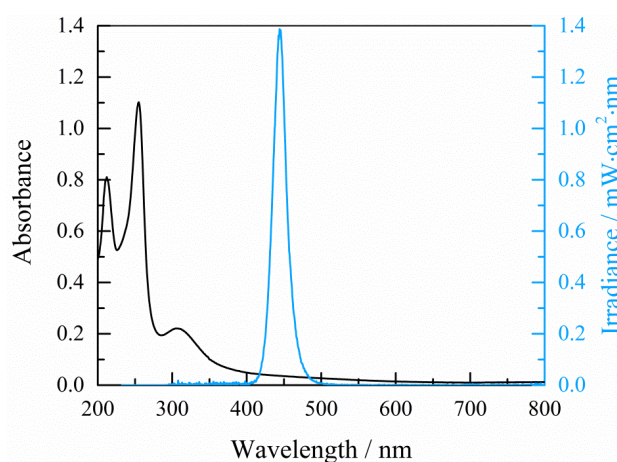
Figure 4-S4. Absorption spectrum of a 100 µM aqueous solution of chlorpromazine (black line), and emission spectrum of the employed light source (blue line).
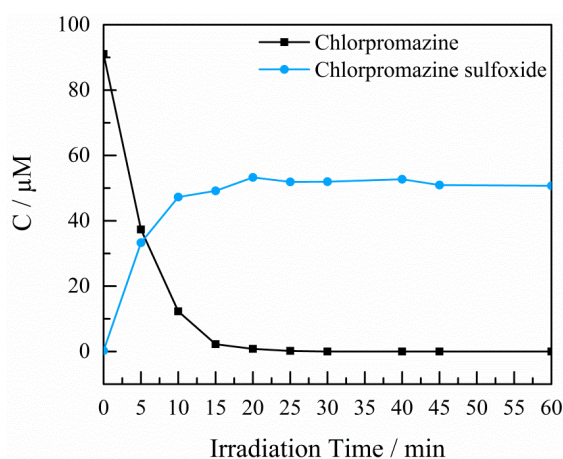
Figure 4-S5. Photocatalytic conversion of chlorpromazine to the main product chlorpromazine sulfoxide in
the presence of K-7000 under visible light irradiation.
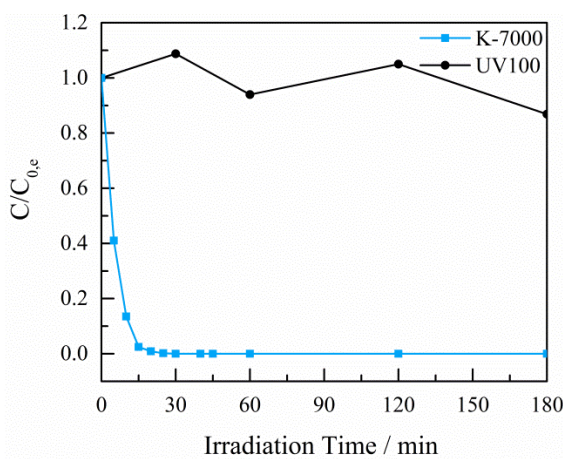
Figure 4-S6. Photocatalytic conversion of chlorpromazine under visible light irradiation in the presence of
K-7000 and Hombikat UV100.
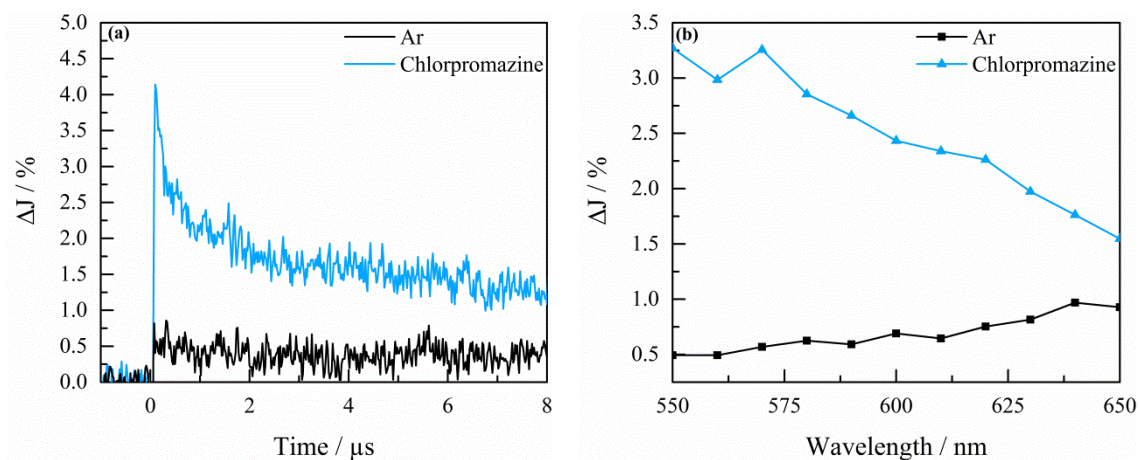
Figure 4-S7. (a) Transient absorption decays of K-7000 observed at 550 nm and (b) transient absorption
spectra of K-7000 measured at 100 ns after the laser excitation in an Ar atmosphere and in the presence of
chlorpromazine after excitation with 455 nm.

4.9. Acknowledgments

4.10. References

1. Fujishima, A.; Honda, K. Electrochemical photolysis of water at a semiconductor electrode. *Nature* **1972**, *238*, 37–38.

2. Schneider, J.; Matsuoka, M.; Takeuchi, M.; Zhang, J.; Horiuchi, Y.; Anpo, M.; Bahnemann, D.W. Understanding TiO_2 photocatalysis: Mechanisms and materials. *Chem. Rev.* **2014**, *114*, 9919–9986.

3. Pelaez, M.; Nolan, N.T.; Pillai, S.C.; Seery, M.K.; Falaras, P.; Kontos, A.G.; Dunlop, P.S.M.; Hamilton, J.W.J.; Byrne, J.A.; O'Shea, K.; et al. A review on the visible light active titanium dioxide photocatalysts for environmental applications. *Appl. Catal. B Environ.* **2012**, *125*, 331–349.

4. Günnemann, C.; Haisch, C.; Fleisch, M.; Schneider, J.; Emeline, A. V; Bahnemann, D.W. Insights into different photocatalytic oxidation activities of anatase, brookite, and rutile single-crystal facets. *ACS Catal.* **2019**, *9*, 1001–1012.

5. Tayade, R.J.; Surolia, P.K.; Kulkarni, R.G.; Jasra, R. V Photocatalytic degradation of dyes and organic contaminants in water using nanocrystalline anatase and rutile TiO_2. *Sci. Technol. Adv. Mater.* **2007**, *8*, 455–462.

6. Grätzel, M.; Rotzinger, F.P. The influence of the crystal lattice structure on the conduction band energy of oxides of titanium(IV). *Chem. Phys. Lett.* **1985**, *118*, 474–477.

7. ASTM International. *ASTM G173-03(2012): Standard tables for reference solar spectral irradiances: Direct normal and hemispherical on 37° tilted surface*; West Conshohocken, PA, 2012.

8. Arimi, A.; Megatif, L.; Granone, L.I.; Dillert, R.; Bahnemann, D.W. Visible-light photocatalytic activity of zinc ferrites. *J. Photochem. Photobiol. A Chem.* **2018**, *366*,

118–126.

9. Curti, M.; Kirsch, A.; Granone, L.I.; Tarasi, F.; López-Robledo, G.; Bahnemann, D.W.; Murshed, M.M.; Gesing, T.M.; Mendive, C.B. Visible-light photocatalysis with mullite-type $Bi_2(Al_{1-x}Fe_x)_4O_9$: Striking the balance between bandgap narrowing and conduction band lowering. *ACS Catal.* **2018**, *8*, 8844–8855.

10. Xu, A.; Gao, Y.; Liu, H. The preparation, characterization, and their photocatalytic activities of rare-earth-doped TiO_2 nanoparticles. *J. Catal.* **2002**, *207*, 151–157.

11. Klosek, S.; Raftery, D. Visible light driven V-doped TiO_2 photocatalyst and its photooxidation of ethanol. *J. Phys. Chem. B* **2001**, *105*, 2815–2819.

12. O'Regan, B.; Grätzel, M. A low-cost, high-efficiency solar cell based on dye-sensitized colloidal TiO_2 films. *Nature* **1991**, *353*, 737–740.

13. Cho, Y.; Choi, W.; Lee, C.; Hyeon, T.; Lee, H. Visible light-induced degradation of carbon tetrachloride on dye-sensitized TiO_2. *Environ. Sci. Technol.* **2001**, *35*, 966–970.

14. Chowdhury, P.; Moreira, J.; Gomaa, H.; Ray, A.K. Visible-solar-light-driven photocatalytic degradation of phenol with dye-sensitized TiO_2: Parametric and Kinetic Study. *Ind. Eng. Chem. Res.* **2012**, *51*, 4523–4532.

15. Ząbek, P.; Eberl, J.; Kisch, H. On the origin of visible light activity in carbon-modified titania. *Photochem. Photobiol. Sci.* **2009**, *8*, 264–269.

16. Sankova, N.; Semeykina, V.; Selishchev, D.; Glazneva, T.; Parkhomchuk, E.; Larichev, Y.; Uvarov, N. Influence of tetraalkylammonium compounds on photocatalytic and physical properties of TiO_2. *Catal. Letters* **2018**, *148*, 2391–2407.

17. Tobaldi, D.M.; Seabra, M.P.; Otero-Irurueta, G.; de Miguel, Y.R.; Ball, R.J.; Singh, M.K.; Pullar, R.C.; Labrincha, J.A. Quantitative XRD characterisation and gas-phase photocatalytic activity testing for visible-light (indoor applications) of KRONOClean 7000®. *RSC Adv.* **2015**, *5*, 102911–102918.

18. Ilan, Y.A.; Czapski, G.; Meisel, D. The one-electron transfer redox potentials of free radical I. The oxygen/superoxide system. *Biochmica er Biophys. Acta* **1976**, *430*, 209–224.

19. Yamakata, A.; Ishibashi, T.; Onishi, H. Water- and oxygen-induced decay kinetics of photogenerated electrons in TiO_2 and Pt/TiO_2: A time-resolved infrared absorption study. *J. Phys. Chem. B* **2001**, *105*, 7258–7262.

20. Schneider, J.; Bahnemann, D.W. Undesired role of sacrificial reagents in photocatalysis. *J. Phys. Chem. Lett.* **2013**, *4*, 3479–3483.

21. Memming, R. Photoinduced charge transfer processes at semiconductor electrodes and particles. In *Electron Transfer I. Topics in Current Chemistry*; Mattay, J., Ed.; Springer-Verlag: Berlin Heidelberg, **1994**; Vol. 169, pp. 105–181.

22. Wang, C.; Pagel, R.; Bahnemann, D.W.; Dohrmann, J.K. Quantum yield of formaldehyde formation in the presence of colloidal TiO_2-based photocatalysts: Effect of intermittent illumination, platinization, and deoxygenation. *J. Phys. Chem. B* **2004**, *108*, 14082–14092.

23. Iorio, Y. Di; Aguirre, M.E.; Brusa, M.A.; Grela, M.A. Surface chemistry determines electron storage capabilities in alcoholic sols of titanium dioxide nanoparticles. A combined FTIR and room temperature EPR investigation. *J. Phys. Chem. C* **2012**, *116*, 9646–9652.

24. Bahnemann, D.; Henglein, A.; Lilie, J.; Spanhel, L. Flash photolysis observation of the absorption spectra of trapped positive holes and electrons in colloidal titanium dioxide. *J. Phys. Chem.* **1984**, *88*, 709–711.

25. Morikawa, T.; Asahi, R.; Ohwaki, T.; Aoki, K.; Taga, Y. Band-gap narrowing of titanium dioxide by nitrogen doping. *Jpn. J. Appl. Phys.* **2001**, *40*, L561–L563.

26. Umebayashi, T.; Yamaki, T.; Itoh, H.; Asai, K. Band gap narrowing of titanium dioxide by sulfur doping. *Appl. Phys. Lett.* **2003**, *81*, 2–5.

27. Qin, P.; Yang, X.; Chen, R.; Sun, L.; Marinado, T.; Edvinsson, T.; Boschloo, G.; Hagfeldt, A. Influence of π-conjugation units in organic dyes for dye-sensitized solar cells. *J. Phys. Chem. C* **2007**, *111*, 1853–1860.

28. Youngblood, W.J.; Lee, S.-H.A.; Kobayashi, Y.; Hernandez-Pagan, E.A.; Hoertz, P.G.; Moore, T.A.; Moore, A.L.; Gust, D.; Mallouk, T.E. Photoassisted overall water splitting in a visible light-absorbing dye-sensitized photoelectrochemical cell. *J. Am. Chem. Soc.* **2009**, *131*, 926–927.

29. Ahmed, A.Y.; Kandiel, T.A.; Ivanova, I.; Bahnemann, D. Photocatalytic and photoelectrochemical oxidation mechanisms of methanol on TiO_2 in aqueous solution. *Appl. Surf. Sci.* **2014**, *319*, 44–49.

30. Somasundaram, N.; Srinivasan, C. Oxidation of aryl methyl sulfides and sulfoxides on irradiated TiO_2. *J. Photochem. Photobiol. A Chem.* **1998**, *115*, 169–173.

31. Merkle, F.H.; Discher, C.A. Electrochemical oxidation of chlorpromazine hydrochloride. *J. Pharm. Sci.* **1963**, *53*, 620–623.

32. Bahnemann, D.; Asmus, K.-D.; Willson, R.L. Phenothiazine radical-cations: Electron

transfer equilibria with iodide ions and the determination of one-electron redox potentials by pulse radiolysis. *J. Chem. Soc. Perkin Trans. II* **1983**, 1669–1673.

33. Feldt, S.M.; Lohse, P.W.; Kessler, F.; Nazeeruddin, M.K.; Grätzel, M.; Boschloo, G.; Hagfeldt, A. Regeneration and recombination kinetics in cobalt polypyridine based dye-sensitized solar cells, explained using Marcus theory. *Phys. Chem. Chem. Phys.* **2013**, *15*, 7087–7097.

34. Marcus, R.A. Chemical and electrochemical electron-transfer theory. *Annu. Rev. Phys. Chem.* **1964**, *15*, 155–196.

35. Maruthamuthu, P.; Sharma, D.K.; Serpone, N. Subnanosecond relaxation dynamics of 2,2′-azinobis(3-ethylbenzothiazoline-6-sulfonate) and chlorpromazine. Assessment of photosensitization of a wide band gap metal oxide semiconductor TiO_2. *J. Phys. Chem.* **1995**, *99*, 3636–3642.

36. Arimi, A.; Dillert, R.; Dräger, G.; Bahnemann, D.W. Light-induced reactions of chlorpromazine in the presence of a heterogeneous photocatalyst: Formation of a long-lasting sulfoxide. *Catalysts* **2019**, *9*, 0627–0643.

37. Lang, X.; Chen, X.; Zhao, J. Heterogeneous visible light photocatalysis for selective organic transformations. *Chem. Soc. Rev.* **2014**, *43*, 473–486.

38. Ito, S.; Chen, P.; Comte, P.; Nazeeruddin, M.K.; Liska, P.; Péchy, P.; Grätzel, M. Fabrication of screen-printing pastes from TiO_2 powders for dye-sensitised solar cells. *Prog. Photovoltaics Res. Appl.* **2007**, *15*, 603–612.

39. Nash, T. The colorimetric estimation of formaldehyde by means of the Hantzsch reaction. *Biochem. J.* **1953**, *55*, 416–421.

Chapter 5: Summarizing Discussion and Conclusions

This chapter includes a general overview of all experimental achievements of this doctoral dissertation and provides a detailed discussion regarding the obtained observations throughout this scientific work.

Initially, an overview of the characterization analysis performed on seven differently prepared zinc ferrite samples will be presented. Also, the results obtained from wavelength dependent photocatalytic methylene blue (MB) degradation experiments will be analyzed. Hereby, the effect of the synthetic method on the photocatalytic activity of zinc ferrite samples as well as the adequacy of MB as a model compound for the determination of the photocatalytic activity of zinc ferrite samples will be evaluated.

Afterwards, the conversion of chlorpromazine under UV and visible light irradiation in the presence of a visible light-absorbing photocatalyst, namely, KRONOClean 7000 (K-7000) will be discussed in detail. The formation of the main reaction intermediate of photocatalytic conversion of chlorpromazine and its high resistance against any further photocatalytic conversion will be assessed. Moreover, based on the intermediates/products evolved throughout these experiments, a respective reaction pathway for the photocatalytic conversion of chlorpromazine upon UV and visible light irradiation under both anaerobic and aerobic conditions will be introduced.

Additionally, the fundamental studies regarding the nature of charge carriers formed in K-7000 after laser excitation by means of laser flash photolysis spectroscopy will be discussed and an interpretation of the transient absorption spectra measured under different atmospheres will be given. In addition, the results of laser experiments and those of the photocatalytic experiments for chlorpromazine and methanol conversion will be mutually evaluated. The discussion will be finalized with a proposed mechanism of the processes taking place after excitation of K-7000 with visible light irradiation. As a final point, the overall conclusions obtained based on the experimental results and the discussion within this doctoral dissertation will be presented.

5.1. Visible-light-driven MB Conversion in the Presence of Zinc Ferrite

As mentioned in **Chapter 1**, visible light-driven photocatalysis can be regarded as an environmental friendly technology, easing the way towards the utilization of the solar light for water and wastewater treatment, especially for the removal of pharmaceuticals from aquatic systems [1–7]. Accordingly, many attempts towards the development of new photocatalytic materials which are able to absorb light in the visible region of the solar spectrum have been made.

Zinc ferrite, with the general formula of $ZnFe_2O_4$, is one of the potential alternative materials which has been widely studied regarding its visible light activity for applications in photocatalytic and photoelectrocatalytic processes [8–10]. With a bandgap of ~1.9-2.3 eV [11], zinc ferrite exhibits a suitable optical absorption for low energy photons and benefits from a proper electronic structure for photocatalytic applications. At standard conditions (273.15 K and 100 kPa), the thermodynamically most stable configuration for this semiconductor is the normal spinel structure ($^T[Zn]^O[Fe_2]O_4$), in which Zn^{2+} ions occupy the tetrahedral sites, while Fe^{3+} ions are located at the octahedral sites of the crystal structure as shown in **Figure 5-1** [12].
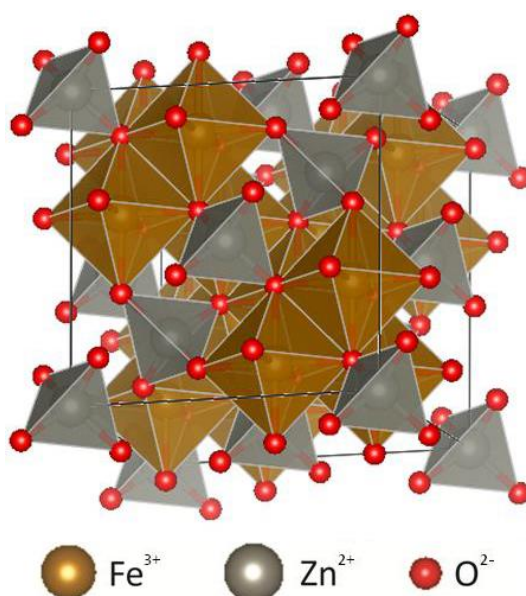

Figure 5-1. Crystallographic 3D structure of zinc ferrite with a normal spinel arrangement [13]; Reproduced from Ref [13]. This figure is a reprint of Figure 1-7 from page 12 in Chapter 1.

The spinel structure of zinc ferrite provides a considerable number of available catalytic sites as a result of the crystal lattice, and should thus enhance the photocatalytic efficiency

of this semiconductor [14]. The number of Fe^{3+} ions in tetrahedral sites divided by the total number of Fe^{3+} ions is defined as the degree of inversion in this spinel lattice. This parameter is dependent on the ionic radius, the configuration of the cations and their relative stabilization energies in the tetrahedral and the octahedral sites, respectively [14].

Nevertheless, very different photocatalytic activities have been reported in the literature for zinc ferrites prepared by different synthetic methods [11,15]. Although these differences might be explained by the variations in the applied synthetic path and the preparation conditions [12], still, in some cases, one might ask the question whether the test system which has been employed to analyze the visible light activity of the respective semiconductor is really appropriate. As suggested by Mills and Wang, when for example using a dye such as MB as a probe molecule, the observed photobleaching is not necessarily due to the dye's photocatalytic oxidation, since other reactions such as the reduction of the dye might lead to the same bleaching effect [16]. Moreover, under visible light irradiation, MB itself is a photosensitive material. Therefore, the overlap of MB's absorption spectra with the incoming visible light and the subsequent reactions of the excited MB molecule is commonly mistaken as a visible-light activity of the investigated semiconductor [17].

In the current study, as described in **Chapter 2**, seven zinc ferrite samples are prepared through four different synthetic pathways adapted from the literature, namely, a reflux method [18], a hydrothermal method [18], a polymer complex method [19,20], and a solid-state reaction [19,20], employing different precursors and reaction temperatures. It is observed that each of these synthetic approaches resulted in products with different colors, magnetic properties, surface area, particle sizes, and photocatalytic activities for the degradation of MB.

A different preparation approach can affect the cation distribution in the spinel lattice and thus, the magnetic and catalytic properties of the semiconducting material. Varying magnetic properties of zinc ferrites prepared via different synthetic methods were reported by Toledo-Antonio *et al.* [21]. These authors claimed that the magnetic and catalytic properties of the prepared zinc ferrite samples are dependent on the occupation of the tetrahedral sites with iron ions as confirmed by the analysis of the local atom distribution by Mössbauer spectroscopy. This occupation was higher in the sample synthesized by the hydrothermal method, as compared to the one synthesized by the co-precipitation approach

[21]. As reported by Chinnasamy *et al*., the magnetic properties of zinc ferrite samples are affected by their particle size. According to these authors, the magnetization seems to increase with a decrease of the particle size and its relatively high values are attributed to the degree of inversion in combination with particle size reduction [22]. Similar observations were reported by Ammar *et al*. who reported an increase in magnetization with the reduction of the particle size [12].

According to the XRD results shown in **Chapter 2, Figure 2-1**, the crystallinity and the purity of the obtained materials are different, depending on the synthetic method. The formation of a pure-phase spinel zinc ferrite cannot be confirmed for all the samples. It is observed that the samples which were prepared at temperatures lower than 800°C, namely, RF-75, HT-135, HT-175, and SN-800 contain some impurities. Spinel structures are known to require extended thermal treatments and elevated temperatures for complete crystallization [14,19,23–25]. Thus, due to the low synthetic temperature used for the preparation of these samples, the formation of the bare spinel zinc ferrite structure cannot be ensured. However, for the samples prepared through high-temperature methods, i.e., SO-1100, SN-1100, and PC-1100, a much higher crystallinity compared to the other synthetic methods is attained. This observation is in good agreement with the literature [14,23–25] and confirms that only at extensively high temperatures a pure-phase zinc ferrite can be obtained.

The results of the Raman measurements (**Figure 2-2**) are consistent with those obtained from the XRD measurements. Only for the samples prepared through high-temperature methods, narrow peaks are detected confirming an increased degree of crystallinity at higher temperatures. The poorest degree of crystallinity is observed for the commercial zinc ferrite and for the RF-75 sample. As a result of the low synthetic temperature in some samples, i.e., HT-135, HT-175, and SN-800, the formation of the spinel structure remains incomplete and thus, traces of hematite impurities are found in these samples. As reported by Shim *et al.*, these impurities corresponding to the absorption bands at 220, 288, 400, 490, and 1300 cm^{-1} can be assigned to the presence of α-Fe$_2$O$_3$ [26]. According to these observations, polymer complex synthesis methods and solid state reactions are the best approaches to obtain pure-phase zinc ferrite samples.

The measured physiochemical properties of the thus prepared zinc ferrite samples are presented in detail in **Chapter 2**, **Table 2-1**. The average crystallite sizes are estimated by the Debye–Scherrer formula. According to the literature, zinc ferrite nanoparticles are synthesized in a size range of 5–45 nm and the particles size is mainly dependent on the calcination temperature [27]. In the current study, for the samples synthesized at higher temperatures, bigger crystallite sizes, and lower specific surface areas are obtained (**Table 5-1**). The smallest crystallite size of 5 nm is achieved by the RF-75 method, while the high temperature methods, namely, PC-1100, SO-1100, and SN-1100 yield products with crystallite sizes of 130, 110, and 100 nm, respectively.

Table 5-1. Properties of the synthesized zinc ferrite samples

Zinc Ferrite Samples Properties	RF-75	HT-135	HT-175	SN-800	SN-1100	SO-1100	PC-1100
Crystallite Size / nm	5	8	10	50	100	110	130
BET Surface Area / m^2g^{-1}	210	120	95	20	11	7.8	8.6

As shown by Martin de Vidales *et al.*, besides the synthetic temperature, also the precursor and the source of the ions in the synthetic method can affect the particle size, the morphology, the thermal properties and the surface area of the prepared zinc ferrites [28]. These authors prepared zinc ferrite particles through a co-precipitation method with ferric nitrate and ferrous sulphate solutions as the starting precursors. Using ferrous sulphate as a precursor resulted in smaller-sized zinc ferrite particles, while the cubic spinel-type structure of zinc ferrite was obtained at a lower temperature when nitrate solutions were used [28].

In the scientific literature, the visible-light activity of zinc ferrite is most often reported in terms of its ability for the photocatalytic degradation of organic dyes such as rhodamine B (RhB), methyl orange (MO), and methylene blue (MB) [10,14,29–34]. However, since zinc ferrite is prepared in each case through a different synthetic procedure, the reported photocatalytic activities of these materials might be a function of the varying particle size, the surface area, the crystallinity, the bandgap energy, the morphology, and even the overall structure. In addition, as highlighted before, choosing an organic dye as a model pollutant

to confirm the visible-light activity of a semiconductor is questionable. Thus, this issue is investigated in detail in the current study.

In this regard, after the primary characterization of the prepared zinc ferrite samples, initial photocatalytic experiments for MB degradation under both UV and visible irradiation are carried out with these samples. Since the reaction suspensions were initially stirred in the dark for 60 min, the fractional conversion of MB during the irradiation time is calculated by $X_{irr} = (A_{60} - A_{300})/A_{60}$ with A_{60} and A_{300} being the absorbance measured 60 min and 300 min after the start of the experimental run, respectively.

In order to get thorough insights into the activity of the SO-1100 zinc ferrite sample, a series of wavelength dependent MB degradation measurements employing four nearly monochromatic light sources with λ_{max} at 365, 455, 505 and 660 nm are performed. However, the four employed LED lamps do not have the same intensities. Therefore, the so-called normalized photocatalytic conversion (X_{norm}) for an equal number of photons (N) for all the lamps is defined. This parameter is the photocatalytic conversion of each experimental run divided by the relative number of photons ($N/N_{365\ nm}$). The X_{norm} for all the lamps are calculated and the respective values are presented in **Table 5-2**.

Table 5-2. Photocatalytic conversion data for degradation of MB in the presence of SO-1100

Wavelength / nm	N = Number of photons / $s^{-1}\,cm^{-2}$	X_{irr}	$X_{norm} = X_{irr} / (N_{365\ nm}/N)$
365	1.12×10^{16}	0.05	0.05
455	7.47×10^{16}	0.27	0.04
505	3.36×10^{16}	0.25	0.08
660	10.9×10^{16}	0.46	0.05

By looking at the MB conversion values in the presence of SO-1100 zinc ferrite, it becomes clear that the initially assumed visible-light activity of zinc ferrite is rather low. The highest MB conversion of only about $X_{norm} = 0.08$ is attained upon irradiation at 505 nm. This conversion value is not far from the value obtained in the presence of TiO_2 P25 ($X_{norm} = 0.05$) under the same irradiation wavelengths (**Figure 2-6**). However, TiO_2 P25 is known as a "UV-active photocatalyst", not being able to absorb visible light. Considering the $X_{norm} = 0.95$ for MB conversion upon UV irradiation in the presence of TiO_2 P25, the term "visible-active photocatalyst" might not be appropriate for zinc ferrites.

Common differences in photocatalytic activities of differently synthesized zinc ferrite samples are also reported in the literature [10,34]. For instance, Shao *et al.* synthesized zinc ferrite nanoparticles with an average particle size of 20 nm through a solvothermal method using zinc nitrate as a precursor and evaluated their photocatalytic activity under UV irradiation using MB as a probe pollutant [35]. They observed only 20% bleaching of MB after 3 hours irradiation. Li *et al.* prepared zinc ferrite nanospheres and nanoparticles *via* a solvothermal method [33]. They compared the photocatalytic activities of these two morphologies following the degradation of RhB in an aqueous solution under irradiation with a 500 W xenon lamp (light intensity: 25.3 m·W·cm^{-2}) [33]. The zinc ferrite nanoparticles showed a removal of 63% of the initially present RhB, while the zinc ferrite nanospheres were able to remove RhB completely during the same illumination time (5 h). Moreover, the zinc ferrite nanospheres exhibited higher specific surface area compared to the zinc ferrite nanoparticles, leading to a higher number of active sites for photocatalytic reactions [33].

Nevertheless, in the current study, after confirming that no OH radicals can be photocatalytically formed with any of the prepared samples under UV or visible light irradiation, the idea of a reaction between the dye molecule and a photocatalytically generated OH radical is excluded. The calculated energetic positions of the conduction and the valence band of the zinc ferrite samples compared with those of TiO$_2$ P25 (**Figure 5-2**) also supported this observation: The formation of OH radicals by hole oxidation of water is thermodynamically not possible, since the energetic positions of the valence bands of all the studied zinc ferrite samples (between 1.74 and 2.41 V (pH 0) *vs.* NHE) are less positive than E(H$_2$O/$^{\bullet}$OH) = 2.8 V (pH 0) *vs.* NHE.

These measurements also show that, considering the redox potential of O$_2$/O$_2^{\bullet-}$ = -0.33 V *vs.* NHE (a pH-independent value [36]), being more negative than the energetic positions of the conduction bands of the zinc ferrite samples (between -0.14 and 0.54 V (pH 0) *vs.* NHE), the reduction of O$_2$ by zinc ferrite is also not likely to happen.
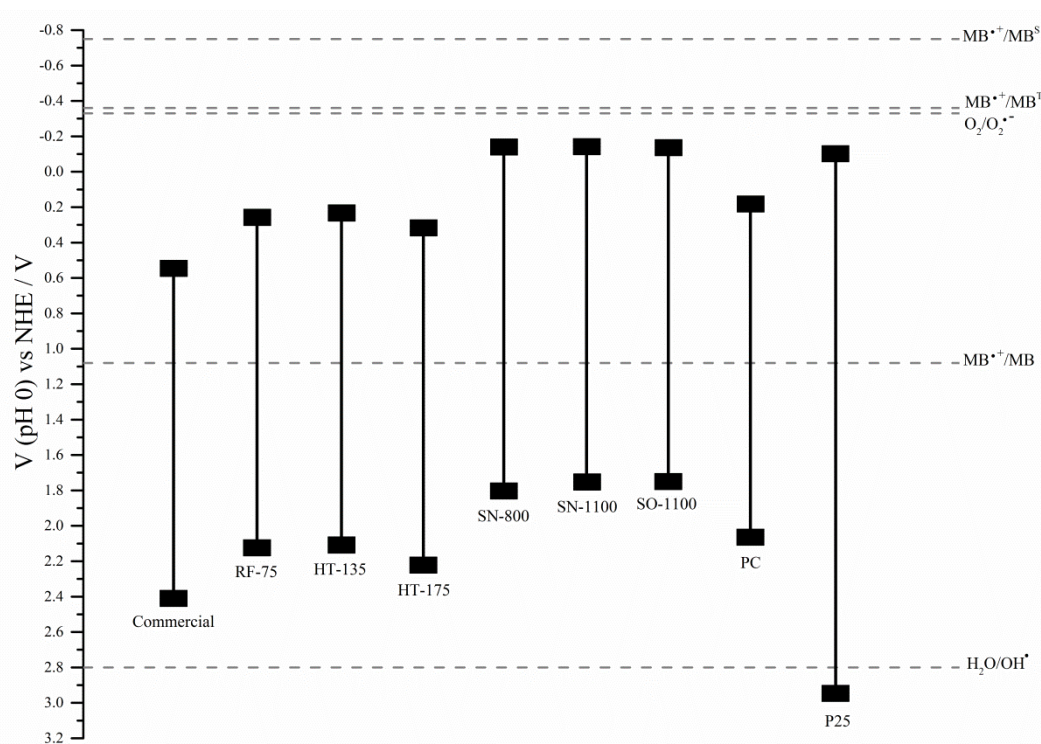
Figure 5-2. Energetic positions of the valance and the conduction band of different zinc ferrite samples and TiO$_2$ P25; MB, MB^T and MB^S denote the MB ground state, the excited triplet state and the excited singlet state of MB, respectively. The one electron reduction potentials are calculated with data given in Ref.[16].

The differences in the measured energetic positions of the conduction band of the synthesized zinc ferrites, can contribute to their different activities. As illustrated in **Figure 5-2**, higher synthetic temperatures yield zinc ferrite samples with more negative conduction band positions and thus, less positive valance band positions; since the bandgap energy of all samples remains constant. These differences might also be due to the variation of degree of inversion between the samples. As reported by Granone *et al.*, a higher calcination temperature results in an enhanced degree of inversion in zinc ferrites. Moreover, with an increase in the degree of inversion, the contribution of the ligand field transitions of the Fe^{3+} ions in the tetrahedral sites of the zinc ferrite will be enhanced. This results in an improved visible light absorptivity of this material. Thus, these authors suggest that the differences in degree of inversion of different spinel zinc ferrite samples affects their optical properties and consequently their visible light absorptivity, while the optical bandgap of zinc ferrite remains unchanged [37]. Therefore, by illuminating the zinc ferrites (having an improved degree of inversion), with an energy equal to or more than the bandgap energy, more electron-hole pairs will be produced in the semiconductor.

Dom *et al.* synthesized zinc ferrite samples through two different approaches, namely, a rapid microwave method and a solid state reaction and reported slight differences in the energetic positions of the conduction band and the valence band between these two samples. They claimed that the conduction band edge of the sample synthesized by the microwave method was positioned at a more negative value than that of the sample obtained through the solid state reaction [10]. In another study, Jia *et al.* prepared porous, one dimensional zinc ferrite nanorods with diameters of 100–200 nm and lengths of several micrometers using a solvothermal method. The bandgap energy of this material was determined to be 1.85 eV. Zinc ferrite nanorods showed higher photocatalytic activity (85%) for MB degradation than bulk zinc ferrite (25%) after 6 hours of irradiation under real sunlight [30].

As mentioned beforehand, in the current study, it is observed that the bleaching of MB cannot be a consequence of a reaction between photocatalytically generated reactive oxygen species such as the OH radical and the dye molecule. However, as illustrated in **Figure 5-2**, the standard reduction potential for the couple $MB^{\bullet+}/MB$ (1.08 V *vs*. NHE [16]) is located within the bandgap of the synthesized zinc ferrite samples. Thus, in the presence of suitable electron acceptors, the light-induced valence band holes might oxidize the absorbed MB molecules on the zinc ferrite surface (MB_s), according to the following equations:

$$ZnFe_2O_4 + h\nu\,(455\ nm) \rightarrow ZnFe_2O_4(h_{VB}^+ + e_{CB}^-) \tag{5-1}$$

$$ZnFe_2O_4(h_{VB}^+ + e_{CB}^-) + MB_s \rightarrow ZnFe_2O_4(e_{CB}^-) + MB^{\bullet+} \tag{5-2}$$
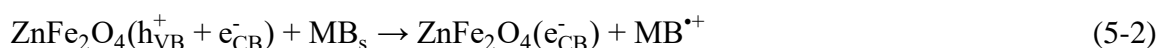
On the other hand, under visible light irradiation, the absorbed MB molecules (λ_{max} = 664 nm) on the surface of the semiconducting zinc ferrite will be excited (MB_s^*) as shown in **Equation 5-3**.

$$MB_s + h\nu\,(455\ nm) \rightarrow MB_s^* \tag{5-3}$$

Due to the adsorption of the excited MB molecules on the surface of zinc ferrite in a most likely energetically favourable position, an interfacial electron transfer between the excited surface-bound MB molecules (MB_s^*) and the semiconducting zinc ferrite is likely to take place (**Equation 5-4**). This interaction can be assumed as a dye-sensitized process.

$$MB_s^* + ZnFe_2O_4 \rightarrow MB^{\bullet+} + ZnFe_2O_4(e_{CB}^-) \tag{5-4}$$

This kind of electron injection has been proposed before in the scientific literature [16,17] and is well-known for dye-sensitized solar cells (DSSC) [38]. As suggested by Takizawa *et al.* [39], the resulting MB radical cation (MB$^{\bullet+}$, λ_{max} = 520 nm [40]) might be reduced back to MB according to the following equations:

$$MB_s^* + O_2 \rightarrow O_2^{\bullet-} + MB^{\bullet+} \tag{5-5}$$

$$O_2^{\bullet-} + MB^{\bullet+} \rightarrow MB + O_2 \tag{5-6}$$

As can be seen from the measured absorption spectrum of MB illustrated in **Figure 5-3**, in the UV(A) region of spectrum (320-400 nm), MB reveals only a small absorption (λ_{max} = 293 nm). Thus, the excitation of MB molecules upon UV(A) irradiation is rather unlikely. However, within the visible range of the spectrum (380-750 nm), a significant absorption with a maximum at 664 nm can be seen.
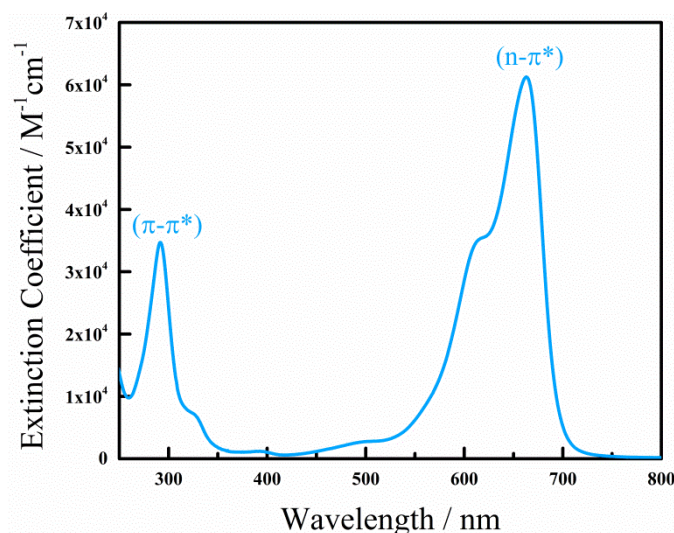
Figure 5-3. Absorption spectrum of MB (20 μM solution); The transitions are adapted from Ref. [41].

Therefore, under visible irradiation, a considerable amount of absorbed MB molecules on the surface of zinc ferrite will be excited. This increases the possible interfacial electron transfer between the surface-bound excited MB molecules and the semiconductor. Hence, a faster bleaching under these conditions is observed.

After all, the obtained experimental data can be summarized as illustrated in **Figure 5-4**. After the proposed injection of an electron from the surface-bound photo-excited MB

molecules to the conduction band of zinc ferrite under visible light irradiation, within the semiconductor, Fe^{3+} can be reduced yielding Fe^{2+}. However, as explained before, due to the redox potential of $O_2/O_2^{\bullet-}$ = -0.33 V (pH 0) *vs.* NHE, being more negative than the energetic positions of the conduction band of the zinc ferrite (between -0.14 and 0.54 V (pH 0) *vs.* NHE), the conduction band electrons are not able to reduce O_2.
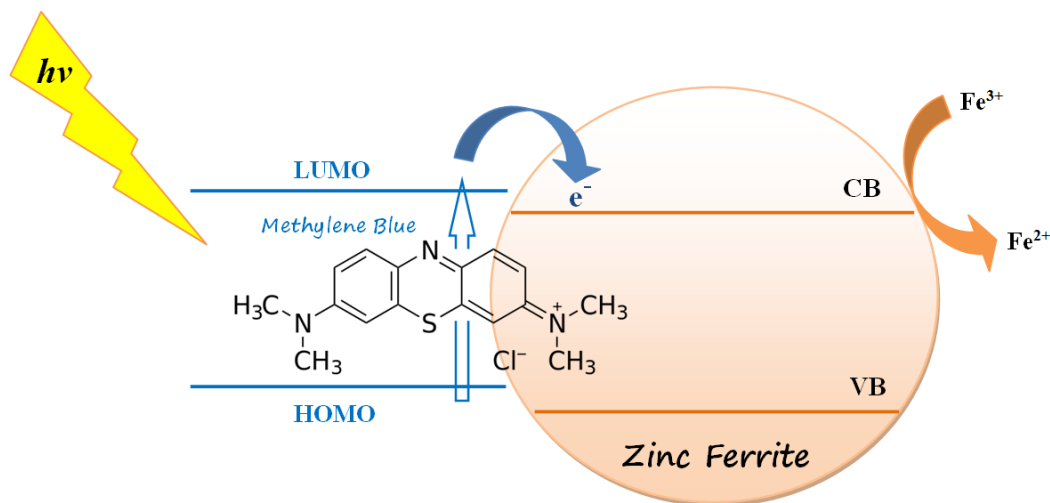
Figure 5-4. Schematic demonstration of the visible light-induced bleaching of MB in the presence of zinc ferrite

This dye-sensitized effect is not observed under UV irradiation due to the low absorption of MB in this region. However, as also suggested by Mills and Wang [16], under strong visible irradiation, this effect can be simply attained. This kind of photo-induced reaction should not be mistaken with the photocatalytic activity of zinc ferrite. However, due to the mentioned adsorption and the interfacial electron injection processes, the nature of the photocatalyst and its physical properties are likely to have an impact on the photoreaction [17].

5.2. Light-Induced Reactions of Chlorpromazine in the Presence of K-7000

Following the previous experiments with MB, the pioneering associate of the phenothiazine group of antipsychotics, as a probe pollutant, in this section, the photocatalytic conversion of chlorpromazine, another important member of this group is evaluated. For this purpose, the visible light-absorbing carbon-modified commercial titanium dioxide photocatalyst, K-7000, is employed throughout the photocatalytic experiments. Under identical experimental conditions, the photocatalytic and the photolytic transformations of chlorpromazine are

compared with each other upon UV(A) and visible light irradiation under both aerobic and anaerobic conditions.

As explained extensively in **Chapter 1**, upon UV light irradiation, chlorpromazine (**Figure 5-5**) is known to undergo photo-transformation *via* oxidation of the amine or sulfur groups, demethylation at the N-chain, and dechlorination and hydroxylation of the benzene ring [42–44]. The products of these photo-induced transformations are commonly called chlorpromazine metabolites in which the aromatic ring of the phenothiazine structure is kept.
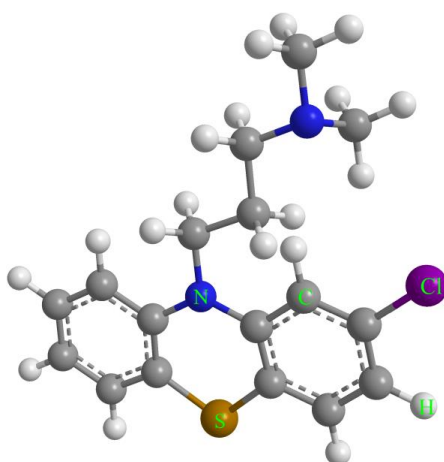
Figure 5-5. 3D scheme of the chemical structure of chlorpromazine

Nevertheless, very little is known about the photocatalytic conversion of chlorpromazine. According to the experimental results presented in **Chapter 3**, under UV(A) irradiation (365 nm), the presence of the K-7000 photocatalyst seems to slow down the photo-induced conversion of chlorpromazine (**Figure 3-1(a)**). Under aerobic conditions and in aqueous solution, chlorpromazine has an absorption maximum at 305 nm ($\varepsilon = 4500$ mol^{-1}·dm^{3}·cm^{-1}) [45] and is hence able to absorb UV light thus undergoing photoexcitation. However, due to the nature of the K-7000 photocatalyst, being an anatase TiO$_2$, a large quantity of the incoming UV photons at 365 nm will be absorbed by the photocatalyst inhibiting the contribution of the photolytic excitation of the probe molecule. This, results into a slower photocatalytic conversion compared to the pure photolytic one, that means, the photocatalyst acts somehow like a "sun-screen".

The situation is, however, completely different under visible irradiation, as for the conversion of chlorpromazine at 455 nm, the presence of K-7000 is found to be

indispensable under aerobic conditions. Although a complete photocatalytic conversion of chlorpromazine is attained within less than 30 minutes of visible light irradiation, this compound is highly stable upon visible light irradiation in the absence of the photocatalyst (**Figure 3-1(b)**).

The different behavior of chlorpromazine under UV(A) and visible irradiation, in the presence and absence of the photocatalyst can be explained by evaluating its absorption spectrum as illustrated in **Figure 5-6**.
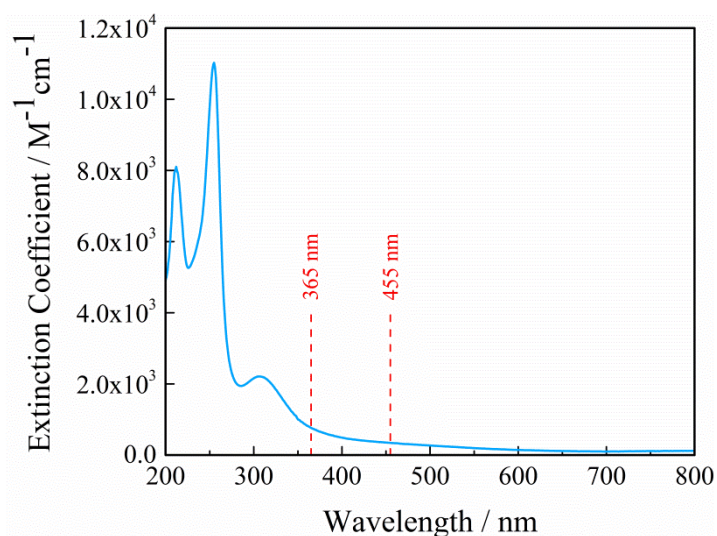
Figure 5-6. Absorption spectrum of a 100 μM aqueous solution of chlorpromazine

A comparison between the two irradiation wavelengths of 365 nm and 455 nm leads to the following explanations. Chlorpromazine reveals a considerably larger absorbance at 365 nm than at 455 nm. Considering the photolytic reaction, the amount of incoming photons absorbed by chlorpromazine at 455 nm compared to that value at 365 nm is negligible. As a result of such a low absorbance under visible irradiation, most of the incoming photons will be transmitted through the suspension and hence, a weak photolysis of chlorpromazine at 455 nm is observed. In the presence of K-7000, however, as explained beforehand, the photocatalyst will be the main absorbing component in the system, and thus, the contribution of the homogeneous reaction (photolytic excitation of chlorpromazine) will be small compared to the photocatalytic one.

Following the above-mentioned differences, further analytical investigations are performed *via* HPLC-MS analysis to study the photocatalytic and photolytic transformation

products/intermediates of the chlorpromazine conversion upon both UV(A) and visible light irradiation. As revealed by this analysis of the stable intermediates, different metabolites/intermediates are detected upon UV(A) and visible light irradiation in the presence and in the absence of K-7000 (**Table 5-3**).

Table 5-3. Products/intermediates of aerobic photocatalytic and photolytic conversion of chlorpromazine

Reactions	UV(A)-Photocatalysis	Vis-Photocatalysis	UV(A)-Photolysis	Vis-Photolysis
m/z	335, 351, 317	335, 351	335, 301, 317	—

Within the first 60 minutes of the photocatalytic experiments, under UV(A) irradiation, products/intermediates with m/z values of 335, 351 and 317 are detected (**Figure 3-3(a)**). Upon visible light irradiation, however, the photocatalytic conversion yields only reaction products/intermediates with m/z values of 335 and 351 (**Figure 3-3(b)**). Under both irradiation wavelengths, the main and most stable product formed within the irradiation period is found to be the one with m/z value of 335. On the other hand, no stable intermediates can be detected under 455 nm irradiation during the aerobic photolytic experiments, evincing the negligible conversion of chlorpromazine under visible irradiation (**Figure 3-3(d)**). During the aerobic photolytic reaction under UV(A) irradiation, however, the main reaction products are found to have m/z values of 301, 335, and 317 (**Figure 3-3(c)**). The possible structures for these detected intermediates/products are shown in **Figure 5-7** and **Figure 5-8**.

The fact that different intermediates are formed during the photocatalytic and photolytic experiments, respectively, leads to the conclusion that the mechanism of the photocatalytic conversion of chlorpromazine is different than that of the pure photolytic process. The formation of some of the metabolites of chlorpromazine during light-induced reactions has been reported before in the literature and their proposed structures are shown in **Table 3-1** [42,46–48]. For instance, similar to the current study, Trautwein and Kümmerer observed three main photo-transformation products of chlorpromazine (with m/z values of 301, 317 and 335) under aerobic conditions within 4 hours of illumination by a xenon arc lamp [42]. They suggested that the metabolite with a m/z value of 301 corresponds to the dechlorination of chlorpromazine followed by a hydroxylation at one of the benzene rings

resulting in the formation of 2-hydroxypromazine (**Figure 5-7(a)**), while for the detected product with a m/z value of 317, a further sulfoxidation step has been assumed corresponding to the structure of 2-hydroxypromazine sulfoxide (**Figure 5-7(b)**).

(a) **(b)** **(c)**
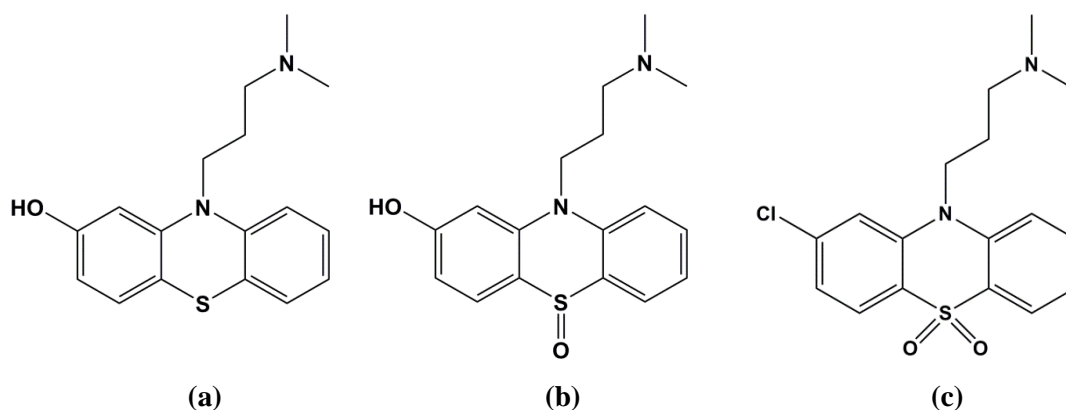
Figure 5-7. Proposed structures for the products with m/z values of (a) 301, (b) 317, and (c) 351

According to Trautwein and Kümmerer, the main product of the photolytic conversion of chlorpromazine can be attributed to chlorpromazine sulfoxide with m/z value of 335 (**Figure 5-8(a)**) [42]. The formation of chlorpromazine sulfoxide has been observed by many authors either as the ultimate reaction intermediate or as the product of the photo-induced conversion of chlorpromazine [43,49–52].

(a) **(b)**
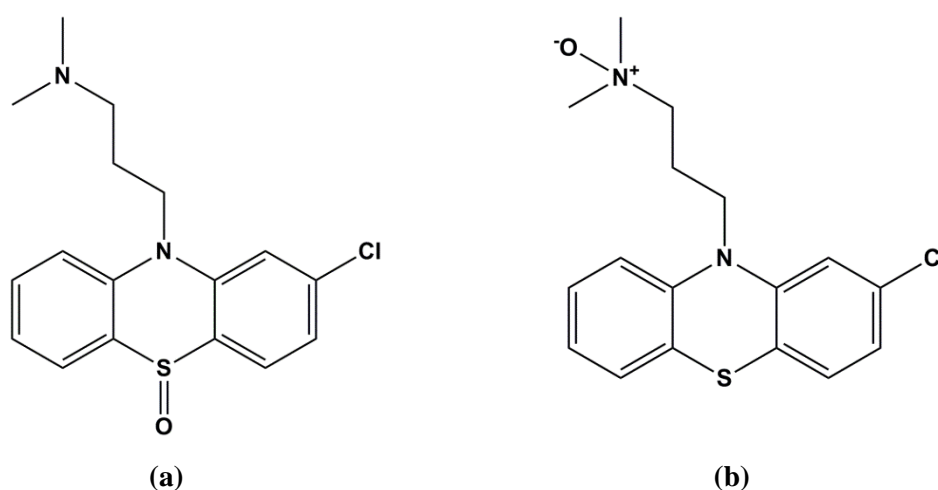
Figure 5-8. Chemical structures of (a) chlorpromazine sulfoxide and (b) chlorpromazine N-oxide, (both with m/z value of 335)

Also in the current study, during the aerobic conversion of chlorpromazine, the formation of a metabolite with m/z value of 335 is detected. However, the m/z value of 335 can also be attributed to chlorpromazine N-oxide (**Figure 5-8(b)**) [48]. Nevertheless, the formation

of chlorpromazine N-oxide is excluded in the current study, since an authentic sulfoxide sample exhibits the same retention time as the photogenerated intermediate. A quantitative calibration with the authentic sulfoxide sample shows that chlorpromazine sulfoxide is clearly the main photo-product of the aerobic chlorpromazine conversion.

The photochemistry of chlorpromazine sulfoxide is reported in the scientific literature with different explanations. As reported by Kochevar, in general under UV irradiation, chlorpromazine (CPZ) either fragments to form radicals or photo-ionizes to form its respective radical cation and an electron (**Equation 5-7**) [53].

$$CPZ \xrightarrow{h\nu < 400 \text{ nm}} \begin{cases} PZ^{\bullet} + Cl^{\bullet} \\ CPZ^{\bullet+} + e^{-} \end{cases} \tag{5-7}$$

Most of the produced radical intermediates of chlorpromazine photodegradation under UV irradiation, including also its excited singlet and triplet states [54] are not stable. However, in aqueous solutions with pH values of 1.5 to 6.5, a free radical intermediate (red) known as the chlorpromazine radical cation ($CPZ^{\bullet+}$, λ_{max} = 530 and 275 nm) has been identified [55]. Felmeister and Discher suggest that several resonance forms of the mentioned free radical cation can possibly be envisioned (**Figure 5-9**) [56].
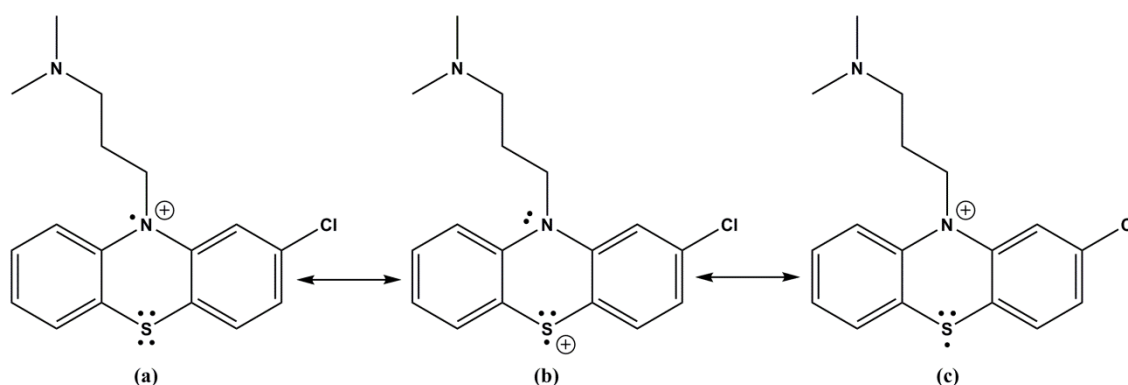
Figure 5-9. Resonance forms of free radical of chlorpromazine; adapted from Ref. [56], copyright (1964), with permission from Elsevier.

Also, in the current study, throughout the experiments upon UV(A) irradiation, the colorless suspension of chlorpromazine turns to pink and ruby (dark red), confirming the formation of the chlorpromazine radical cation. Merkle and Discher have suggested that the chlorpromazine free radical intermediate, $CPZ^{\bullet+}$, which is the product of the one-electron oxidation of chlorpromazine in aqueous media, might be the origin of the

formation of chlorpromazine sulfoxide [49]. As proposed by these authors, in a dilute aqueous acidic solution (1 N sulfuric acid), $CPZ^{\bullet+}$ is rather unstable and disproportionates rapidly to form chlorpromazine and chlorpromazine sulfoxide (CPZ=O) (**Equation 5-8**) [49].

$$2\ CPZ \xrightarrow{\text{1 N sulfuric acid (+0.70 V. } vs.\ \text{SCE)}} \underbrace{2CPZ^{\bullet+}}_{\downarrow} + 2e^{-} \tag{5-8}$$

$$CPZ \xleftarrow{\text{Spontaneous}} CPZ=O$$
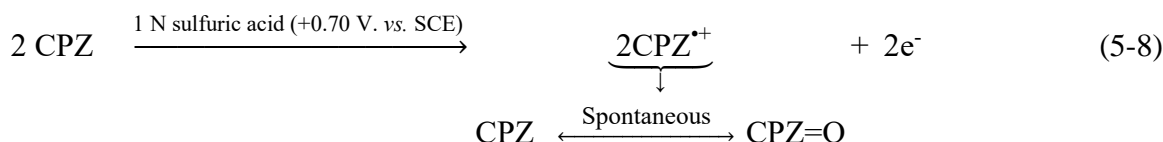
However, in a concentrated acidic solution (9 N sulfuric acid), it is possible to stabilize $CPZ^{\bullet+}$ by electrolysis at a potential of +0.50 V. *vs.* SCE (**Equation 5-9**). Thus, by choosing a proper potential, $CPZ^{\bullet+}$ can be selectively either oxidized or reduced. The one-electron oxidation of $CPZ^{\bullet+}$ yields chlorpromazine sulfoxide (**Equation 5-10**), while the one-electron reduction of $CPZ^{\bullet+}$ (at lower potentials) results in the formation of chlorpromazine (**Equation 5-11**) [49].

$$CPZ \xrightarrow{\text{9 N sulfuric acid (+0.50 V. } vs.\ \text{SCE)}} CPZ^{\bullet+} + e^{-} \tag{5-9}$$

$$CPZ^{\bullet+} \longrightarrow CPZ=O + e^{-} \tag{5-10}$$

$$CPZ^{\bullet+} + e^{-} \longrightarrow CPZ \tag{5-11}$$
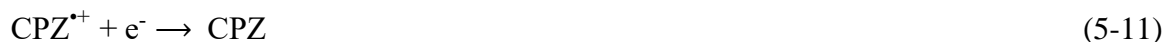
Cheng *et al.* however, disagreed with a mechanism involving a disproportionation of the free radical cation and alternatively proposed a further oxidation step of a formed cation radical/buffer adduct by another chlorpromazine radical cation, leading to its rearrangement to the sulfoxide metabolite [51]. These authors were able to show that, in aqueous buffers in the pH range between 2 and 7, a cation radical/buffer adduct (**Equation 5-12**) is formed. The oxidation of this adduct by another $CPZ^{\bullet+}$ (**Equation 5-13**), will eventually result in the formation of chlorpromazine sulfoxide (**Equation 5-14**). In the following equations, RCO_2^- refers to a representative buffer constituent [51].

$$CPZ^{\bullet+} + RCO_2^- + H_2O \leftrightarrows [CPZ(RCO_2)(OH)]^{\bullet-} + H^+ \tag{5-12}$$

$$[CPZ(RCO_2)(OH)]^{\bullet-} + CPZ^{\bullet+} \leftrightarrows CPZ + [CPZ(RCO_2)(OH)] \tag{5-13}$$

$$[CPZ(RCO_2)(OH)] \longrightarrow CPZ=O + RCO_2H \tag{5-14}$$

These reactions propose a direct reaction of CPZ$^{\bullet+}$ with the buffer or with water.

After all, according to the performed intermediates analysis in the current study, the aerobic photolytic conversion of chlorpromazine upon UV(A) irradiation can be summarized in the following reactions. Photo-ionization of chlorpromazine upon UV(A) irradiation results in the formation of its radical cation and an aqueous electron (e_{aq}^-) (**Equation 5-15**). This electron is able to reduce molecular oxygen yielding $O_2^{\bullet-}$ (**Equation 5-16**) which then reacts with chlorpromazine radical cation to produce eventually the main reaction intermediate, namely, the sulfoxide metabolite (CPZ=O, m/z: 335) (**Equation 5-17**) [57].

$$CPZ \xrightarrow{hv\ (365\ nm)} CPZ^{\bullet+} + e_{aq}^- \tag{5-15}$$

$$e_{aq}^- + O_2 \rightarrow O_2^{\bullet-} \tag{5-16}$$

$$CPZ^{\bullet+} + O_2^{\bullet-} \xrightarrow{+\ CPZ} 2\ CPZ{=}O \tag{5-17}$$
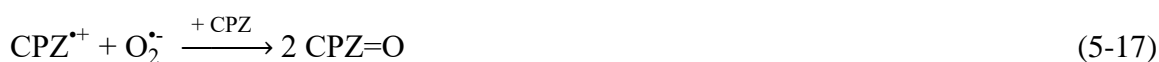
On the other hand, chlorpromazine might also be fragmented upon UV(A) excitation yielding a promazine radical and a chlorine radical (**Equation 5-18**). The formed chorine radical reacts with water forming hydroxyl radicals (**Equation 5-19**) which then react further with the promazine radical forming a hydroxylated promazine molecule (PZ-OH, m/z: 301) (**Equation 5-20**).

$$CPZ \xrightarrow{hv\ (365\ nm)} PZ^{\bullet} + Cl^{\bullet} \tag{5-18}$$

$$Cl^{\bullet} + H_2O \rightarrow {}^{\bullet}OH + H^+ + Cl^- \tag{5-19}$$

$$PZ^{\bullet} + {}^{\bullet}OH \rightarrow PZ\text{-}OH \tag{5-20}$$

Similar to chlorpromazine, the formed chlorpromazine sulfoxide might be also fragmented upon UV(A) excitation (**Equation 5-21**) and undergo a dechlorination step, forming a radical, (PZ=O)$^{\bullet}$, and a chlorine radical (which reacts further with water as shown in **Equation 5-19**). The reaction between the (dechlorinated) sulfoxide radical and a hydroxyl radical, results in the formation of the detected intermediate with m/z value of 317 (PZ=O)-OH as shown in **Equation 5-22**.

$$CPZ{=}O \xrightarrow{hv\ (365\ nm)} (PZ{=}O)^{\bullet} + Cl^{\bullet} \tag{5-21}$$

$$(PZ{=}O)^{\bullet} + {}^{\bullet}OH \rightarrow (PZ{=}O)\text{-}OH \tag{5-22}$$

However, in the presence of the photocatalyst, K-7000, the situation will be completely different. It should be considered that, K-7000 is basically anatase TiO_2 covered with a carbon-based sensitizer layer. Thus, upon irradiation at 365 nm, mainly the TiO_2 bandgap will be illuminated resulting in the formation of electron-hole pairs in the semiconductor (**Equation 5-23**). In this case, most of the incoming UV(A) photons will be absorbed by K-7000. Thus, the contribution of the homogenous photolytic reaction of chlorpromazine (**Equation 5-24**) is not significant (but still not neglected). According to the analysis of the products, during the photocatalytic conversion of chlorpromazine upon UV(A) irradiation, intermediates with m/z values of 335, 351 and 317 are found. The respective reactions can be summarized as following. Some of the above-mentioned reactions are written again to keep the consistency of the proposed mechanism.

$$K\text{-}7000 \xrightarrow{h\nu\ (365\ nm)} e^-_{CB} + h^+_{VB} \tag{5-23}$$

$$CPZ \xrightarrow{h\nu\ (365\ nm)} CPZ^{\bullet+} + e^-_{aq} \tag{5-24}$$

$$O_2 + \begin{cases} e^-_{CB} \\ e^-_{aq} \end{cases} \rightarrow O_2^{\bullet-} \tag{5-25}$$

$$h^+_{VB} + CPZ \rightarrow CPZ^{\bullet+} \tag{5-26}$$

$$h^+_{VB} + H_2O \rightarrow {}^{\bullet}OH + H^+ \tag{5-27}$$

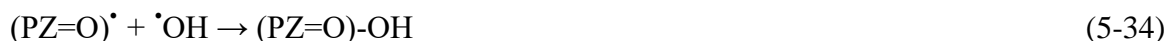$$CPZ + {}^{\bullet}OH \rightarrow CPZ^{\bullet+} + OH^- \tag{5-28}$$

$$CPZ^{\bullet+} + O_2^{\bullet-} \xrightarrow{+\ CPZ} 2\ CPZ{=}O \tag{5-29}$$

For the formation of the intermediate with m/z value of 351, which corresponds to chlorpromazine sulfone (**Figure 5-7(c)**) [58], a further oxidation step of the produced chlorpromazine sulfoxide is required (**Equation 5-30**) [57]. This results in the formation of its respective radical cation which yields eventually chlorpromazine sulfone (O=(CPZ)=O) (**Equation 5-31**).

$$CPZ{=}O + h^+_{VB} \rightarrow (CPZ{=}O)^{\bullet+} \tag{5-30}$$

$$2\ (CPZ{=}O)^{\bullet+} + 2\ O_2^{\bullet-} \rightarrow 2\ [O{=}(CPZ){=}O] + O_2 \tag{5-31}$$
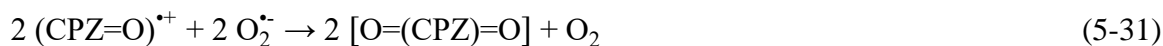
Similar to the photolytic pathway, also here, the formation of the intermediate with m/z value of 317 will proceed through the reactions shown in **Equation 5-32** to **Equation 5-34**.

$$CPZ=O \xrightarrow{h\nu \ (365 \ nm)} (PZ=O)^{\bullet} + Cl^{\bullet} \tag{5-32}$$

$$Cl^{\bullet} + H_2O \rightarrow {}^{\bullet}OH + H^+ + Cl^- \tag{5-33}$$

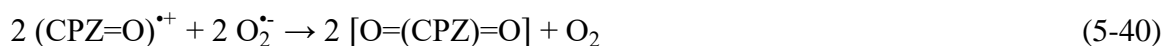$$(PZ=O)^{\bullet} + {}^{\bullet}OH \rightarrow (PZ=O)\text{-}OH \tag{5-34}$$

Nevertheless, under visible light irradiation, a completely different mechanism for the conversion of chlorpromazine is proposed. To explain this mechanism, K-7000 is considered as anatase TiO_2 covered with a carbon-based sensitizer layer. Upon visible irradiation, the excitation energy of 2.73 eV (corresponding to 455 nm) is not enough to generate electron-hole pairs in TiO_2. Thus, at 455 nm, only the carbon-based sensitizer layer (CS) will be excited. Similar to a dye-sensitizer system, the excited sensitizer will inject an electron into the conduction band of TiO_2, yielding a sensitizer radical cation ($CS^{\bullet+}$) as shown in **Equation 5-35**. This radical cation is then able to oxidize the chlorpromazine molecule from which chlorpromazine radical cation ($CPZ^{\bullet+}$) will be formed (**Equation 5-36**). The conduction band electron is able to react with molecular oxygen producing a superoxide radical (**Equation 5-37**), which is required (as mentioned before) to yield chlorpromazine sulfoxide (**Equation 5-38**).

$$CS \xrightarrow{h\nu \ (455 \ nm)} CS^{\bullet+} + e^-_{CB} \tag{5-35}$$

$$CS^{\bullet+} + CPZ \rightarrow CPZ^{\bullet+} + CS \tag{5-36}$$

$$e^-_{CB} + O_2 \rightarrow O_2^{\bullet-} \tag{5-37}$$

$$CPZ^{\bullet+} + O_2^{\bullet-} \xrightarrow{+ \ CPZ} 2 \ CPZ=O \tag{5-38}$$

The second detected intermediate, namely chlorpromazine sulfone (m/z: 351), is most likely produced through a further oxidation of chlorpromazine sulfoxide with $CS^{\bullet+}$ (**Equation 5-39**) and the reaction of its respective radical cation with a superoxide radical (**Equation 5–40**).

$$CPZ=O + CS^{\bullet+} \rightarrow (CPZ=O)^{\bullet+} + CS \tag{5-39}$$

$$2 \, (CPZ{=}O)^{\bullet+} + 2 \, O_2^{\bullet-} \rightarrow 2 \, [O{=}(CPZ){=}O] + O_2 \qquad\qquad (5\text{-}40)$$

These reactions are discussed in more detail later on in this chapter (**Section 5.3**).

Interestingly, in the current study, chlorpromazine sulfoxide is found to be highly persistent within the reaction period upon both UV(A) and visible irradiation even in the presence of K-7000. The high stability of chlorpromazine sulfoxide has been also reported by Ljunggren *et al.*[43]. Thus, in order to have a better understanding on the stability of chlorpromazine sulfoxide, further long-term experiments (24 hours) under both UV(A) and visible light irradiation are also carried out in the current study.

In the presence of K-7000, chlorpromazine sulfoxide reveals a high resistance against visible light irradiation. During 24 hours of visible light irradiation, only 27% conversion of sulfoxide is observed. From the overall conversion, 20% occurs in the first two hours, while throughout the remaining 22 hours only 7% decrease in the concentration of chlorpromazine sulfoxide is detected. A similar trend is attained for the photolytic reaction under visible light irradiation, confirming the high stability of chlorpromazine sulfoxide upon visible irradiation (**Figure 5-10**).

Figure 5-10. Long term photocatalytic and photolytic conversion of chlorpromazine sulfoxide (100 μM) upon visible light irradiation

Moreover, the reaction intermediates of the photocatalytic and photolytic processes under visible irradiation are evaluated and compared with each other. This analysis reveals the formation of an intermediate with a m/z value of 321 over the photocatalytic path, while during the photolytic experiments no intermediates are detected (**Figure 5-11**). The structure of this intermediate, however, is not determined in this study.

Figure 5-11. Chromatograms of chlorpromazine sulfoxide (m/z: 335) under both photocatalytic and photolytic conditions after 24 h visible light irradiation

Nevertheless, in both cases the signal intensity of the sulfoxide metabolite seems to be rather stable from 2 hours to 24 hours of irradiation, as for the photocatalytic path only 7% decrease and for the photolytic path 17% decrease in concentration of chlorpromazine sulfoxide is detected in this time period (**Figure 3-6**).

On the other hand, under UV(A) irradiation, chlorpromazine sulfoxide is found to be converted over the long-term experiments in both the presence and the absence of K-7000 (**Figure 5-12**).
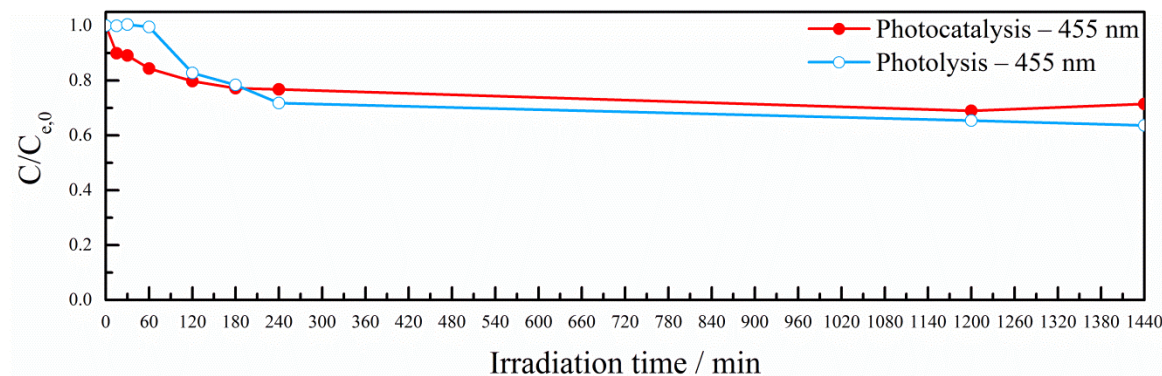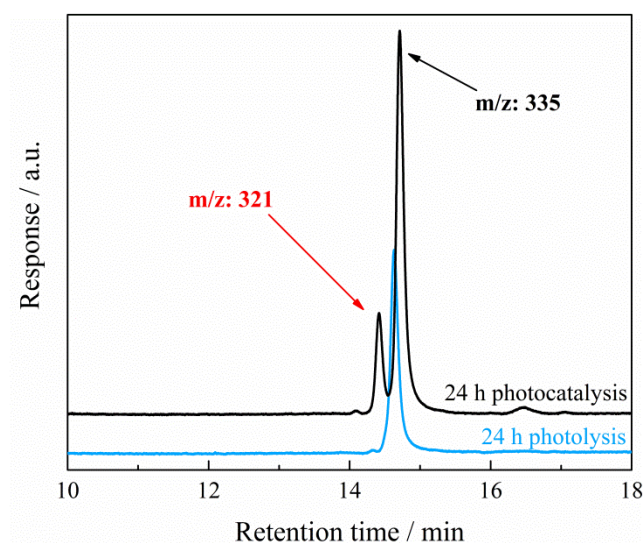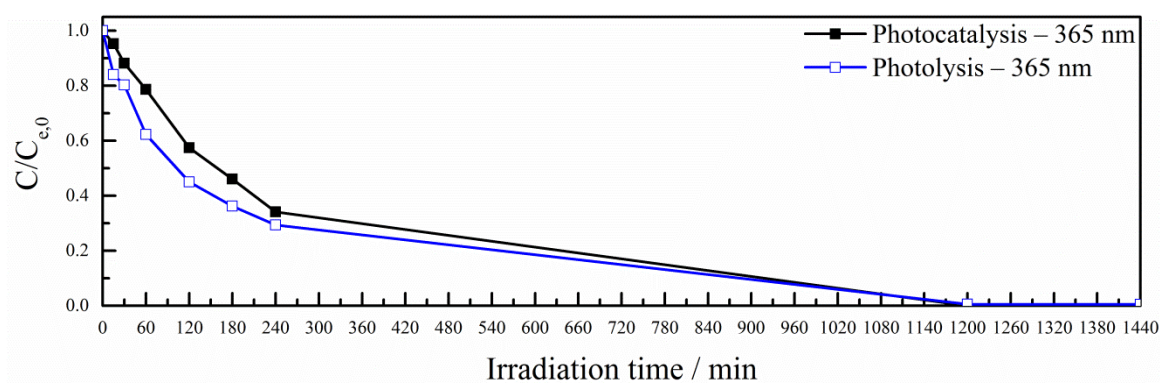

Figure 5-12. Long term photocatalytic and photolytic conversion of chlorpromazine sulfoxide (100 µM) upon UV(A) irradiation

However, this reaction seems to proceed much slower as compared to chlorpromazine conversion. After 30 minutes of UV(A) irradiation, only 12% decrease in concentration of

chlorpromazine sulfoxide is observed, while in previous experiments (**Figure 3-1(a)**), a complete conversion of chlorpromazine is achieved within 30 minutes under identical conditions. Therefore, for the complete photocatalytic conversion of the sulfoxide metabolite under UV(A) irradiation, compared to that of chlorpromazine, under identical conditions a much longer irradiation time (almost 12 times longer) is required. Also here, the same trend is observed for the photolytic conversion of chlorpromazine sulfoxide upon UV(A) irradiation. Nevertheless, the presence of the photocatalyst seems to slow down the conversion process. Thus, possible different reaction pathways for the photocatalytic and photolytic experiments are suggested.

According to the intermediates analysis performed on the conversion of chlorpromazine sulfoxide under UV(A) irradiation (**Figure 5-13**), not only the product distributions between the photocatalytic and the photolytic pathways are different, but also the produced intermediates over the photocatalytic reaction are completely removed at the end of irradiation period (**Figure 5-13(a)**). However, during the photolytic reaction, other than the initial intermediates, some new ones (marked with red * in **Figure 5-13(b)**) are also formed after all (not identified). This aspect indicates that the photocatalytic path is superior in removal of the produced intermediates compared to the photolytic path.
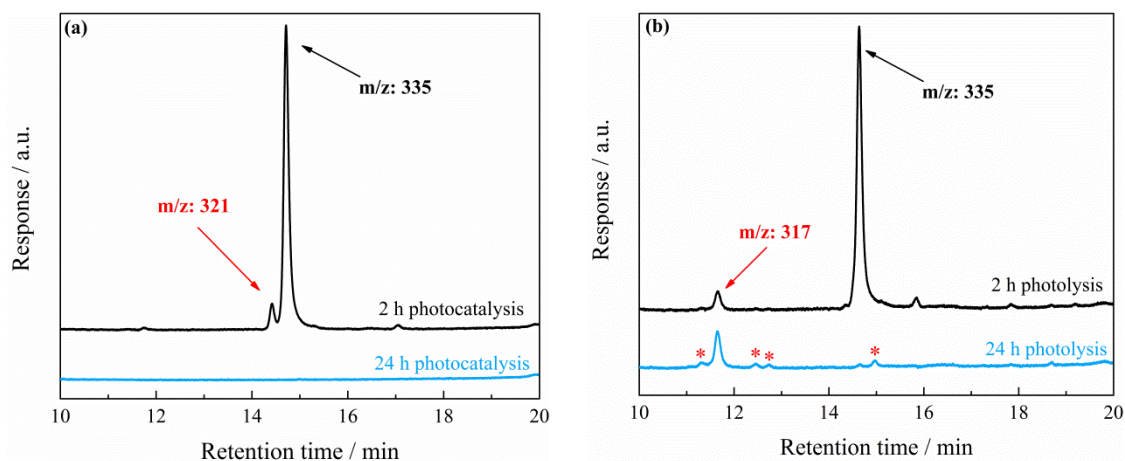

Figure 5-13. Chromatograms of chlorpromazine sulfoxide (m/z: 335) under (a) photocatalytic and (b) photolytic conditions after 2h and 24 h UV(A) irradiation

So far, all the discussions were based on the presence of molecular oxygen. However, in general, the photodegradation of chlorpromazine is strongly dependent on the reaction

medium, so that in a deoxygenated atmosphere, the photodegradation products of its transformation are different from those formed in the presence of molecular oxygen [7].

Similar to Merkle and Discher [49] and Cheng *et al.* [51] (mentioned before), Iwaoka and Kondo also showed that chlorpromazine sulfoxide is formed by its respective radical cation. However, they have claimed to have experimental evidence confirming that the oxygen atom in the sulfoxide structure originates from the molecular oxygen and not from water and that in the absence of molecular oxygen, no chlorpromazine sulfoxide will be formed [52].

In the current study, similar observations are attained under anaerobic conditions. In the absence of molecular oxygen and upon visible light irradiation, chlorpromazine cannot be converted (neither in the presence nor in the absence of K-7000). Under UV(A) irradiation, however, it is converted in the absence of molecular oxygen through both the photocatalytic and the photolytic pathways (**Figure 3-7**). Nevertheless, the reaction intermediates formed through the anaerobic pathway are completely different from those formed through the aerobic path. Interestingly, no trace of chlorpromazine sulfoxide is found in the absence of molecular oxygen.

Davies and Navaratnam found experimental evidence for the formation of free radicals on photolysis of chlorpromazine in the absence of molecular oxygen and explained its photochemistry in propan-2-ol as a solvent [59]. According to their observations, the photoreaction of chlorpromazine occurs through the first excited triplet state. This includes the absorption of light by the chlorpromazine molecule (CPZ) yielding its singlet state ($^1CPZ^*$), followed by an intersystem transformation to its triplet state ($^3CPZ^*$), as shown in **Equation 5-41** [59].

$$CPZ + hv\,(<400\ \text{nm}) \rightarrow\ ^1CPZ^* \longrightarrow\ ^3CPZ^* \tag{5-41}$$
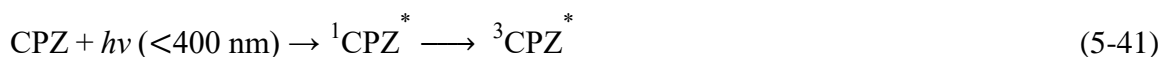
In an oxygen-saturated solution, $^3CPZ^*$ reacts directly with molecular O_2 (due to the quenching by molecular oxygen), forming chlorpromazine in its ground state and an excited singlet oxygen molecule (**Equation 5-42**) [59].

$$^3CPZ^* +\ ^3O_2 \rightarrow CPZ +\ ^1O_2^* \tag{5-42}$$

However, in the absence of molecular oxygen, excited chlorpromazine is subjected to a C-Cl bond splitting yielding a promazine free radical (PZ$^\bullet$) (**Figure 5-14**), and a chlorine free radical as follows [59]:

$$^3CPZ^* \longrightarrow PZ^\bullet + Cl^\bullet \tag{5-43}$$

These radicals were found to react further with the solvent yielding products such as promazine, isopropoxypromazine, HCl, and acetone [59]. According to Davies and Navaratnam [59], singlet oxygen is not able to oxidize chlorpromazine, which also explains the conclusions of Iwaoka and Kondo [52].
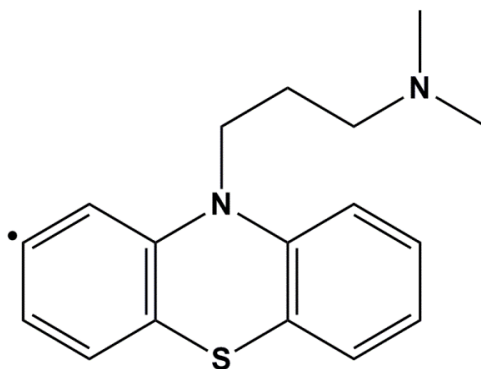

Figure 5-14. The structure of the dechlorinated chlorpromazine molecule (promazine radical (PZ$^\bullet$))

Thus, the fact that in the current study no formation of chlorpromazine sulfoxide in the absence of molecular oxygen is observed, leads to the conclusion that under anaerobic conditions, PZ$^\bullet$ is more likely to be formed (rather than CPZ$^{\bullet+}$). However, the formation of CPZ$^{\bullet+}$ can still not be excluded.

This conclusion is also in good agreement with the intermediate analysis performed for the anaerobic pathway (**Figure 3-7(a)**) revealing the formation of different chlorpromazine dimers during the photolytic reaction. As reported by Huang and Sands, the free radicals (PZ$^\bullet$) formed after the cleavage of the C-Cl bond in chlorpromazine (shown in **Equation 5-43**), promote the polymerization and dimerization processes [60]. Therefore, the observed large m/z values of 631, 599, and 583 under anaerobic conditions in the current study can be assigned to the dimers of chlorpromazine formed during the photolytic reaction upon UV(A) irradiation. These dimers are most probably the products of the interactions between the promazine radical with another molecule of chlorpromazine or with another radical, leading to a rearrangement to the dimers of this compound.

Nevertheless, no information about the possible structures of these dimers is found in this work.

Besides the dimer intermediates observed during the anaerobic photolytic conversion of chlorpromazine, two other products with m/z values of 301 and 285 are also detected for both, the photolytic and the photocatalytic pathway (**Figure 5-15**).
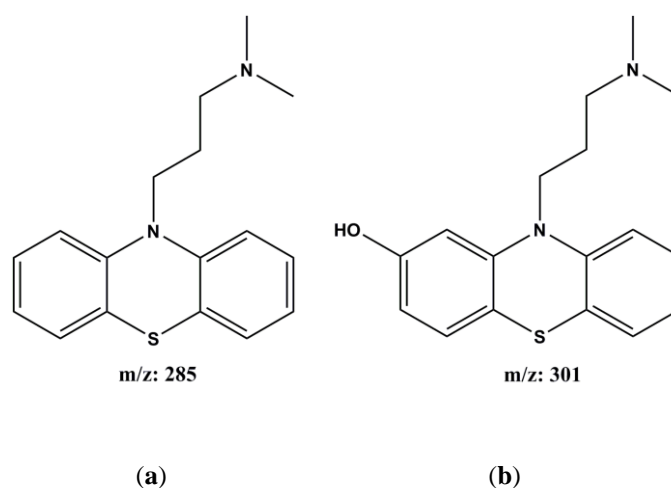

| (**a**) | (**b**) |

Figure 5-15. Proposed structures of the two most stable products under anaerobic conditions

Considering the structures of these products (PZ-H (m/z: 285) and PZ-OH (m/z: 301)), in both of them, the C-Cl bond is replaced with a C-OH or a C-H bond (**Figure 5-15**). For these products to be formed, a reaction between PZ$^{\bullet}$ and $^{\bullet}$OH radicals has to take place, which is likely to be originated from the reaction of the dechlorinated radical with water. Although the reactions between the organic radicals and water are usually somewhat unlikely, such reactions have been reported before under anaerobic conditions [61]. The formation of these products under anaerobic conditions has been reported before in the literature and the m/z value of 285 was attributed to the promazine metabolite (**Figure 5-15(a)**), while the m/z value of 301 was assigned to 2-hydroxypromazine (**Figure 5-15(b)**) [59,62]. After all, based on the performed intermediate analysis in the current study, the following processes are proposed for the anaerobic photolytic conversion of chlorpromazine upon UV(A) irradiation. As explained before, in the absence of molecular oxygen, the photo-excited chlorpromazine molecule undergoes a dechlorination step to form free radicals (**Equation 5-44**). The formed chlorine radical can possibly react with water yielding a hydroxyl radical (**Equation 5-45**) which is likely to react further with the promazine radical (**Equation 5-46**) resulting in the formation of PZ-OH (m/z: 301). On the

other hand, the promazine radical is likely to react with water to form PZ-H (m/z: 285) (**Equation 5-47**). The promazine radical might also react with another chlorpromazine molecule or other radicals or intermediates to produce the dimers as mentioned before (**Equation 5-48**).

$$CPZ \xrightarrow{h\nu\,(365\,nm)} PZ^{\bullet} + Cl^{\bullet} \qquad (5\text{-}44)$$

$$Cl^{\bullet} + H_2O \rightarrow {}^{\bullet}OH + H^+ + Cl^- \qquad (5\text{-}45)$$

$$PZ^{\bullet} + {}^{\bullet}OH \rightarrow PZ\text{-}OH \qquad (5\text{-}46)$$

$$PZ^{\bullet} + H_2O \rightarrow PZ\text{-}H + {}^{\bullet}OH \qquad (5\text{-}47)$$

$$PZ^{\bullet} + \begin{cases} CPZ \\ PZ^{\bullet} \\ \text{other radicals} \end{cases} \longrightarrow \text{Dimers} \qquad (5\text{-}48)$$

A comparison between the photocatalytic and photolytic conversion of chlorpromazine under anaerobic conditions (**Figure 3-7**) yields the following observations: (I) in the presence of K-7000, only PZ-OH and PZ-H are formed and no formation of dimers is detected, (II) PZ-OH and PZ-H are apparently rather stable products at least within the irradiation period, and (III) the presence of K-7000 seems to limit the conversion of chlorpromazine.

These observations can be explained when considering the photocatalytic pathway. In this case, the probability of a direct photo-excitation of the chlorpromazine molecule is rather low but it is not excluded. Thus, the reactions shown in **Equation 5-44** and in **Equation 5-45** might occur (not shown again). However, In the presence of K-7000, most of the incoming UV(A) photons will be absorbed by this photocatalyst resulting into its photo-excitation (**Equation 5-49**). In the absence of molecular oxygen, however, the only electron acceptor in the reaction medium will be the chlorpromazine itself. As a result, the photo-generated conduction band electrons will react with chlorpromazine causing it to undergo a dechlorination step yielding the promazine radical and a chloride ion (**Equation 5-50**). The photogenerated valence band holes might oxidize water forming hydroxyl radicals (**Equation 5-51**).

$$\text{K-7000} \xrightarrow{\textit{hv (365 nm)}} e^-_{CB} + h^+_{VB} \tag{5-49}$$

$$e^-_{CB} + CPZ \rightarrow PZ^{\bullet} + Cl^- \tag{5-50}$$

$$h^+_{VB} + H_2O \rightarrow {}^{\bullet}OH + H^+ \tag{5-51}$$
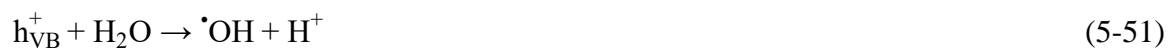
The formed promazine radical, $PZ^{\bullet}$, is likely to react with ${}^{\bullet}OH$ or water to form PZ-OH and PZ-H as described in **Equation 5-46** and **Equation 5-47**, respectively. Nevertheless, in the photocatalytic procedure under anaerobic conditions no formation of the chlorpromazine dimers is observed. A possible explanation might be that, in this case, the formed promazine radicals are most likely absorbed on the surface of the photocatalyst which inhibits the interaction between these radicals and the formation of their respective dimers. However, in the photolytic process, these free radicals are present in the solution and can easily react with each other.

It has to be noted that these systems (including all the mentioned active radical species) are rather complicated and besides these proposed reactions, other processes might occur as well. In any case, it can be concluded that in the absence of oxygen, the photocatalytic pathway proceeds through possible reactions of conduction band electrons. It seems to be likely that the anaerobic photocatalytic products are formed through the reduction reaction of chlorpromazine which is more expected to take place in the absence of oxygen.

As can be seen in **Figure 5-16**, the detected intermediates of the photocatalytic conversion of chlorpromazine are different under aerobic and anaerobic conditions using different irradiation wavelengths.
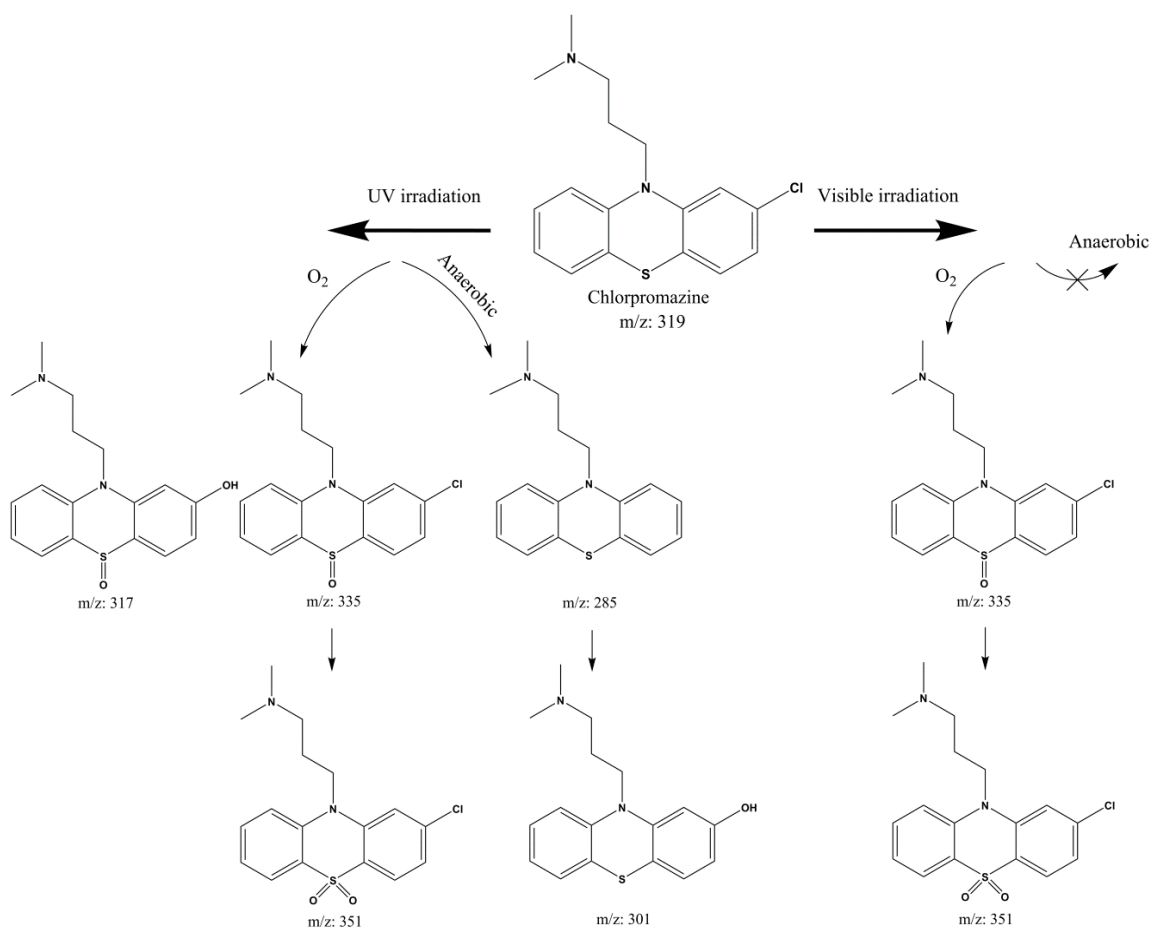
Figure 5-16. The detected reaction intermediates during the photocatalytic conversion of chlorpromazine

The main difference between the products obtained over UV(A) and visible irradiation, is the dechlorination of the chlorpromazine molecule. Under visible light irradiation, chlorpromazine is converted to chlorpromazine sulfoxide (m/z: 335) and chlorpromazine sulfone (m/z: 351). Interestingly, in the structure of both of these products, the C-Cl bond remains unchanged (see **Figure 5-16**). As mentioned before, upon visible light irradiation (455 nm), no excitation of chlorpromazine occurs. Therefore, the dechlorination step and consequently, the formation of promazine radical will be inhibited. This might explain the mentioned difference observed in reaction intermediates using different irradiation wavelengths.

After all, due to the observed differences between the photolytic and photocatalytic experiments, it is of high importance to further evaluate the mechanism of the photocatalytic conversion of chlorpromazine in the presence of K-7000 under both UV(A) and visible irradiation.

5.3. Nature of Charge Carriers Formed by UV or Visible Excitation in K-7000

After investigating the photocatalytic conversion of chlorpromazine in the presence of K-7000 and following the assessment of the formed intermediates throughout this process, a deeper analysis on the origin of the visible light activity of K-7000 is required. As it was observed so far, K-7000 is able to convert chlorpromazine under visible light irradiation, while, its sulfoxide metabolite is found to be highly persistent even in the presence of K-7000. Therefore, in order to have a better understanding of the mechanism behind these observations, in diffuse reflectance transient absorption spectroscopic measurements on K-7000 is performed in different atmospheres using excitation with UV light (355 nm) and visible light (455 nm) and the nature of the photo-generated charge carriers formed by excitation of this photocatalyst is investigated in detail in **Chapter 4**.

As explained in **Chapter 1**, K-7000 is reported to be anatase titanium dioxide which is modified with carbon-based materials [63]. In the current study, the reported [63] anatase crystalline structure of K-7000 is confirmed through XRD analysis (**Figure 4-1**) as well as UV-vis diffuse reflectance measurements (**Figure 4-2(a)**). Accordingly, no effect of the carbon-based layer on the crystalline structure of the titanium dioxide is observed.

As a commercially developed product, K-7000 was originally introduced as carbon-doped TiO_2. However, as demonstrated for instance, in N- and S-doped TiO_2, doping is known to cause bandgap narrowing [64,65]. Nevertheless, in the current study, no bandgap narrowing is observed for K-7000, while an absorption band in the visible range is found. The obtained optical bandgap value of 3.31 eV for K-7000 (**Figure 4-S1**) is in good agreement with values reported in the literature [63,66]. The effect of the carbon-based layer on the absorption properties of titanium dioxide is observed in terms of a broad absorption band in the visible region for K-7000, while this effect is not observed for Hombikat UV100 (pure anatase) (**Figure 4-2**). Moreover, the determined flatband potential of K-7000 being −0.46 V *vs.* NHE at pH 7 (-0.047 V *vs.* NHE at pH 0) is found to be similar to that of Hombikat UV100 being −0.51 V *vs.* NHE at pH 7 (-0.097 V *vs.* NHE at pH 0) (**Figure 4-3**). It has to be noted that, since all the measurements in the current study are carried out at neutral pH, the potentials are presented as V *vs.* NHE at pH 7. These results are in good agreement with those obtained in the group of Prof. Kisch [63]. Similar to the current study, they were also able to verify experimentally that the carbon-based modification does not

affect the position of the conduction band of K-7000 [63]. Their obtained experimental results also excluded the original assumption of the incorporation of the carbon-based material into the lattice, but rather confirmed its deposition on the surface of TiO_2 in the form of a molecular sensitizer. Thus, regarding this description, K-7000 can be considered similar to a dye-sensitized photocatalytic particle, in which, the electronic structure is characterized by well-defined HOMO (highest occupied molecular orbital) and LUMO (lowest unoccupied molecular orbital) levels of the dye [67]. This sensitizer–TiO_2 assembly is schematically illustrated in **Figure 5-17**.
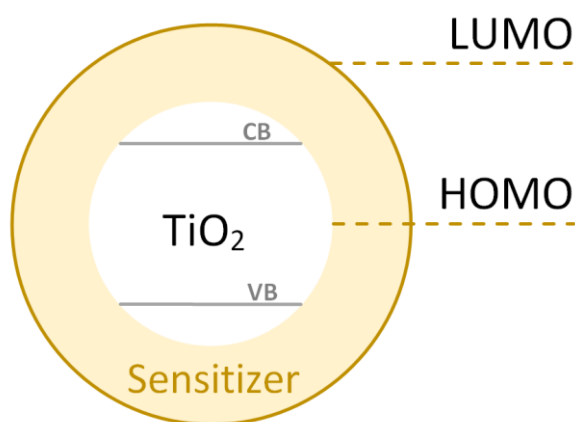

Figure 5-17. Schematic of K-7000 illustrated as TiO_2 with a carbon-based sensitizer layer

In addition to the characterizing assessments, transient absorption spectroscopy measurements are performed *via* excitation with UV light (355 nm) and visible light (455 nm) in Ar, methanol and oxygen atmospheres. These measurements also reveal interesting information on visible light activity K-7000. An Ar atmosphere is normally considered as an inert one; since due to the absence of any active species in Ar atmosphere, the photogenerated charge carriers can only recombine with each other. In contrast, considering the role of oxygen as an active electron scavenger, it is expected to observe different absorption spectra and decays in the oxygen atmosphere compared to the Ar atmosphere. Moreover, since the reduction potential of oxygen ($O_2/O_2^{\bullet-}$ = -0.33 V *vs.* NHE [68]), which is a pH-independent value [36], is located at a more positive value than the flatband potential of K-7000 (-0.46 V *vs.* NHE in neutral solution), the transfer of conduction band electrons of TiO_2 to O_2 molecules is thermodynamically foreseeable.

However, as reported by Yamakata *et al.*, for the photogenerated electrons in TiO_2 to be scavenged by O_2 molecules in the gas phase, a reaction time of more than 10 µs is required

[69]. Therefore, in the current study, regardless of the irradiation wavelengths, due to the limited considered time scale of 8 μs, this effect is observed neither in the transient absorption spectra (**Figure 4-4**), nor in the transient absorption decays (**Figure 4-5**). On the other hand, after excitation with 355 nm laser light, clear differences are observed between the absorption spectra (**Figure 4-4(a)**) and decays (**Figure 4-5(a)**) obtained in the methanol and the Ar atmospheres. To explain this effect, one should consider that as a well-known hole scavenger, methanol can be oxidized by the photogenerated valence band holes and form an α-hydroxyl radical (**Equation 5-52**) [70,71].

$$CH_3OH \rightarrow {}^{\bullet}CH_2OH + H^+ + e^- \tag{5-52}$$

However, for this reaction to happen, the valence band edge and thus the potential of the photogenerated holes must be more positive compared to the redox potential of the methanol oxidation. The valence band edge of K-7000 can be easily calculated from its determined flatband potential (−0.46 V *vs.* NHE at pH 7) and bandgap value (3.31 eV) to be at 2.85 V *vs.* NHE at pH 7. Also the oxidation potential of methanol is reported to be at 1.03 V *vs.* NHE at pH 7 [72]. Considering these values, the abstraction of an electron from the methanol molecule (**Equation 5-52**) is possible. Therefore, in the presence of methanol as a hole scavenger, the transient absorption spectrum is attributed only to the photogenerated electrons; since due to an eminent phenomenon for TiO_2 [73], in the absence of an electron scavenger, the photogenerated electrons tend to accumulate in the particles. Thus, the observed higher absorption at longer wavelengths seen in **Figure 4-4(a)**, which is attributed to the photogenerated electrons [74], clarifies the different absorption spectra obtained under Ar and methanol atmospheres.

Nonetheless, the obtained results of transient absorption spectroscopy experiments using 455 nm light excitation show a completely different aspect, since no significant variations between the transient absorption spectra (**Figure 4-4(b)**) and decays (**Figure 4-5(b)**) measured in methanol and Ar atmospheres are attained. Considering the determined bandgap value of K-7000 (3.31 eV), for this photocatalyst to be photo-excited, an energy equal to or more than the bandgap energy is required. Hence, at 455nm excitation wavelengths, the corresponding photon energy of 2.73 eV will not be enough for bandgap excitation in anatase TiO_2. This fact is also confirmed by transient absorption measurements performed for anatase UV100 which reveals no transient response after

visible light excitation (**Figure 4-6**). Contradictorily, for K-7000 an outstanding and long-lived signal is obtained under identical conditions. The presence of the sensitizer molecule on the surface of TiO_2 is reflected through the above-mentioned long-lived signal which is originated from its light absorption in the visible range. Thus, the photocatalytic mechanism under visible light in K-7000 is profoundly different than in normal anatase TiO_2. Considering the TiO_2-sensitizer assembly, under excitation with visible light, the transition is rather correlated to the HOMO and LUMO levels of the sensitizer, instead of the valence band and the conduction band of TiO_2 (**Figure 5-18**).
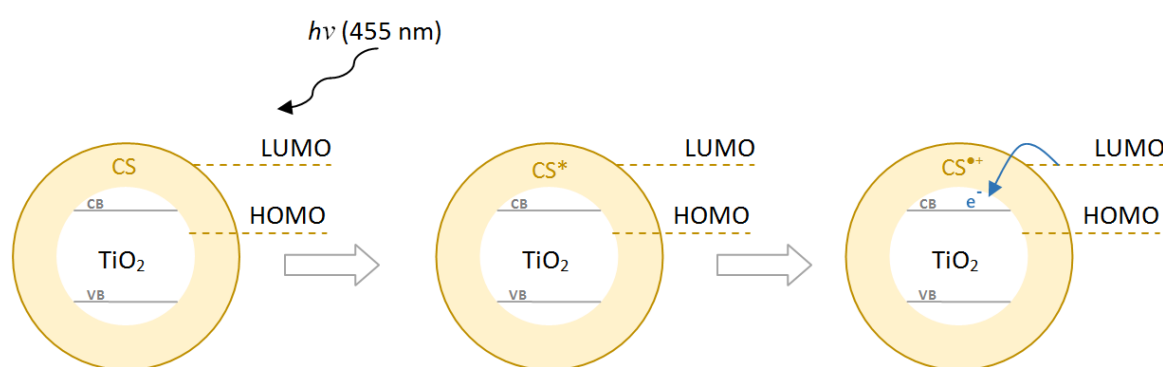

Figure 5-18. Schematic of visible light (455 nm) excitation of K-7000; CS, CS* and CS•+ represent respectively, the carbon-based sensitizer, its excited state, and its radical cation.

Similar to UV light excitation, the transient absorption spectra (**Figure 4-4(b)**) and decays (**Figure 4-5(b)**) in Ar and oxygen atmosphere after visible light excitation of K-7000 are observed to be similar to each other. Resembling dye-sensitized solar cells, after excitation of the sensitizer, the electrons are likely to be transferred from the LUMO to the conduction band of TiO_2 and accumulate in the TiO_2 particles as schematically shown in **Figure 5-18** [67]. Thus, also here, oxygen reduction will be restricted in the same way as for bandgap excitation under visible light irradiation [69].

It has been reported that the presence of the sensitizer layer could increase the visible light activity of K-7000 compared to Evonik P25 TiO_2, for the photocatalytic removal of NO_x under white light excitation [66] as well as for the degradation of acetone under visible light irradiation [75]. In addition, the photocatalytic experiments (also presented in **Section 5.2**) reveal that K-7000 is able to convert the resistant molecule of chlorpromazine within the first 30 minutes of visible light irradiation (**Figure 4-7**).

However, the similar decays and spectra obtained in methanol and inert atmospheres indicate that under visible light excitation, the degradation of methanol in the presence of K-7000 does not proceed within the considered time scale. A trend akin to that of the transient absorption measurements is also observed during the photocatalytic experiments under visible irradiation performed with an aerated aqueous methanol suspension. So that after 60 minutes of constant irradiation of the suspension at 455 nm wavelengths in the presence of K-7000, only less than 2% conversion of methanol to formaldehyde is attained (**Figure 4-7** & **Figure 4-S2**).

In addition to these experiments, transient absorption spectroscopy measurements with the K-7000 powder in the presence of pre-adsorbed chlorpromazine result into similar observations (**Figure 5-19**).
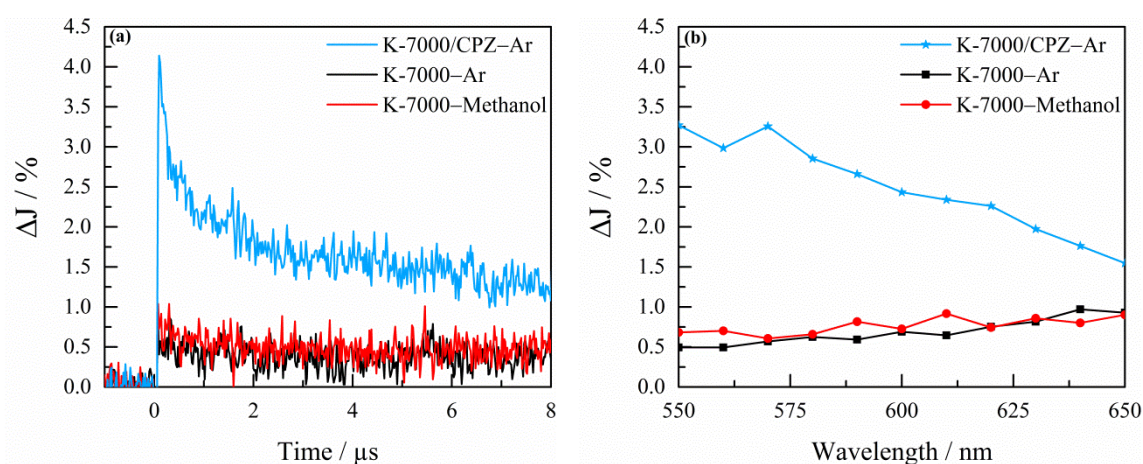

Figure 5-19. (a) Transient absorption decays observed at 550 nm after excitation with 455 nm, and (b) transient absorption spectra measured at 100 ns after the laser excitation after excitation with 455 nm for: K-7000 with pre-adsorbed chlorpromazine (CPZ) in Ar atmosphere (blue line), bare K-7000 in Ar atmosphere (black line), and bare K-7000 in methanol atmosphere (red line)

A strongly increased transient absorption signal right after the laser pulse is detected for the K-7000 with pre-adsorbed chlorpromazine (see **Figure 5-19-**blue line). This signal can be assigned to the chlorpromazine radical cation [76]. The formation of this radical cation is in good agreement with the discussions presented before in **Section 5.2** for the photocatalytic conversion of chlorpromazine. However, the transient absorption spectra and decays of bare K-7000 in the presence of methanol (see **Figure 5-19-**red line) and in inert atmosphere (see **Figure 5-19-**black line) are found to be almost identical revealing that the photocatalytic conversion of methanol is almost negligible.

These results bring up the question: "Why is the degradation of methanol under visible light irradiation in the presence of K-7000 limited (or extremely slow), while this photocatalyst is able to successfully convert chlorpromazine under identical conditions?"

To answer this question, initially, the possible mechanism of the photocatalytic degradation of methanol under UV irradiation has to be taken into consideration. After irradiation with UV light, most likely TiO_2 and the carbon-based sensitizer will both be excited. However, the impact of sensitizer's excitation is negligible in the mechanism, due to the smaller amount of the sensitizer layer compared to TiO_2. Nevertheless, in the TiO_2 particles, electron-hole pairs will be generated after UV light excitation (**Equation 5-53**).

$$TiO_2 + hv \rightarrow e_{CB}^- + h_{VB}^+ \tag{5-53}$$

Following the photogeneration of electrons and holes, the conduction band electrons are likely to react with molecular oxygen and form a superoxide radical ($O_2^{-\bullet}$) as follows [77]:

$$O_2 + e_{CB}^- \rightarrow O_2^{-\bullet} \tag{5-54}$$

On the other hand, the photogenerated valence band holes might get trapped at protonated bridging oxygen ions (OH_{br}^-) and form a hydroxyl radical ($-OH_{br}^\bullet$) [77]:

$$OH_{br}^- + h_{VB}^+ \rightarrow -OH_{br}^\bullet \tag{5-55}$$

The photogenerated holes can also be trapped at adsorbed methanol molecules (CH_3OH_{ads}) yielding an α-hydroxyl radical ($^\bullet CH_2OH$) [77]:

$$CH_3OH_{ads} + h_{VB}^+ \rightarrow {}^\bullet CH_2OH + H^+ \tag{5-56}$$

This radical ($^\bullet CH_2OH$) can also be formed through the oxidation of methanol molecules in aqueous solution (CH_3OH_{aq}) via hydroxyl radicals [77]:

$$CH_3OH_{aq} + -OH_{br}^\bullet \rightarrow {}^\bullet CH_2OH + -OH_{2\,br} \tag{5-57}$$

Thus, in an aerated suspension, formaldehyde will be a product of the further oxidation of the produced α-hydroxyl radicals with molecular oxygen as following [77]:

$$^\bullet CH_2OH + O_2 \rightarrow CH_2O + O_2^{-\bullet} + H^+ \tag{5-58}$$
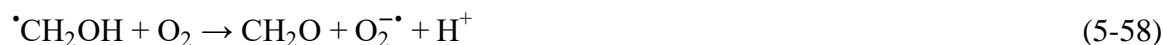
Nevertheless, under visible light excitation, the possible mechanism of methanol degradation in the presence of K-7000 is a completely different one. In this case, as explained before, the excitation energy of 2.73 eV (corresponding to 455 nm) will not be enough for the excitation of TiO_2 and hence, only the carbon-based sensitizer layer (named here as CS) will be excited (CS^*). This excitation is followed by the injection of an electron from the LUMO into the conduction band of TiO_2 forming the sensitizer radical cation ($CS^{\bullet+}$) as presented in the following equation:

$$CS + h\nu \rightarrow CS^* \rightarrow CS^{\bullet+} + e^-_{CB} \qquad (5\text{-}59)$$

The conduction band electrons can react as before with molecular oxygen (**Equation 5-54**), while the sensitizer radical cation could react with methanol as following:

$$CS^{\bullet+} + CH_3OH \rightarrow CS + {}^{\bullet}CH_2OH + H^+ \qquad (5\text{-}60)$$

The formed α-hydroxyl radical (${}^{\bullet}CH_2OH$) is able to be further oxidized as shown before (**Equation 5-58**) and form formaldehyde. However, since the degradation of methanol could not be observed according to the experimental results, the reaction shown in **Equation 5-60** is not likely to happen.

As described before, **Figure 5-20** reveals that under excitation with UV light, electron-hole pairs will be generated in the anatase particles as well as in the carbon-based sensitizer, while under visible light irradiation, only the carbon-based sensitizer will be excited.
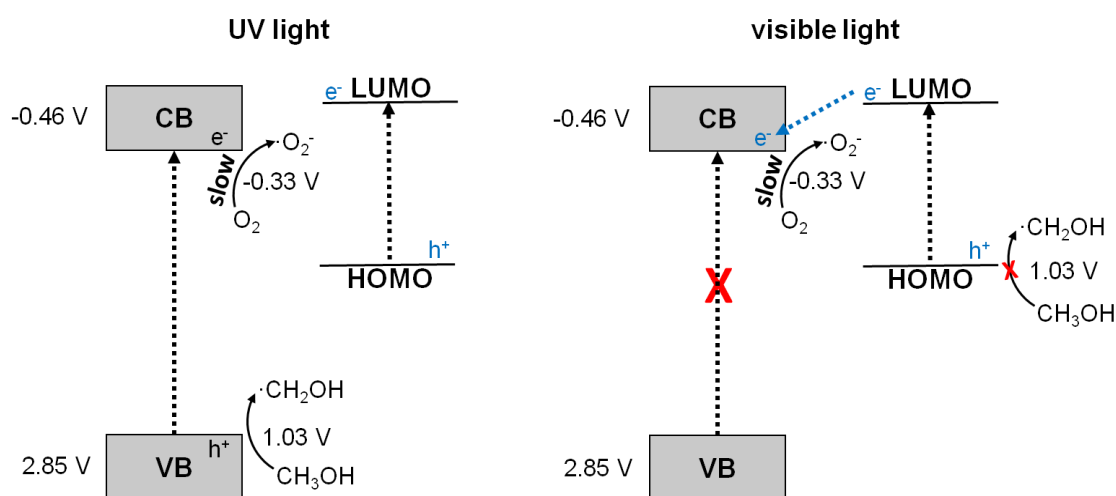

Figure 5-20. Proposed processes taking place after excitation of K-7000 with UV light and visible light; This figure is a reprint of Scheme 4-1 from page 124 in Chapter 4. Since all the measurements were carried

out at neutral pH, the potentials are presented as V *vs.* NHE at pH 7. ($O_2/O_2^{\cdot-}$ = -0.33 V *vs.* NHE is a pH-independent value [36])

Figure 5-20 helps to clarify the different photocatalytic activities of K-7000 observed for the conversion of methanol and chlorpromazine under visible light excitation. Considering the mechanism of the chlorpromazine conversion under visible light excitation, the excitation of the sensitizer layer and consequently, the injection of electrons to the conduction band of TiO_2 (**Equation 5-59**) should be taken into account. In the presence of molecular oxygen, conduction band electrons will slowly reduce the oxygen molecule as described before (**Equation 5-54**) and produce a superoxide radical ($O_2^{\cdot-}$). The sensitizer radical cation ($CS^{\cdot+}$) formed through the reaction shown in **Equation 5-59** is however, able to oxidize chlorpromazine and to form a chlorpromazine radical cation and a regenerated sensitizer molecule (**Equation 5-61**).


$$(5\text{-}61)$$
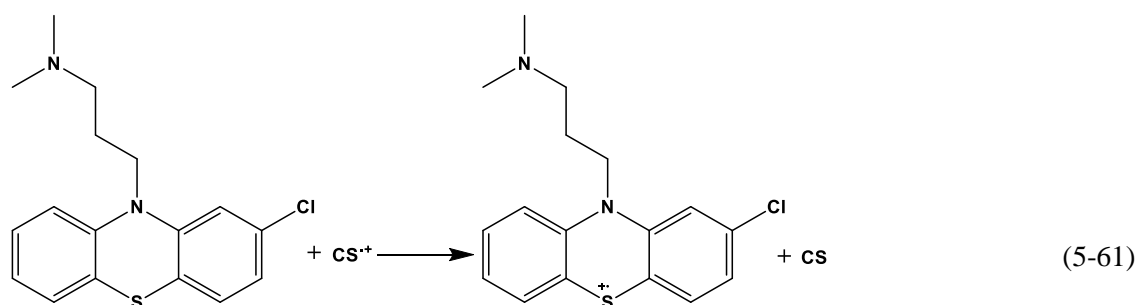
The formed chlorpromazine radical cation is the able to react with the superoxide radical ($O_2^{\cdot-}$) formed through the reaction shown in **Equation 5-54**, to form a persulfoxide molecule (**Equation 5-62**). This kind of reaction is reported before for similar compounds [57].

$$(5\text{-}62)$$
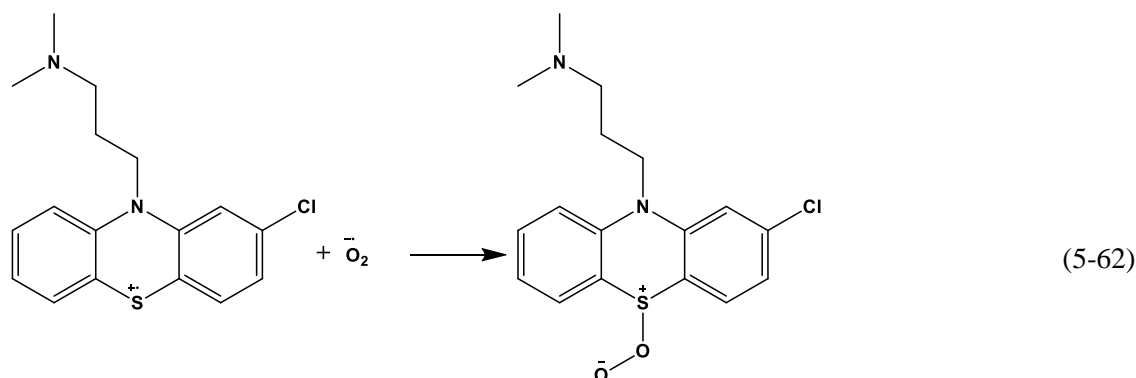
The next reactions are expected to occur as following based on the mechanism proposed by Somasundaram and Srinivasan for the oxidation of aryl methyl sulfides in the presence of irradiated TiO_2 [57]. The persulfoxide molecule which is yielded in the reaction shown in **Equation 5-62** is likely to form a thiadioxirane molecule (**Equation 5-63**):

$$(5\text{-}63)$$
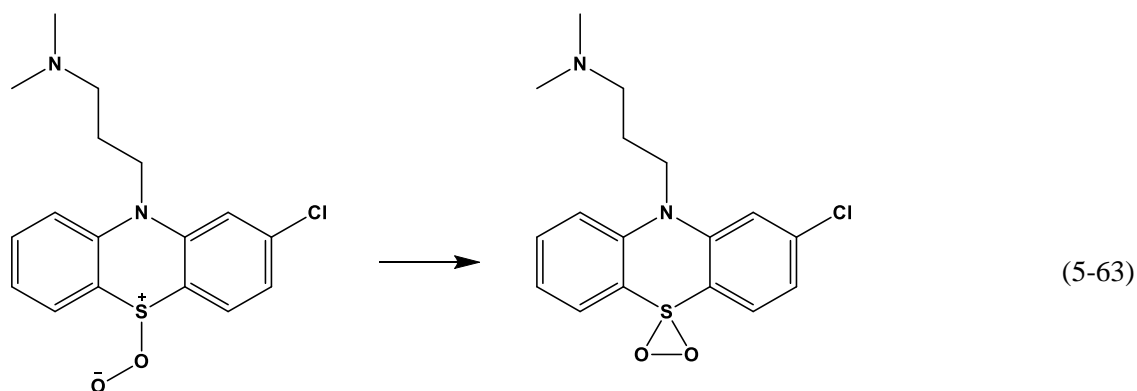
Further, the thiadioxirane molecule can react with another chlorpromazine molecule forming two chlorpromazine sulfoxide molecules as shown in the following equation:

$$(5\text{-}64)$$
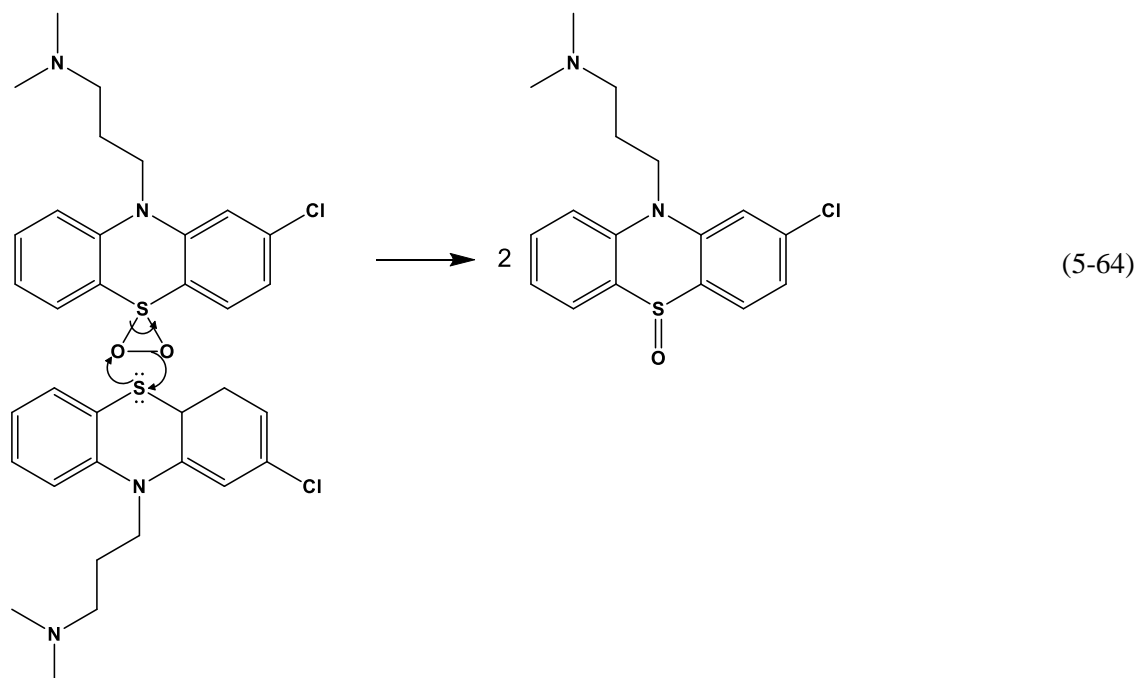
This proposed pathway including the formation of the chlorpromazine sulfoxide is also in good agreement with the experimental results discussed in **Section 5.2**, for the photocatalytic conversion of chlorpromazine.

According to these reactions confirming the ability of chlorpromazine to react with the sensitizer radical cation, and considering the lack of methanol degradation upon visible light irradiation in the presence of K-7000, one comes to the conclusion that an essential initial step, namely, the reaction between methanol and the sensitizer radical cation must be missing for the photocatalytic conversion of methanol under visible light irradiation. In other words, without the reaction of the organic compound with the sensitizer radical cation, further photocatalytic reaction steps will not be able to occur as well. After all, this step seems to happen with chlorpromazine and not with methanol. This difference is originated from the variations between the redox potentials of the corresponding reactions.

Figure 5-21 helps to obtain a better understanding of these observations. Considering the redox potential of the one-electron oxidation of chlorpromazine (0.53 V *vs.* NHE at pH 7 [49,78]) and the required potential for the methanol oxidation (1.03 V *vs.* NHE at pH 7 [72]), the redox potential of the sensitizer radical cation should be more positive than that of the chlorpromazine oxidation and either more negative or close to that of the methanol oxidation (the possible position of the HOMO shown in **Figure 5-21**). This might explain the lack of methanol oxidation. On the other hand, due to the possibility of the electron transfer from the excited sensitizer to the conduction band of TiO_2, the position of LUMO can be estimated to be at a less positive potential than the conduction band edge of TiO_2. However, a precise position for the LUMO of the sensitizer cannot be specified from the performed experiments (see **Figure 5-21**).
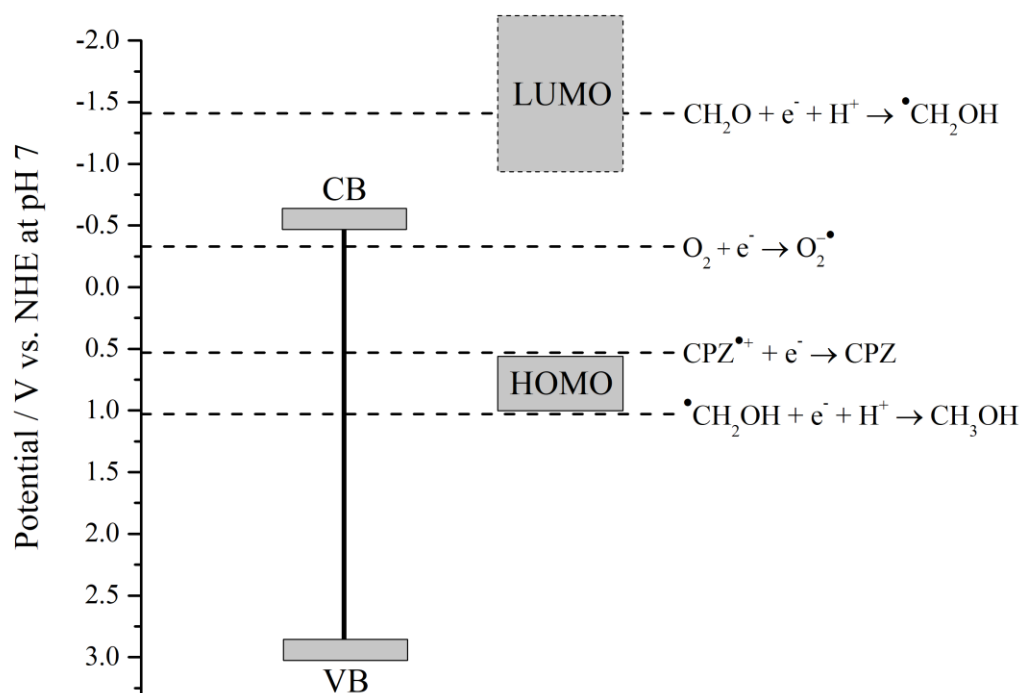
Figure 5-21. Band positions of K-7000 with the corresponding redox potentials of the oxygen reduction, methanol oxidation, and chlorpromazine (CPZ) oxidation at pH 7 and the possible positions of the LUMO and the HOMO of the sensitizer [68,72]; This figure is a reprint of Scheme 4-2 from page 127 in Chapter 4.

Accordingly, the strong stability of chlorpromazine sulfoxide, the long-lasting main product of the photocatalytic conversion of chlorpromazine under visible light irradiation (described in **Section 5.2**) can be explained also by means of the proposed mechanism for methanol and chlorpromazine. For this purpose, the redox potential for the one-electron oxidation of chlorpromazine sulfoxide has to be known. However, to the best of the author's knowledge, this value has not been determined before. Nevertheless, for similar sulfoxides, potentials in the range of 2.5 V to 2.8 V can be found in the literature [57]. These values are very close to the valence band edge of K-7000. Assuming a redox potential value for the one-electron oxidation of chlorpromazine sulfoxide in this range, would explain the stability of this compound upon oxidation; as this value would be positioned even more positive than the methanol oxidation.

5.4. Conclusions and Outlook

In conclusion, the experimental results of this study provide a better understanding of the principles of the photocatalytic conversion of organic molecules, specifically from the group of phenothiazine antipsychotic pharmaceuticals.

Despite the assumed high capacity of zinc ferrite for the removal of organic materials, it is shown in the current study that the photocatalytic activity of this semiconductor upon visible light irradiation might be often overestimated. Most commonly, for the evaluation of the photocatalytic activity of newly developed semiconducting materials, organic dyes are chosen as model pollutants. Nevertheless, depending on the irradiation wavelengths, organic dyes are likely to undergo photo-excitation and thus, a photo-bleaching effect might be observed which is usually mistaken with the photocatalytic transformation of the dye. In such cases, the photocatalytic effect is hardly distinguishable from the homogeneous photolysis of the dye molecule. Moreover, despite the observed photobleaching of the MB dye (a member of the phenothiazine group) under visible light irradiation, it is shown that this effect is initiated by an electron transfer from the photo-excited MB molecule adsorbed on the zinc ferrite surface, into the conduction band of this semiconductor. Thus, the performed investigations on photocatalytic conversion of MB in the presence of zinc ferrite in this study recommend that organic dyes such as MB are inadequate model compounds for the evaluation of the photocatalytic activity of semiconducting materials.

Furthermore, photocatalytic experiments with chlorpromazine in the presence of K-7000 reveal that for the conversion of this persistent organic pharmaceutical under visible light irradiation, the presence of the photocatalyst is essential. This work provides useful information on the differences between the photolytic and photocatalytic procedures and suggests possible reaction pathways for the photocatalytic removal of chlorpromazine under different conditions. Nevertheless, despite the ability of K-7000 to convert chlorpromazine under visible light irradiation, the observed high stability of the main product of its conversion, namely, chlorpromazine sulfoxide, points out some limitations regarding the visible light activity of the K-7000 semiconductor.

These observations are supported also by laser flash photolysis spectroscopy measurements which reveal the inadequate ability of K-7000 for photocatalytic conversion of methanol (compared to chlorpromazine) under visible light excitation. The transient absorption spectroscopic analysis performed on the photogenerated charge carriers upon UV and visible light excitation in K-7000, along with considering it as a TiO_2-sensitizer assembly, leads to helpful conclusions which are used to determine the possible photocatalytic reactions under these conditions. The proposed mechanism in this regard serves to explain

the reason behind the varying visible light activity of K-7000 for the photocatalytic transformation of different organic molecules, by considering the redox potentials of the corresponding reactions.

All in all, the experiments carried out within the purpose of this doctoral thesis contribute to the evaluation of the possible visible-light driven photocatalytic removal of pharmaceuticals. The obtained results provide a deeper insight into the visible light activity of semiconducting materials. Despite the generally assumed high oxidizing ability of the photogenerated holes in semiconductors, this study illustrates that the photogenerated charge carriers in visible light active materials may have a limited ability to drive oxidation reactions. This piece of information is highly valuable as it can be used to enhance the selectivity of the oxidation half-reaction in photocatalytic procedures. This idea might as well be employed in the application of visible active materials in environmental remediation, such that, under the right circumstances, they would be used to oxidize an unwanted compound selectively and transform it into a valuable product.

5.5. References

1. Spasiano, D.; Marotta, R.; Malato, S.; Fernandez-Ibañez, P.; Di Somma, I. Solar photocatalysis: Materials, reactors, some commercial, and pre-industrialized applications. A comprehensive approach. *Appl. Catal. B Environ.* **2015**, *170–171*, 90–123.

2. Robertson, P.K.J.; Bahnemann, D.W.; Robertson, J.M.C.; Wood, F. Photocatalytic detoxification of water and air. *Environ. Photochem. Part II* **2005**, *2*, 367–423.

3. Malato, S.; Fernández-Ibáñez, P.; Maldonado, M.I.; Blanco, J.; Gernjak, W. Decontamination and disinfection of water by solar photocatalysis: Recent overview and trends. *Catal. Today* **2009**, *147*, 1–59.

4. Mills, A.; Hunte, S. Le An overview of semiconductor photocatalysis. *J. Photochem. Photobiol. A Chem.* **1997**, *108*, 1–35.

5. Hoffmann, M.R.; Martin, S.T.; Choi, W.; Bahnemann, D.W. Environmental applications of semiconductor photocatalysis. *Chem. Rev.* **1995**, *95*, 69–96.

6. Bahnemann, D. Photocatalytic water treatment: Solar energy applications. *Sol. Energy* **2004**, *77*, 445–459.

7. Trawiński, J.; Skibiński, R. Studies on photodegradation process of psychotropic

drugs: a review. *Environ. Sci. Pollut. Res.* **2017**, *24*, 1152–1199.

8. Sato, T.; Haneda, K.; Seki, M.; Iijima, T. Morphology and magnetic properties of ultrafine $ZnFe_2O_4$ particles. *Appl. Phys. A Solids Surfaces* **1990**, *50*, 13–16.

9. Boumaza, S.; Boudjemaa, A.; Bouguelia, A.; Bouarab, R.; Trari, M. Visible light induced hydrogen evolution on new hetero-system $ZnFe_2O_4/SrTiO_3$. *Appl. Energy* **2010**, *87*, 2230–2236.

10. Dom, R.; Subasri, R.; Hebalkar, N.Y.; Chary, A.S.; Borse, P.H. Synthesis of a hydrogen producing nanocrystalline $ZnFe_2O_4$ visible light photocatalyst using a rapid microwave irradiation method. *RSC Adv.* **2012**, *2*, 12782–12791.

11. Dillert, R.; Taffa, D.H.; Wark, M.; Bredow, T.; Bahnemann, D.W. Research Update: Photoelectrochemical water splitting and photocatalytic hydrogen production using ferrites (MFe_2O_4) under visible light irradiation. *APL Mater.* **2015**, *3*, 104001-1–15.

12. Ammar, S.; Jouini, N.; Fiévet, F.; Beji, Z.; Smiri, L.; Moliné, P.; Danot, M.; Grenèche, J.M. Magnetic properties of zinc ferrite nanoparticles synthesized by hydrolysis in a polyol medium. *J. Phys. Condens. Matter* **2006**, *18*, 9055–9069.

13. Granone, L.I. An Iron-Based Photoelectrode, Gottfried Wilhelm Leibniz Universität Hannover, 2019.

14. Dom, R.; Subasri, R.; Radha, K.; Borse, P.H. Synthesis of solar active nanocrystalline ferrite, MFe_2O_4 (M: Ca, Zn, Mg) photocatalyst by microwave irradiation. *Solid State Commun.* **2011**, *151*, 470–473.

15. Taffa, D.H.; Dillert, R.; Ulpe, A.C.; Bauerfeind, K.; Bredow, T.; Bahnemann, D.; Wark, M. Photoelectrochemical and theoretical investigations of spinel type ferrites ($M_xFe_{3-x}O_4$) for water splitting: A mini-review. *J. Photonics Energy* **2016**, *7*, 1–24.

16. Mills, A.; Wang, J. Photobleaching of methylene blue sensitised by TiO_2: an ambiguous system? *J. Photochem. Photobiol. A Chem.* **1999**, *127*, 123–134.

17. Yan, X.; Ohno, T.; Nishijima, K.; Abe, R.; Ohtani, B. Is methylene blue an appropriate substrate for a photocatalytic activity test? A study with visible-light responsive titania. *Chem. Phys. Lett.* **2006**, *429*, 606–610.

18. Diodati, S.; Pandolfo, L.; Caneschi, A.; Gialanella, S.; Gross, S. Green and low temperature synthesis of nanocrystalline transition metal ferrites by simple wet chemistry routes. *Nano Res.* **2014**, *7*, 1027–1042.

19. Jang, J.S.; Borse, P.H.; Lee, J.S.; Jung, O.-S.; Cho, C.-R.; Jeong, E.D.; Ha, M.G.; Won, M.S.; Kim, H.G. Synthesis of nanocrystalline $ZnFe_2O_4$ by polymerized

complex method for its visible light photocatalytic application: An efficient photo-oxidant. *Bull. Korean Chem. Soc.* **2009**, *30*, 1738–1742.

20. Sarkar, J.; Bhattacharyya, S. Operating characteristics of transcritical CO_2 heat pump for simultaneous water cooling and heating. *Arch. Thermodyn.* **2013**, *33*, 23–40.

21. Toledo-Antonio, J.A.; Nava, N.; Martínez, M.; Bokhimi, X. Correlation between the magnetism of non-stoichiometric zinc ferrites and their catalytic activity for oxidative dehydrogenation of 1-butene. *Appl. Catal. A Gen.* **2002**, *234*, 137–144.

22. Chinnasamy, C.N.; Narayanasamy, A.; Ponpandian, N.; Chattopadhyay, K.; Guerault, H.; Greneche, J.-M. Magnetic properties of nanostructured ferrimagnetic zinc ferrite. *J. Phys. Condens. Matter* **2000**, *12*, 7795–7805.

23. Ahmed, Y.M.Z.; Ewais, E.M.M.; Zaki, Z.I. In situ synthesis of high density magnetic ferrite spinel ($MgFe_2O_4$) compacts using a mixture of conventional raw materials and waste iron oxide. *J. Alloys Compd.* **2010**, *489*, 269–274.

24. Jang, J.S.; Hong, S.J.; Lee, J.S.; Borse, P.H.; Jung, O.-S.; Hong, T.E.; Jeong, E.D.; Won, M.S.; Kim, H.G. Synthesis of zinc ferrite and its photocatalytic application under visible light. *J. Korean Phys. Soc.* **2009**, *54*, 204–208.

25. Jeong, E.D.; Borse, P.H.; Jang, J.S.; Lee, J.S.; Cho, C.R.; Bae, J.S.; Park, S.; Jung, O.-S.; Ryu, S.M.; Won, M.S.; et al. Physical and optical properties of nanocrystalline calcium ferrite synthesized by the polymerized complex method. *J. Nanosci. Nanotechnol.* **2009**, *9*, 3568–3573.

26. Shim, S.-H.; Duffy, T.S. Raman spectroscopy of Fe_2O_3 to 62 GPa. *Am. Mineral.* **2001**, *87*, 318–326.

27. Kharisov, B.I.; Dias, H.V.R.; Kharissova, O. V. Mini-review: Ferrite nanoparticles in the catalysis. *Arab. J. Chem.* **2014**, *In press*, 1–13.

28. Martín De Vidales, J.L.; López-Delgado, A.; Vila, E.; López, F.A. Effect of the starting solution on the physico-chemical properties of zinc ferrite synthesized at low temperature. *J. Alloys Compd.* **1999**, *287*, 276–283.

29. Singhal, S.; Sharma, R.; Singh, C.; Bansal, S. Enhanced photocatalytic degradation of methylene blue using $ZnFe_2O_4$/MWCNT composite synthesized by hydrothermal method. *Indian J. Mater. Sci.* **2013**, *2013*, 1–6.

30. Jia, Z.; Ren, D.; Liang, Y.; Zhu, R. A new strategy for the preparation of porous zinc ferrite nanorods with subsequently light-driven photocatalytic activity. *Mater. Lett.* **2011**, *65*, 3116–3119.

31. Cao, X.; Gu, L.; Lan, X.; Zhao, C.; Yao, D.; Sheng, W. Spinel $ZnFe_2O_4$ nanoplates embedded with Ag clusters: Preparation, characterization, and photocatalytic application. *Mater. Chem. Phys.* **2007**, *106*, 175–180.

32. Jadhav, S.D.; Hankare, P.P.; Patil, R.P.; Sasikala, R. Effect of sintering on photocatalytic degradation of methyl orange using zinc ferrite. *Mater. Lett.* **2011**, *65*, 371–373.

33. Li, X.; Hou, Y.; Zhao, Q.; Wang, L. A general, one-step and template-free synthesis of sphere-like zinc ferrite nanostructures with enhanced photocatalytic activity for dye degradation. *J. Colloid Interface Sci.* **2011**, *358*, 102–108.

34. Dom, R.; Chary, A.S.; Subasri, R.; Hebalkar, N.Y.; Borse, P.H. Solar hydrogen generation from spinel $ZnFe_2O_4$ photocatalyst: effect of synthesis methods. *Int. J. Energy Res.* **2015**, *39*, 1378–1390.

35. Shao, R.; Sun, L.; Tang, L.; Zhidong Chen Preparation and characterization of magnetic core-shell $ZnFe_2O_4@ZnO$ nanoparticles and their application for the photodegradation of methylene blue. *Chem. Eng. J.* **2013**, *217*, 185–191.

36. Wood, P.M. The potential diagram for oxygen at pH 7. *Biochem. J.* **1988**, *253*, 287–289.

37. Granone, L.I.; Ulpe, A.C.; Robben, L.; Klimke, S.; Jahns, M.; Renz, F.; Gesing, T.M.; Bredow, T.; Dillert, R.; Bahnemann, D.W. Effect of the degree of inversion on optical properties of spinel $ZnFe_2O_4$. *Phys. Chem. Chem. Phys.* **2018**, *20*, 28267–28278.

38. Lang, X.; Chen, X.; Zhao, J. Heterogeneous visible light photocatalysis for selective organic transformations. *Chem. Soc. Rev.* **2014**, *43*, 473–486.

39. Takizawa, T.; Watanabe, T.; Honda, K. Photocatalysis through excitation of adsorbates. 2. A comparative study of Rhodamine B and methylene blue on cadmium sulfide. *J. Phys. Chem.* **1978**, *82*, 1391–1396.

40. Bauldreay, J.M.; Archer, M.D. Dye-modified electrodes for photogalvanic cells. *Electrochim. Acta* **1983**, *28*, 1515–1522.

41. Párkányi, C.; Boniface, C.; Aaron, J..; Maafi, M. A quantitative study of the effect of solvent on the electronic absorption and fluorescence spectra of substituted phenothiazines: evaluation of their ground and excited singlet-state dipole moments. *Spectrochim. Acta Part A Mol. Spectrosc.* **1993**, *49*, 1715–1725.

42. Trautwein, C.; Kümmerer, K. Degradation of the tricyclic antipsychotic drug

chlorpromazine under environmental conditions, identification of its main aquatic biotic and abiotic transformation products by LC-MS[n] and their effects on environmental bacteria. *J. Chromatogr. B Anal. Technol. Biomed. Life Sci.* **2012**, *889–890*, 24–38.

43.   Ljunggren, B.; Moller, H. Phenothiazine phototoxicity: an experimental study on chlorpromazine and related tricyclic drugs. *Acta Derm. Venereol.* **1977**, *57*, 325–329.

44.   Jiménez, J.J.; Muñoz, B.E.; Sánchez, M.I.; Pardo, R.; Vega, M.S. Fate of the drug chlorpromazine in river water according to laboratory assays. Identification and evolution over time of degradation products. Sorption to sediment. *Chemosphere* **2016**, *162*, 285–292.

45.   Bahnemann, D.; Asmus, K.-D.; Willson, R.L. Free radical induced one-electron oxidation of the phenothiazines chlorpromazine and promethazine. *J. Chem. Soc. Perkin Trans.* **1983**, *2*, 1661–1668.

46.   Boehme, C.L.; Strobel, H.W. High-performance liquid chromatographic methods for the analysis of haloperidol and chlorpromazine metabolism in vitro by purified cytochrome P450 isoforms. *J. Chromatogr. B Biomed. Sci. Appl.* **1998**, *718*, 259–266.

47.   Wilde, M.L.; Schneider, M.; Kümmerer, K. Fenton process on single and mixture components of phenothiazine pharmaceuticals: Assessment of intermediaries, fate, and preliminary ecotoxicity. *Sci. Total Environ.* **2017**, *583*, 36–52.

48.   Kigondu, E.M.; Njoroge, M.; Singh, K.; Njuguna, N.; Warner, D.F.; Chibale, K. Synthesis and synergistic antimycobacterial screening of chlorpromazine and its metabolites. *Med. Chem. Commun.* **2014**, *5*, 502–506.

49.   Merkle, F.H.; Discher, C.A. Electrochemical oxidation of chlorpromazine hydrochloride. *J. Pharm. Sci.* **1963**, *53*, 620–623.

50.   Motten, A.G.; Buettner, G.R.; Chignell, C.F. Spectroscopic studies of cutaneous photosensitizing agents--VIII. A spin-trapping study of light induced free radicals from chlorpromazine and promazine. *Photochem. Photobiol.* **1985**, *42*, 9–15.

51.   Cheng, H.Y.; Sackett, P.H.; Mccreery, R.L. Kinetics of chlorpromazine cation radical decomposition in aqueous buffers. *J. Am. Chem. Soc.* **1978**, *100*, 962–967.

52.   Iwaoka, T.; Kondo, M. Mechanistic studies on the photooxidation of chlorpromazine in water and ethanol. *Bull. Chem. Soc. Jpn.* **1974**, *47*, 980–986.

53. Kochevar, I.E. Phototoxicity mechanisms: Chlorpromazine photosensitized damage to DNA and cell membranes. *J. Invest. Dermatol.* **1981**, *77*, 59–64.

54. Saucin, M.; Van de Vorst, A. Photodynamic potentialities of some phenothiazine derivatives. *Radiat. Environ. Biophys.* **1980**, *17*, 159–168.

55. Ateş, S.; Somer, G. Photodegradation of chlorpromazine in aqueous solutions as studied by ultraviolet-visible spectrophotometry and voltammetry. *J. Chem. Soc. Faraday Trans. 1* **1981**, *77*, 859–867.

56. Felmeister, A.; Discher, C.A. Photodegradation of chlorpromazine hydrochloride. *J. Pharm. Sci.* **1964**, *53*, 756–762.

57. Somasundaram, N.; Srinivasan, C. Oxidation of aryl methyl sulfides and sulfoxides on irradiated TiO_2. *J. Photochem. Photobiol. A Chem.* **1998**, *115*, 169–173.

58. Chagonda, L.F.S.; Millership, J.S. High-performance liquid chromatographic determination of chlorpromazine and its degradation products in pharmaceutical dosage forms: A stability-indicating assay. *Analyst* **1988**, *113*, 233–237.

59. Davies, A.K.; Navaratnam, S.; Phillips, G.O. Photochemistry of chlorpromazine [2-chloro-N-(3-dimethylaminopropyl)phenothiazine] in propan-2-ol solution. *J. Chem. Soc. Perkin Trans. 2* **1976**, 25–29.

60. Huang, C.L.; Sands, F.L. Effect of ultraviolet irradiation on chlorpromazine II: Anaerobic condition. *J. Pharm. Sci.* **1967**, *56*, 259–264.

61. Hamid, S.; Ivanova, I.; Jeon, T.H.; Dillert, R.; Choi, W.; Bahnemann, D.W. Photocatalytic conversion of acetate into molecular hydrogen and hydrocarbons over Pt/TiO_2: pH dependent formation of Kolbe and Hofer-Moest products. *J. Catal.* **2017**, *349*, 128–135.

62. Grant, F.W.; Greene, J. Phototoxicity and photonucleophilic aromatic substitution in chlorpromazine. *Toxicol. Appl. Pharmacol.* **1972**, *23*, 71–74.

63. Ząbek, P.; Eberl, J.; Kisch, H. On the origin of visible light activity in carbon-modified titania. *Photochem. Photobiol. Sci.* **2009**, *8*, 264–269.

64. Morikawa, T.; Asahi, R.; Ohwaki, T.; Aoki, K.; Taga, Y. Band-gap narrowing of titanium dioxide by nitrogen doping. *Jpn. J. Appl. Phys.* **2001**, *40*, L561–L563.

65. Umebayashi, T.; Yamaki, T.; Itoh, H.; Asai, K. Band gap narrowing of titanium dioxide by sulfur doping. *Appl. Phys. Lett.* **2003**, *81*, 2–5.

66. Tobaldi, D.M.; Seabra, M.P.; Otero-Irurueta, G.; de Miguel, Y.R.; Ball, R.J.; Singh, M.K.; Pullar, R.C.; Labrincha, J.A. Quantitative XRD characterisation and gas-

phase photocatalytic activity testing for visible-light (indoor applications) of KRONOClean 7000®. *RSC Adv.* **2015**, *5*, 102911–102918.

67.   Qin, P.; Yang, X.; Chen, R.; Sun, L.; Marinado, T.; Edvinsson, T.; Boschloo, G.; Hagfeldt, A. Influence of π-conjugation units in organic dyes for dye-sensitized solar cells. *J. Phys. Chem. C* **2007**, *111*, 1853–1860.

68.   Ilan, Y.A.; Czapski, G.; Meisel, D. The one-electron transfer redox potentials of free radical. I. The oxygen/superoxide system. *Biochmica er Biophys. Acta* **1976**, *430*, 209–224.

69.   Yamakata, A.; Ishibashi, T.; Onishi, H. Water- and oxygen-induced decay kinetics of photogenerated electrons in TiO_2 and Pt/TiO_2: A time-resolved infrared absorption study. *J. Phys. Chem. B* **2001**, *105*, 7258–7262.

70.   Schneider, J.; Bahnemann, D.W. Undesired role of sacrificial reagents in photocatalysis. *J. Phys. Chem. Lett.* **2013**, *4*, 3479–3483.

71.   Memming, R. Photoinduced charge transfer processes at semiconductor electrodes and particles. In *Electron Transfer I. Topics in Current Chemistry*; Mattay, J., Ed.; Springer-Verlag: Berlin Heidelberg, 1994; Vol. 169, pp. 105–181.

72.   Wang, C.; Pagel, R.; Bahnemann, D.W.; Dohrmann, J.K. Quantum yield of formaldehyde formation in the presence of colloidal TiO_2-based photocatalysts: Effect of intermittent illumination, platinization, and deoxygenation. *J. Phys. Chem. B* **2004**, *108*, 14082–14092.

73.   Iorio, Y. Di; Aguirre, M.E.; Brusa, M.A.; Grela, M.A. Surface chemistry determines electron storage capabilities in alcoholic sols of titanium dioxide nanoparticles. A combined FTIR and room temperature EPR investigation. *J. Phys. Chem. C* **2012**, *116*, 9646–9652.

74.   Bahnemann, D.; Henglein, A.; Lilie, J.; Spanhel, L. Flash photolysis observation of the absorption spectra of trapped positive holes and electrons in colloidal titanium dioxide. *J. Phys. Chem.* **1984**, *88*, 709–711.

75.   Sankova, N.; Semeykina, V.; Selishchev, D.; Glazneva, T.; Parkhomchuk, E.; Larichev, Y.; Uvarov, N. Influence of tetraalkylammonium compounds on photocatalytic and physical properties of TiO_2. *Catal. Letters* **2018**, *148*, 2391–2407.

76.   Maruthamuthu, P.; Sharma, D.K.; Serpone, N. Subnanosecond relaxation dynamics of 2,2′-azinobis(3-ethylbenzothiazoline-6-sulfonate) and chlorpromazine. Assessment of photosensitization of a wide band gap metal oxide semiconductor

TiO$_2$. *J. Phys. Chem.* **1995**, *99*, 3636–3642.

77.   Ahmed, A.Y.; Kandiel, T.A.; Ivanova, I.; Bahnemann, D. Photocatalytic and photoelectrochemical oxidation mechanisms of methanol on TiO$_2$ in aqueous solution. *Appl. Surf. Sci.* **2014**, *319*, 44–49.

78.   Bahnemann, D.; Asmus, K.-D.; Willson, R.L. Phenothiazine radical-cations: Electron transfer equilibria with iodide ions and the determination of one-electron redox potentials by pulse radiolysis. *J. Chem. Soc. Perkin Trans. II* **1983**, 1669– 1673.

Publications

Journal Publications

Arimi, A.; Günnemann, C.; Curti, M.; Bahnemann, D. W., Regarding the Nature of Charge Carriers formed by UV or Visible Light Excitation of carbon-modified Titanium Dioxide, *Catalysts* **2019**, 9 (8), 697-712 (doi:10.3390/catal9080697).

Arimi, A.; Dillert, R.; Dräger, G.; Bahnemann, D. W., Light-Induced Reactions of Chlorpromazine in the Presence of a Heterogeneous Photocatalyst: Formation of a Long-Lasting Sulfoxide, *Catalysts* **2019**, 9 (7), 627-644 (doi:10.3390/catal9070627).

Arimi, A.; Megatif, L.; Granone, L. I.; Dillert, R.; Bahnemann, D. W., Visible-light Photocatalytic Activity of Zinc Ferrites, *Journal of Photochemistry and Photobiology A: Chemistry* **2018**, 366,118-126 (doi:10.1016/j.jphotochem.2018.03.014).

Arimi, A.; Farhadian, M; Solaimany Nazar; A. Z.; Assessment of operating parameters for photocatalytic degradation of a textile dye by Fe_2O_3/TiO_2/clinoptilolite nanocatalyst using Taguchi experimental design, *Research on chemical Intermediates* **2016**, 42 (5), 4021-4040 (doi:10.1007/s11164-015-2255-3).

Megatif, L.; Ghozatloo, A.; Arimi, A.; Shariati-Niasar, M., Investigation of Laminar Convective Heat Transfer of TiO_2-CNT Hybrid Water Base Nano Fluid, *Experimental Heat Transfer Journal* **2016**, 29 (1), 124-138 (doi:10.1080/08916152.2014.973974).

Book Chapter

Megatif, L.; Arimi, A.; Dillert, R.; Bahnemann, D. W., Reactors for Artificial Photosynthesis in Heterogeneous Systems, In *Artificial Photosynthesis*, World Scientific Series in Current Energy Issues: Solar Energy, Volume 6, **2019**, World Scientific Publishers Ltd. submitted for publication.

Oral Presentations

Arimi, A., Dillert, R.; Bahnemann, D. W., "Photocatalytic Visible-Light Activity of Zinc Ferrite", Russian-German Workshop, National University of St. Petersburg, October 2017, St. Petersburg, Russia.

Arimi, A., Dillert, R.; Bahnemann, D. W., "Investigation of Zinc Ferrite as a Visible-Light Active Photocatalyst", New Photocatalytic Materials for Environment, Energy and Sustainability 2 (NPM-2), July 2017, Ljubljana, Slovenia.

Arimi, A., Dillert, R.; Bahnemann, D. W., "Zinc Ferrite: A visible light active photocatalyst", Russian-German Workshop, Laboratorium für Nano- und Quantenengineering (LNQE), Leibniz University Hannover, November 2016, Hannover, Germany.

Poster Presentations

Arimi, A., Dillert, R.; Bahnemann, D. W., "Wavelength Dependent Measurements to investigate the Visible-Light Activity of Zinc Ferrite", Nanoday 2017, Laboratorium für Nano- und Quantenengineering (LNQE), Leibniz University Hannover, September 2017, Hannover, Germany.

Arimi, A., Megatif, L.; Granone, L. I.; Dillert, R.; Bahnemann, D. W., "Visible-Light Photocatalytic Activity of Zinc Ferrites", 6th International Conference on Semiconductor Photochemistry (SP6), Carl von Ossietzky University, September 11-14, 2017, Oldenburg, Germany.

Arimi, A.; Megatif, L.; Granone, L. I., Dillert, R.; Bahnemann, D. W., "Ferrites for Photoelectrochemical Water Splitting", DFG SPP 1613 Summer School, Hotel Teikyo, September 2016, Berlin-Schmoeckwitz, Germany.

Curriculum Vitae

Personal data

Name   **Arimi, Arsou**

Address   **Podbielskistrasse. 116, 30177 Hannover**

Date of Birth   **30.03.1989**

Place of Birth   **Sari, Iran**

Education

Since 10/2015	Ph.D. Student at Institute of Technical Chemistry, Leibniz University of Hannover, Hannover, Germany Ph.D. Thesis: "Visible Light Active Photocatalysts for the Degradation of Drug Residues in Polluted Waters"
10/2012 – 10/2014	Master of Science in Chemical Engineering (M.Sc.Eng) at Institute of Chemical Engineering, University of Isfahan, Isfahan, Iran Major: Environmental Engineering Master Thesis: "Textile wastewater treatment through Advanced Oxidation Processes (AOPs) by a novel TiO_2/Fe_2O_3/natural zeolite nano-photocatalyst"
10/2007 – 09/2011	Bachelor of Science in Chemical Engineering (B.Sc.Eng) at Institute of Chemical Engineering, University of Tehran, Tehran, Iran Bachelor Thesis: "Separation of heavy metal ions such as Cu(II) from wastewater by adsorption on carbon nano-tubes (CNTs)"
10/2003-09/2007	Diploma and Pre-University at Farzanegan High School (National Organization for Development of Exceptional Talents (NODET)), Sari, Iran Major: Mathematical Sciences

Work Experience

10/2015 – now	Ph.D. Fellow at Institute of Technical Chemistry, Leibniz University of Hannover, Hannover, Germany
10/2014 – 03/2015	Process engineer, Nilfam Engineering Wastewater Treatment Design Co., Isfahan, Iran
07/2010 – 09/2010	Intern, Roshangaran Polyethylene Industries, Sari, Iran